The Involvement of RS2Z Proteins in Tomato Heat Stress Response and Thermotolerance

Dissertation

zur Erlangung des Doktorgrades
der Naturwissenschaften

vorgelegt beim Fachbereich Biowissenschaften
der Johann Wolfgang Goethe-Universität
in Frankfurt am Main

Von Remus Richard Elrik Rosenkranz
aus Dieburg

Frankfurt 2022
(D 30)

vom Fachbereich Biowissenschaften der

Johann Wolfgang Goethe-Universität als Dissertation angenommen.

Dekan: Prof. Dr. Sven Klimpel

Gutachter: Prof. Dr. Enrico Schleiff

Zweitgutachter: Prof. Dr. Michaela Müller-McNicoll

Datum der Disputation: _____

I Table of contents

II Abstract

Due to their sessile nature, plants are constantly exposed to an everchanging environment. When these changes exceed certain limits, they can significantly impact plant growth and development, which, in case of crop plants, has consequences on food security. Exposure to high temperatures can cause heat stress (HS), one of the most devastating stresses that plants can face. The survival and recovery from HS are dependent on the activation of the HS response (HSR), a collection of molecular mechanisms conferring HS tolerance by maintaining the cellular homeostasis. Stress responses follow a strictly orchestrated network of signal perception and -transduction, ultimately resulting in an adaptive cellular output. Thereby, the massive reshaping of the transcriptome plays a major part, in which heat stress transcription factors (HSFs) play the key role by inducing the expression of HS-responsive genes, including heat shock proteins and other transcription factors. Additionally, alternative splicing (AS), the selective usage of splice sites, contributes to the rapid adjustment of the transcriptome landscape by producing different mRNA variants from a single gene. Consequently, this results in the reduction of translatable transcripts by nonsense-mediated mRNA-decay or nuclear retention, but also enhances the proteome diversity by allowing the synthesis of protein isoforms with distinct functions. AS thereby modulates the activity of important regulatory factors like HSFA2 in *Solanum lycopersicum* (tomato). HSFA2 is the key factor of acquired thermotolerance (ATT), which enables the ability to survive a potentially lethal HS through pre-exposure to a preceding mild HS. Temperature-dependent AS leads to the synthesis of two HSFA2 protein variants, whereby inhibition of splicing ensures the synthesis of the stable isoform HSFA2-I that is required for ATT.

Transcriptome analysis of several plant species exposed to HS has highlighted the strong impact of high temperatures on the regulation of pre-mRNA splicing. Despite its importance, little is known about the molecular basis of the AS regulation in plants. Particularly for an economically important crop like tomato, understanding the regulation of HS-sensitive AS will contribute to the description of such an important regulatory mechanism but also might offer new insights for increasing HS resilience. Serine/arginine-rich proteins (SR proteins) are central regulators of constitutive and AS by modulating the splice site selection by the spliceosome. This study describes two members of this protein family in tomato, namely RS2Z35 and RS2Z36, which act as core regulators of AS under HS and consequently as central factors for HSR and thermotolerance. This study investigates the interaction of the two RS2Z proteins with the *HSFA2* pre-mRNA and provides evidence for their function as splicing repressors in this particular AS event. Thereby, RS2Z proteins play an important role in the HSR by modulating the AS of the key factor of the ATT. Furthermore, based on global transcriptome analysis of knockout mutants of single or both *RS2Z* genes, it is demonstrated that RS2Z proteins are involved in the splicing of pre-mRNAs of almost 2000 genes. Moreover, RS2Z proteins act as splicing regulators and take part in more than half of the HS-induced AS events, thus playing a broader role in AS regulation. Furthermore, the HS-induced *RS2Z36* is involved in basal thermotolerance (BTT), highlighting its importance for the basic HS resilience capacity of tomato. In addition, RNA sequencing demonstrates that RS2Z proteins–especially RS2Z36–regulate the expression of proteins involved in plant immunity. The study thereby, for the first time, provides experimental evidence for the important and essential

role of SR proteins in the plant HSR and on top suggests the existence of RS2Z-mediated crossroads of different stress responses.

III Zusammenfassung

Durch ihre sessile Lebensweise sind Pflanzen diversen Umwelteinflüssen ausgesetzt, denen sie nicht durch Ortswechsel entkommen können (Zhang et al., 2020a). Vor allem Perioden extremer Hitze mit langanhaltenden oder stark frequentierten Temperaturspitzen gefährden ihre Reproduktionsfähigkeit oder, im schlimmsten Fall, das Überleben (Rahmstorf and Coumou, 2011). Bei fruchttragenden Pflanzen, z. B. Tomate (*Solanum lycopersicum*), führt dies zu Ernteeinbußen, die hinsichtlich der globalen Erwärmung und einer gleichsam ansteigenden Weltbevölkerung ein weitreichendes Problem darstellen (Lobell und Field, 2007; Lobell et al., 2011; Gerland et al., 2014). Pflanzen schützen sich gegenüber stark schwankenden Umwelteinflüssen durch sogenannte Stressantworten, die in einem gewissen Rahmen das Überleben der Pflanze durch molekulare Anpassungsmechanismen sichern. Ein umfassendes Verständnis der zellulären Hitzestressantwort trägt somit wesentlich zur Entwicklung robuster Arten bei, die durch selektive Zuchtwahl, aber auch durch biotechnologische Verfahren erzeugt werden können (Fragkostefanakis et al., 2015).

Umwelteinflüsse, die die individuellen Toleranzgrenzen einer Pflanze überschreiten, beeinträchtigen die zelluläre Homöostase und verursachen dadurch die Akkumulation zellschädigender Substanzen, darunter die Aggregation ungefalteter oder falsch gefalteter Proteine (Vigh et al., 2007; Saidi et al., 2011). Die Hitzestressantwort (engl. *heat stress response*, HSR) reagiert auf die Akkumulation jener Proteine mit der Synthese sogenannter Hitzeschockproteine (engl. *heat shock proteins*, HSPs), die mitunter an der Proteinrückfaltung beteiligt sind (Grossman et al., 1984). Stressantworten folgen einem strikt regulierten, komplexen System aus Signalperzeption und -transduktion, das schließlich zur Ausprägung adaptiver Mechanismen führt (Pandey et al. 2015). Die Stellschrauben der Stressantwort sind Transkriptionsfaktoren, die nach Perzeption der durch Stress verursachten zellulären Stresssignale aktiviert werden und transkriptionelle Anpassungen initiieren (Scharf et al., 2012). Hitzestress-transkriptionsfaktoren (engl. *heat stress transcription factors*, HSFs) sind die Hauptakteure der HSR, indem sie die Synthese von HSPs und weiterer Proteine mit schützender Funktion aktivieren (Scharf et al., 2012). In der Tomate bilden zwei HSFs die Kernkomponente der HSR. Der konstitutiv exprimierte Faktor HSFA1a ist essenziell für die Ausprägung der inhärenten Fähigkeit zur basalen Thermotoleranz (engl. *basal thermotolerance*, BTT) (Mishra et al., 2002; Bokszczanin et al., 2013). Der durch Hitze induzierte Faktor HSFA2 wird zunächst in zytosolischen Strukturen gespeichert und bei langanhaltender oder wiederkehrender Hitzeeinwirkung freigesetzt (Port et al., 2004). Dies verleiht der Pflanze die Fähigkeit der erworbenen Thermotoleranz (engl. *acquired thermotolerance*, ATT). Dabei ermöglicht die Präakklimatisierung durch vorausgegangenen Stress das Überleben eines sonst tödlichen Stresses (Song et al., 2012), indem durch das Zusammenwirken von HSFA1a und HSFA2 eine stärkere Hitzestressantwort erzielt werden kann (Schramm et al., 2006; Chan-Schaminet et al., 2009).

Die stressinduzierte, massive Umstrukturierung des Transkriptoms wird durch alternatives Spleißen (AS) noch erweitert. Spleißen ist ein essenzieller Bestandteil des mRNA-Metabolismus, in dem nicht-kodierende Bereiche (Introns) aus der prä-mRNA entfernt (gespleißt) werden. Beim alternativen Spleißen führt die selektive Erkennung von Spleißstellen in der prä-mRNA zur Produktion unterschiedlicher mRNA-Transkripte, welche potenziell für Proteinisoformen mit unterschiedlichen

Eigenschaften kodieren und damit die Proteinvielfalt erweitern (Mastrangelo et al., 2012). Oftmals führt alternatives Spleißen jedoch zur Verschiebung des Leserasters eines Gens und ruft dadurch ein vorzeitiges Stopcodon hervor (Filichkin et al., 2010). Viele solcher nicht-produktiven Transkripte werden anschließend durch den *Nonsense-mediated mRNA Decay* (NMD)-Mechanismus abgebaut (Isken and Maquat, 2007). AS spielt eine maßgebliche Rolle unter HS, indem es einerseits das Vorkommen translatierbarer Transkripte reduziert und damit durch Verminderung neu-synthetisierter Proteine die Last auf das HSP-system minimiert, und andererseits das Vorkommen oder die Eigenschaften von bedeutenden regulatorischen Faktoren moduliert. Eines von vielen Beispielen ist die Regulation des Transkriptionsfaktors HSFA2. Hierbei führt temperaturabhängiges alternatives Spleißen zur Ausprägung zweier Proteinisoformen: Während die korrekt gespleißte Isoform HSFA2-II eine hohe Instabilität aufweist und nicht in zytosolischen Strukturen gespeichert werden kann, führt die Inhibierung des Herausspleißens des zweiten Introns unter höheren Temperaturen zur Ausprägung der stabilen Isoform HSFA2-I (Hu et al., 2020a). Die Inhibierung des *HSFA2*-Spleißvorgangs unter höheren Temperaturen stellt damit die Fähigkeit zur ATT sicher (Hu et al., 2020a).

Obwohl alternatives Spleißen eine wichtige Rolle in der pflanzlichen Entwicklung und vor allem bei Stressantworten spielt (Staiger and Brown, 2013; Filichkin et al., 2015), sind die molekularen Details dieses regulatorischen Mechanismus noch nicht vollständig geklärt. Das Spleißen von Introns aus der prä-mRNA wird durch die Aktivität verschiedener Spleißfaktoren bestimmt. Am besten erforscht ist dabei die Familie der Serin/Arginin-reichen Proteine (SR-Proteine). SR-Proteine sind evolutionär konservierte, dynamisch phosphorylierte RNA-Bindeproteine, die die Erkennung der Spleißgrenzen durch das Spleißosom modulieren (Golovkin and Reddy, 1998; Shepard and Hertel, 2009). SR-Proteine weisen sowohl RNA-Erkennungssequenzen (engl. *RNA recognition motif*, RRM), als auch eine Protein-Protein-Interaktionsfläche, die sogenannte RS-Domäne, auf. Sie werden anhand ihrer Domänenarchitektur in sechs Untergruppen eingeordnet, wobei pflanzliche SR-Proteine zusätzliche Eigenschaften aufweisen, die sie von den SR-Proteinen der Säugetiere abheben (Barta et al., 2010). Durch den erhöhten Anspruch der sessilen Pflanzen an ihre Anpassungsfähigkeit, lässt die höhere Anzahl und Diversität pflanzlicher SR-Proteine spezialisierte Funktionen dieser Proteine vermuten. Die pflanzenspezifische Untergruppe der RS2Z-Proteine besitzt z. B. zusätzlich zur RRM zwei RNA-bindende Zinkfinger-Motive des z*inc knuckle*-Typs (Barta et al., 2010).

Alternatives Spleißen wird auf vielen Ebenen reguliert, wobei vor allem die stressabhängige Regulation der Aktivität von Spleißfaktoren das Spleißprofil wichtiger Transkripte beeinflusst und damit zur Ausprägung des adaptiven Transkriptoms beitragen kann. Die Häufigkeit alternativen Spleißens in Pflanzen wurde lange unterschätzt, was zur Folge hatte, dass die Relevanz dieses Vorgangs und die Rolle von Spleißfaktoren ebenso lange unerforscht blieben. Obgleich bereits für manche Spleißfaktoren gezeigt werden konnte, dass sie temperaturabhängige Spleißvorgänge regulieren (Kim et al. 2018; Li et al., 2021) und obwohl AS ein wichtiger Bestandteil der Hitzestressantwort ist (Verhage et al., 2017), wurde die Rolle von SR-Proteinen in der Hitzestressantwort bislang nicht adressiert.

Die Ihnen vorliegende Studie befasst sich mit der Charakterisierung der pflanzenspezifischen RS2Z-Untergruppe der SR-Proteine mit dem Ziel, ihre Rolle in der Hitzestressantwort und folglich ihren

Einfluss auf die pflanzliche Thermotoleranz zu beschreiben. Hierbei dient die Tomatenpflanze als Modellorganismus für die Hitzestressantwort in fruchttragenden Pflanzen.

Das temperaturabhängige alternative Spleißen des Faktors HSFA2 dient dabei als Ansatzpunkt, da die Konsequenz dieses wichtigen Vorgangs zwar gut beschrieben (Hu et al., 2020a), dessen ursächliche Regulation aber gänzlich unbekannt ist. SR-proteine kommen durch ihre bedeutende Rolle in der Modulation alternativen Spleißens dabei als potenzielle Regulatoren in Frage. Die Regulation des *HSFA2*-Spleißens durch die 17 in der Tomate identifizierten SR-proteine (Rosenkranz et al., 2021) wird mithilfe eines Reporterkonstrukts untersucht, welches aus dem zweiten Intron des *HSFA2*-Gens und den flankierenden Exonbereichen besteht. Zur Analyse des *HSFA2*-Spleißprofils in Tomaten-Mesophyllprotoplasten wird neben dem Reporterkonstrukt zusätzlich jeweils eines der 17 SR-Proteine überexprimiert. Während mehrere SR-Proteine das Spleißen des *HSFA2*-Introns inhibieren, sind lediglich zwei dieser Proteine selbst hitzereguliert: SC30b und RS2Z36. RS2Z36 ist dabei ein durch Hitze induzierbarer Faktor der pflanzenspezifischen RS2Z-Proteine und fungiert als Repressor des *HSFA2*-Spleißereignisses. Ferner kann gezeigt werden, dass das zweite Mitglied der RS2Z-Untergruppe, RS2Z35, ebenfalls dazu befähigt ist, das Herausspleißen des zweiten Introns aus *HSFA2* zu inhibieren.

Natürlich vorkommende Polymorphismen innerhalb des *HSFA2*-Introns in Kultur- und Wildsorten korrelieren mit der Ausprägung der Thermotoleranz (Hu et al., 2020a). Folglich wird die Regulation des *HSFA2*-Spleißereignisses durch SR-Proteine in Abhängigkeit jener Polymorphismen untersucht. Während die meisten SR-Proteine das *HSFA2*-Spleißprofil ungeachtet der Intron-lokalisierten Polymorphismen regulieren, zeigen RS2Z-Proteine ein in Abhängigkeit des Haplotyps verändertes Verhältnis der HSFA2-Proteinisoformen. Folglich konzentriert sich die Studie auf die nähere Charakterisierung dieser beiden RS2Z-Proteine, zunächst hinsichtlich der Regulation des AS-Ereignisses in *HSFA2*, und in Bezug auf ihre Beteiligung an der Ausprägung der Thermotoleranz.

Da das Ausschalten eines Faktors Rückschlüsse auf dessen Funktion erlaubt, werden mithilfe CRISPR/Cas9-vermittelter Genommutation homozygote Knockout-Mutanten für *rs2z35* und *rs2z36* generiert. Dabei zeigt nur der simultane Knockout beider Faktoren in Form einer *rs2z35 rs2z36* Doppelmutante eine signifikante Änderung des *HSFA2*-Spleißprofils. RS2Z35 und RS2Z36 agieren demnach in redundanter Weise hinsichtlich dieses Spleißereignisses. In Folge des veränderten Spleißprofils zugunsten der instabilen Isoform HSFA2-II in der *rs2z*-Doppelmutante wird die Expression der durch HSFA2 regulierten Transkripte negativ beeinflusst. Der Einfluss des *rs2z*-Knockouts auf die Fähigkeit zur ATT wird mittels eines Hypokotyl-Elongations-Experiments ermittelt. Hierbei werden junge Keimlinge zunächst einem milden Hitzestress (40°C) ausgesetzt. In der darauffolgenden Erholungsperiode synthetisieren die Keimlinge die zur Akklimatisierung nötigen Proteine, darunter HSFA2. Dies ermöglicht das Überstehen eines zweiten Stresses (47.5°C), der ohne vorherige Exposition letal wäre. Die Elongationsrate des Hypokotyls nach der Stress-Exposition wird anschließend als Indikator für Thermotoleranz herangezogen, wobei nicht-tolerante Keimlinge in ihrem Wachstum beeinträchtigt sind. Schließlich weist die *rs2z*-Doppelmutante dabei tatsächlich einen Phänotyp mit verminderter ATT auf. Demnach spielen RS2Z-Proteine durch die Modulierung von HSFA2, dem Hauptfaktor der ATT, eine wichtige Rolle für die Thermotoleranz. Hierbei üben beide RS2Z-Proteine

dieselbe Rolle hinsichtlich des *HSFA2*-AS-Events aus und sind zur gegenseitigen Kompensation befähigt.

Ferner wird durch RNA Immunpräzipitation (RIP) und anschließender Transkriptquantifikation mittels qRT-PCR untersucht, ob RS2Z-Proteine *in-vivo* mit der *HSFA2* prä-mRNA assoziiert sind. Hierfür werden transgene Pflanzenlinien erzeugt, welche GFP-RS2Z-Fusionsproteine überexprimieren. Mit gegen GFP gerichteten Nanobodies werden die GFP-RS2Z-Proteine, sowie die durch vorausgehende Formaldehyd-Behandlung mit den Proteinen vernetzte RNAs, aus dem Zelllysat HS-exponierter Blätter aufgereinigt. Tatsächlich sind sowohl RS2Z35 als auch RS2Z36 mit der für HSFA2 kodierenden RNA assoziiert. Die Interaktion der RS2Z-Proteine mit dem *HSFA2*-Intron wird zudem mittels *RNA Electrophoretic Mobility Shift Assay* (REMSA) untersucht. Hierfür wird die Bindeaffinität aufgereinigter RS2Z-Proteine zu verschiedenen *in-vitro* synthetisierten Regionen des Introns ermittelt. Dieses Experiment zeigt, dass RS2Z-Proteine mehrfache Bindestellen besitzen, aber eine Präferenz für die 3'-Region des Introns aufweisen. Zusätzlich wird die Rolle der einzelnen Proteindomänen der RS2Z-Proteine für ihre Funktion als *HSFA2*-Spleißrepressoren ermittelt. Dies wird mithilfe von transienter Expression von mutierten RS2Z-Konstrukten in Protoplasten und anschließender Analyse des *HSFA2*-Spleißprofils durchgeführt. Dabei stellt sich heraus, dass für die Inhibition des *HSFA2*-Spleißens nicht etwa die RRM der RS2Z-Proteine, sondern die Zinkfinger-Motive die essenziellen Komponenten darstellen.

Mikroskopie-Analysen und Auftrennung von RS2Z-Proteinen in Anwesenheit Phosphatgruppen-bindender Agenzien (Phos-tag PAGE) stellen dar, dass weder RS2Z35 noch RS2Z36 durch Hitze in ihrer Lokalisation oder Phosphorylierung reguliert werden. Dies lässt darauf schließen, dass es die transkriptionelle Induktion von RS2Z36 ist, welche die Inhibition des *HSFA2*-Spleißens unter erhöhten Temperaturen sicherstellt. Dabei wirkt RS2Z36 einem Mitglied einer anderen Gruppe von Spleißfaktoren, den *heterogeneous ribonucleoprotein particles* (hnRNPs), entgegen.

Obwohl beide Mitglieder der RS2Z-Familie dieselbe Funktion zu haben scheinen, lässt die Induzierbarkeit von *RS2Z36* auf einen spezifischen Bedarf unter Hitzebedingungen schließen. Darüber hinaus zeigen Analysen der Transkriptvorkommen sowie der Spleißprofile von *RS2Z35* und *RS2Z36*, dass RS2Z35 einen negativen Effekt auf *RS2Z36* ausübt. Ferner regulieren die RS2Z-Proteine ihr eigenes Transkriptvorkommen sowie das des jeweils anderen RS2Z-Mitglieds, sobald ein beliebiges RS2Z-Protein überexprimiert wird. Dies impliziert, dass RS2Z-Proteine – und RS2Z36 im Speziellen – einer strikten Kontrolle unterliegen. Dies wird ebenfalls durch einen negativen Einfluss einer RS2Z-Protein-Überexpression auf die Reproduktion der Tomatenpflanze deutlich. Hierbei führt die Überexpression eines beliebigen RS2Z-Proteins zur Verminderung des Fruchtgewichts und der Samenausbeute.

Erstaunlicherweise ist nicht nur die *rs2z*-Doppelmutante in ihrer Fähigkeit zur ATT beeinträchtigt, sondern auch die beiden *rs2z*-Einzelmutanten, obwohl das *HSFA2*-Spleißen in diesen nicht verändert ist. Eine globale Analyse von AS-Ereignissen mittels RNA-Sequenzierung (RNA-Seq) im Wildtyp (WT) und in den *rs2z*-Mutanten unter Kontroll- und HS-bedingungen zeigt auf, dass mehr als die Hälfte der durch Hitze bedingten AS-Ereignisse ebenfalls durch RS2Z-Proteine reguliert werden. Dabei agieren

RS2Z35 und RS2Z36 als neutrale Spleißfaktoren und regulieren AS-Ereignisse eines breiten Transkriptspektrums. Dies impliziert eine globalere und umso bedeutendere Rolle der RS2Z-Proteine in der HSR jenseits der Regulation von *HSFA2*. Eine Analyse der mit RS2Z-Proteinen assoziierten RNAs mittels einer auf RIP folgenden RNA-Sequenzierung (RIP-Seq) zeigt zudem, dass mit RS2Z-Proteinen assoziierte RNAs, deren Spleißprofil durch *rs2z*-Mutation beeinflusst ist, hauptsächlich durch alternative Erkennung der 3‘ Spleißstelle (A3’SS) reguliert werden. Die Assoziation der RS2Z-Proteine mit Transkripten, deren alternatives Spleißen nicht durch die *rs2z*-Mutation beeinträchtigt wird, weist darüber hinaus auf mögliche zusätzliche Funktionen von RS2Z-Proteinen in weiteren Aspekten des RNA-Metabolismus hin.

Ferner, und überraschenderweise, weist die *rs2z36*-Einzelmutante nicht nur eine verminderte ATT, sondern ebenfalls eine verminderte BTT auf. Zur Evaluation der BTT werden Keimlinge im Hypokotyl-Elongation-Experiment einem HS von 40°C über einen Zeitraum von 2-4 h ausgesetzt. Eine globale Analyse differenziell exprimierter Gene nach 1 h HS-Exposition (40°C) in Blättern des WT und der *rs2z*-Mutanten mittels RNA-Seq zeigt dabei, dass RS2Z-Proteine, und im Speziellen RS2Z36, die Expression von Genen der pflanzlichen Immunantwort regulieren. Dies repräsentiert eine RS2Z36-spezifische Rolle in der BTT, die sich auf Wegkreuzungen verschiedener Stressantworten abzuspielen scheint.

Zusammenfassend spielen RS2Z-Proteine eine wichtige Rolle für die Thermotoleranz der Tomate. Dabei regulieren sie das alternative Spleißen des Hauptregulators der ATT, *HSFA2*, auf redundante Art und Weise und sind über der Hälfte der HS-induzierten AS-Ereignisse beteiligt. RS2Z-Proteine – und RS2Z36 im Speziellen – sind darüber hinaus an der Regulation von Genen beteiligt sind, welche für Proteine der pflanzlichen Immunabwehr kodieren. Die Studie liefert damit erstmalig experimentelle Belege für eine bedeutende Rolle pflanzlicher SR-Proteine in der HSR und eröffnet darüber hinaus die Möglichkeit für RS2Z-regulierte Wegkreuzungen verschiedener Stressantworten.

IV Table of figures

Main figures

Supplemental figures

V Table of tables

VI Abbreviations

Abbreviation	Meaning
A3'SS	alternative 3' acceptor splice site
A5'SS	alternative 5' donor splice site
aa	amino acid
AHA	activator motif
amp	ampicillin
APX	ascorbate peroxidase
AS	alternative splicing
ATT	acquired thermotolerance
BTT	basal thermotolerance
BV	bed volume
CaMV	cauliflower mosaic virus
cDNA	complementary DNA
CDS	coding sequence
CHX	cycloheximide
CK	cytokinin
CLSM	confocal laser scanning microscope
CRF	cytokinin response factor
cv	cultivar
DAS	differential alternative splicing
DBD	DNA binding domain
ddH_2O	distilled deionized water
DE	differential expression
DEPC	diethyl pyrocarbonate
DNA	deoxyribonucleic acid
dNTP	deoxynucleotide
DREB	dehydration-responsive element binding protein
EDTA	ethylenediaminetetraactic acid
EMSA	electromobility shift assay
ERF	ethylene response transcription factor
ES	exon skipping
ESR	exonic regulatory sequences
ET	ethylene
EtBr	ethidium bromide
FDR	false discovery rate
GFP	green fluorescent protein
GO	gene ontology
HA	hemagglutinin
hnRNP	heterogeneous nuclear ribonucleoprotein
HRP	horseradish peroxidase
HS	heat stress
HS (context: buffers)	high salt
HSE	heat shock element
HSF	heat stress transcription factor
HSG	heat stress granule
HSP	heat shock protein
IEX	ion exchange chromatography
IGC	interchromatin granule clusters
IMAC	immobilized metal affinity chromatography
IP	immunoprecipitation
IPTG	isopropyl ß-D-1-thiogalactopyranoside

Abbreviation	Meaning
IR	intron retention
ISR	intronic regulatory sequences
IVT	*in vitro* transcription
JA	jasmonic acid
JAZ	jasmonate zim-domain
kan	kanamycin
K_D	dissociation constant
LFC	log2foldchange
lncRNA	long non-coding RNA
LSV	local splice variants
MACE	massive analysis of cDNA ends
mc	monoclonal
mRNA	messenger RNA
MS	Murashige and Skoog
MW	molecular weight
NES	nuclear export signal
NF-Y	nuclear factor Y
Ni-NTA	nickel nitrilotriacetic acid
NLS	nuclear localisation signal
NMD	nonsense mediated RNA decay
nt	nucleotide
OD (context: HSF)	oligomerization domain
OD (context: spectrophotometry)	optical density
OX	overexpression
padj	false discovery rate-adjusted p-value
PAGE	polyacrylamide gel electrophoresis
PBS	phosphate-buffered saline
pc	polyclonal
PCA	principal component analysis
PCR	polymerase chain reaction
PEG	polyethylene glycol
pI	isoelectric point
PPT	polypyrimidine tract
Pre-mRNA	precursor messenger RNA
PSI	percent selected index
PTB	polypyrimidine-tract binding protein
PTC	premature termination codon
qRT-PCR	quantitative real-time polymerase chain reaction
RBD	RNA binding domain
RIP	RNA immunoprecipitation
RIP-Seq	RNA immunoprecipitation followed by rna-seq
RIPxDAS	differential alternative spliced genes that were enriched in RIP-seq
RIPxDE	differential expressed genes that were enriched in RIP-seq
RNA	ribonucleic acid
RNA POL II	RNA polymerase ii
RNAi	RNA interference
RNA-Seq	RNA sequencing
ROS	reactive oxygen species

Abbreviation	Meaning
RRM	RNA recognition motif
RS domain	region rich in serine- and arginine residues
RS2Z-regulated	genes regulated by RS2Z proteins indicated by regulation in any *rs2z* mutant in a direct or indirect fashion
RT	Room temperature
RT-PCR	reverse transcription polymerase chain reaction
RUST	regulated unproductive splicing and translation
SA	salicylic acid
SDS-PAGE	sodium dodecyl sulfate polyacrylamide gel electrophoresis
SEA	singular enrichment analysis
SGN	Sol Genomics Network
sgRNA	Single guide RNA
sHSP	small HSP
SNP	single nucleotide polymorphisms
snRNP	small nuclear ribonucleoprotein particle
spec	spectinomycin
SR protein	serine/arginine-rich protein
SS	splice site
T7RNAP	T7 rna-polymerase
TCA	trichloroacetic acid
T-DNA	transfer dna
TEMED	tetramethylenediamin
TF	transcription factor
Tris	tris(hydroxymethyl)aminomethane
tRNA	transfer RNA
U2AF	U2 auxiliary factor
UTR	untranslated region
vol	volume
WT	wild type
ZnK	zinc knuckle

Units	
Abbreviation	**Meaning**
°C	degree Celsius
g (context: centrifugation)	relative centrifugal force
h	hour
kb, bp	kilo- , base pairs
kDa, Da	kilo-, dalton
mA	milliampere
min	minute
ng, µg, mg, g	nano-, micro-, milli-, gram
nm, cm, m	nano-, centi-, meter
pM, nM, µM, mM, M	pico-, nano-, micro-, milli-, molar
psi	Pound-force per square inch
rpm	rounds per minute
sec	second
U (context: enzyme activity)	unit
µl, ml, L	micro-, milli-, liter
V	volt
v/v	volume per volume
w/v	weight per volume

1. Introduction

1.1 The impact of heat

Plants are vulnerable towards fluctuations in their environment and must cope with undesirable conditions threatening growth and reproduction, which they cannot escape due to their sessile nature (Zhang et al., 2020a). Extreme environmental conditions, such as high temperature, high salinity, or drought (abiotic stress) along with attacks by pathogens such as bacteria, fungi, or nematodes (biotic stress) endanger plant fitness by disturbing the cellular homeostasis. This consequently negatively impacts essential mechanisms such as photosynthesis, ultimately resulting in loss of biomass or, in the worst case, even death of the entire plant (Vara Prasad et al., 2002; Pushpalatha et al., 2008). The maintenance of high crop yield however is crucial to supply a constantly increasing global population that is estimated to reach up to 12 billion by the end of the century (Gerland et al., 2014).

Plant survival is especially threatened by heat stress (HS), occurring either as elevated absolute surface temperature or as heat waves with increasing frequency, severity, and duration with temperatures 5°C higher than the climatic normal (Rahmstorf and Coumou, 2011). The onset of global warming, which is estimated to reach 1.5°C above pre-industrial levels in the near future, thereby threatens biodiversity and food security (Lobell and Field, 2007, Lobell et al., 2011; IPCC 2022). Plants are vulnerable even to small temperature fluctuations and can perceive changes as little as 1°C (Kumar and Wigge, 2010). While all plant organs are sensitive to temperatures above their species-specific range optimal for growth and reproduction, reproductive organs are particularly sensitive (Zinn et al., 2010; Hatfield et al., 2011), hence why yield loss reported for many crop species has been attributed to the current rise in global temperature and is expected to increase in severity in the future (Vara Prasad et al., 2002; Lobell and Field, 2007; Battisti and Naylor, 2009; Lobell et al., 2011). To sustain food security in the era of global warming, which is estimated to rise to 2.2-3.5% by 2100 (IPCC 2022), it is of particular interest to understand the mechanisms involved in establishing heat tolerance. Understanding the principles of heat acclimation could ultimately be utilized to develop heat-tolerant crops, employing both traditional breeding and genetic engineering (Singh et al., 2013; Fragkostefanakis et al., 2015). However, many aspects of the complex and intertwined processes conferring heat tolerance are yet to be uncovered and subject of thorough research for many decades and ongoing (Gray and Brady, 2016).

1.2 Thermotolerance

The inherent ability of an organism to survive elevated temperatures above the growth optimum is collectively referred to as basal thermotolerance (BTT) (Bokszczanin et al., 2013). As sessile organisms, plants are often exposed to reoccurring high temperature events or to gradually increasing temperatures. This pre-exposure to a nonlethal stress, so-called priming, thereby poses as a pre-conditioning that allows the plant to survive reoccurring and otherwise lethal stress, which is referred to as acquired thermotolerance (ATT) (Hong and Vierling, 2000; Song et al., 2012; Bokszczanin et al., 2013). While ATT lasts for up to two days, the long-term maintenance of ATT over extended periods (up to 14 days), driven by chromatin modification, is referred to as HS memory (Lämke et al., 2016;

Balazadeh, 2022). All types of thermotolerance, however, rely on the initial response to HS (Liu and Charng, 2012).

1.3 Stress response

To cope with damaging changes in their environment and build up stress tolerance, plants evolved sophisticated mechanisms (stress responses) to maintain and rebuild cellular homeostasis, thereby ensuring their survival. The plant stress response is a complex network of multifaceted, interdependent and interconnected systems, responding to the exposure to a single but often times many concurrent stresses, for example drought and heat (Rizhsky et al., 2002; Pandey et al., 2015).

Stress response pathways mediate survival through the transduction of stress signals into transcriptome- and proteome reshaping to produce an adaptive cellular output (Pandey et al., 2015). The damaging effects of a suboptimal environment caused by abiotic or biotic stresses produce a multitude of intracellular stress signals caused by the disturbance of cellular homeostasis (Saidi et al., 2011; Pandey et al., 2015). These stress signals initiate the respective stress response to rapidly adapt to the unfavourable condition, whereby stress pathways generally are interconnected and thus interdependent on many levels (Scharf et al., 2012; Pandey et al., 2015). The major stressors are, among others, an accumulation of intracellular Ca^{2+}, reactive oxygen species (ROS), and unfolded proteins (Fig. 1, left side). HS impacts membrane integrity (Vigh et al., 2007), thereby disturbing pH and ion homeostasis, provoking accumulation of intracellular Ca^{2+}, as well as the disruption of photosynthesis and respiration (Wahid et al., 2007; Mittler et al., 2012). Consequently, ROS accumulate, either acting as a signal molecule, such as H_2O_2, or causing further damages to other biomolecules, including nucleic acids and proteins (Nosaka, 2017). Many stresses, but especially the high temperatures, negatively impact protein homeostasis by misregulation of protein synthesis and - folding, which causes an accumulation of toxic protein aggregates. Collectively, these stress signals are perceived through numerous and diverse signal transduction networks that often include plant hormones (phytohormones), ultimately initiating the appropriate stress response pathways, including the expression of stress-responsive genes (Fig. 1, left side). These genes encode for proteins that aid in the maintenance of cellular homeostasis or in the transduction of stress signals, e. g. ROS scavengers such as ascorbate peroxidase (APX), calcium-dependent protein kinase (CDPK) cascades, molecular chaperones, or transcription factors (TFs) (Baniwal et al., 2004). TFs thereby act as key players of response pathways by facilitating the expression of stress genes and amplifying stress responses through transcriptional cascades (Mishra et al., 2002; Liu et al., 2011; Ohama et al., 2016).

Stress responses, however, are a trade-off between growth and survival (Zhang et al., 2020a), and thus can only serve as a temporary adjustment to the particular stress and follow strictly orchestrated and complex regulatory pathways. Additional layers of regulation, such as alternative splicing (AS), emerged as newly discovered and important acclimation strategies whose relevance and regulation are largely unknown to date (reviewed in Staiger and Brown, 2013 and recently in Rosenkranz et al., 2022).

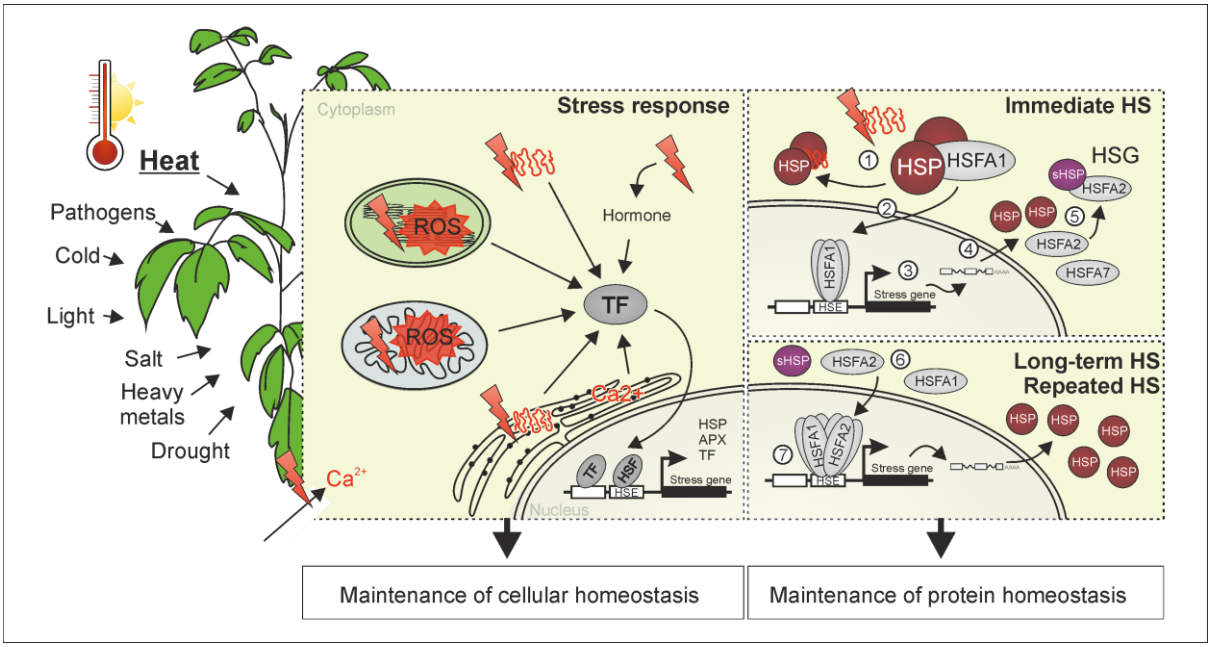

Figure 1. Plant stress response. Left: Stress signals trigger stress responses. Abiotic or biotic stresses provoke intracellular stress signals and consequent intracellular signal transduction cascades. These initiate the differential expression of stress-responsive genes through the modulation of transcription factor (TF) activity. HSP: heat shock protein. APX: ascorbate peroxidase. HSF: heat stress transcription factor. HSE: heat stress element. **Right: Tomato heat stress response**. (1) HSFA1, the master regulator of the heat stress response (HSR), is kept inactive under control conditions by interaction with HSP90 and HSP70. (2) Upon accumulation of unfolded proteins, HSFA1 is activated by dissociation from HSPs. (3) In a trimeric state, HSFA1 binds to HSEs in the promoters of HS-genes. (4) HSFA1 promotes stress tolerance through the activation of HSPs but also other HSFs, for example HSFA2 and HSFA7. (5) HSFA2 is bound by small HSPs (sHSP) and kept inactive in cytosolic foci (heat stress granules, HSGs). (6) Upon prolonged or repeated HS, HSFA2 is released from HSGs. HSFA1 and HSFA2 interact in the cytosol which facilitates the localisation into the nucleus. (7) HSFA1 and HSFA2 activate the transcription of HS-genes as synergistic hetero-oligomeric super activator complex and promote a stronger HSR.

1.3.1 Transcriptional regulation of the plant heat stress response

The response to HS, usually occurring at temperatures 10-15°C above ambient (Wahid et al., 2007), involves multiple signalling pathways and adaptive mechanisms that are collectively referred to as heat stress response (HSR) (Baniwal et al., 2004; Larkindale et al., 2005). The transcriptional induction of heat shock proteins (HSPs) is the most characteristic and evolutionary conserved aspect of the HSR (Grossman et al., 1984). HSPs are the major regulators of protein homeostasis, which includes their function as molecular chaperones by binding to unfolded proteins to keep them in a folding-competent state and aid in their refolding, thereby rebuilding and maintaining protein homeostasis (Vierling, 1991; Parsell and Lindquist, 1993). Since proteins are involved in every biological process, the maintenance of protein homeostasis is one of the most crucial aspects of plant survival under stress conditions.

The induction of HSP expression, as well as other genes involved in thermotolerance (e. g. proteins involved in protein processing, metabolism, and transport), is mediated by a transcriptional cascade of heat stress transcription factors (HSFs) (Busch et al., 2004; Scharf et al., 2012). Plant genomes encode for a high number of HSFs, e. g. 21 in *Arabidopsis thaliana* (further referred to as Arabidopsis) and 27 in *Solanum lycopersicum* (further referred to as tomato) (Nover et al., 2001; Scharf et al., 2012). HSFs have a modular domain structure: an N-terminal DNA binding domain (DBD) recognizes specific

cis-regulatory elements in promoters of heat-inducible genes, called heat shock elements (HSE) (Pelham and Bienz, 1982; Schultheiss et al. 1996) and an oligomerisation domain (OD or HR-A/B domain) is required for protein-protein interaction (Peteranderl et al., 1999, Scharf et al, 2012). Plant HSFs differ mainly in their C-termini and are classified into three classes (A, B, C) based on characteristics of their oligomerisation domains (Nover et al., 1996; Nover et al., 2001; Scharf et al, 2012). Along with a nuclear localisation signal (NLS) which positions them in the nucleus, class A HSFs possess an additional nuclear export signal (NES) in their C-terminus that enables nuclear-cytosolic shuttling (Kotak et al., 2004).

Class A HSFs act as transcriptional activators, characterised by the presence of a C-terminal activator motif (AHA motif), a region rich in aromatic and large hydrophobic amino acids (aa) embedded in an acidic context (Döring et al., 2000). Members of the HSFA1 subfamily are the master regulators of HSR (Mishra et al., 2002; Liu et al., 2011). In Arabidopsis, four HSFA1 members share the master regulator function redundantly and their activity attributes for the upregulation of more than 65% of HS-induced genes, but they also display additional roles in growth and development (Liu et al., 2011). In tomato, out of four HSFA1 proteins, HSFA1a was identified as single master regulator of the HSR (Mishra et al., 2002, El-shershaby et al., 2019). The basic core principle of the HSFA1-mediated induction of the HSR is depicted in Figure 1 (right side). Under non-stress conditions, HSFA1a is kept inactive by interaction with HSP70 and HSP90, as well as by proteasomal degradation (Hahn et al., 2011; Mesihovic et al., 2022). Upon accumulation of unfolded proteins, HSFA1 is derepressed by dissociation from HSPs and binds to HSEs in the promoters of HS-genes in a trimeric state (Schultheiss et al., 1996; Hahn et al., 2011). Thereby, HSFA1 promotes stress tolerance through the activation of HSPs but also other HSFs, for example HSFA2 and HSFA7 (Mishra et al., 2002; Mesihovic et al., 2022).

Additionally, HSFs are involved in various other stress response pathways besides heat, for example high light and drought, highlighting extensive crosstalk between stress responses (Nishizawa et al., 2006; Andrási et al., 2021). For example, HSFA1 induces the transcription of other TFs such as DEHYDRATION-RESPONSIVE ELEMENT-BINDING (DREB) PROTEIN 2A (DREB2A), a key regulator of drought response (Yoshida et al., 2011). Furthermore, crosstalk between temperature stress and pathogen defence has been observed as well (Pandey et al., 2015; Zhou et al., 2018), further indicating an interplay even between biotic and abiotic stresses.

1.3.2 The role of HSFA2

Other HSFs, for example HSFA2 and HSFA7, are downstream targets of HSFA1 (Fig. 1, right side) and act as its coactivators, thereby amplifying and fine-tuning the HSR (Mishra et al., 2002; Rao et al., 2021; Mesihovic et al., 2022). In tomato, *HSFA7* is expressed at mildly elevated temperatures of 35°C, while *HSFA2* is the strongest HS-induced HSF with an expression peak at 40°C in both tomato (Mesihovic et al., 2022) and Arabidopsis (Schramm et al., 2006).

Tomato HSFA2, however, is not essential for the initial stress response (BTT) (Mishra et al. 2002; Fragkostefanakis et al., 2016). Instead, HSFA2 is the key regulator of ATT by establishing and maintaining tolerance against otherwise lethal temperatures upon pre-treatment or prolonged HS by

promoting stress gene expression in a cooperative fashion with HSFA1a (Charng et al., 2007; Li et al., 2010; Fragkostefanakis et al., 2016). While HSFA2 is synthesized upon HS, the interaction with HSP17.4-CII enforces its accumulation in cytosolic foci, so-called heat stress granules (HSGs), providing storage and protection against degradation (Scharf et al., 1998; Port et al., 2004) (Fig. 1, right side). Upon a re-occurring HS incident (or prolonged HS), the pre-synthesized HSFA2 is released from HSGs and interacts with HSFA1a (Scharf et al., 1998). HSFA1a and HSFA2 form a so-called super activator complex that is subsequently translocated to the nucleus (Chan-Schaminet et al., 2009) and enables a very strong expression of HS genes, including APX and several members of the HSP and small HSP (sHSP) family (Panchuk et al., 2002; Charng et al., 2006; Schramm et al., 2006) (Fig. 1, right side).

In the past decade, it became more and more evident that stress responses are further shaped through AS, highlighted by the regulation of many key factors by stress-induced splicing alterations, including *HSFA2* (Hu et al., 2020a) and *HSFA7* (Mesihovic et al., 2022) which are described in more detail in section 1.5.3.

1.4 Pre-mRNA splicing

Splicing is a crucial step of messenger RNA (mRNA) processing, in which non-coding introns are removed from mRNA precursors (pre-mRNA) and the residual exons are ligated (see Wilkinson et al., 2020 for an extensive review). Introns usually interrupt the coding sequence and thus their removal is pivotal for the generation of mature protein-coding mRNAs. The splicing process is a strictly orchestrated procedure carried out by the spliceosome, a large and dynamic RNA-protein complex composed of five major small nuclear ribonucleoprotein particles (snRNPs) consisting of an RNA component (U1, U2, U4, U5, U6) and hundreds of associated proteins (Nilsen, 2003). For proper splicing, assembly of the early spliceosome at the splice sites and extensive structural rearrangement during the splicing process are required (Wilkinson et al., 2020). The discrimination between introns and exons is achieved by the recognition of consensus *cis*-elements at the exon/intron borders, conserved nucleotides at the 5’ donor splice site (5’SS, GU) and the 3’ acceptor splice site (3’SS, AG), as well as by sequences within the intron, a branchpoint adenine required for the splicing reaction in the 3’-region of the intron and a region enriched in polypyriminde nucleotides (polypyrimidine tract, PPT) downstream of the branchpoint (Fig. 2A; Wang and Burge, 2008). The spliceosome assembly is initiated by the recognition of the 5’SS by the U1 snRNP and the interaction of splicing factor 1 (SF1) with the branchpoint, which further facilitates the binding of U2 auxiliary factors (U2AF) with the branchpoint and the PPT, followed by binding of the U2snRNP (Fig. 2A; Wilkinson et al., 2020). Together with the U5/U4/U6 tricomplex, a pre-spliceosome complex is formed that bridges the splice sites. Structural rearrangements including the displacement of U1 and U4 lead to the formation of the enzymatically active spliceosome which removes the intron via two transesterification steps (Wilkinson et al., 2020). The branchpoint and the 5’SS of the intron are ligated first by nucleophilic attack of the 5’SS by the branchpoint, followed by joining of the flanking exons by nucleophilic attack

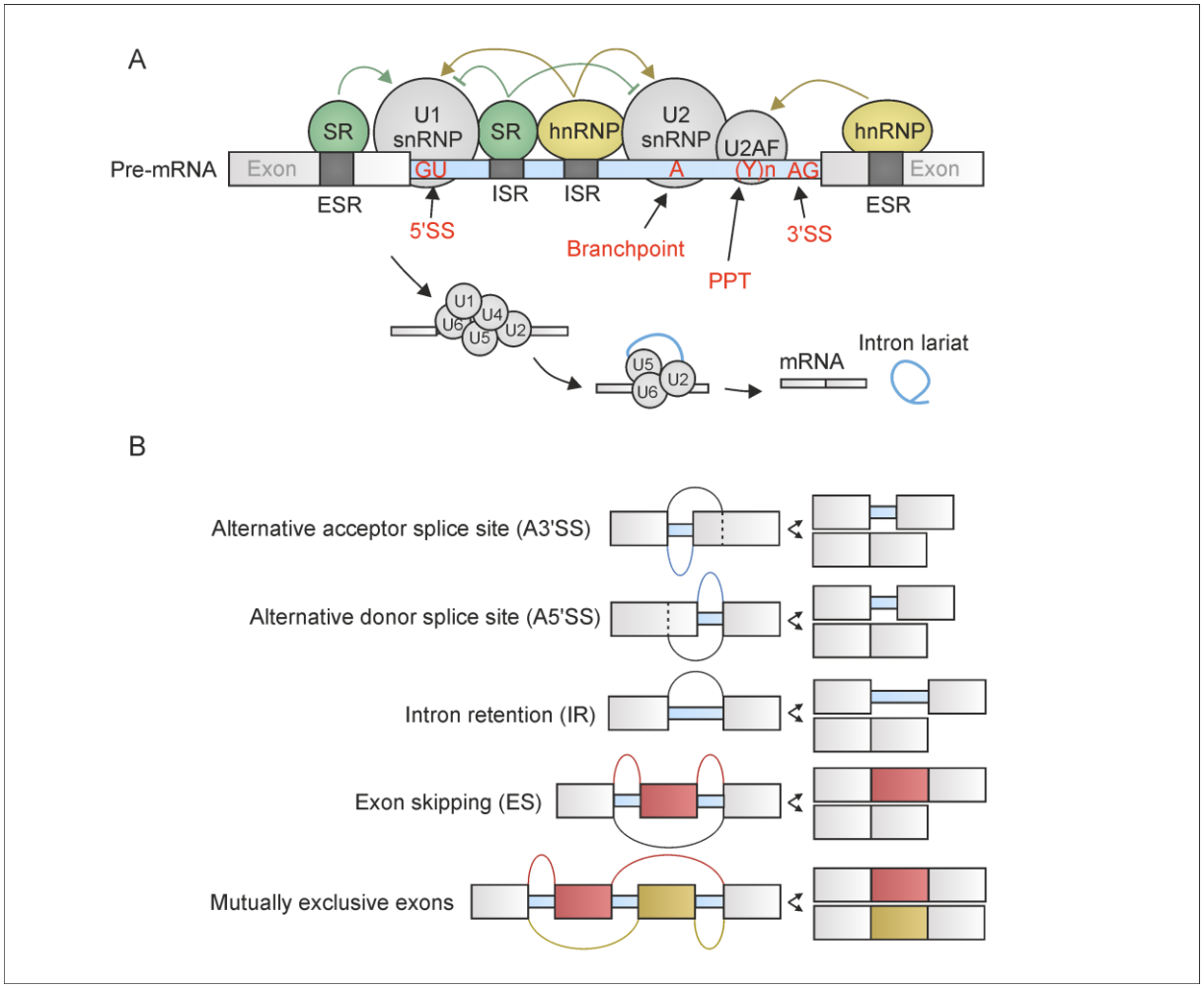

Figure 2. Schematic representation of the splicing process and alternative splicing outcomes. **(A)** Cis-regulatory sequences (exonic splicing regulators (ESR) and intronic splicing regulators (ISR)) define the binding of trans-acting factors (Serine/Arginine-rich (SR) proteins and heterogeneous nuclear ribonucleoproteins (hnRNPs), that in turn influence the selection of consensus sequences (donor (5'SS) and acceptor splice sites (3'SS), adenosine branchpoint (A) and polypyrimidine tract ((Y)n); PPT) by spliceosomal components U1 snRNP and U2 snRNP. The formation of a catalytically active spliceosome by association of U1 and U2 with the U4/U6/U5 tricomplex and subsequent displacement of U1 and U4 facilitates the removal of the intron via two transesterification reactions, thereby releasing the intron as a lariat and joining the flanking exons. **(B)** Selective usage of splice sites produces multiple transcript variants from a single gene, shortens exonic or retains intronic sequences (A3'SS, A5'SS), retains entire introns (IR) or modulates the skipping of exons (ES and mutually exclusive exons).

of the 3'SS by the 5' exon, thereby releasing the intron as a lariat (Fig. 2A; Wilkinson et al., 2020). Non-snRNP proteins, primarily splicing factors of the serine/arginine-rich (SR) and heterogeneous nuclear ribonucleoprotein (hnRNP) families, as well as polypyrimidine-tract binding proteins (PTB) (Lambermon et al., 2000), assist in the spliceosome assembly and splice site recognition, whereby their impact on the spliceosome is achieved in a context-dependent and combinatorial manner and is often found to be antagonistic (Cáceres et al., 1994; Eperon et al., 2000; Fu and Ares, 2014). These non-snRNP proteins act as *trans*-acting factors by binding to *cis*-regulatory sequences in the pre-mRNA through their RNA binding domains (RBDs) on one hand and with spliceosomal proteins or other splicing factors on the other hand (Golovkin and Reddy, 1998; Tanabe et al., 2009; Day et al., 2012).

Cis-regulatory sequences are small degenerate exonic or intronic regulatory sequences (ISR, ESR), further termed exonic/intronic splicing enhancers/silencers (ESE, ESS, ISE, ISS) (Wang and Burge,

2008), depending on the protein bound and the splicing outcome (Fig. 2A; Fu, 2004). *Trans*-acting factors bind to a diverse set of overlapping *cis*-elements and can compete for the same binding site (Wang et al., 2013, Fu and Ares, 2014). Ultimately, the activity and abundance of splicing factors determine the SS usage, for example as splicing enhancers by recruiting U1 and U2 to the pre-mRNA, by stabilizing the snRNP-pre-mRNA interaction or by facilitating the bridging of the 3' and 5' SS (Robberson et al., 1990). Alternatively, splicing factors can act as splicing silencers by masking binding sites or by impacting RNA structure, thereby preventing U1 or U2 association with the pre-mRNA (Hönig et al., 2002; Shin et al., 2004; Warf et al., 2009).

1.5 Alternative splicing

Splicing factors determine the selective usage of (alternative) splice sites (SS), thereby allowing the generation of many different mature mRNAs from a single gene (Staiger and Brown, 2013). This process, AS, commonly follows five archetypes (Fig. 2B) that also co-occur, thus producing more complex AS types. The usage of alternative 3' (A3'SS) or 5' SS (A5'SS) either shortens exonic sequences or retains part of an intron, while the inhibition of SS recognition leads to intron retention (IR). By alternative SS usage, an entire exon can be skipped (exon skipping, ES) or the choice between mutually exclusive exons can be modulated. This way, AS greatly increases the transcriptome diversity by giving rise to multiple transcript variants. AS shapes the transcriptome in a tissue type and developmental stage specific manner (Staiger and Brown, 2013). Moreover, it is a common occurrence in response to environmental fluctuations, such as temperature changes, and provides a mechanism for rapid acclimation (Staiger and Brown, 2013; Chang et al., 2014; Jiang et al., 2017; Keller et al., 2017; Ling et al., 2018; Lee and Adams, 2020). Many AS events, especially IR, cause frameshifts that in turn lead to the formation of premature termination codons (PTC) (Filichkin et al., 2010). The occurrence of a PTC upstream of the last exon-exon junction marks the transcript for degradation via the nonsense mediated decay (NMD) pathway in the cytosol within the pioneer round of translation (Ishigaki et al., 2001; Isken and Maquat, 2007). The regulation of transcript abundance through coupling of AS and mRNA decay is also referred to as regulated unproductive splicing and translation (RUST) (Kalyna et al., 2012; Reddy et al., 2013; Neumann et al., 2020). In contrast, AS potentially leads to the generation of multiple coding transcript variants, coding for protein isoforms with altered and potentially opposing properties, e. g. in protein stability, activity, or localisation, which is suggested to enhance transcriptome plasticity, especially in response to environmental stress (Nilsen and Graveley, 2010; Filichkin et al., 2010; Mastrangelo et al., 2012). Thereby, AS not only controls transcript abundance, but also contributes to proteome diversity.

1.5.1 Splicing in plants

The eukaryotic spliceosome has been extensively studied primarily in yeast and humans with a substantial lack of plant studies. However, the conservation of core spliceosomal elements between plants and metazoans led to the assumption that the core principles of splicing would be conserved across all eukaryotes (Wang and Brendel, 2004; Richardson et al., 2011; Reddy et al., 2013). Nevertheless, the fine-tuning of splicing differs between plant and metazoan systems, indicated by reduced efficiency or entirely absent splicing of metazoan introns in a plant context and vice versa

(Wiebauer et al., 1988), pointing towards differences in intron recognition. Since most metazoan introns are rather long in size relative to the neighbouring exons, the recognition of splice sites is often defined by bridging of the U1 and U2 snRNPs across the relatively short exons (Robberson et al., 1990). In contrast, plant introns are generally short in size (Reddy et al., 2013). Thereby, SS recognition may differ due to the differences in intron structure, whereby plant splicing likely follows intron definition rather than exon definition. This is further supported by the reduced conservation of the polypyriminde tract which is dispensable for the splicing of many plant introns, likely due to their generally high AU-content relative to their neighbouring exons (Wiebauer et al., 1988). Like the expanded families of plant TFs, genes coding for spliceosomal components and regulators are expanded as well, indicating functional diversification, likely attributed to the sessile nature of plants and thus a need for tightly regulated adaptive mechanisms (Wang and Brendel, 2004; Richardson et al., 2011).

In human cells, AS is a prevalent mechanism found in more than 95% of multiexon genes (Pan et al., 2008). AS in plants however was long underestimated, but with increasing application of high throughput RNA sequencing (RNA-Seq), it was now shown to occur in 40-70% of plant multiexon genes as well and plays important roles in plant development and stress responses (Marquez et al., 2012; Ding et al., 2014; Chamala et al., 2015). While underrepresented in humans, intron retention (IR) is the most prevalent AS type in plants (Ner-Gaon et al., 2004; Marquez et al., 2012). Recent transcriptome analyses in tomato, integrating a multitude of RNA-Seq datasets, revealed an AS frequency of 65% with mixed AS types as the most prevalent (more than 50%) (Clark et al., 2019). This indicates that, while the core mechanisms of splicing are shared, plant splicing regulation likely follows more complex and plant-specific routes.

1.5.2 Alternative splicing in response to heat stress

An increasing number of studies emerge that describe AS as a means of rapid acclimation to HS through quantitative and qualitative reshaping of the plant transcriptome (Duque 2011; Chang et al., 2014; Jiang et al., 2017; Keller et al., 2017; Ling et al., 2018; Zhu et al., 2018; Lee and Adams, 2020; Punzo et al., 2020; Liu et al., 2022a). IR thereby is the most prevalent AS type in response to HS in both plants (Ner-Gaon et al., 2004; Marquez et al., 2012; Chang et al., 2014; Jiang et al., 2017; Verhage et al., 2017) and humans (Shalgi et al., 2014), and most IR events lead to the generation of PTC containing transcript variants (Filichkin et al., 2010). IR is thus associated with expression control through RUST but also has the potential to give rise to multiple protein-coding transcripts (Filichkin et al., 2010). Further, stress priming was shown to impact AS frequency in response to HS, in which repression of splicing was less frequent in pre-exposed plants that quickly reset to constitutive splicing after the second exposure to HS is relieved, linking splicing ability to thermotolerance (Yost and Lidquist, 1986; Ling et al., 2018). Whether repression of splicing during HS is an adverse effect caused by the impairment of the spliceosome, or whether it is a controlled mechanism, remains yet to be elucidated. Furthermore, not all PTC-containing transcripts are degraded through the NMD pathway (Kalyna et al., 2012). Instead, many PTC-containing transcripts are retained in the nucleus and thereby resilient against degradation by NMD, thus again reducing the pool of translatable transcripts (Göhring et al., 2014; Shalgi et al.,

2014). The accumulation of unspliced or partially spliced transcripts under HS could therefore represent a reservoir of splicing-competent transcripts that are retained in the nucleus and spliced after HS (Shalgi et al., 2014; Ling et al., 2018; Jia et al., 2020). In addition to the general inhibition of translation under HS (Yánguez et al., 2013), the AS-dependent reduction of translatable transcripts, either by RUST or through nuclear retention, is hypothesized to provide regulatory control in a cost-effective manner by reduction of *de novo* protein synthesis, thereby simultaneously reducing the burden on the chaperone system (Yángüez et al., 2013; Chaudhary et al., 2019; Rosenkranz et al., 2022). A reduced repression of splicing in primed plants could thereby represent a reduced necessity for acclimation through AS. Furthermore, splicing memory requires a proper HSR as opposed to a simple induction of HSPs (Corell et al., 1994) and the HS-induced expression of key splicing regulators has recently been shown to be dependent on HSF1a (Rosenkranz et al., 2021), which suggests feedback loops between the HSR and AS regulation.

Different stress responses trigger AS in individual subsets of genes and through different types of AS events (Punzo e al, 2020). For example, while HS predominantly represses splicing (IR events) (Ner-Gaon et al., 2004), salt stress predominantly induces A3'SS events (Ding et al., 2014). This hints towards an at least partially controlled mechanism, rather than a dysregulation of splicing per se.

1.5.3 Modulation of transcription factors through temperature-dependent alternative splicing

In contrast to the global splicing repression upon HS, many transcripts coding for proteins involved in ROS scavenging and protein folding, continue to be efficiently spliced (Shalgi et al., 2014) and their translation is further facilitated by circumventing nuclear quality control (Zander et al., 2016). Thereby, the protein landscape is shifted in favour of stress response mechanisms by ensuring continued expression of essential HS genes and repressing the translation of non-HS-genes until the stress subsides (Shalgi et al., 2014). However, in plants, a wide range of HS-genes is subject to AS, including several essential regulatory genes (Filichkin et a., 2010; Chang et al., 2014; Jiang et al., 2017; Keller et al., 2017; Ling et al., 2018; Lee and Adams, 2020; Liu et al., 2022a). AS of regulatory genes, such as TFs, thereby allows precise fine-tuning of stress responses by modulating TF abundance or properties.

An example for TF regulation by HS-dependent AS is *DEHYDRATION-RESPONSIVE ELEMENT-BINDING PROTEIN 2 B* (*DREB2B*) in *Oryza sativa* (rice), representing an HS-induced member of the DREB family of TFs involved in enhanced response to drought and HS (Matsukura et al., 2010; Mizoi et al., 2012). HS-dependent AS produces two protein isoforms: The inclusion of exon 2 generates a shorter protein DREB2B1, while skipping of exon 2 generates the longer isoform DREB2B2. DREB2B2 possesses an NLS and a AP2/ERF DNA-binding domain, which are both missing in the non-functional DREB2B1 (Matsukura et al., 2010). HS thereby not only promotes the overall induction of *DREB2B* but facilitates the production of DREB2B2 by ES, ensuring accumulation of the transcriptionally active variant (Matsukura et al., 2010). Moreover, Os-DREB2B2, but not Os-DREB2B1, improved the HSR of transgenic Arabidopsis plants, but negatively impacted plant growth under non-stress conditions, suggesting AS as a mechanism to fine-tune ODREB2B2 accumulation (Matsukura et al., 2010).

Additionally, HS-dependent AS occurs in various plant HSFs, for example *Lilium spp*. (lily) *HSFA3* (Wu et al., 2019), or *HSFA2* in both tomato and Arabidopsis. HSFA2 is the key player of ATT and stress memory (section 1.3.2) and therefore under strict transcriptional and co-transcriptional control. Upon severe HS, AS of At-*HSFA2* intron 1 produces a largely truncated and C-terminally modified protein isoform At-HSFA2-III, capable of binding to the At-*HSFA2* promoter and thus stimulating its own transcription, representing a positive feedback loop mediated by temperature-dependent AS (Liu et al., 2013). In tomato, AS of Sl-*HSFA2* produces six transcript variants (Fig. 3; Hu et al., 2020). In contrast to Arabidopsis, AS in Sl-*HSFA2* intron 1 represents a rare event under severe HS and the generated transcripts are NMD-targets (Liu et a., 2013; Hu et al. 2020a). In tomato, AS of intron 2, however, is mediated in a temperature-dependent manner, giving rise to two distinct protein isoforms, HSFA2-I and HSFA2-II, whereby increasing temperatures correlate with the inclusion of intron 2 and thus preferential accumulation of the HSFA2-I protein (Hu et al., 2020a). HSFA2-I encoding transcripts, resulting from partial, as well as entire, intron 2 retention, possess an NES in the C-terminus (Fig. 3; Hu et al., 2020a), allowing nucleocytoplasmic shuttling, as well as interaction with Hsp17.4-CII, thereby facilitating sequestration of HSFA2-I in HSGs (Scharf et al., 1998). In contrast, the absence of an NES in the fully spliced variant, HSFA2-II, causes the retention of this isoform in the nucleus where the protein is rapidly degraded (Hu et al., 2020a). Thereby, AS ensures the accumulation of HSFA2-I, which is released from HSGs upon repeated HS, conferring ATT (section 1.3.2). Interestingly, *HSFA2* splicing efficiency correlates with genetic diversity between tomato species, whereby three intronic single nucleotide polymorphisms (SNPs) between wild and domesticated species determine the splicing profile of *HSFA2* intron 2. Higher splicing efficiency and therefore reduced accumulation of HSFA2-I in wild tomato species correlate with lowered ATT compared to modern species (Hu et al., 2020a). In this notion, global differences in AS were observed between closely related species (Keller et al, 2017; Kannan et al., 2018), suggesting that AS could modulate species-specific stress responses.

Furthermore, tomato HSFA7, a coactivator in the HSR, is regulated through AS as well, in which temperature-dependent IR favours the more stable protein isoform HSFA7-I upon early onset of HS over the less stable isoforms HSFA7-II/III (Mesihovic et al., 2022). These examples highlight the importance of AS-regulation for proper thermotolerance in plants.

In addition, beyond stress responses, temperature responsive AS is associated with the circadian clock, a mechanism that is regulated by AS across eukaryotes (Filichkin et al., 2015; Yang et al., 2020). In humans, acclimation to body temperature fluctuations during day-night cycles is triggered by AS events that consequently shape gene expression (Preußner et al., 2017). Similarly, temperature-sensitive AS mediates temperature-adaption in *Drosophila melanogaster* (Anduaga et al., 2019). In Arabidopsis, the circadian clock and flowering time are regulated through temperature dependent AS of key TFs (Park et al., 2012; Lee et al., 2017; Steffen et al., 2019; Lee et al., 2020). Due to its large impact on the circadian rhythm and flowering control in a temperature-dependent manner, AS was suggested as ‘molecular thermometer’, allowing rapid adjustment to temperature changes (Capovilla et al., 2015).

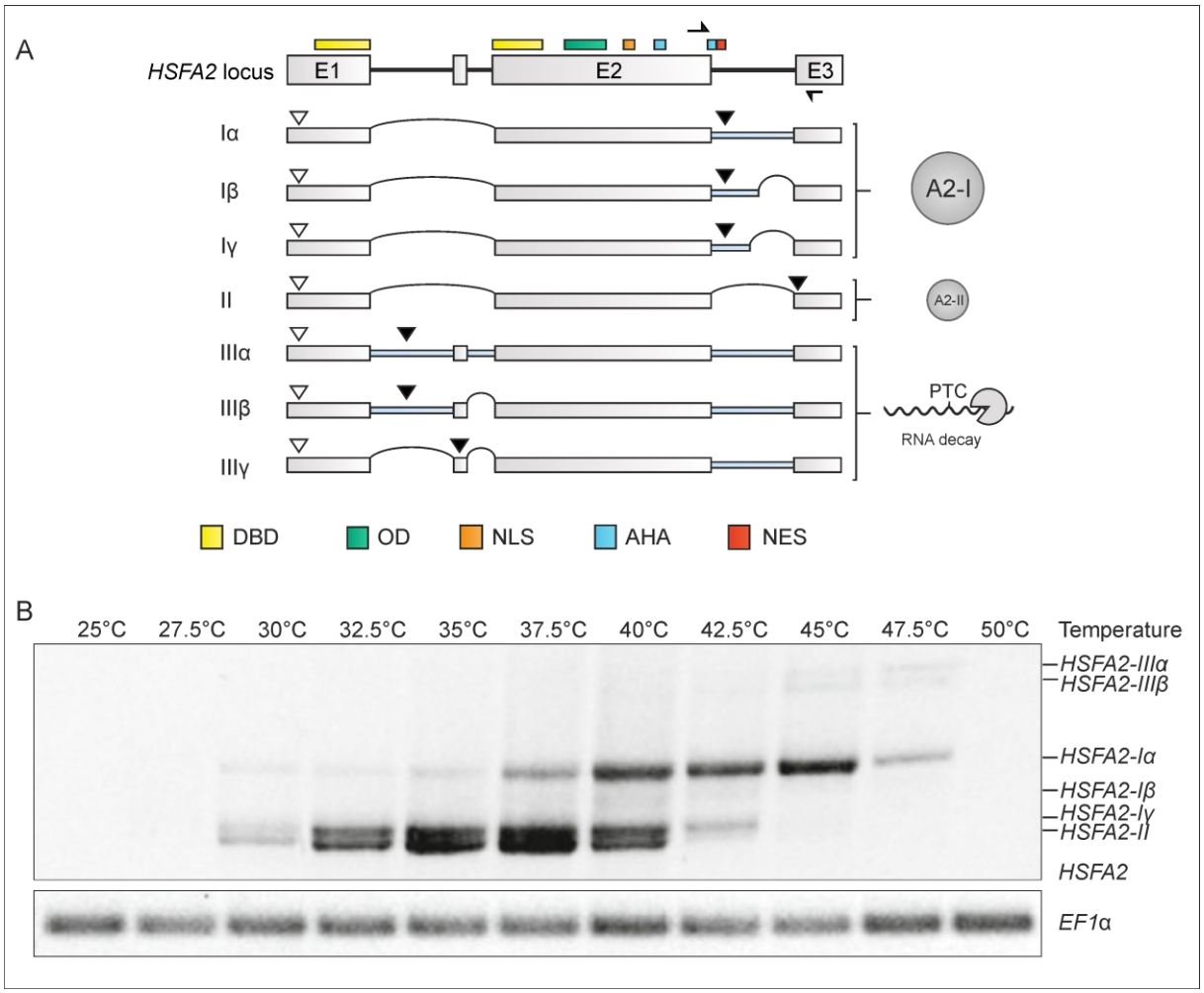

Figure 3. Temperature-dependent alternative splicing of tomato *HSFA2* based on Hu et al. (2020a). (A) Depiction of *HSFA2* splice variants and domain structure. Exons and introns are depicted by boxes and lines, respectively. Curved lines indicate spliced regions, thin blue lines indicate retained intron sequences. Start and stop codons are indicated by white and black triangles, respectively. Coloured boxes represent domain encoding regions: DNA binding domain (DBD, yellow), oligomerisation domain (OD, green), nuclear localisation signal (NLS, orange), activation domain (AHA motif, blue), nuclear export signal (NES, red). Right side symbols indicate the fate of the respective transcripts: translation into protein isoforms HSFA2-I and HSFA2-II, or degradation via nonsense-mediated RNA decay (NMD). (B) *HSFA2* intron 2 splicing profile in seedlings exposed to increasing temperatures for 1 h each. Arrows in (A) indicate primer positions. *EF1α* serves as control. *HSFA2* splice variants and RT-PCR splicing profiles were adopted and modified from Hu et al. (2020a).

1.6 Serine/Arginine-rich proteins

SR proteins are a highly conserved family of RNA binding proteins involved in both constitutive and alternative splicing by modulating SS recognition and spliceosome assembly (Golovkin and Reddy, 1998; Gao et al., 2004; Isshiki et al., 2006; Shepard and Hertel, 2009; Day et al., 2012). SR proteins play key roles in growth, development, and plant stress responses (Reddy and Ali, 2011) and fulfil additional roles in various aspects of RNA processing beyond splicing (Howard and Stanford, 2015), including mRNA decay (Zhang and Krainer, 2004), nuclear export (Huang and Steitz, 2001), and translation efficiency (Sanford et al., 2004; Windgassen et al., 2004). Compared to the 12 SR proteins identified in humans to date (Manley and Krainer, 2010), the repertoire of SR proteins in many plants extends to almost twice the amount, e. g. 18 in *Arabidopsis*, 22 in rice and 17 in tomato (Fig. 4, right side; Barta et al., 2010; Butt et al., 2019; Rosenkranz et al, 2021).

SR proteins usually harbour one or two RNA recognition motifs (RRM) in their N-terminus conferring RNA binding specificity, and a C-terminus rich in serine- and arginine dipeptides (RS domain), defining the name of the protein family (Fig. 4). The RS domain serves as a protein-protein interaction platform on the one hand and the RRM enables RNA binding on the other hand, which allows SR proteins to function as mediators between the spliceosomal protein components and the pre-mRNA (Shepard and Hertel, 2009). Based on their domain architecture, SR proteins are classified into six subfamilies, whereby three subfamilies are orthologous to their mammalian counterparts (SR, SC, RSZ) and three subfamilies exhibit additional features specific to plants (RS, SCL, RS2Z; Fig. 4; Barta et al., 2010). The RS subfamily shares the general composition of the SR subfamily but lacks a highly conserved SWQDLKD motif in the second RRM, while the SCL subfamily differs from mammalian SR proteins through an N-terminal extension not present in the SC subfamily (Fig. 4). The plant-specific RS2Z subfamily shares the general features of the RSZ subfamily but possesses an additional zinc knuckle (ZnK) following the RRM as well as a C-terminal extension rich in serine- and proline residues (Fig. 4; Barta et al., 2010). Moreover, the length and RS/SR content in plant RS domains are more divergent compared to mammalian SR proteins (Barta et al., 2010). Based on the nomenclature for SR proteins, proteins like At-SR45, that possess an RRM flanked by RS domains, are not considered canonical SR proteins anymore and will therefore further be referred to as SR-like proteins (Fig. 4; Barta et al., 2010). The extended number and diversified features of plant SR proteins could be a result of genome and gene duplications and therefore exert redundancy in plant SR protein functions (Kalyna and Barta, 2004). However, the expanded repertoire of splicing factors in plants could also be attributed to the necessity for a more refined and complex fine-tuning of adaptive mechanisms to their environment, representing diversity of SR protein functions (Kalyna and Barta, 2004).

1.7. The role of Serine/Arginine-rich proteins in plant heat stress response

To this date, the role of individual plant SR proteins in the HSR has not been addressed. However, splicing factors of other types have been reported to influence important temperature sensitive AS events, for example *Arabidopsis* SPLICING FACTOR 1 (SF1), that stimulates flowering and thermotolerance by AS regulation of *HSFA2* and *FLOWERING LOCUS M* (*FLM*), thereby also linking thermotolerance and the circadian clock (Lee et al., 2017; Lee et al., 2020; Hirsz and Dixon, 2021). Another example is the role of STABILIZED 1 (STA1) in thermotolerance by AS-regulation of *HSFA3* and several *HSP* genes (Kim et al., 2017; Kim et al. 2018). Furthermore, SR-like protein At-SR45 (Arabidopsis) and Os-SR45 (rice) play roles in plant development and in diverse stress responses with functions beyond splicing (Ali et al. 2007; Albaqami et al., 2019; Park et al., 2020), and Zm-SR45a has been reported to shape the transcriptome in response to daily temperature cycles in *Zea mays* (maize; Li et al., 2021).

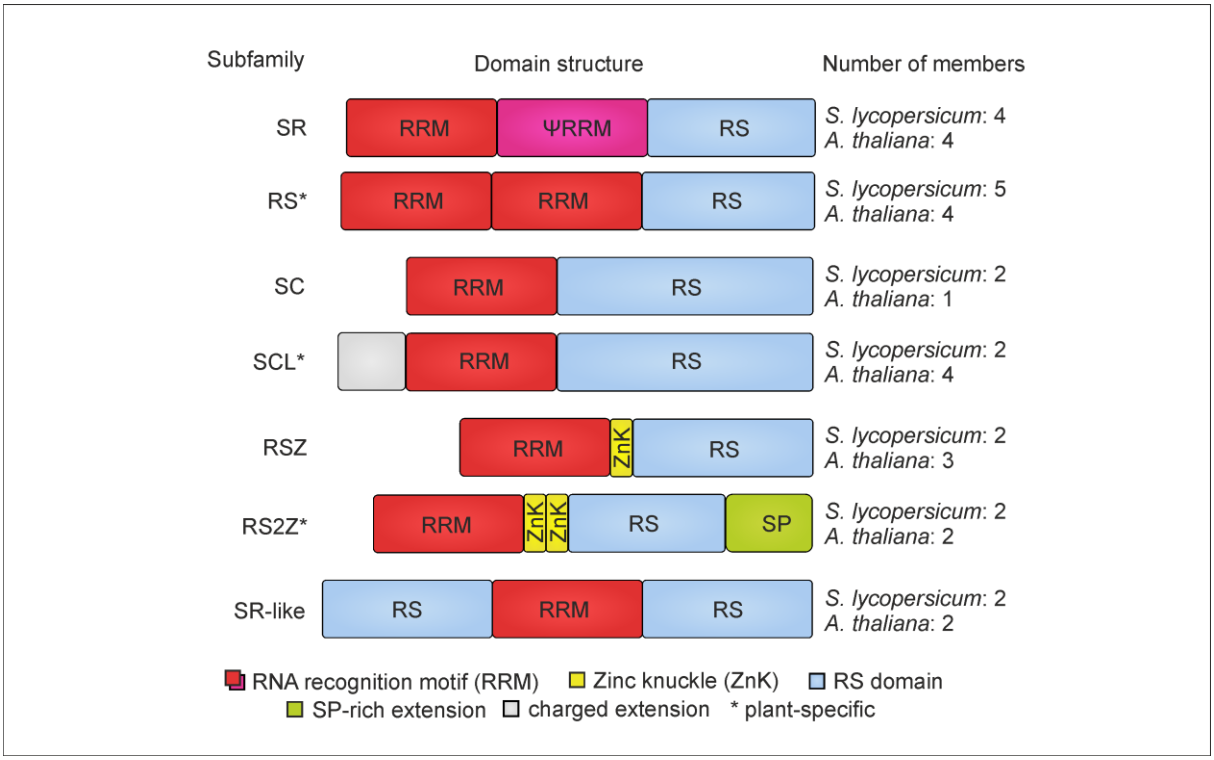

Figure 4. Serine/Arginine-rich (SR) protein families and domain structure. SR proteins are classified into six subfamilies based on their domain architecture. The domain structure of SR and SR-like proteins is depicted with coloured boxes: RNA recognition motif (RRM, red. RRM with conserved SWQDLKD motif in pink), Zinc knuckle (ZnK, yellow), Domain rich in Arginine/Serine dipeptides (RS domain, blue), region rich in serine and proline (SP-rich extension, light green), charged extension (grey). Asterisks indicate plant-specific subfamilies. Members of all subfamilies were described in *Solanum lycopersicum* (tomato) and *Arabidopsis thaliana* (right side) (Barta et al., 2010; Richardson et al., 2011; Rosenkranz et al., 2021).

1.8 Regulation of SR proteins

While the long-underestimated extent of AS in plants was revised during the past century, the questions about the mechanisms conferring HS-induced AS changes persist. Reshaping of splicing factor abundance, activity and localisation could be the link between stress occurrence and rapid adjustment through AS. Figure 5 provides an overview.

1.8.1 Regulation of SR proteins through transcription

SR proteins are expressed in a tissue, developmental stage, and stress dependent manner (Fang et al., 2004; Neumann et al., 2020; Rosenkranz et al., 2021). In many cases, one member in a paralogous pair is dominant over the other, for example tomato RS28 over RS29 and SC30a over SC30b (Richardson et al., 2011; Rosenkranz et al., 2021). In this notion, expression patterns of paralogous pairs, e. g. Arabidopsis SR30 and SR34, can differ in a cell-type or developmental stage-specific manner, in which they overlap in one but separate in other cases, suggesting redundant as well as specialised functions for closely related plant SR proteins (Lopato et al., 1999). Similarly, the response to environmental stresses by members of the same subfamily does not necessarily follow the same trends either, as shown for tomato SC and RS2Z subfamilies under HS, in which only one member is transcriptionally induced (Rosenkranz et al., 2021). Each stress condition induces a specific set of SR proteins (Staiger and Brown, 2013; Cruz et al. 2014; Rosenkranz et al., 2021) and promoters of SR genes contain *cis*-elements for various types of stress-related TFs, for example HSE elements in the promoters of

HS-induced tomato SR proteins (Rosenkranz et al., 2021), further suggesting specialised roles of individual SR proteins under certain conditions and an involvement of splicing factors in the respective stress responses.

1.8.2 Regulation of SR proteins through alternative splicing

The abundance of SR proteins is modulated through extensive AS of their own transcripts in a tissue type or developmental stage specific manner, as well as in response to hormonal and environmental stimuli, giving rise to a plethora of transcript variances, whereby most possess a PTC and fulfil the criteria for NMD decay (Lazar and Goodman, 2000; Isshiki et al., 2006; Palusa et al., 2007; Verhage et al., 2017; Gu et al., 2020; Rosenkranz et al., 2021), suggesting modulation of SR protein abundance by regulated unproductive splicing and translation (RUST) (Palusa and Reddy, 2010). AS of SR proteins is prominent in response to HS and likely poses an evolutionary conserved mechanism to modulate SR protein abundance (Chamala et al., 2015; Verhage et al., 2017). Some SR protein splice variants, however, potentially encode for different protein isoforms, as for example in the case of At-SR45 (Zhang and Mount, 2009). The two At-SR45 protein isoforms differ in their RS domains by the substitution of one aa in SR45-1 by eight aa in SR45-2 and exhibit specialised functions in which SR45-1 plays a role in flower development and SR45-2 plays a role in root growth (Zhang and Mount, 2009). Similarly, maize SR-like protein SR45a is alternatively spliced in response to daily temperature cycles giving rise to two distinct protein isoforms (Li et al., 2021). Here, elevated temperatures shift the splicing profile in favour of the protein isoform harbouring both RS domains and exhibiting higher splicing activity, thereby shaping splicing factor activity in a temperature-dependent manner (Li et al., 2021). However, for most SR proteins, the role of potential isoforms is unclear. Despite many of the

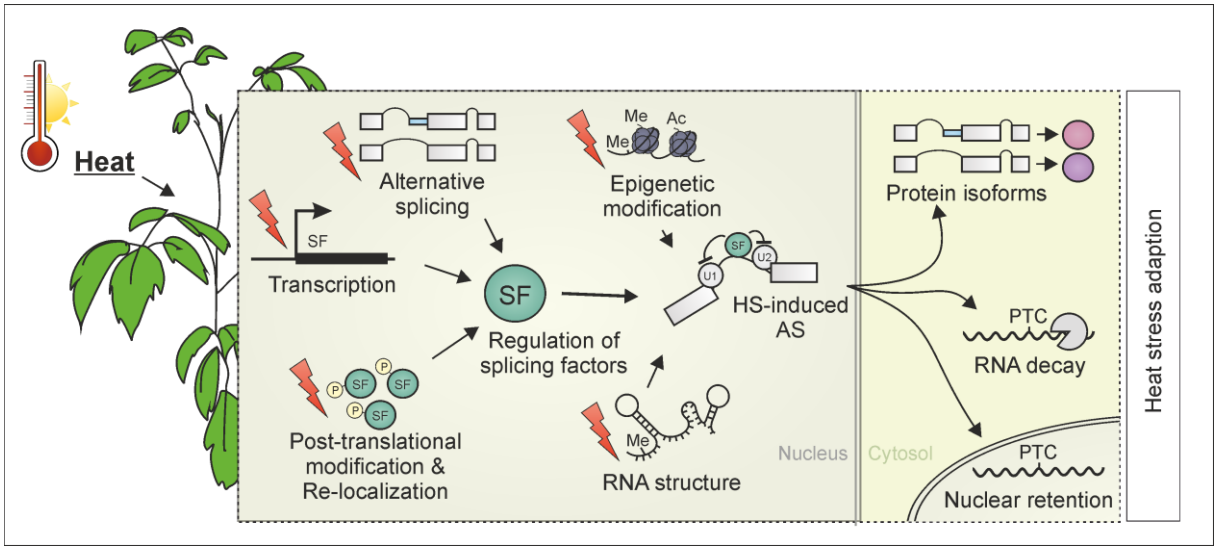

Figure 5. Schematic representation of various mechanisms impacting alternative splicing upon heat stress. Splicing factors are regulated in many ways, e. g. by transcriptional induction, AS, or post-translational modification which collectively determine their abundance, availability, and activity. The regulation of splicing factors, along with changes in the chromatin environment (e. g. DNA methylation, histone acetylation, nucleosome occupancy and RNA polymerase II processivity) and RNA structure (e. g. through RNA modification), impact global AS upon HS. The mechanisms are described in more detail in sections 1.8-1.9. HS-induced AS potentially results in the formation of protein isoforms, thereby diversifying the activity of important regulatory factors, but also promotes the accumulation of PTC-containing transcripts that are either degraded in the cytosol or retained in the nucleus.

splice variants being potential NMD targets, only about half were identified as real NMD targets (Palusa and Reddy, 2010) and some are even recruited to polysomes in an organ- and stress specific manner, suggesting a role for truncated SR proteins under both control and stress conditions, further expanding the complexity of plant SR proteins in response to stress (Palusa and Reddy, 2015).

AS of SR proteins is mediated both in an auto- and cross regulatory fashion, representing a self-restricting system to balance the abundance of a defined set of splicing factors (Lopato et al., 1999; Kalyna et al., 2003; Isshiki et al., 2006). Overexpression of At-*RS2Z33*, for example, impacted AS of its own transcripts (auto regulation) as well as of At-*SR30* and At-*SR34* (cross regulation) (Kalyna et al., 2003). The balance of SR protein levels thereby seems to be crucial to sustain normal growth and reproduction as indicated by pleiotropic effects of SR overexpression (Lopato et al., 1999; Kalyna et al., 2003), suggesting that stress-induction of SR proteins indeed reflects a need for the particular splicing factor under the respective condition.

1.8.3 Regulation of SR proteins through phosphorylation

SR proteins are extensively post-translationally modified through reversible phosphorylation of the serine residues in the RS domain (Fuente van Bentem et al., 2006) which determines their subcellular and subnuclear localisation, as well as their activity by modulating the interaction with other proteins, such as spliceosomal components (Xiao and Manley, 1997; Prasad et al., 1999; Yeakley et al., 1999; Zhou and Fu, 2013). SR proteins undergo a cyclic phosphorylation/dephosphorylation, in which phosphorylation promotes their mobility, releases them from subnuclear bodies and facilitates spliceosome assembly (Roscigno and Garcia-Blanco, 1995), while dephosphorylation during splicing subsequently promotes re-localisation to nuclear speckles (Xiao and Manley, 1997; Zhou and Fu, 2013). Nuclear speckles are subnuclear condensates that appear in irregular speckled patterns of variable sizes (Spector and Lamond, 2011). These biomolecular condensates are predominantly located in the inter-chromatin space and are therefore also termed interchromatin granule clusters (IGCs) (Spector and Lamond, 2011). Other nuclear bodies, such as perichromatin fibrils and Cajal bodies, appear in a speckled formation and contain splicing factors as well (Spector and Lamond, 2011), while the term ‘nuclear speckles’ usually refers to IGCs. Perichromatin fibrils represent sites of active transcription that are assumed to supply the nascent pre-mRNA with splicing factors (Fakan, 1994). In contrast, nuclear speckles primarily act as SR protein modification and storage sites, so-called molecular sponges, and thus modulate SR protein availability by sequestration, as demonstrated for human SR protein SRSF9 which is associated with an architectural RNA in response to HS (Ninomiya et al., 2020). Human SR proteins are rapidly dephosphorylated upon HS (Shi and Manley, 2007) and re-phosphorylated after stress by CDC2-like kinases 1 and 4 (Ninomiya et al., 2011). Specifically, CDC2-like kinase 1 (CLK1), a kinase that undergoes temperature-dependent structural changes in its catalytic domain (Haltenhof et al., 2020), modulates the re-phosphorylation and release of SRSF9 from nuclear speckles during stress recovery and thus promotes global IR (Ninomiya et al., 2020). Furthermore, the regulation of temperature-sensitive AS of *U2AF26* by SRSF2 and SRSF7 is mediated by temperature-controlled phosphorylation (Preußner et al., 2017; Haltenhof et al., 2020). In this notion, human SR protein SRSF10 (former SRp38) acts as a splicing repressor in response to HS only in its

dephosphorylated state (Shi and Manley, 2007). Protein kinases were thus hypothesized to function as temperature sensors by transducing temperature signals into SR protein phosphorylation states, thereby regulating their activity or availability and consequently shifting splicing profiles (Preußner et al., 2017; Haltenhof et al., 2020).

While nuclear bodies exist in plants, they are less extensively studied than mammalian subnuclear structures (Lorković and Barta, 2004). Many plant SR proteins primarily show a speckle-like accumulation driven by phosphorylation of the RS domain (Fang et al., 2004; Tillemans et al., 2006; Lorković et al., 2008; Reddy et al., 2012), and do not necessarily co-localise in the same speckles (Lorković et al., 2008). However, the nature and function of these condensates is not well understood, especially since IGCs and perichromatin fibrils are not distinguishable by using fluorescence microscopy (Spector and Lamond, 2011). Upon HS, At-SR45 accumulates in enlarged nuclear speckles (Ali et al., 2003) and the cyclin-dependent protein kinase CDK2 co-localises with spliceosomal components in enlarged speckles upon HS treatment (Kitsios et al., 2008), indicating potential dynamic SR protein re-localisation upon HS in plants as well. Furthermore, the CYCLIN-DEPENDENT KINASE (G2) (CDKG2)-CYCLIN L1 (CYCL1) complex (Cavallari et al., 2018) and the LAMMER kinase AFC2, a CLK homolog, are involved in temperature-dependent AS (Lin et al., 2022). The latter was shown to regulate the phosphorylation status of SR Protein At-RSZ21 (Lin et al., 2022) but the detailed relationships between SR protein phosphorylation and splicing control were not addressed.

Furthermore, like mammalian SR proteins (Cáceres et al., 1998), some plant SRs were reported to shuttle between the nucleus and the cytosol (Rausin et al., 2010). Nuclear export of SR proteins is mediated by their phosphorylation state-dependent interaction with nuclear export factors (Huang and Steitz, 2005; Müller-McNicoll et al., 2016), which enables SR proteins to take part in nucleocytoplasmic RNA export (Valencia et al., 2008) and to accompany the bound mRNA to the cytosol. Nuclear re-import is subsequently facilitated by transportin-SR following SR protein phosphorylation in the cytosol (Lai et al., 2001). Nucleocytoplasmic shuttling allows additional functions of SR proteins in mRNA metabolism beyond splicing, e. g. in nuclear export (Huang and Steitz, 2001), RNA surveillance through interaction with the NMD pathway (Zhang and Krainer, 2004) or modulation of translation efficiency (Sanford et al., 2004; Windgassen et al., 2004). However, functions of plant SR proteins beyond splicing were so far only addressed for SR-like protein At-SR45, a homolog of the exon junction complex component RNPS1 (Zhang et al., 2009).

1.9 Regulation of alternative splicing beyond splicing factors

AS is further impacted through other mechanisms that largely do not result from direct regulation of splicing factors but by impacting their binding to the pre-mRNA. Since this study focusses on SR proteins, the additional mechanisms are only described briefly.

1.9.1 Regulation of alternative splicing by RNA structure

RNA molecules form complex secondary structures through intramolecular interactions that impact AS by modulating the accessibility of *cis*-regulatory elements for splicing factors and spliceosomal proteins (Hiller et al., 2007; Warf et al. 2009; Meyer et al., 2011). In addition, secondary structures potentially

mask cryptic SS or bring SS closer together, thereby promoting splicing (Shepard and Hertel, 2008; Warf and Berglund, 2010). RNA structures are altered for example through RNA modifications such as N^6-methyladenosine (m^6A), the most prevalent type of eukaryotic RNA modifications (Liu et al, 2015; Deng et al., 2018). Moreover, m^6A modification regulates splicing not only by structure alterations, but also through the interaction of m^6A reader proteins with splicing factors (Xiao et al., 2016). For example, the repression of m^6A-dependent splicing following HS in human cells was associated with the sequestration of the YTHD1 reader protein in nuclear stress bodies (Ninomiya et al., 2021). Efforts to uncover the role of HS-specific RNA modifications in plants were taken by analysing the global Arabidopsis RNA structurome (Li et al., 2021) and by obtaining a HS map of the m^6A transcriptome in *Brassica rapa* (Liu et al., 2020), but further insights are lacking. Furthermore, since distinct pre-mRNA structure features regulate constitutive- as well as alternative splicing in plants (Liu et al., 2021), temperature-dependent RNA folding, as recently described for *HSFA2* (Broft et al., 2022), could provide an additional layer for HS-responsive splicing regulation (Su et al., 2018).

1.9.2 Coupling of transcription and alternative splicing

Since splicing occurs primarily co-transcriptionally (Li et al., 2020), the processes of transcription and splicing are coupled in a temporal and spatial manner, which allows the chromatin environment to impact both transcription and splicing (Das et al., 2006; Jabre et al., 2019). Two models describe the relationship between transcription and splicing (Muñoz et al., 2010). The kinetic model describes the impact of RNA polymerase II (RNA POL II) processivity on splicing, in which mechanisms impacting elongation speed, such as nucleosome occupancy, DNA methylation and histone modification, also impact splicing outcomes (Dujardin et al., 2014; Godoy Herz and Kornblihtt, 2019). For example, day/night-dependent AS changes could be attributed to alterations in RNA POL II elongation rates, in which light promotes higher RNA POL II processivity (Godoy Herz et al., 2019). Similarly, mutation of *TRANSCRIPTION ELONGATION FACTOR TFIIS*, a HS-induced gene crucial for RNA POL II elongation, caused changes in global AS, as well as reduced thermotolerance (Szádeczky-Kardoss et al., 2022). Secondly, the recruitment model describes direct interaction between proteins involved in transcription and those involved in splicing, supported by the co-purification of splicing factors along with RNA POL II (Das et al., 2007) and the direct interaction of splicing factors with chromatin (Loomis et al., 2009). While the reciprocal regulation of splicing and transcription is a relatively newly discovered phenomenon that requires further exploration, it further supports the relevance of AS in shaping the plant transcriptome.

1.10 Objectives

AS plays an important part in the fine-tuning of HSR as exemplified not only by global changes in splicing profiles in response to HS, but also by temperature-dependent splicing of important TFs such as *Os-DREB2B* and *Sl-HSFA2*, by regulating their abundance and/or activity through the generation of protein isoforms. AS could thereby allow the integration of temperature signals into rapid transcriptome alterations. However, the mechanisms leading to HS-induced AS events and their biological relevance are largely unknown.

Moreover, functional characterisation of SR proteins, the key regulators of splicing, is scarce in plants and a link between HS-induced AS alterations and specific SR proteins has not been described. In response to environmental cues, the abundance and activity of several plant SR proteins is impacted through altered expression, AS profiles and phosphorylation states, strongly suggesting a role for these proteins in stress responses and in conferring stress tolerance.

This study aims to elucidate the impact of SR proteins on the HSR and thermotolerance in tomato, an important crop plant serving as a model for HSR. This is addressed by employing genetic, biochemical and bioinformatic approaches, thereby providing experimental evidence for the role of splicing factors in the tomato HSR. The study thereby initially focusses on the regulation of thermotolerance through HS-dependent AS of *HSFA2*, an important regulator of ATT. While the function of HSFA2 and the consequences of its temperature-dependent AS are well described in tomato, the mechanisms regulating this event are not known. SR protein domain deletion mutants as well as *in vitro* and *in vivo* binding assays provide further insight into how specific SR proteins engage with *HSFA2* pre-mRNA and confer splicing profile alterations.

Furthermore, the study aims to provide a general picture on the HS-regulation and function of the plant-specific RS2Z subfamily in tomato, and particularly its HS-induced member RS2Z36. Transient expression in tomato protoplasts, genetic manipulation using the CRISPR/Cas9 system as well as transgenic lines overexpressing RS2Z proteins provide insight into the functionality of these proteins, including their regulation in response to HS. Moreover, the general involvement of RS2Z proteins in thermotolerance is assessed by their impact on HS gene abundance and through physiological assays observing BTT and ATT in young seedlings of *rs2z* knockout lines, providing an understanding on how individual and plant-specific splicing factors contribute to HS tolerance.

The global picture of the effect of *rs2z* mutations on transcriptome diversity through transcript abundance and AS is provided by RNA-Seq and by RNA immunoprecipitation followed by RNA-Seq (RIP-Seq), thus providing a landscape of *RS2Z*-regulated genes and RS2Z-associated RNAs. Thereby, the functional basis of these splicing factors is expanded beyond the regulation of *HSFA2* and thus opening opportunities for the exploration of their role in interconnected stress response pathways and additional functions beyond splicing.

Collectively, this study expands the fragmented knowledge on plant splicing factors and their versatile functions in abiotic and biotic stress responses. It further supports the importance of AS in stress response pathways and describes the essential role of plant-specific splicing factors of the RS2Z subfamily for heat acclimation.

2. Materials

2.1 Chemicals and Disposables

Basic chemicals were purchased from Carl Roth GmbH + Co. KG (Karlsruhe, Germany), Sigma-Aldrich (St. Louis, Missouri, USA) or Merck KGaA (Darmstadt, Germany). Disposables were purchased from Sarstedt AG & Co (Nümbrecht, Germany). Further, specific chemicals are referred to along with the experimental procedures.

2.2 Technical equipment

Table 1. Basic technical equipment

Instrument	Manufacturer
2100 Bioanalyzer instrument	Agilent Technologies (Santa Clara, California, USA)
Agarose gel electrophoresis system	Built in-house
Amersham™ TE 77 semi-dry transfer unit	Amersham plc (Amersham, UK)
Biostep UV transilluminator UST-30M-BE	Biostep GmbH (Burkhardtsdorf, Germany)
Centrifuge SORVALL Evolution RC	Thermo Fisher Scientific (Waltham, Massachusetts, USA)
Centrifuge SORVALL RC6 Plus	Thermo Fisher Scientific (Waltham, Massachusetts, USA)
ECL ChemoStar 6	Intas Science Imaging (Göttingen, Germany)
Electrophoresis power supply EPS 1001	Amersham plc (Amersham, UK)
Electrophoresis system (Mini-PROTEAN Tetra Cell)	Bio-Rad Laboratories, Inc. (Hercules, California, USA)
Electroporation system EASYJECT optima	EquiBio Ltd. (London, UK).
Eppendorf BioPhotometer 6131	Eppendorf AG (Hamburg, Germany)
Eppendorf centrifuge 5417 R	Thermo Fisher Scientific (Waltham, Massachusetts, USA)
Eppendorf centrifuge 5804 R	Thermo Fisher Scientific (Waltham, Massachusetts, USA)
French press cell disruptor with French Pressure cell	Thermo Fisher Scientific (Waltham, Massachusetts, USA)
Incubator (Bacteria)	Heraeus instruments (Hanau, Germany)
MiniAmp™ Plus thermal cycler	Thermo Fisher Scientific (Waltham, Massachusetts, USA)
NanoDrop 1000 Spectrophotometer	Thermo Fisher Scientific (Waltham, Massachusetts, USA)
PAGE running chamber	Micro - Bio - Tec Brand Albrecht Brand e. K. (Gießen, Germany)
Plant growth chamber: CLF Plant Climatics (CU-22CD)	CLG Plant Climatics GmbH (Wertingen, Germany)
Qubit 4 Fluorometer	Thermo Fisher Scientific (Waltham, Massachusetts, USA)
Roll mixer RM5.40	Ingenieurbüro CAT, M. Zipperer GmbH (Ballrechten-Dottingen, Germany)
Rotator 2-1175	neoLab Migge GmbH (Heidelberg, Germany)
Shaking incubator Multitron	Infors AG (Basel-Landschaft, Austria)
Sonicator: Sonoplus HD 70	BANDELIN electronic GmbH & Co. KG (Berlin, Germany)
StepOne™ Plus Real-Time PCR system	Thermo Fisher Scientific (Waltham, Massachusetts, USA)
Thermomixer comfort 5355	Eppendorf AG (Hamburg, Germany)
TissueLyser MM300	Retsch GbmH (Haan, Germany)
Typhoon 9400 fluorescence scanner	GE Healthcare (Chicago, Illinois, USA)

Table 2. Basic technical equipment (continued).

Instrument	Manufacturer
VIBRAX-VXR (shaker for 15 ml-falcon tubes)	IKA-Werke (Staufen im Breisgau, Germany)
Waterbath julabo 8A with heating circulator julabo UC	JULABO GmbH (Seelbach, Germany)
Zeiss LSM 780 microscope; objective: Plan Apochromat 63x/1.2	Carl Zeiss AG (Oberkochen, Germany)

2.3 Plasmid constructs

Genomic and cDNA sequences were obtained from the Sol Genomics Network (SGN) (Fernandez-Pozo et al., 2015). Gene nomenclature was adopted from the ITAG 4.0 provided by the SGN except for Solyc08g062960 that was manually curated as *HSFA2*. Tomato SR proteins were described in Rosenkranz et al. (2021) and the nomenclature for ERF genes was adopted from Liu et al. (2016). Generally, the style for genes, transcripts and proteins follows the guidelines for the model plant *Arabidopsis thaliana* (https://www.arabidopsis.org/portals/nomenclature/namerule.jsp).

2.3.1 Plasmid constructs for bacterial and protoplast transformation

Table 3. Plasmid constructs for bacterial and protoplast transformation. amp^R: ampicillin resistance. HA: hemagglutinin. All constructs are driven by the Cauliflower mosaic virus 35S rRNA (CaMV35S) promoter.

Plasmid ID	Insert gene ID	Tags, resistance	Designation	Cloning strategy, primer ID	Source
SR and SR-like protein constructs					
pRT-35S-3HA-RS2Z35 (S02-V320)	*RS2Z35* (Solyc05g054920)	3xHA; amp^R	Protein expression in protoplasts	-	Rosenkranz et al. (2021)
pRT-35S-3HA-RS2Z36 (S02-V239)	*RS2Z36* (Solyc09g005980)				
pRT-35S-RS28 (S02-V372)	*RS28* (Solyc10g009330)				
pRT-35S-RS29 (S02-V321)	*RS29* (Solyc01g096180)				
pRT-35S-RS30 (S02-V322)	*RS30* (Solyc01g091750)				
pRT-35S-RS41 (S02-V323)	*RS41* (Solyc11g072340)				
pRT-35S-RS42 (S02-V373)	*RS42* (Solyc03g026240)				
pRT-35S-3HA-SR32 (S02-V246)	*SR32* (Solyc03g082380)				
pRT-35S-3HA-SR33 (S02-V329)	*SR33* (Solyc01g099810)				
pRT-35S-3HA-SR35 (S02-V330)	*SR35* (Solyc09g075090)				
pRT-35S-3HA-SR41 (S02-V331)	*SR41* (Solyc06g009060)				

Table 4. Plasmid constructs for bacterial and protoplast transformation (continued). amp^R: ampicillin resistance. All constructs are driven by the CaMV35S promoter.

Plasmid ID	Insert gene ID	Tags, resistance	Designation	Cloning strategy, primer ID	Source
pRT-35S-3HA-SC30a (S02-V242)	*SC30a* (Solyc04g074040)	3xHA; amp^R	Protein expression in protoplasts	-	Rosenkranz et al. (2021)
pRT-35S-3HA-SC30b (S02-V243)	*SC30b* (Solyc01g105140)				
pRT-35S-3HA-SCL29 (S02-V244)	*SCL29* (Solyc01g005820)				
pRT-35S-3HA-SCL31 (S02-V327)	*SCL31* (Solyc01g080660)				
pRT-35S-3HA-RSZ21a (S02-V240)	*RSZ21a* (Solyc08g006430)				
pRT-35S-3HA-RSZ21b (S02-V324)	*RSZ21b* (Solyc08g069120)				
pRT-35S-3HA-SR46 (S02-V374)	*SR-like 46* (Solyc10g005590)				
pRT-35S-3HA-SCL46 (S02-V328)	*SR-like 46a* (Solyc06g076670)				
RS2Z domain mutant constructs					
pRT-3HA-RS2Z36-ΔRRM1-80 (S02-V299)	*RS2Z36* (Solyc09g005980)	3xHA; amp^R	Protein expression in protoplasts	Deletion PCR on S02-V239 Primers: 10246, 10247	Created in this study
pRT-3HA-RS2Z36-ΔZnK (S02-V300)	*RS2Z36* (Solyc09g005980)			Deletion PCR on S02-V239 Primers: 10248, 10249	
pRT-35S-3HA-RS2Z36ΔRS (S02-V416)	*RS2Z36* (Solyc09g005980)			Deletion PCR on S02-V239 Primers: 11196, 11197	
pRT-35S-3HA-RS2Z35ΔRRM (S02-V418)	*RS2Z35* (Solyc05g054920)			Deletion PCR on S02-V320 Primers: 11194, 11195	
pRT-35S-3HA-RS2Z35ΔZnk (S02-V419)	*RS2Z35* (Solyc05g054920)			Deletion PCR on S02-V320 Primers: 11192, 11103	
pRT-35S-3HA-RS2Z35ΔRS (S02-V417)	*RS2Z35* (Solyc05g054920)			Deletion PCR on S02-V320 Primers: 11198, 11199	

Table 5. Plasmid constructs for bacterial and protoplast transformation (continued). amp^R: ampicillin resistance. All constructs are driven by the CaMV35S promoter unless specified differently.

Plasmid ID	Insert gene ID	Tags, resistance	Designation	Cloning strategy, primer ID	Source
Mutant plant mimicking constructs					
pRT-d35S-3HA-gRS2Z35 (S02-V462)	Genomic WT *RS2Z35* (Solyc05g054920)	3xHA; amp^R	Protein expression in protoplasts	Traditional cloning: Acc65I/XbaI Primers: 10398, 10399	Created in this study
pRT-d35S-3HA-gRS2Z36 (S02-V464)	Genomic WT *RS2Z36* (Solyc09g005980)			Traditional cloning: Acc65I/XbaI Primers: 9082, 9083	
pRT-d35S-3HA-gRS2Z36m2 (S02-V466)	Genomic mutant *RS2Z36* (Solyc09g005980) . Origin: S02-38.16			Traditional cloning: Acc65I/XbaI Primers: 9082, 9083	
Further protoplast expression constructs					
pRT-3HA-hnRNP (S02-V525)	*GR-RBP3* (hnRNP 1/3 ortholog) (Solyc02g088790)	3xHA; amp^R	Protein expression in protoplasts	Traditional cloning: *SalI/XbaI* Primers: 10422, 13979	Created in this study
pRT-GFP-A2-minigene-lyco (GGG) (S02-V276)	*HSFA2* (Solyc08g062960)	GFP; amp^R	Protein expression in *E. coli*; backbone for IVT templates; Minigene assay	-	Hu et al. (2020a)
pRT-GFP-A2-minigene-peru (AAA) (S02-V281)	*HSFA2* (Solyc08g062960-peru)		Minigene assay		
pRT-PHSP21.5-GFP-A2-minigene-lyco (GGG) (S02-V444)	*HSFA2* (Solyc08g062960)	GFP; amp^R; *HSP21.5* promoter	Minigene assay	Gibson assembly. PHSP21.5 primers: 11894, 11895. Vector (SO2-V276) linearization primers: 11896, 11897	Created in this study
pRT-PHSP21.5-GFP-A2-minigene-peru (AAA) (S02-V445)	*HSFA2* (Solyc08g062960-peru)			Same as for S02-V444 Vector: (SO2-V281)	
pRT103-Neo (S02-V52)	Neomycin phosphatase (Neo)	amp^R	Protein expression in protoplasts, mock plasmid	-	Töpfer et al. (1987)

Table 6. Plasmid constructs for bacterial and protoplast transformation (continued). amp^R: ampicillin resistance. kan^R: kanamycin resistance. All constructs are driven by the T7 promoter.

Plasmid ID	Insert gene ID	Tags, resistance	Designation	Cloning strategy, primer ID	Source
Plasmid templates for *in vitro* transcription					
pRT-T7-A2L-RiJ- SP6 (S02-V537)	*HSFA2* (Solyc08g062960)	amp^R	Template for *in vitro* transcription	Traditional cloning: Acc65I/XbaI Backbone: S02-V276 Primers: 14207, 14208	Created in this study
pRT-T7-A2L-RiK-SP6 (S02-V538)	*HSFA2* (Solyc08g062960)			Traditional cloning: Acc65I/XbaI Backbone: S02-V276 Primers: 14209, 14210	
pRT-T7-A2L-RiN-SP6 (S02-V539)	*HSFA2* (Solyc08g062960)			Traditional cloning: Acc65I/XbaI Backbone: S02-V276 Primers: 14211, 14212	
Protein expression and purification constructs					
pOPINE GFP nanobody (S02-V483)	GFP Nanobody	kan^R	Protein expression in *E. coli*	-	Addgene
pL91-GB1-His-SAP25 (S02-V527)	GB1-6xHis tag	GB1-6xHis; amp^R	Source for GB1-6xHis tag for S02-V528	-	
pMAL-TEV-His-RS2Z36 (S02-V369)	*RS2Z36* (Solyc09g005980)	MBP, 6xHis; amp^R	Backbone for S02-V528	-	Rosenkranz (2017)
pMAL-c4x-GB1-His-RS2Z36(RBD) (S02-V528)	*RS2Z36* (Solyc09g005980)	GB1-6xHis; amp^R	Backbone for S02-V550, V545, V554	Traditional cloning: NdeI/BamHI Replace MBP-tag in S02-V528 with GB1-tag from S02-V527	Created in this study
pMAL-c4x-GB1-His-RS2Z36(RBD2) (S02-V545)	*RS2Z36* (Solyc09g005980)		Protein expression in *E. coli*	Traditional cloning: BamHI,XbaI Backbone: (S02-V528) 14136, 14137	
pMAL-c4x-GB1-GB1-His-RS2Z35(RBD) (S02-V550)	*RS2Z35* (Solyc05g054920)			Traditional cloning: BamHI,XbaI Backbone: (S02-V528) 14138, 14139	
pMAL-c4x-GB1-His-SC30b(RRM) (S02-V554)	*SC30b* (Solyc01g105140)			Traditional cloning: BamHI,XbaI Backbone: (S02-V528) Primers: 14463, 14494	

Table 7. Plasmid constructs for bacterial and protoplast transformation (continued). amp^R: ampicillin resistance. All constructs are driven by the CaMV35S promoter.

Plasmid ID	Insert gene ID	Tags, resistance	Designation	Cloning strategy, primer ID	Source
Constructs for microscopy studies					
pRT-35S-GFP (S02-V484)	*GFP*	GFP; amp^R	Protein expression in protoplasts	-	Provided by Dr. Sotirios Fragkostefanakis
pRT-35S-GFP-RS2Z35 (S02-V398)	*RS2Z35* (Solyc05g054920)				
pRT-GFP-RS2Z36 (S02-V253)	*RS2Z36* (Solyc09g005980)				Streit (2016)
pRT-GFP-SC30b (S02-V256)	*SC30b* (Solyc01g105140)				
pRTdsAtEnp1-mCherry (S02-V41)	*ENP1* (At1g31660)	mcherry; amp^R			Röth et al. (2017)

2.3.2 Plasmid constructs for plant transformation

Table 8. Plasmid constructs for plant transformation and generation of plant transformation constructs. spec^R: spectinomycin resistance. kan^R: kanamycin resistance.

Plant line	Plasmid ID	Gene ID	Tags, Resistance	Cloning strategy, primer ID	Source
	pICSL01009::AtU6p (S02-V228)	At-U6 promoter	spec^R	Source for PAtU6 sequence (CRISPR construct assembly)	Addgene #46966
	pICSL002208 (S02-V227)	-	kan^R	Level 2 vector for Golden Gate; Binary backbone for plant transformation	Provided by Dr. Nicola Patron (Earlham Institute, UK)
	pICHL41744	-	spec^R	End linker for level 2 Golden Gate (assembly of the binary vector)	MoClo Toolkit (Engler et al, 2014)
rs2z35 (S02.37)	pICSL002208-RS2Z35-RNA1-2 (S02-V420)	*RS2Z35* (Solyc05g054920)	kan^R	Golden Gate; sgRNA primers: 11125, 11126	Created in this study
rs2z36 (S02.38)	pICSL002208-RS2Z36-RNA1-2 (S02-V421)	*RS2Z36* (Solyc09g005980)		Golden Gate; sgRNA primers: 11127, 11128	
	pICH86966 (S02-V453)	-	lacZ; kan^R	Acceptor plasmid	Addgene #48075
PCaMV35S:GFP (S02.42)	pICH86966-P35S-GFP (S02-V480)	GFP	GFP; kan^R	Golden Gate into pICH86966; Fragment1: 11903, 13322 Fragment 2: 11904, 13323	Created in this study
PCaMV35S:GFP-RS2Z35 (S02.40)	pICH86966-P35S-GFP-RS2Z35 (S02-V455)	*RS2Z35* (Solyc05g054920)		Golden Gate into pICH86966	Löchli (2020)
PCaMV35S:GFP-RS2Z36 (S02.41)	pICH86966-P35S-GFP-RS2Z36 (S02-V456)	*RS2Z36* (Solyc09g005980)		Golden Gate into pICH86966	

2.4 Oligonucleotides

Oligonucleotides were purchased from Eurofins Genomics (Ebersberg, Germany) and are depicted in Table 9-13.

Table 9. Oligonucleotides used in this study. IVT: *in vitro* transcription

Construct ID	Designation	Primer ID	Sequence (5‘ to 3‘)
Cloning oligonucleotide primers			
S02-V299	*RS2Z* domain mutant, Deletion PCR	10246	CGCTGCTCAGGTACCTGGTGTGCCACGTGGACCAGGCG
		10247	TCCACGTGGCACACCAGGTACCTGAGCAGCGTAATCTGG
S02-V300		10248	CCTGGGTCAGGTAGTCCTAAAAAACTCAGTAGACGCAG
		10249	GTTTTTTAGGACTACCTGACCCAGGAGCGGGTCC
S02-V416		11196	CCTAAAAAACTCCCGCCACCAAAGAGAGAAC
		11197	TGGTGGCGGGAGTTTTTTAGGACTATTTGGGCAT
S02-V418		11194	GGTGGCACATTCGCCAAAGGGGTGCCTCGTG
		11195	CTTTGGCGAATGTGCCACCATACCTGTC
S02-V419		11192	GGTACTGGTAGCCCCAAGAAATTGAAACGTG
		11193	TCTTGGGGCTGTCCTCCTCCAGGTACTGGT
S02-V417		11198	GAAACGTGACCCTGTGAAGAGGGACCGTAG
		11199	CTTCACAGG GTCACGTTTCAATTTCTTG
S02-V462 S02-V487	Mutant mimic constructs, *RS2Z35*	10398	TCAGGTACCTCCGCGGTATGATGACAGGTATG
		10399	GACTCTAGATTAGGGTGACTCACTGCC
S02-V464 S02-V466	Mutant mimic constructs, RS2Z36	9082	ACCGGTACCTCCTCGTTATGATGATCGT
		9083	ACCTCTAGAGCGCAAGTTTCAAGGTGACT
S02-V537	IVT, Whole *HSFA2* intron	14207	ACGGGTACCTAATACGACTCACTATAGGGTGAGGAATTACAAGACC
		14208	TGGTCTAGAACTAGTATTTAGGTGACACTATAGCTGAAAAATTGAATCAAATG
S02-V538	IVT, *HSFA2* 5'SS region	14209	ACGGGTACCTAATACGACTCACTATAGGGTGGAAGTTGAAGATCTTG
		14210	TGGTCTAGAACTAGTATTTAGGTGACACTATAGCAAGAGTGACCTCTAAAGGAAAC
S02-V539	IVT, *HSFA2* 3'SS region	14213	ACGGGTACCTAATACGACTCACTATAGGGTGAAGTGCAGAATTGATATTTTTCTTTTC
		14212	TGGTCTAGAACTAGTATTTAGGTGACACTATAGTCAAAGCTTCCTGAAATGAAAG
S02-V550	Expression construct (*E. coli*): GB1-His-RS2Z35(RBD)	14138	CATGGATCCCCGCGGTATGATGACAG
		14139	GTATCTAGACTAGGGGCTATTCTGACAGTTC
S02-V545	Expression construct (*E. coli*): GB1-His-RS2Z36(RBD)	14136	CATGGATCCCCTCGTTATGATGATC
		14137	GTATCTAGACTATTTAGGACTATTTGGGC
S02-V554	Expression construct (*E. coli*): GB1-His-SC30b(RRM)	14463	GACTCTAGACTAACTTTCTCAATGATCCTCCCTTG
		14494	GACTCTAGACTAAACTTTCTCAATGATCCTCCCTTG

Table 10. Oligonucleotides used in this study (continued).

Construct ID	Designation	Primer ID	Sequence (5‘ to 3‘)
S02-V480	Transgenic plant: PCaMV35S:GFP; GFP input fragment 1	11903	CTAGGTCTCTGGAGTAGGCTTTACACTTTATGC
		13322	TACGGTCTCTCTCTTTTCGTTGGGATCTTTC
	Transgenic plant: PCaMV35S: GFP; GFP input fragment 2	11904	TACGGTCTCTAGCGTACGGTCACAGCTTGTCTG
		13323	ACAGGTCTCAAGAGGGACCACATGGTCCTT
S02-V420	Mutant *rs2z35* plant; sgRNA 1	11125	TGTGGTCTCAATTGGTGGCACACGCCTATATGTGTTT TAGAGCTAGAAATAGCAAG
	Mutant *rs2z35* plant; sgRNA 2	11126	TGTGGTCTCAATTGTGGAAGACGGTAGCCCAACGTTT TAGAGCTAGAAATAGCAAG
S02-V420; S02-V421	Mutant RS2Z plant, tracrRNA sequence	8297	TGTGGTCTCAAGCGACAAAAAAGCACCGACTCG
S02-V421	Mutant *rs2z36* plant; sgRNA 1	11127	TGTGGTCTCAATTGACGGACCCGTTCACGTGATCGTT TTAGAGCTAGAAATAGCAAG
	Mutant *rs2z36* plant; sgRNA 2	11128	TGTGGTCTCAATTGTGATGGACGCCGCATAATTGGTT TTAGAGCTAGAAATAGCAAG
S02-V444, S02-V445	PHSP21.5 fragment for PHSP21.5-GFP-A2 minigene	11894	CTATGACCATGATTACGCCAGGTACCTTCATCCTAATT TTAC
		11895	TATATGTTGTGTTGAGAATTCTCGAGACTATACACTGT AG
	Backbone linearization	11896	AATTCTCAACACAACATATACAAAAC
		11897	GGCGTAATCATGGTCATAGC
S02-V525	*GR-RBP3* insert (Solyc02g088790)	14022	TCAAGTCGACTGCTTTTGTCAATAAAATTGGG
		13979	CCTATCTAGATCAGCTCCTGGTGTTGGCGTA
		3967	GGAACAGGTAGTTTTCCAGTAGTGCAAATAAA
Genotyping oligonucleotide primers			
Cas9	genotyping of T-DNA-free mutants	8794	CTTCGACCTGGCCGAAGATG
		8795	CGTATTTGACCTTGGTGAGC
GFP	genotyping of transgenic plants	12115	ATGGGTAAAGGAGAAGAAC
		3967	GGAACAGGTAGTTTTCCAGTAGTGCAAATAAA
RS2Z35 (Solyc05g054920)	Amplification of genomic sequence for sequencing, sequencing	11965	CGGGAAGATGCGCTATCATG
		11968	ATAGAACACAGCATGTGCAAGG
	sequencing	12618	CGACTAGTGTGTCTCATCTC
RS2Z36 (Solyc09g005980)	Amplification of genomic sequence for sequencing, sequencing	11969	ATGCCTCGTTATGATGATCGT
	Amplification of genomic sequence for sequencing	12143	TCACTGCAAATTCATCAGAGG
	sequencing	12564	AATGCTAGACCCTAAGGAACC
		11971	AAGCACGACTATGCCTTCGT
Solyc06g048090	Sequencing of potential *RS2Z35* CRISPR off-target	13666	GCTAACGACACTCGTCTA
		13667	GTAGTTGTTCTTACGCTGCTC

Table 11. Oligonucleotides used in this study (continued). OX: overexpression

Construct ID	Designation	Primer ID	Sequence (5‘ to 3‘)
Solyc02g093970	Sequencing of potential *RS2Z36* CRISPR off-target	13664	GTATTCAACTCCTTTGCCATTG
		13665	GAGGGTCTATGCTATATGG
RT-PCR oligonucleotide primers			
HSFA2 (Solyc08g062960)	endogenous *HSFA2* splicing	6026	AGGCCGGATTCTGTTGTGAC
	endogenous and minigene *HSFA2* splicing	7332	GAGACCGCCTCAAAGCTTCCTG
	minigene *HSFA2* splicing	7611	GAGTTTGTAACAGCTGCTG
		11068	GAAGCAACGCGCACGACAAG
RS2Z35 (Solyc05g054920)	*RS2Z35* AS	11087	GATGACAGGTATGGTGGCAC
		11088	CGCTTCATATCCACATCACG
	RS2Z35 AS (cross- and autoregulation)	10372	GCGGTATGATGACAGGTATGG
		11068	GAAGCAACGCGCACGACAAG
RS2Z36 (Solyc09g005980)	*RS2Z36* AS	11089	ATGATCGTGTGGGAAATAGC
		11090	CCAAGATACTCACGCGAACC
	RS2Z36 AS (cross- and autoregulation)	7071	AATAGCACTCGTCTCTATGTG
		12143	TCACTGCAAATTCATCAGAGG
Solyc01g005440	RT-PCR RNA-Seq AS validation	15064	CAATGTCGAGCAAGGTTG
		15065	GTTCGGTTGTTCCAGCC
qRT-PCR oligonucleotide primers			
EF1α (Solyc06g005060)	Housekeeping ene, normalisation qRT-PCR and RIP-qPCR	5957	TGATCAAGCCTGGTATGGTTGT
		5958	CTGGGTCATCCTTGGAGTT
RS2Z35 (Solyc05g054920)	full-length protein-coding *RS2Z35* (P)	10372	GCGGTATGATGACAGGTATGG
		10373	CCACATCACGTACTCTCCCA
	endogenous *RS2Z35* in OX plants (endo)	13422	TATCTCATCCTTGCACTTTGAT
		11968	ATAGAACACAGCATGTGCAAGG
	RIP-qPCR	11967	GATCCAGGTCTCCTGTGAAGA
		7060	TTTGATGGAGGTGGTGATGA
RS2Z36 (Solyc09g005980)	full-length protein-coding *RS2Z36*(P)	7071	AATAGCACTCGTCTCTATGTG
		7906	GGATCACTAAATTCTACGAAGG
	endogenous *RS2Z36* in OX plants (endo), RIP-qPCR	12142	TGCAGTGCTTGGTATTTGATG
		12143	TCACTGCAAATTCATCAGAGG
RS28 (Solyc10g009330)	full-length protein-coding *RS28*	10356	CGAGTCGACATGAAATCTGGGT
		10357	GCGCCTTTCATAACCAAATG
RS29 (Solyc01g096180)	full-length protein-coding *RS29*	10358	CGTCTTGACATGAAATCTGGCT
		10359	ATAACCGGCGCTTGTCATAC
RS30 (Solyc01g091750)	full-length protein-coding *RS30*	10354	GAGTTTGACGCTCGCCAG
		10355	CTCCATATAAATGAAAGCAAATCCAGA

Table 12. Oligonucleotides used in this study (continued).

Target	Designation	Primer ID	Sequence (5‘ to 3‘)
RS41 (Solyc11g072340)	full-length protein-coding *RS41*	10362	TGGATAGAGTGGATATGAAATCTGGT
		10363	GAAGTCTGCGTCCCTTTCTG
RS42 (Solyc03g026240)	full-length protein-coding *RS42*	10360	TTTGAGTTTGAAACCAGACAGC
		10361	CATATAAACAAAAGCAAAACCAGAC
SR32 (Solyc03g082380)	full-length protein-coding *SR32*	10366	AGCAGGAGCAAGACTCCAAG
		10367	TGGACCTGGTCGACTTTACAG
SR33 (Solyc01g099810)	full-length protein-coding *SR33*	10364	CAGCCAGAGCGGAAGTGTAT
		10365	ATCTGGATCTTGATAGAGATCTTGA
SR35 (Solyc09g075090)	total *SR35*	10368	TTTCGAAATGCCTTTTCTCG
		10369	GCTTCGGCTTCGACTAACAC
SR41 (Solyc06g009060)	total *SR41*	10370	GCTGAGCTGTTGGTGTCATC
		10371	TCCCCAAGTCAAAGGTTCAC
SC30a (Solyc04g074040)	total *SC30a*	10338	CAAGGCATCGTGATCATAGG
		10339	GCGCCTGTCCTCATCATATT
SC30b (Solyc01g105140)	total *SC30b*	10340	GCAGAAGCCCTCGTAGAAGA
		10341	ATGTTTTCTGTCCCGTCTCC
SCL29 (Solyc01g005820)	full-length protein-coding *SCL29*	10348	AAACCTTCGCCATGATTGTC
		10349	AAGCCTCGTGGTTCACCAGTG
SCL31 (Solyc01g080660)	full-length protein-coding *SCL31*	10350	CCAGCAAGACGTGACTCAAGGGA
		10351	CCTTGGAGAAATAGACCGAGAC
RSZ21a (Solyc08g006430)	*total RSZ21a*	10374	CGGAGGAGTCCAAGTTATGGTC
		10375	CTGACACCATTTCCATTGGAG
RSZ21b (Solyc08g069120)	*total RSZ21b*	10376	CAGGAGCCCAAGTTATGGTC
		10377	CACTCTCTAAGTCCATTTCCATTAAC
SR46 (Solyc10g005590)	*total SR46*	13400	AGCCCCAGCAACAGTAACAG
		13401	ACAAAGCTCATCCGTCAAGG
SR46a (Solyc06g076670)	*full-length protein-coding SR46a*	10352	GTTATCACCGTGGAGAAGGCC
		10353	CCTTGAATAATGAGGATAAGTTCG
Hsp17.7A-CI (Solyc09g015010)	HS-genes in *rs2z* mutants	6263	ATGGAGAGAAGCAGCGGTAA
		6264	ATGTCAATGGCCTTCACCTC
APX3 (Solyc09g007270)	HS-genes in *rs2z* mutants	6259	CCGCCCTCTAGTCGAGAAAT
		6260	AGAACCAGACTGATCTCCAGAGA
HSFA2 (Solyc08g062960)	HS-genes in *rs2z* mutants; RIP-qPCR	9800	TTCCACCACATTGTTGCCTA
		9801	GCAAGCACCAGATCCTTGTT

Table 13. Oligonucleotides used in this study (continued).

Target	Designation	Primer ID	Sequence (5‘ to 3‘)
Solyc05g052570	RNA-Seq validation	15046	GTATGCGTCCACTGGTTC
		15047	GAACATGTAACAGCAGGAGAC
Solyc06g074030		15048	CTGTAATAGCCTTTATGGTGG
		15049	CTTTCTGCTCCGTTATTCAC
Solyc03g121940		15050	GAAGAAGCCTGGAGAGTCC
		15051	CGGAGAAGGCGGAGTAG
Solyc09g075600		15052	GGAACAATTGGATACGGC
		15053	CAGTTTTCACCACGAAGC
Solyc02g090770		15054	GGAGGAGGAGGAATACGAAG
		15055	CATCATTGGGGAACTGTTG
Solyc03g093540		15056	GCATATGACAGGGCAGC
		15057	GACCAATTCGACGGTG
Solyc03g093550		15058	GCAATATTGAATTTCCCACTC
		15059	GGTGTTAATGGAGATGCC
Solyc05g024230		15062	GATTTGTTTCAGTTCGAGAAC
		15063	CACAAGCGGGTTAGACC
Other oligonucleotides			
5'Cy5- SP6 oligonucleotide for RNA labeling		12490	Cy5-TATTTAGGTGACACTATAG
Oligo(dT) for cDNA synthesis		6530	TTTTTTTTTTTTTTTTTTTTTTTTVN

2.5 Antibodies

Table 14. Antibodies used in this study. mc = monoclonal; pc = polyclonal.

Antibody	Antigen	Organism	Dilution	Source
Primary antibodies				
αHA (mc)	Hemagglutinin (HA) tag	Mouse	1:2,000	BioLegend (San Diego, California, USA)
αGFP (mc)	GFP		1:5,000	Roche (Basel, Switzerland)
αHSC70 (Spa-820) (mc)	Cognate Hsp70 (Hsc70)		1:10,000	StressGen Biotechnologies (San Diego, California USA)
30HN (pc)	SlHSFA2	Rabbit	1:10,000	Scharf et al., 1998
αHSP17-CI (pc)	Ps17Ci		1:3,000	Port et al.,2004
αAtBRX1 (pc)	AtBRX1		1:5,000	Weis (2015)
Secondary antibodies				
αMouse IgG, HRP-conjugated (pc)	Mouse IgG	Rabbit	1:10,000	Sigma-Aldrich (St. Louis, Missouri, USA)
αRabbit IgG, HRP-conjugated (pc)	Rabbit IgG	Goat	1:10,000	Sigma-Aldrich (St. Louis, Missouri, USA)

2.6 Software and bioinformatic tools

Table 15. Software and tools used in this study.

Software/package	Version	Purpose	Source
agriGO	2.0	GO term enrichment analysis	Tian et al 2017
apeglm	1.14.0	LFC shrinkage	Zhu et al. (2019)
Clone manager	9.0	Molecular cloning, Sanger sequencing analysis	Sci Ed Software LLC (Westminster, CO, USA)
ComplexHeatmap	2.8.0	Generation of heat maps	Gu et al. (2016)
CorelDRAW	2020	Figure processing	Corel Corporation (Ottawa, Ontario, Canada)
DESeq2	1.32.0	DE analysis, RIP-Seq analysis	Love et al. (2014)
Expasy (ProtParam)		Calculation of protein-specific A280 coefficients	Duvaud et al. (2021)
Htseq (Galaxy Version)	0.9.1	Read counting	Anders et al. (2015)
IBM SPSS Statistics	21.0	Statistical analysis	IBM Corporation (Armonk, New York, USA)
ImageJ	1.52p	Hypocotyl elongation, Protein quantification (SDS-PAGE), Relative protein abundance (Immunoblot)	Schneider et al. (2012)
ImageLab	6.0.1	Splice variant quantification from EtBr-stained agarose gels	Bio-Rad Laboratories, Inc. (Hercules, California, USA
Majiq	2.2	AS analysis	Vaquero-Garcia et al. (2016)
Microsoft excel		Data management	Microsoft Corporation (Redmond, Washington, USA)
OrgDb object (Genome wide annotation for *Arabidopsis*)	3.15.1	Annotation package	Carlson (2017)
Pfam	35.0	Analysis of protein domain architecture	Mistry et al., (2021)
Photoshop	CC 2019-2021	Figure processing	Adobe Inc. (San José, Calfironia, USA)
rrvgo	1.8.0	Reduction and visualisation of GO terms	Sayols (2020)
Rstudio	4.1.1	Bioinformatic analyses, data processing	RStudio Team (2020)
Star (Galaxy Version	2.7.8a	Read mapping	Dobin et al. (2013)
Sva package (ComBat-seq function)	3.42.0	Removal of batch effects in DE analysis	Zhang et al. (2020b); Leek et al. (2021)
UpSetR	1.4.0	Visualisation of intersections (upset plots)	Conway et al. (2017)
Venny	2.1.0	Analysis of overlapping sets	Oliveros (2007)
ZEN	2 (blue edition)	Confocal microscopy image processing	Carl Zeiss AG (Oberkochen, Germany)

2.7 Biological material

2.7.1 Plant lines

Plant lines are listed in below. The position of mutations is indicated as nucleotide position in the genomic sequence of the respective gene as annotated in the tomato gene annotation ITAG 2.50 (Fernandez-Poco et al., 2014).

Table 16. Plant lines used in this study.

Plant line	Genotype	Source
Solanum lycopersicum cv. Moneymaker	Wild type	
hsfA2 (S02-31/15-6) *(CR-a2-1)*	Δ57-58(GC)	Hu et al. (2020a)
rs2z35 (S02.37/10.20-20)	1383DelA, 3944InsC	Generated in this study
rs2z36 (S02.38/9-23-3)	Ins79T; 1402DelT	Generated in this study
rs2z35 rs2z36 (S02.45/01.63)	*RS2Z35*: 1383DelA, 3944InsC *RS2Z36*: Ins79T; 1402DelT	Generated in this study
PCaMV35S:GFP (S02.42)	T-DNA insertion: PCaMV35S:GFP	Generated in this study
PCaMV35S:GFP-RS2Z35 (S02.40)	T-DNA insertion: PCaMV35S:GFP-RS2Z35	Löchli (2020)
PCaMV35S:GFP-RS2Z36 (S02.41)	T-DNA insertion: PCaMV35S:GFP-RS2Z36	Löchli (2020)

2.7.2 Bacterial strains

Table 17. Bacterial strains used in this study.

Strain	Genotype	Source
E. coli DH5a	F– Φ80lacZΔM15 Δ(lacZYA-argF) U169 recA1 endA1 hsdR17 (rK–, mK+) phoA supE44 λ– thi-1 gyrA96 relA1	Thermo Fisher Scientific (Waltham, Massachusetts, USA)
E. coli BL21 LEMO (DE3)	*fhuA2 [lon] ompT gal (λ DE3) [dcm] ΔhsdS/ pLemo*(Cam^R) *λ DE3 = λ sBamHIo ΔEcoRI-B int::(lacI::PlacUV5::T7 gene1) i21 Δnin5* pLemo = pACYC184-*PrhaBAD-lysY*	New England BioLabs Inc. (Ipswich, Massachusetts, UK)
*E. coli B*L21 star (DE3) pRARE	F^- *ompT* $hsdS_B$(r_B^- m_B^-) *gal dcm rne131* (DE3) pRARE (Cam^R)	Thermo Fisher Scientific (Waltham, Massachusetts, USA)
A. tumefaciens GV3101::pMP90	C58 (rif^R), pMP90 (pTiC58DT-DNA; gen^R), Nopaline	Kindly provided by A. Batauscher, Marburg
A. tumefaciens EHA 105	C58 (rif^R) Ti pEHA105 (pTiBo542DT-DNA), Succinamopine	Kindly provided by the Buschmann lab (Hochschule Mittweida, Mittweida, Germany)

3. Experimental procedures

3.1 Plant tissue and growth conditions

Plants were grown in the green house with a day/night cycle of 16h/8h under temperature-controlled conditions of 24°C/20°C diurnal temperature.

Plants for protoplasts were grown in climate chambers with a day/night cycle of 16h/8h under temperature-controlled conditions of 25°C/22°C diurnal temperature and 120 µmol m^{-2} s^{-1} light on half-strength Murashige and Skoog (MS) medium (Murashige and Skoog, 1962), solidified by addition of 3 g L^{-1} gelrite, supplemented with 0.05 mg L^{-1} vitamin B1, 0.25 mg L^{-1} vitamin B6 and 0.5 mg L^{-1} Niacinamide, and adjusted to pH 5.8.

3.2 Hypocotyl elongation assay

Thermotolerance of mutant plants was assessed by hypocotyl elongation under different temperature conditions. The approach was based on the method described for Arabidopsis by Queitsch et al. (2000) and adopted for tomato in Fragkostefanakis et al. (2016).

Seeds of indicated genotypes were surface sterilized by shaking in 15% sodium hypochlorite for 4 minutes, followed by 2x5 minutes in 70% ethanol and 5 washes in sterile distilled deionized water (ddH_2O) for 5 minutes each. The seeds were germinated in sterile ddH_2O in the dark at 25°C for 3 days and subsequently placed on square petri dishes containing half-strength MS medium (pH 5.8, supplemented with 10 g L^{-1} sucrose, 0.96 g L^{-1} MS and 8 g L^{-1} Phyto agar) (7-10 etiolated seedlings per plate). The seedlings were then grown for 4 days in climate chambers as described in section 3.1 until approximately 1 cm hypocotyl length. Then, seedlings were exposed to indicated temperature regimes by placing the plates in growth chambers for the indicated duration. For ATT, seedlings were allowed to recover for three hours at 25°C under light conditions. Seedlings were imaged directly after application of the respective stress regime, allowed to grow under constant 25°C and a day/night cycle of 16h/8h for two days and were then imaged again. Absolute hypocotyl length was measured using ImageJ (Schneider et al., 2012)). Hypocotyl elongation was calculated as hypocotyl growth rate in cm/day. Relative hypocotyl elongation was expressed as hypocotyl elongation relative to control per replicate per genotype by normalising the growth rate of each genotype to the mean of the growth rates under control conditions. This was performed separately for each replicate. The experiment was performed in at least three independent biological replicates that consisted of 5-10 seedlings each for every treatment. Statistical analysis was performed using one-way ANOVA with Duncan posthoc test and a significance threshold of 0.05 using SPSS statistics software (IBM Corporation, Armonk, New York, USA). Normal distribution of relative hypocotyl elongation values was validated using the Shapiro-Wilk normality test ($p < 0.05$) (performed in R) along with visual inspection of Q-Q plots generated in R.

3.3 Protoplast isolation

Isolation of tomato mesophyll protoplasts was performed for transient protein expression and subsequent HS experiments. The procedure was previously described by Mishra et al. (2002). Leaves

from 6-week-old tomato plants were cut with a sterile surgical scalpel and incubated in enzyme solution containing 0.5% (w/v) cellulase (Duchefa Biochemie, Haarlem, Netherlands) and 0.2% macerozyme (Duchefa Biochemie, Haarlem, Netherlands) in the dark for 16 hours. Next, residual leaf tissue was removed by transferring the solution into glass vials through a metal mesh, and subsequently mixed K32S buffer (K3M buffer without mannitol, but 13.7% (w/v) sucrose instead). Protoplasts were separated via centrifugation at 460 pm for 7 min at room temperature (RT) with slow acceleration and brakes. The protoplast-containing supernatant was then transferred to new glass vials, mixed with 2 volumes (vol) W5 wash buffer (2.74% (w/v $CaCl_2$ x 6H2O, 0.9% (w/v) NaCl, 0.04% (w/v) KCl, 0.1 % (w/v) glucose, 0.5 mM MES) and centrifuged at 670 rpm for 10 min at RT with slow acceleration and brakes. The protoplast pellet was washed again with W5, followed by centrifugation. Finally, the protoplasts were resuspended in K3M buffer (3% (w/v) sucrose, 0.4 M mannitol, 24.73 mM KNO_3, 1.01 mM $MgSO_4$ x $7H_2O$, 1.09 mM NaH_2PO_4 x H_2O, 1.01 mM $(NH_4)_2SO_4$, 6.12 mM $CaCl_2$ x $2H_2O$, 560 µM m-inositol, 3 mM NH_4NO_3, 165 µM $FeSO_4$EDTA, trace elements (45.2 nM KI, 0.59 µM $MnSO_4$ x H_2O, 69.6 nM $ZnSO_4$ x $7H_2O$, 0.485 µM H_3BO_3, 10.3 nM Na_2MoO_4 x $2H_2O$, 1.1 nM $CoCl_2$ x $6H_2O$, 15 nM $CuSO_4$), hormones 5.37 µM NES and 0.89 µM BA, vitamins 29.65 µM B1, 4.86 µM B6, 8.12 µM nicotinamide, and 5 mM MES; pH adjusted with KOH to 5.8), counted using a Fuchs-Rosenthal counting chamber and adjusted to 1 million/ml.

3.4 Protoplast transformation and heat stress treatment

Transient expression of plasmid DNA in protoplasts was obtained via polyethylene glycol (PEG)-mediated transformation as described by Mishra et al. (2002). 50,000 protoplasts were mixed with 10 µg plasmid DNA and 1 vol of 25% PEG (25% PEG 6000, 0.45 M mannitol, 0.1 M $Ca(NO_3)_2$x$4H_2O$, pH 6.0), incubated at RT for 25 minutes. DNA amounts were used as indicated in the results section and filled up with pRT-Neo as mock plasmid. The reaction was stopped by addition of 400 µl K3M buffer. Volumes were scaled up proportionally if different amounts of protoplasts were used (amounts are indicated in results section). Proteins of interest were expressed in the presence of light at constant 25°C for the indicated duration. HS treatment was performed in Eppendorf-tubes in a water bath at the indicated temperature and for the indicated time. Immediately after stress, the protoplasts were harvested by centrifugation at 14,000 rpm at 4°C for 5 minutes. The pellets were snap-frozen in liquid N_2 and stored at -80°C until further use.

3.5 Protein turnover in protoplasts

The stability of proteins transiently expressed in was conducted similarly to Röth et al. (2017). In brief, following tomato protoplast transformation and 16 hours of expression, cycloheximide (CHX) was added to a final concentration of 40 µM. Protoplasts were then subjected 37.5°C (HS) or remained at 25°C (control). Samples were harvested at the indicated time points and kept at -80°C until further use. Proteins were extracted, separated on denaturing polyacrylamide gels, and detected by immunoblot as described in sections 3.8, 3.10 and 3.12. Protein signals were measured following background subtraction using ImageJ (Abràmoff et al., 2004), further normalised to cognate HSP70 (HSC70) and calculated as relative to time point t0 (timepoint of CHX addition and onset of HS treatment).

3.6 Microscopy analysis

For assessment of intracellular SR protein localisation, 10^{-5} protoplasts were transformed with 12 µg *ENP1-mCherry* and 8 µg *GFP-SR* encoding plasmid. Due to strong GFP expression, only 2 µg GFP encoding plasmid was used for localisation of GFP. Following 20 hours of expression, protoplasts were either exposed to 38°C for 1 h in an Eppendorf thermomixer or kept at 25°C and subsequently imaged using the confocal laser scanning microscope (CLSM; Zeiss LSM 780; objective: Plan Apochromat 63x/1.2). Excitation and emission spectra for GFP- and mCherry fusion proteins were defined as follows: GFP: excitation at 488 nm, emission at 490-548 nm. mCherry: excitation at 561 nm, emission at 570-656 nm. Emission of chlorophyll-b autofluorescence was detected with excitation at 633 nm and an emission filter of 665-738 nm. Excitation was performed in a sequential manner to prevent crosstalk between channels.

3.7 Leaf heat stress treatment

Excised young leaves from mature plants were exposed to HS by incubation on wetted paper towel in sealed petri dishes in a water bath of the indicated temperature. Samples were harvested after the indicated treatment duration by snap freezing in liquid N_2 and subsequent storage at -80°C until further use.

3.8 Protein extraction from plant material

For immunoblot analysis, proteins from protoplasts or leaves were extracted using high salt (HS) buffer (20 mM Tris-HCl, pH 7.8; 0.5 M NaCl; 25 mM KCl; 5 mM $MgCl_2$; 30 mM EDTA; 0.5% Nonidet P40 (NP40 substitute); 0.2% sarcosyl; 5% sucrose; 5% glycerol; 0.1% ß-mercaptoethanol; protease inhibitor cocktail, EDTA-free (Roche, Basel, Switzerland). Frozen young leaves were homogenized using a tissue lyser (2x 30 seconds at a frequency of 30/s). Ground tissue was subsequently mixed with 150 µl HS buffer, while protoplast pellets were directly mixed with 40 µl HS buffer, followed by thorough vortexing. Lysates were cleared by centrifugation at 20,000 x g for 5 minutes at 4°C and finally mixed with 4x Laemmli buffer (Laemmli, 1970) (200 mM Tris-HCl, pH 6.8; 8% (w/v) SDS; 40% (w/v) glycerol, 0.4 M DTT, 0.4% bromophenolblue).

3.9 Protein quantification

3.9.1 Bradford protein quantification

To ensure equal protein amounts used for protein dephosphorylation (section 3.13), protoplast protein extracts were quantified using the colorimetric Bradford assay (Bradford, 1976). 3 µl total protein extract were mixed with 797 µl H_2O and 200 µl Bradford reagent (Bio-Rad protein assay, Bio-Rad Laboratories, Inc. (Hercules, California, USA)) and incubated for 5 min at RT. As blank, lysis buffer was used instead of protein extract. Dye-protein complexes were measured at 595 nm and protein concentrations were determined by employing a BSA standard curve.

3.9.2 Amidoblack protein quantification

For leaf extracts, protein quantification was performed via amidoblack originally described by Schaffner and Weissmann (1973), following an in-house protocol. Amidoblack forms a stable dye-

protein complex under acidic conditions. 2 µl lysate were diluted with ddH_2O to a total volume of 100 µl, followed by addition of 400 µl amidoblack solution (0.01% (w/v) amidoblack 10B, 90% (v/v) methanol, 10% (v/v) acetic acid), mixing and centrifugation at 20,000 x g for 15 min at 4°C. The supernatant was removed, and the coloured precipitate was washed with 1 ml wash solution (90% (v/v) methanol, 10% (v/v) acetic acid) followed by centrifugation at the same conditions. The precipitate was air dried and resolubilised in 1 ml 200 mM NaOH. The amount of pelleted dye-protein complex was quantified via absorbance at OD_{615} and protein concentration was then calculated using a BSA standard in parallel.

3.9.3 NanoDrop protein quantification

Quantification of pure purified protein was carried out utilizing absorption at 280 nm using the NanoDrop spectrophotometer. For this, the protein-specific coefficient for A_{280} was calculated using the ProtParam tool of the Expasy resource portal (Duvaud et al., 2021).

3.9.4 Protein quantification via SDS-PAGE

Purified recombinant SR proteins were quantified via SDS-PAGE, whereby different amounts of final protein sample were run along increasing amounts of BSA of known concentration. Using ImageJ, a BSA standard curve was calculated for each gel by using the area under peak-method. The concentration of SR proteins was quantified by determining the area corresponding to protein signals and subsequent calculation of protein concentration using the BSA standard curve.

3.10 Sodium dodecyl sulfate polyacrylamide gel electrophoresis (SDS-PAGE)

Proteins from protein extracts or after heterologous protein expression were separated according to their molecular weight using discontinuous sodium dodecyl sulfate polyacrylamide gel electrophoresis (SDS-PAGE) (Laemmli, 1970). First, the protein samples were mixed with 4x Laemmli buffer and were entirely denatured by boiling for 5 min at 95°C, rapid cooling for a short time followed by centrifugation at max. speed for 1 min at RT. Then, the samples were loaded onto a gel along with a Protein Molecular Weight Marker (Pierce™ unstained protein molecular weight (MW) marker, Thermo Fisher Scientific (Waltham, Massachusetts, USA)). Protoplast samples were loaded in equal volumes unless stated otherwise. Leaf protein extracts were quantified, and equal absolute protein amounts were loaded. Gels were composed of 5 ml resolving gel (390 mM Tris-HCl, pH 8.8; 10-15% acrylamide mix (Rotiphorese® Gel 30 (37.5:1), 0.1% (w/v SDS), 0.1% (w/v) APS, 0.1% (v/v) TEMED) topped with 2.5 ml stacking gel (130 mM Tris-HCl, pH 6.8; 5% acrylamide mix (Rotiphorese® Gel 30 (37.5:1), 0.1% (w/v) SDS, 0.1% (w/v) APS, 0.3% TEMED). Separation took place in SDS running buffer (49.5 mM Tris, 197.8 mM glycine, 0.1% (w/v) SDS) at 90V (60V until the sample entered the separation gel) for approximately 1 h. Next, the gel was either stained (section 3.11) or the proteins were blotted onto a nitrocellulose membrane (section 3.12).

3.11 Coomassie staining

Staining of polyacrylamide gels was performed by incubation in Coomassie (0.125 % (w/v) R250, 0.125% (w/v) G250, 50% (v/v) methanol, 40% (v/v) acetic acid) for 30 min under gentle agitation,

followed by rinsing with water and destained using destainer (10% (v/v) methanol, 7% (v/v) acetic acid) (Neuhoff et al, 1988).

3.12 Immunoblot analysis (Western blot)

For immunoblot detection of proteins of interest, proteins were transferred onto nitrocellulose blotting membranes (0.45 µm; GE Healthcare) by semi-dry blotting (Towbin et al, 1992). For this, the membrane was placed on top of two Whatman papers and was subsequently topped with the gel and two additional Whatman papers. Transfer was performed in transfer buffer (48 mM Tris, 39 mM glycine, 0.037% (w/v) SDS, 20% (v/v) methanol) at 1 mA/cm² for 75 min. Successful transfer was examined by either Ponceau S staining (0.4% (w/v) Ponceau S, 3% (v/v) trichloroacetic acid, 1% (v/v) acetic acid) for 5 minutes following washes with ddH_2O, or by DB71 staining for 1 minute. After imaging of DB71 stain (0.008 % (w/v) DB71, 36.8% (v/v) ethanol, 9.2% (v/v) acetic acid) the blot was briefly washed with wash solution (40% (v/v) ethanol, 10% (v/v) acetic acid) (Hong et al., 2000). After documentation, the blot was destained using destain solution (50% (v/v) ethanol, 150 mM $NaHCO_3$) and final washed using ddH_2O for 10 minutes. RuBisCo large subunit served as loading control if no Hsc70 antibody control was performed.

To detect proteins of interest, the membrane was first blocked with 5% milk powder in phosphate-buffered saline (PBS) (137 mM NaCl, 2.7 mM KCl, 10 mM $Na_2HPO_4xH_2O$, 1.8 mM KH_2PO_4) and subsequently incubated with primary antibody for 1 hour at RT (or overnight at 4°C). Next, the membrane was washed in PBS four times for 5-15 minutes and subsequently incubated with horseradish peroxidase (HRP)-coupled secondary antibody in 5% milk powder in PBS for 1 hour. After yet again four wash steps of 5-15 minutes each, signals were detected by luminescence by addition of substrate solutions (ECL Kit, Perkin-Elmer Life Sciences, Waltham, Massachusetts, USA) and imaging in the ECL ChemoStar 6 (Intas Science Imaging, Göttingen, Germany).

3.13 Protein dephosphorylation

Phosphorylation changes were examined by dephosphorylation followed by SDS-PAGE or by Phos-tag PAGE (section 3.10 and 3.14). 3 x 10^{-5} protoplasts were transformed with hemagglutinin (HA)-tagged RS2Z encoding plasmid (15 µg/10^5 protoplasts) (section 3.4). SR proteins were expressed at 25°C for 4.5 hours, followed by 1 h HS at 37.5°C. Pelleted protoplasts were then resolubilised in 40 µl RIP C2 lysis buffer (buffer (50 mM Tris-HCl pH 7.6, 4 mM $MgCl_2$, 500 mM NaCl, 1% NP40 substitute, 1% Sodium deoxycholate, 10% glycerol, 0.1% SDS, 1 mM NaF, 5 mM DTT, 1x EDTA-free Protease inhibitor cocktail (1 tablet/10 ml buffer, Roche), Ribolock [100 U/ml]) without NaF and lysed by thorough vortexing. Next, the lysate was cleared by centrifugation at 20,000 x g for 5 min at 4°C. The supernatant was transferred to a new tube and subsequently mixed with 2 vol dilution buffer to reduce salt concentration to 167 mM. Protein concentration was determined via Bradford assay (section 3.9.1). 15 µg protein extract was mixed with 37.5 U FastAP (Thermo Fisher Scientific, Waltham, Massachusetts, USA). Non-phosphatase treated samples were instead mixed with lysis and dilution buffer in a ratio of 1:2. All samples were then incubated at 37°C for 30 min at 300 rpm and subsequently mixed with 4x Laemmli buffer. Samples were run either on 10% SDS-PPA gels (see section 3.10) or loaded on a Phos-tag PPA-gel (section 3.14).

3.14 Phos-tag PAGE

To evaluate the protein phosphorylation in more detail, Phos-tag (Wako Pure Chemical Industries, Ltd., Osaka, Japan) PAGE was performed. Phos-tag is a chemical compound that traps phosphate groups to form a stable complex (Kinoshita et al., 2006). The presence of Phos-tag in the gel reduces the migration velocity of phosphorylated proteins proportionally to the number of phosphate groups present. Thereby, the occurrence of multiple phosphorylation states can be observed. Phos-tag PAGE was performed according to the manufacturer's instructions, using the Mn^{2+}-Phos-tag method. Protein extracts were prepared as described in section 3.8 and run on a Phos-tag containing 8% resolving gel (375 mM Tris-HCl pH 8.8; 8% acrylamide mix (Rotiphorese® Gel 30 (37.5:1), 15 µM Phostag (Wako Pure Chemical Industries, Ltd., Osaka, Japan), 80 µM $MnCl_2$, 0.1 % (w/v) APS, 0.1% (v/v) TEMED 0.1%), topped with a 4.5% stacking gel (187.5 mM Tris-HCl pH 6.8; 4.5% acrylamide mix (Rotiphorese® Gel 30 (37.5:1), 0.1 % (w/v) APS, 0.1% (v/v) TEMED), alongside a prestained protein marker (PageRuler™ Prestained Protein Ladder, Thermo Fisher Scientific, Waltham, Massachusetts, USA) in running buffer (section 3.10). Gels were prepared the same day and polymerized for at least one hour after casting. After protein separation at 110 V for approximately 90 minutes, Mn^{2+} ions were removed from the gel by incubation of the gel in 100 ml transfer buffer (25 mM Tris, 19.2 mM glycine, 20% (v/v) methanol) supplemented with 50 mM EDTA (pH 8.0). Four EDTA-washes of 10 minutes at 50 rpm were performed in total. Afterwards, the proteins were blotted onto a PVDF membrane (AmershamTM Hybond P Western blotting membrane, 0.45 µm, Amersham plc, Amersham, UK) by wet-tank blotting in a Bio-Rad blotting chamber (Bio-Rad Laboratories, Inc. (Hercules, California, USA) at 115 V for 2-2.5 hours in transfer buffer (without EDTA). After blotting at 4°C, the membrane was stained with DB71 and specific proteins were detected by immunodetection (section 3.12).

3.15 Minigene splicing reporter assay (*in vivo* splicing assay)

A minigene reporter assay was performed to rapidly screen the regulation of *HSFA2* splicing by many SR proteins simultaneously. The reporter assay was adapted from Hu et al. (2020a) and is composed of a genomic segment of the *HSFA2* gene fused in-frame to an N-terminal GFP-tag and driven by the CaMV35S promoter. The *HSFA2* segment includes the intron 2 flanked by the 3'-end of exon 2 and the entire exon 3. In order to investigate different regulation of natural *HSFA2* variants, minigenes harbouring the *HSFA2* sequence from *S. lycopersicum* cv Moneymaker and *S. peruvianum* were used (Hu et al., 2020a). Protoplasts were transformed with 2 µg minigene along with 5 µg HA-SR protein encoding plasmid. After 4.5 h expression at 25°C, protoplasts were exposed to 37.5°C for 1 hour. *HSFA2* splicing efficiency was calculated using immunoblot analysis and expressed as the fraction of GFP-HSFA2-II relative to all GFP-HSFA2 protein signals.

A subset of combinations was validated via RT-PCR (section 3.18.1) using a *GFP-HSFA2* minigene reporter driven by the heat inducible *HSP21.5* promoter in order to mimic the natural heat induction of endogenous *HSFA2*. After expression and HS treatment as described above, total RNA was extracted as described in section 3.16. Complete removal of *HSFA2*-encoding plasmid was ensured by overnight DNA digestion. 300-1,000 ng isolated RNA was incubated overnight at 37°C in a total volume of 10 µl, including 10 U RNase-free DNaseI (Roche, Basel, Switzerland), 0.5 µl Ribolock and 0.5 µl *DpnI* (Thermo

Fisher Scientific, Waltham, Massachusetts, USA), whereby the presence of *DpnI* facilitated plasmid digestion. Following cDNA synthesis (section 3.17), *GFP-HSFA2* splicing profiles were assessed by RT-PCR using a forward primer located in GFP and a reverse primer located in *HSFA2* exon 3. The absence of plasmid was confirmed by simultaneously performing the same RT-PCR using RNA as template.

3.16 RNA extraction from plant material

Frozen plant tissue was mechanically homogenized using a tissue lyser. Frozen protoplast pellets were directly resolubilised in the appropriate lysis buffer. Total plant RNA for RT- and qRT-PCR purposes was isolated using either the E.Z.N.A.® Plant RNA Kit (Omega Bio-Tek Inc.) or the standard TRIzol™ (Thermo Fisher Scientific Inc.) procedure. Using the plant RNA kit, extraction was performed following the manufacturer's instructions with slight modifications: 1 h DNaseI treatment instead of 15 min; 15 min incubation in 40 µl pre-warmed ddH_2O for elution instead of 2 min.

The TRIZol procedure was performed following the manufacturer's instructions with slight modifications: The RNA was pelleted at 18,000 x g, followed by three washes with 70% ethanol at the same speed and subsequent air dry for 15 min at RT. The RNA was then resolubilised in 25 µl (protoplasts) or 100 µl (leaves) diethyl pyrocarbonate (DEPC)-treated ddH_2O. Tri-reagent was prepared following the protocol described in Köster et al. (2014). The amount of TRIZol used depended on the starting material: 350 µl TRIZol for extraction from 3 x 10^5 protoplasts, 1,000 µl TRIZol for extraction from leaves.

RNA-extraction for RIP-qPCR and RIP-Seq is described in detail in section 3.29.5. and additional steps for RNA extracted for RNA-Seq are described in section 3.30.

The RNA was quantified by absorption at 260 nm using the NanoDrop spectrophotometer. Purity was evaluated based on A260/280 ratio > 1.8 (protein) and A260/A230 ratio > 2 (organic compounds).

3.17 cDNA synthesis

Total RNA was used for first-strand cDNA synthesis using the RevertAid Reverse Transcriptase (200 U/µL, Thermo Fisher Scientific, Waltham, Massachusetts, USA) and oligo(dT) primers. Prior to reverse transcription, residual genomic DNA was removed by DNaseI treatment: up to 1 µg RNA was incubated with 0.3 µl RNase-free DNaseI (Roche, Basel, Switzerland) with supplied DNaseI buffer in a total volume of 10 µl for 1 hour at 37°C. The reaction was stopped by addition of 1 µl 50 mM EDTA pH 8.0 and incubation at 75°C for 10 min. The successful gDNA removal was verified by amplification of *EF1α* via PCR on DNase-treated RNA (diluted to 10 ng/µl). Oligo(dT) primers were annealed to the residual DNAse-free RNA by addition of 1 µl oligo(dT) [100 µM] following 5 min incubation at 70°C and subsequent 5 min incubation on ice. Reverse transcription was initiated by addition of 9 µl mastermix (1 µl reverse transcriptase, 4 µl 5x RT buffer, 2 µl 10 mM dNTPs, 2 µl RNase-free ddH_2O) and 1 h incubation at 42°C. The reaction was stopped by 15 min incubation at 70°C. Finally, the cDNA was diluted to a final concentration of 10 ng/µl and stored at -20°C. Successful cDNA synthesis was verified by amplification of *EF1α* via PCR.

3.18 Polymerase chain reaction (PCR)

Amplification of DNA (e. g. for cloning purposes) was performed via polymerase chain reaction (PCR) (Mullis et al., 1986) using in-house purified Pfu turbo polymerase in appropriate buffer (10 mM Tris-HCl pH 8.8, 25 mM KCl, 5 mM $(NH_4)_2SO_4$, 2 mM $MgSO_4$). Standard reactions consisted of 1 µ template DNA (10 ng cDNA, 1 ng plasmid, 100 ng genomic DNA), 2 µl 2 mM dNTP, 1 µl 10 µM forward primer, 1 µl 10 µM reverse primer, 1 µl 10x Pfu buffer and 0.2 µl Pfu polymerase in a total volume of 20 µl. Typical thermal cycler profiles were set up as follows: Initial denaturation for 2 min at 95°C, followed by 30 cycles consisting of 30 seconds denaturation at 95°C, 30 seconds annealing at temperatures between 58°C and 63°C, and elongation at 72°C for 2 min/kb product length. The profile ended with a final elongation step at 72°C for 7 minutes. Amplification of large products (>3 kb) were performed using Phusion™ High-Fidelity DNA Polymerase (Thermo Fisher Scientific, Waltham, Massachusetts, USA) according to the manufacturer's instructions.

3.18.1 Reverse transcription-polymerase chain reaction (RT-PCR)

PCR was used for analysis of splice variants using cDNA as template. The procedure was performed using Pfu polymerase as described above. The number of thermal cycles were adjusted according to expression levels to avoid saturation and ranged from 25 to 30 cycles.

3.18.2 Colony PCR

For verification of positive clones after cloning, colony PCR was performed. A single colony was streaked on a fresh plate containing LB medium and antibiotics using a pipette tip. The residual bacteria cells left on the tip were then mixed with 50 µl of ddH_2O and thoroughly mixed. 1 µl of diluted bacterial cells were used as template for PCR. The initial denaturation was prolonged to 3 min for cell lysis.

Colony PCR after transformation of *Agrobacterium tumefaciens* was performed as following: A single colony was cultivated as 5 ml overnight-culture. Cells were collected by centrifugation and resuspended in 100 µl ddH_2O. The cells were then lysed by boiling for 10 min in a hot block set to 95°C and centrifuged at max. speed for 30 sec to pellet cell debris. 5 µl supernatant were used as PCR template.

3.18.3 Quantitative real-time PCR (qRT-PCR)

Assessment of relative transcript levels was performed using quantitative real-time PCR (qRT-PCR) in a thermal cycler. qRT-PCR was performed in three technical replicates in 96-well plates. Each sample contained 2 µl cDNA [2 ng/µl], 1 µl forward primer [3 µM], 1 µl reverse primer [3 µM] and 5 µl PowerUp™ SYBR™ Green Master Mix (Thermo Fisher Scientific, Waltham, Massachusetts, USA). The thermal cycling profile was set up as follows: initial step at 50°C for 2 min, followed by initial denaturation for 3 min at 95°C, then 40 cycles of 15 sec 95°C denaturation, 30 sec annealing at 58°C, 30 sec elongation at 72°C. In addition to the thermal cycling, a melting curve analysis was performed to validate the synthesis of a single product: 15 sec 95°C, followed by 60°C for 1 min and then ramp up in steps of 0.3°C until 95°C, lastly 95°C on hold for 15 sec.

Relative transcript levels were calculated using the $2^{-\Delta\Delta Ct}$ method described by Livak and Schmittgen (2001). Mean Ct values of three technical replicates were first normalised against an internal control, the housekeeping gene *EF1α* (Solyc06g005060), and subsequently normalised against the indicated control. qRT-PCR was performed in biological replicates of the indicated amount.

3.19 Gel electrophoresis

Nucleic acids were separated based on their size in agarose gels of the indicated percentage, along with GeneRuler™ DNA Ladder Mix (Thermo Fisher Scientific) as size reference. Prior to loading, the samples were mixed with 6x orange G loading buffer (0.1% (w/v) orange G, 10% (w/v) glycerol). RNA was denatured at 70°C for 2 min, followed by cooling on ice for 3 minutes. Agarose gels were prepared with and run in TTE buffer (90 mM Tris, 30 mM taurine, 1 mM EDTA pH 8.0) at 300 V for the desired duration. The nucleic acids were visualised on a UV trans-illuminator following staining of the gel in 0.5 mg/ml ethidium bromide for 5-10 minutes.

3.20 Transformation of competent bacteria

Chemically competent *E. coli* DH5α (Dagert and Ehrlich, 1979) were transformed for plasmid amplification (section 3.21). Chemically competent *E. coli* LEMO21 (DE3) and *E. coli* BL21 star (DE3) pRARE were transformed for heterologous protein expression and subsequent protein purification (section 3.28). For plant transformation (section 3.24), chemically competent *Agrobacterium tumefaciens* strain GV3101 or strain EHA105 were used. Transformation was performed by heat stock similarly to the protocol described in Sambrook and Russel (2001). First, 50 µl of cells were mixed with 1 vol of transformation buffer (10 mM MOPS, 100 mM KCl, 45 mM $MnCl_2$, 10 mM $CaCl_2$,10 mM KAc) and the desired amount of DNA. After incubation on ice for 25 minutes, transformation was performed via 2 min heat shock at 42°C and subsequent chilling on ice for 5 minutes. Afterwards, 700 µl LB medium (1 % (w/v) bactotrypton, 0.5 % (w/v) yeast extract, 1 % (w/v) NaCl) was added and the cells were incubated at 37°C *(Agrobacterium*: 28°C) for 1.5 hours at 750 rpm to establish antibiotic resistance. Cells were collected by centrifugation at 5,000 rpm for 5 min at RT, resolubilised in 100 µl residual LB medium and subsequently plated on LB plates (LB medium with 20 g/L agar) containing desired antibiotics. Antibiotics were dependent on the plasmid that was introduced. 50 µg/ml kanamycin or 100 µg/ml ampicillin were commonly used. *E. coli* BL21 star (DE3) pRARE and *E. coli* LEMO21 (DE3) were grown in the presence of 34 µg/ml chloramphenicol. Single colonies could be obtained after incubation at 37°C overnight (*Agrobacterium*: 28°Cfor 2 days).

For generation of plant lines overexpressing GFP, *Agrobacterium tumefaciens* strain EHA 105 was transformed. For this, 50 µl cells were mixed with 1 µl DNA, transferred into a chilled cuvette and electroporated with the following settings: 1.8 kV, 335Ω, 15µF. Immediately after, the cells were mixed with 1 ml LB medium, transferred to a 1.5 ml tube, and then incubated at 28°C for 2 hours at 850 rpm. 100 µl of transformed cells were plated in LB plates containing 50 µg/ml rifampicin.

3.21 Plasmid isolation

Plasmid isolation procedures for sequencing during cloning processes (miniprep) or for protoplast transformation and preparation of IVT templates, were adapted based on the protocols described by Sambrooks and Russel (2001) and Ausubel et al. (2003).

3.21.1 Plasmid isolation (midi-preparation)

Plasmids of high concentration and purity were extracted from 100 ml transformed *E. coli* DH5α culture. The bacterial cells were pelleted by centrifugation at 11,000 rpm at 4°C for 2 minutes, followed by resolubilising in 3 ml lysis buffer (50 mM Tris/HCl, pH 8.0; 50 mM EDTA, pH 8.0; 15% sucrose). Then, the cells were lysed by alkaline lysis by addition of 7 ml 0.2 M NaOH/1% SDS, careful mixing and incubation at RT for 10 minutes. The pH was recovered by addition of 3.5 ml 5M KAc (295 g/L potassium acetate 115 ml/L acetic acid glacial, adjusted to pH 5.0) and plasmids were allowed to renature for 20 minutes on ice. Cellular debris was pelleted at 5,000 x g for 20 minutes at 4°C. Debris was further removed by passing the supernatant through wool. Next, nucleic acids were precipitated by adding 7 ml isopropanol, thorough mixing, and incubation at -20°C for at least 1 hour, followed by centrifugation at 11,000 rpm at 4°C for 20 minutes. The pellet was air-dried and subsequently resolubilised in 1 ml TE-buffer (10 mM Tris/HCl, pH 7.5; 1 mM EDTA, pH 8.0). Bacterial RNA was removed by addition of 1 ml 5 M LiCl/50 mM MOPS (pH 8.0), mixing and incubation on ice for at least 30 minutes, followed by centrifugation at 8,000 rpm for 10 minutes. Plasmid DNA was then precipitated from the supernatant by adding 0.1 vol 3 M NaOAc (pH 5.2) and 2.5 vol ethanol, mixing and incubation at -20°C for at least 30 minutes, followed by centrifugation at 11,000 rpm at 4°C for 20 minutes. The DNA pellet was air-dried and resolubilised in 300 µl TE-buffer. Residual bacterial RNA was removed by addition of 5 U RNase A (Roth) and 5 U RNase T1 (Thermo fisher) and incubation at 37°C for 30 minutes, followed by protein removal through addition of 30 µl proteinase K [100 mg/ml] (AppliChem GmbH) and 15 min incubation at 37°C. Finally, the plasmid DNA was purified by adding 1 vol phenol:chloroform:isoamylalcohol (25:24:1), thorough mixing and subsequent centrifugation at 14,000 rpm for 2 minutes at RT. Traces of phenol were removed by mixing the aqueous phase with 1 vol chloroform, mixing and 2 min centrifugation at 14,000 rpm. The plasmid DNA was precipitated from the aqueous phase by addition of 1/10 vol 3M NaOAc (pH 5.2) and 2.5 vol ethanol, followed by incubation at -20°C for at least 30 minutes and centrifugation at 14,000 rpm for 15 min at 4°C. The pellet was washed using 70% ethanol followed by 5 min centrifugation at 4°C. Then, the DNA pellet was air-dried at 42°C for 15 minutes and resolubilised in TE-buffer at 37°C for 30 minutes at 400 rpm. DNA was quantified using the NanoDrop spectrophotometer and adjusted to 1 µg/µl.

3.21.2 Plasmid isolation (mini-preparation)

Plasmids for sequencing after cloning were isolated using a shortened midi-preparation protocol.

1.5 ml transformed *E. coli* DH5α culture was pelleted by centrifugation at 8,000 rpm for 5 minutes, followed by solubilisation of the cell pellet in lysis buffer (50 mM Tris/HCl, pH 8.0; 50 mM EDTA, pH 8.0; 100 µg/ml RNase A) and lysed via alkaline lysis by addition of 200 µl 0.2 M NaOH/1% SDS and careful mixing. After incubation at RT for 5 minutes, the pH was recovered by addition of 150 µl 5M KAC (295 g/L potassium acetate, 115 ml/L acetic acid glacial, adjusted to pH 5.0) and careful mixing.

The samples were incubated on ice for 10 minutes. Cell debris was removed by centrifugation at 15,000 rpm for 15 minutes at 4°C. Afterwards, the supernatant was carefully transferred to a new tube and the plasmid DNA was precipitated by addition of 240 µl isopropanol followed by incubation on ice for at least 40 minutes. Following centrifugation at 15,000 rpm for 15 minutes at 4°C, the DNA pellet was washed with 500 µl 70% ice-cold ethanol and repeated centrifugation. The pellet was then dried at 55°C for 5 min and resolubilised in 30 µl pre-warmed ddH_2O at 55°C for 10 min.

3.22 Molecular cloning

Plasmids created in this study were cloned using the Traditional cloning approach, site-directed mutagenesis PCR (deletion PCR), Gibson assembly or Golden Gate cloning. Section 2.3 contains all plasmids with the corresponding cloning strategy, section 2.4 contains corresponding primer sequences. Constructs for protein expression in *E. coli* were cloned into a pMAL vector in which the MBP-His tag was removed and instead GB1-His was used. Constructs for expression in protoplasts or for IVT were cloned into a pRT vector. Binary vectors for *Agrobacterium tumefaciens* for plant transformation were cloned into pICH vectors using Golden Gate cloning. General cloning strategies are described below.

3.22.1 Traditional cloning

Traditional, T4-ligase based, cloning was performed similarly to the description by Sambrook and Russel (2001). The gene of interest was first amplified via PCR using primers with restriction sites as extensions. The PCR product was purified either by gel extraction using the E.Z.N.A Gel Extraction Kit (Omega Bio-Tek) or by precipitation: The PCR reactions were supplemented with 1/10 vol 3M NaOAc pH 5.2 and 2.5 vol ethanol, mixed and incubated at -20°C overnight. The DNA was pelleted by centrifugation at max. speed for 30 min at 4°C, followed by a wash step using 70% ethanol and subsequent centrifugation. After entire removal of the supernatant, the pellet was dried at 55°C for 5 min and resolubilised in ddH_2O. Purified PCR products as well as the vector with corresponding restriction sites were digested with the indicated restriction enzymes in appropriate buffer at 37°C overnight (reactions involving *BamHI* were performed in *BamHI* buffer for 1 hour). Digested products were separated on an agarose gel, subsequently gel purified and ligated over night at 16°C using T4 DNA ligase [5 U/µl] (Thermo fisher scientific) in the appropriate buffer in a total volume of 10-20 µl. The entire ligation was then transformed into *E. coli* DH5α. Positive clones were verified by colony-PCR, cultivated in 3 ml LB medium supplemented with antibiotics, followed by miniprep plasmid extraction (section 3.21.2) and further verification by digestion and sequencing. Constructs and details are listed in section 2.3.

3.22.2 Deletion PCR

Generation of domain mutant constructs was performed by PCR amplification of the entire plasmid using Phusion™ High-Fidelity DNA Polymerase (Thermo Fisher Scientific, Waltham, Massachusetts, USA) and phosphorylated primers flanking the deleted sequence, whereby both primers start exactly after the deleted sequence in a blunt-end fashion. Primers were phosphorylated by T4-polynucleotide kinase (PNK) (Thermo Fisher Scientific, Waltham, Massachusetts, USA) in buffer A at 37°C for 30 minutes, according to the manufacturer's instructions, and the reaction was stopped by incubation

at 70°C for 10 minutes. Following PCR, the template plasmid was removed by *DnpI* digestion (Thermo fisher scientific) (0.5 µl/20 µl PCR reaction) for 2 hours thrice. Next, the PCR products were purified by precipitation, resolubilised in 17 µl ddH_2O, self-ligated and introduced into *E. coli* DH5α (section 3.20 and 3.22.1). Generation of domain mutant constructs were generated using deletion PCR with help from Stavros Vraggalas. Domains were predicted using Pfam (Mistry et al., 2020). Constructs and details are listed in section 2.3.

3.22.3 Gibson assembly

Gibson assembly was used to assemble several DNA fragments into one final construct using overlapping sequences (Gibson et al., 2009). In brief, the 5' ends of the overlapping sequences are chewed back by exonuclease, followed by annealing of DNA fragments and 3' extension by DNA polymerase. Finally, the residual DNA nicks are sealed by DNA ligase or by endogenous *E. coli* ligases. Generation of Gibson primers was performed using the NEBuilder Assembly tool version 2.5.6 (New England Biolabs). Insert fragments were generated by PCR, followed by *DpnI* digestion and purification as described in section 3.22.1. 15 µl Gibson mastermix (133 mM Tris-HCl pH 7.5, 13.3 mM $MgCl_2$, 0.27 mM of dGTP, dATP, dTTP and dCTP each (NEB), 13.3 mM DTT, 6.67 % (w/v) PEG-8000, 1.33 mM NAD, 5.3 U/ml T5 exonuclease (NEB), 0.03 U/µl Phusion™ High-Fidelity DNA Polymerase (Thermo Fisher Scientific, Waltham, Massachusetts, USA) was mixed with 5 µl DNA (50-100 ng vector and a molar vector:insert ratio of 1:2). Assembly was carried out at 50°C for 1 hour. 4 µl of the reaction were transformed into *E. coli* DH5α (section 3.20). Constructs and details are listed in section 2.3.

3.22.4 Golden Gate cloning

The Golden gate procedure adapted from Engler et al (2014) was used to generate binary plasmids for *Agrobacterium*-mediated plant transformation. The procedure takes advantage of type IIs restriction enzymes (e. g. *BsaI*) whereby cleavage is performed outside of the recognition site. As the recognition sites are lost once the desired fragments are ligated, a cyclic digestion-ligation (dig/lig reaction) can be performed in which each cycle increases the number of final constructs. Construct generation is further described in sections 3.22.4.1 and 3.22.4.2; final constructs are listed in section 2.3.2.

3.22.4.1 Transgene constructs

Constructs for *Agrobacterium*-mediated introduction of transgenes into tomato plants were generated as follows. An already existing PCaMV35S:GFP fusion was PCR-amplified with primers introducing *BsaI* sites. The presence of an internal *BsaI* site was tackled by amplification of two fragments whereby the internal site was destroyed during dig/lig reaction. PCR amplicons for the inserts were purified by gel extraction. For cyclic dig/lig reactions, the following reaction was set up in 15 µl final volume: 100-200 ng of acceptor plasmid (here: pICH86966), insert PCR products in a molar vector:insert ratio of 1:2, 1x T4 ligase buffer and 5 Weiss U/µl T4 ligase (Thermo Fisher Scientific, Waltham, Massachusetts, USA), 10 U/µl *BsaI* (Thermo Fisher Scientific, Waltham, Massachusetts, USA). Dig/lig reactions were carried out in a thermocycler using the following profile: 20 sec 37°C, 26 cycles of 37°C for 3 min followed by 16°C for 4 min. The profile ended with 5 min 50°C followed by 5 min 80°C. The transfer DNA (T-DNA) in the final constructs finally consisted of the transgene driven by the CaMV35S promoter followed by the Cas9 gene driven by a d35S promoter along with a 35S-driven kanamycin

resistance cassette present on the destination vector for subsequent selection of successful transformants. 5 µl construct was transformed in *E. coli* DH5α (section 3.20). Selection was carried out by blue-white screening by addition of 0.02 % (w/v) X-gal to the LB plates. White colonies were further verified as described for Traditional cloning (section 3.22.1). Plant transformation is described in section 3.24.3.

3.22.4.2 Constructs for CRISPR/Cas9-mediated mutagenesis

Constructs for CRISPR/Cas9-mediated mutagenesis were generated using a two-step Golden Gate procedure.

First, the sequences of two crRNAs (two per *RS2Z* gene) were designed using CRISPR-PLANT (https://www.genome.arizona.edu/crispr/) (Table 18). Next, the crRNA encoding sequences were assembled with the tracrRNA encoding sequence to form the single guide RNAs (sgRNAs). This was achieved by PCR using a reverse primer containing the tracrRNA sequence. Simultaneously, *BsaI* sites were introduced. Next, the two sgRNA sequences were assembled with the *Arabidopsis thaliana* U6 promoter sequence (PAthU6) encoded in plasmid pICL01009 and flanked by *BsaI* sites. Using a dig/lig reaction as described above, the sgRNA and PAthU6 were assembled in a level 1 target vector (pICH47732) using the MoClo Toolkit (Addgene Kit #1000000044). In a second step, using *BpiI* type IIs restriction sites, the PAtU6:sgRNA1 PAtU6:sgRNA2 construct was subcloned to the final binary vector pICSL002208 (level 2 reaction), using pICHL41744 as end-linker. The T-DNA finally consisted of PAtU6:sgRNA1, PAtU6:sgRNA2, Pd35S:Cas9, along with a PCaMV35S-driven kanamycin resistance gene, neomycin phosphotransferase II (nptII), present on the destination vector for subsequent selection of successful transformants.

Table 18. sgRNA sequences for CRISPR/Cas9-mediated generation of *rs2z* mutant plant lines.

Plant line	Target gene	sgRNA1 (5'->3')	sgRNA2 (5'->3')	Construct
rs2z35 (S02.37)	*RS2Z35* (Solyc05g054920)	GGTGGCACACGCCTATATGT	GTGGAAGACGGTAGCCCAAC	S02-V420
rs2z36 (S02.38)	*RS2Z36* (Solyc09g005980)	GACGGACCCGTTCACGTGATC	GTGATGGACGCCGCATAATTG	S02-V421

3.23 DNA sequencing

Sequencing of DNA (plasmids, PCR products) was performed by Eurofins Genomics (Ebersberg, Germany) according to the company's requirements. Sequencing of large quantities of PCR products was conducted by Senckenberg institute (Frankfurt, Germany). Evaluation of sequencing results was obtained by sequence alignments in Clone manager.

3.24 Generation of mutant and transgenic plant lines

3.24.1 Generation of RS2Z mutant lines: CRISPR/Cas9-mediated mutagenesis

RS2Z mutant plants were generated by *Agrobacterium*-mediated introduction of a CRIPSR/Cas9 cassette into the tomato genome with the help of Daniela Bublak. The T-DNA-constructs included two

sgRNAs in one single construct targeting two different positions in the RRM. The generation of the constructs is described in section 3.22.4.

Wild type *Solanum lycopersicum* cv. Moneymaker plants were sown, germinated, and grown on ½-strength MS plates as described in section 3.2. *Agrobacterium tumefaciens* were transformed with the plasmid coding for the respective CRISPR/Cas9 cassette (section 3.20), verified using colony PCR (section 3.18.2), and cultivated in 3 ml LB with antibiotics (kanamycin for transformed plasmid, gentamycin or rifampicin for helper plasmid, depending on the strain used) at 28°C and 120 rpm overnight. A 20 ml main culture was inoculated using 100 µl preculture, supplemented with 50 µg/ml kanamycin and 200 µM acetosyringone in DMSO, and subsequently grown at 28°C and 120 rpm until OD_{600} of 1.0. The doubling time was empirically determined as 1.75 h.

Agrobacterium-mediated transformation is based on the procedure described by McCormick (1986). Cotyledons of 1-week-old seedlings were cut into pieces of 5x5 mm using a sterile surgical scalpel. Efficient penetration was improved by slight cutting of the adaxial leaf surface. Cut cotyledons were placed on sterile wet filter paper in glass dishes with the adaxial side facing downwards. Afterwards, the 20 ml bacterial culture was added to the glass dish and incubated for 10 min. The cotyledon pieces (explants) were then transferred onto petri-dishes containing co-cultivation medium (1x MS medium, 0.8% (w/v) agar, 2% (w/v) glucose, 1 mM MES, 0.75 µg/ml trans-Zeatin, 1 µg/ml IAA, 200 µM acetosyringone. Adjusted to pH 5.7 using KOH) with the adaxial side facing down, following removal of excess bacterial suspension by dipping on sterile filter paper. Explants and bacteria were co-cultivated in the dark at 25°C for two days. Afterwards, agrobacteria were removed by washing explants in sterile ddH_2O, followed by two washes in 100 mg/ml Timentin (Duchefa Biochemie, Haarlem, Netherlands), followed by one final wash in sterile ddH_2O. Washed explants were then placed on sterile filter paper to remove excess liquid and subsequently transferred onto shoot induction medium (1x MS medium, 0.8% (w/v) agar, 2% (w/v) glucose, 1 mM MES, 0.75 µg/ml trans-Zeatin, 1 µg/ml IAA, 300 µg/ml Timentin, 100 µg/ml kanamycin, adjusted to pH 5.7 using KOH) with the adaxial side facing down. Explants were transferred onto fresh medium every two weeks. Transformed explants developed a callus-structure while non-transformed explants were kanamycin-sensitive. As soon as shoots emerged, explants were transferred onto shoot elongation medium (1x MS medium, 0.8% (w/v) agar, 2% (w/v) glucose, 1 mM MES, 0.1 µg/ml trans-Zeatin, 0.05 µg/ml IAA, 300 µg/ml Timentin, 100 µg/ml kanamycin, adjusted to pH 5.7 using KOH) in Magenta plant tissue culture boxes (Magenta LLC, New Ave, Lockport, USA). Explants were transferred onto fresh medium every two weeks until the shoots reached 3-4 cm in height. Then, the explant was detached from the callus and transferred into root inducing medium (1x MS medium, 0.8% (w/v) agar, 2% (w/v) glucose, 1 mM MES, 0.2 µg/ml IBA, 400 µg/ml carbenicillin, adjusted to pH 5.7 using KOH). Subsequently, plants with developed roots were transferred to soil and grown in the green house. These plants represent the T0 generation. Selfed T0 plants gave rise to the T1 generation. Mutant *rs2z35* and *rs2z36* plants were generated with the help of Daniela Bublak, Stavros Vraggalas and Sotirios Fragkostefanakis.

3.24.2 Screening of mutant plants

Mutant plants were genotyped in every generation by genomic DNA extraction (section 3.24.6) followed by PCR-amplification of the *RS2Z35* or *RS2Z36* locus, respectively, purification of PCR products and sequencing (section 3.23). Heterozygous plants showed overlapping peaks in electropherograms coming from the wild type (WT) and mutant allele, respectively. In The T2 generation, the absence of the T-DNA was verified using PCR-amplification of the Cas9 gene.

Potential CRISPR/Cas9 off-targets were predicted using CCTop (Stemmer et al., 2015) allowing up to 4 mismatches. The onset of off-targets in exonic regions were ruled out by PCR-amplification of the genomic sequence of the potentially impacted genes (Solyc02g093970 and Solyc08g048090) from homozygous mutant plants, followed by purification of PCR products and sequencing.

3.24.3 Generation of transgenic plants

Plants stably overexpressing GFP were generated by agrobacterium-mediated introduction of a gene cassette including GFP downstream of a CaMV35S promoter into the tomato genome. For this, *Agrobacterium tumefaciens* was transformed with the plasmid coding for PCaMV35S:GFP (S02-V480). Generation of the construct is described in section 3.22.4. The protocol for plant transformation was otherwise identical to the generation of mutant plants (section 3.24.1). *GFP-RS2Z35* and *GFP-RS2Z36* overexpression lines were generated by Löchli (2020) using the same approach.

3.24.4 Screening of transgenic plants

Transgenic plants of the T0 generation were genotyped first by genomic DNA extraction followed by PCR-amplification of GFP, and second by verification of expression by protein extraction followed by immunoblot analysis. Genotyping of *GFP-RS2Z* plants of the T0 generation was carried out by Löchli (2020) the same way. Plants of the T1 generation and higher were first screened by kanamycin spray (Weide and Zabel, 1989). 3-4 weeks after germination, leaves of young plants were sprayed with kanamycin solution (0.5 mg/ml kanamycin sulfate, 0.05% sapogenat) on three consecutive days. Leaf bleaching of WT and non-transgenic plants could be observed approximately two days after the last spraying. Kanamycin tolerant plants were further genotyped by immunoblot analysis detecting GFP. Only plants expressing the respective transgene were kept.

3.24.5 Crossing of plant lines

Double mutants were created by crossing homozygous, T-DNA-free single mutants following the guidelines described by Chetelat and Peacock (2013). In short, flowers were emasculated by removal of petals. Pollen was collected from the male parent plant and applied to the stigma of the emasculated flower. Presence of both mutations in the following generation (F1) was confirmed by PCR amplification of genomic regions coding for *RS2Z35* and *RS2Z36* and subsequent sequencing (section 3.24.2). F1 plants were selfed and resulting F2 plants were screened for homozygous mutation for both genes via PCR amplification of the mutated gene followed by sequencing.

3.24.6 Genomic DNA extraction from plant leaves

Extraction of genomic DNA (gDNA) was performed following homogenization of one young tomato leaf (approximately 30 µg) using a 1.5 ml-Eppendorf tube micropestle in the presence of 200 µl DNA

extraction buffer (100 mM Tris-HCl, pH 8.0; 700 mM NaCl; 50 mM EDTA, pH 8.0). The lysate was mixed by vortexing and incubated for 15 min at 65°C and 600 rpm in a total volume of 800 µl extraction buffer. Afterwards, the lysate is thoroughly mixed by vortexing and cooled down at RT for 1 minute, followed by addition of 390 µl of chloroform:isoamylalcohol (24:1). Phase separation is aided by incubation at RT for 5 minutes at 600 rpm with occasional inverting, followed by centrifugation at 14,000 rpm for 2 minutes. 720 µl of the aqueous phase was then transferred to a new tube and incubated with 10 µl RNase A [1 µg/µl] for 10 min at 37°C. Genomic DNA is precipitated by adding 700 µl isopropanol, careful mixing, incubation at RT for 2 minutes and subsequent centrifugation at 14,000 rpm for 5 to 10 minutes. The DNA pellet is then washed using 1 ml ice-cold 70% ethanol followed by centrifugation at 14,000 rpm for 5 minutes. After complete removal of the supernatant, the pellet was dried at 42°C for 15 minutes and resolubilised in 100 µl prewarmed (65°C) ddH_2O. Resolubilisation was aided by incubation at 65°C for 10 minutes at 300 rpm. Genomic DNA integrity was evaluated by gel electrophoresis as well as by PCR amplifying *EF1α*. Isolated gDNA was stored at 4°C.

3.25 *In vitro* transcription (IVT)

RNAs used for RNA electromobility shift assay (RNA EMSA) were *in vitro* transcribed using plasmid templates. Each RNA sequence was cloned downstream of a T7-promoter and upstream of the SP6 promoter sequence followed by a *SpeI* restriction site (see section 2.3 for the plasmid constructs). The RNA sequences are depicted in Supplemental Figure 1.

Purified template plasmids were linearised using *SpeI* at 37°C overnight in corresponding buffer. Templates were purified following verification of complete linearisation via gel electrophoresis. First, samples were diluted to 400 µl total volume and mixed with 1 vol phenol:chloroform:isoamylalcohol (25:24:1), centrifuged at maximum speed for 2 min at RT. Phenolic residues were removed by mixing the aqueous phase with 1 vol chloroform, followed by centrifugation. DNA was then precipitated from the aqueous phase by addition of 1/10 vol 3M NaOAc pH 5.2 and 2.5 vol ethanol and kept at -20°C for at least 30 minutes. DNA pellets were obtained by centrifugation at max. speed at 4°C for 30 minutes, followed by two washes using 70% ethanol. DNA pellets were dried for 5 min at 55°C and subsequently resolubilised in 20 µl DEPC-treated ddH_2O. The DNA concentration was determined using the NanoDrop spectrophotometer.

RNA was *in vitro* transcribed using the T7 High Yield RNA Synthesis Kit (NEB) following the manufacturer's instructions. After transcription at 37°C for 2 hours, DNA templates were removed by addition of 2 µl RNase-free DNaseI (10 U/µl; Roche) and incubation at 37°C for 30 min. Afterwards, the RNA was purified by addition of 1 vol acidic phenol:chloroform:isoamylalcohol (25:24:1), thorough mixing and centrifugation at max. speed for 2 min at RT. Phenolic residues were removed by mixing the aqueous phase with 1 vol chloroform, followed by centrifugation. The chloroform step was repeated once more. Next, the RNA was precipitated from the aqueous phase by addition of 1/10 vol 3M NaOAc pH 5.2 and 2.5 vol ethanol and kept at -20°C overnight. After centrifugation at max. speed for 30 min at 4°C, the RNA pellet was washed with 70% ethanol at least thrice. Finally, the RNA pellet was air dried at 55°C for 4 minutes, followed by resolubilisation in 25 µl DEPC-treated ddH_2O at 55°C

for 10 min. RNA concentration was determined by absorption at 260 nm using the NanoDrop spectrophotometer. RNA purity and integrity were evaluated by gel electrophoresis followed by ethidium bromide (EtBr) staining.

3.26 RNA labeling

For RNA EMSA, *in vitro* transcribed RNAs were indirectly fluorescence-labelled using a method described by Wang et al. (2010). Hereby, RNAs were mixed with a 5'Cy5-labelled DNA oligonucleotide (Cy5-oligo) complementary to the SP6 promoter sequence located downstream of the RNA sequence of interest. RNA and Cy5-oligo were mixed in a molar ratio of 2:1 (optimal ratio was empirically determined) in RNA annealing buffer (10 mM Tris-HCl pH 8.0, 50 mM NaCl, 1 mM EDTA pH 8.0) and annealed by denaturation and slow cool down to RT to allow refolding of the RNA and simultaneous annealing of RNA and Cy5-oligo. Annealing was performed in a PCR thermocycler with the following settings: 3 min 90°C denaturation, 45 min ramp to 25°C with 0.1°C/s. RNA was kept at 4°C and used for RNA EMSA the same day to avoid structure changes that could arise from freezing and thawing. Labelling reactions were calculated so that they could directly be used for EMSA further dilutions. RNA labelling was evaluated via PAGE using native 5% polyacrylamide gels (0.5x TBE, 5% acrylamide, 0.035 % APS, 0.18 % TEMED) in 0.5x TBE (44.58 mM Tris, 44.45 mM boric acid, 0.5 mM EDTA pH 8.0).

3.27 RNA electromobility shift assay (RNA EMSA)

Investigation of binding affinities of RS2Z proteins towards HsfA2 intron 2 were performed using RNA EMSA based on the protocol by Rio (2014). For this, indirectly fluorescence labelled RNAs (section 3.26) were incubated with purified recombinant RS2Z proteins (section 3.28) and subsequently run on native polyacrylamide gels. Recombinant GB1-His-RS2Z proteins were diluted to the desired concentrations using protein storage buffer (section 3.28.6). Binding reactions were composed of 1 µl labelled RNA (0.6 pmol/reaction = 30 nM), 4 µl recombinant protein and 11 µl binding buffer (20 mM Tris-HCl pH 8.0, 100 mM KCl, 1 mM $MgCl_2$, 5% (w/v) glycerol, 0.01 % (v/v) NP40 substitute, 1 mM DTT, 10 µg/ml BSA, 0.1 mM $ZnSO_4$, 1 U/µl Ribolock, 28x molar access tRNA *E. coli* MRE600, 1x protease inhibitor cocktail, EDTA-free). tRNA content in binding buffer was adjusted based on the final concentration of labelled RNA to be used. In all reactions, tRNA was present in 28x molar excess compared to RNA of interest. In competitor assays, instead of tRNA, unlabelled RNA of interest was added to the binding buffer resulting in a 28x molar excess. Binding reactions were mixed by brief vortexing, subsequent quick spin in a tabletop centrifuge and incubated at RT for 35 min. Afterwards 4 µl 6x red loading buffer (10 mM Tris-HCl pH 8.0, 100 mM KCl, 30% (w/v) glycerol, 0.02% (w/v) cresol red, 0.02 % (w/v) bromophenol blue) were added and samples were mixed carefully by flicking against the tubes followed by a quick spin in a tabletop centrifuge. The emission of light at the same wavelength as Cy5 prohibited the use of xylene cyanole in the loading buffer. Samples of 20 µl total volume were then loaded onto 5% native polyacrylamide gels entirely to resolve the binding products. Gels described in section 3.26 were polymerized at RT for at least 1 hour and pre-run at 200 V for at least 30 minutes. RNAs and RNA-protein complexes were separated at 200V for approximately 45 minutes. Fluorescent signals were detected in-gel using a Typhoon scanner with the following settings: Laser 633 nm, Emission filter 670 BP 30 Cy5, Gel + 3 mm.

3.28 Expression and purification of recombinant proteins in *E. coli*

3.28.1 Expression and lysis

GFP-V_HH nanobodies (further referred to as nanobodies) for RIP as well as GB1-His-RS2Z fusion proteins for EMSA, were expressed and purified from transformed *E. coli* based on the workflow described by Schlegel et al. (2012). The GFP nanobody expressed in *E. coli B*L21 star (DE3) pRARE which supplements rare tRNAs. GB1-His-RS2Z proteins were expressed in *E. coli* LEMO21 (DE3) which allows tunable expression of the recombinant protein. Addition of L-rhamnose activates the transcription of T7Lys, a natural inhibitor of the T7 RNA-polymerase (T7RNAP), under the control of the rhaBAD promoter, thereby allowing controlled T7RNAP induction by isopropyl-ß-D-1-thiogalacto-pyranoside (IPTG) and ultimately fine tuning of recombinant protein expression (Wagner et al., 2008).

Plasmids for protein expression are described in section 2.3. Single colonies were used for inoculation of 100 ml pre-culture (100 ml LB-medium supplemented with appropriate antibiotics). For *E. coli* LEMO21 (DE3) cells, 0.5 µM L-Rhamnose was added to prevent leaky expression. Following incubation overnight at 37°C, a 2 L main culture was inoculated with a starting OD_{600} of 0.1 and grown until OD_{600} of 0.6. Expression was induced by addition of 0.1-1 mM IPTG (Thermo Fisher Scientific, Waltham, Massachusetts, USA). RS2Z-protein expressing cultures were further supplemented with 0.1 mM $ZnSO_4$. Expression took place for 16 hours at 37°C and 120 rpm. An 800 µl aliquot was taken prior to induction and again after expression for expression control. The cells were pelleted and resuspended in 100 µl 1x SDS buffer. To normalise for the density of the culture, the pellet after expression was resuspended in ((ODend/ODstart) x 100 µl) SDS buffer. Cultures were supplemented with 1 mM PMSF [stock solution: 100 mM in isopropanol] 15 minutes prior to harvest to inhibit protease activity. Afterwards, cell pellets were collected by centrifugation at 5,000 x g and 4°C for 15 minutes and stored at -20°C until further use. The pellets were resuspended in 5 ml lysis buffer/g pellet (50 mM HEPES, pH 8.5 (for nanobody: pH 7.6); 0.5 M NaCl; 0.1x protease inhibitor cocktail, EDTA-free (Roche); 5% glycerol, 2 mM ß-mercaptoethanol, for RS2Z proteins: 0.2 mM $ZnSO_4$). Cells were lysed by incubation with a spatula tip of lysozyme for 30 min at 4°C. Due to the similar size of lysozyme and GFP-nanobodies, this was omitted for nanobody purification. A spatula tip of DNaseI was added to remove DNA and therefore ensure a lighter consistency of the lysate. Next, complete lysis was conducted via French press at 1,200 psi twice (alternatively, sonication at 80% power and 40 cycles with 20 strokes thrice and 20 seconds break in between), followed by lysate clearing via centrifugation at 6,000 x g at 4°C for 15 minutes and subsequent transfer of the supernatant to new falcon tubes. The pellet containing insoluble proteins was resolubilised in (50 mM Tris-HCl, pH 8.0; 8 M Urea) using the same volume as lysis buffer used. A sample was taken from resolubilised pellet (P, pellet, insoluble proteins) and supernatant (Lysate).

3.28.2 Removal of endogenous RNAs

For SR proteins, endogenous RNAs were removed by incubation with Polymin P (=polyethyleneimine). Polymin P [2.5% (w/v), pH 7.2] was added dropwise with simultaneous shaking of the samples until a final concentration of 0.3 % (w/v). The samples were further incubated at 4°C for 20 minutes while

shaking and subsequently cleared by centrifugation in SS-34 buckets at 11,000 rpm and 4°C for 30 minutes. The supernatant was transferred into new falcon tubes. Subsequently, residual traces of Polymin P that would interfere with downstream purification were removed by protein precipitation.

3.28.3 Protein precipitation

Proteins were precipitated by addition of $(NH_4)_2SO_4$ at 60% saturation (0.36 g/ml lysate) and incubation at 4°C overnight with gentle agitation. Proteins were collected by centrifugation in SS-34 buckets at 27,000 x g and 4°C for 20 minutes. Following removal of the supernatant, protein pellets were resolubilised in lysis buffer. The samples were then cleared by 10 minutes centrifugation at 27,000 x g and 4°C. Finally, the supernatant was transferred into a new falcon tube and an aliquot was taken for SDS-PAGE (Input).

3.28.4 Immobilized metal affinity chromatography

His-tagged recombinant proteins were purified using the immobilized metal affinity chromatography (IMAC) procedure based on the interaction of histidine with transition metals like Ni^{2+} (Porath et al., 1975). 0.5 - 1 ml (=1 bed volume (BV)) nickel nitrilotriacetic acid (Ni-NTA) matrix (Ni-NTA agarose, Qiagen, Düsseldorf, Germany) was equilibrated using 10 BV lysis buffer, then mixed with lysate and subsequently incubated with gentle agitation for 1 h at 4°C (batch binding). Afterwards, the flowthrough was collected, and an aliquot was taken for SDS-PAGE (flowthrough). The matrix was then washed with 10 BV wash buffer 1 (30 mM HEPES, pH 8.5 (nanobody: pH 7.6); 0.3 M NaCl (nanobody: 0.15 M); 15 mM imidazole, for SR proteins: 2 mM ß-mercaptoethanol. For RS2Z proteins: 0.2 mM $ZnSO_4$), followed by 10 BV buffer 2 (30 mM HEPES, pH 8.5 (nanobody: pH 7.6); 1 M NaCl; 15 mM imidazole, for SR proteins: 2 mM ß-mercaptoethanol) containing high salt in order to remove impurities bound due to electrostatic effects; and again 10 BV wash buffer 1 to reduce the salt concentration. Proteins were eluted five in 5 steps using 1 BV elution buffer (30 mM HEPES pH 8.5 (nanobody: pH 7.6); 0.3 M NaCl (nanobody: 0.15 M); 10% glycerol; 500 mM imidazole; 1x protease inhibitor cocktail, EDTA-free; for SR proteins: 2 mM ß-mercaptoethanol; for RS2Z proteins: 0.2 mM $ZnSO_4$). An aliquot was taken from each fraction.

Successful expression and purification were determined via SDS-PAGE (section 3.10). Sample amounts were adjusted to the total volume of each fraction; volumes used are indicated in the results section, e. g. pre-induction 0.001 % correspond to 0.001% of the total sample volume (2 L).

3.28.5 Ion exchange chromatography (IEX)

SR proteins were further purified using cation exchange chromatography to remove the contamination of an approximately 66 kDa *E. coli* protein that is co-eluted using Ni-NTA purification. For this, elution fractions following Ni-NTA purification were pooled and precipitated using $(NH_4)_2SO_4$ as described above (section 3.28.3). Proteins were resolubilised in 3 ml IEX start buffer (50 mM MES, pH 6.0; 10 mM NaCl) at pH 6.0 to ensure a positive charge (Table 19). This allowed separation from endogenous *E. coli* proteins mostly having an isoelectric point (pI) of around 5 (Schwartz and Russell, 2001) and thus predominantly negative charge at pH 6.0. The cation exchange matrix (CM-Sephadex C-50-120) was previously quelled at 95°C for 2 h in 150 mM NaCl and subsequently washed with 10 BV 20% ethanol

and stored as 75% slurry in 20% ethanol at 4°C until further use. 4 ml matrix (5.33 ml slurry) were equilibrated using 10 BV start buffer. Next, the eluate was added to the matrix and incubated for 1 h at 4°C with gentle agitation. The flowthrough was collected, and the matrix was then washed with 1 BV start buffer, followed by another wash using 3 BV start buffer. Afterwards, the proteins were eluted step-wise using 1 BV each with increasing amounts of NaCl (0.1 increments from 0.1 to 0.9 M). Samples were taken from the input, the flowthrough, first wash and every elution fraction. Elution profiles were evaluated using SDS-PAGE and desired fractions were pooled and supplemented with 5% glycerol and 0.1 mM $ZnSO_4$ (RS2Z proteins only).

Table 19. **Size and pI of recombinant SR proteins and the respective expected net charge at pH 6.0**

	MW [kDa]	pI	Net charge at pH 6.0
GB1-His-RS2Z35(RBD)	23.36	7.69	+
GB1-His-RS2Z36(RBD)	23.75	8.48	+
GB1-His-SC30b(RRM)	19.77	6.5	(+)

3.28.6 Protein concentration and buffer exchange

Elution fractions after IEX purification (SR proteins) or directly after IMAC purification (GFP-nanobody) were concentrated to 2.5 ml using an Amicon®Ultra-15 centrifugal filter with 3 kDa cutoff (Millipore, München, Germany). Subsequently, protein samples were passed to PD-10 buffer exchange columns (Cytiva, Marlborough, Massachusetts, USA) to exchange the buffer to protein storage buffer (50 mM Tris pH 7.6, 0.15 M NaCl, 10% glycerol, RS2Z proteins: 0.1 mM $ZnSO_4$). Nanobodies were further purified by passing the protein sample through an Amicon®Ultra-15 centrifugal filter (Millipore, München, Germany) with a 50 kDa cutoff, allowing 15 kDa-nanobodies to pass through while retaining larger *E. coli* proteins. Nanobodies were quantified using the NanoDrop as described in 3.9.3. GB1-His-SR proteins were quantified via SDS-PAGE as described in 3.9.4.

3.29 RNA immunoprecipitation (RIP)

The RIP procedure was adapted and modified from Köster et al. (2014) and carried out as described in detail in the following sections 3.29.

3.29.1 Heat stress treatment and formaldehyde crosslinking

Young leaves from transgenic plants (PCaMV35S:GFP, PCaMV35S:GFP-RS2Z35, PCaMV35S:GFP-RS2Z36) were subjected to 1 h 40°C in sealed petri dishes in a water bath, whereby leaves from several heterozygous plants were pooled to equalize expression levels. Following HS, RNA-protein interactions were maintained by formaldehyde crosslinking. For this, leaves were placed in glass dishes containing 0.5% formaldehyde in PBS and kept in solution by placing a light-weight metal mesh on top. Vacuum infiltration was performed for 20 min at 900 mbar, followed by formaldehyde quenching by replacing the formaldehyde solution with 125 mM Glycine in PBS, followed by vacuum infiltration for 5 min at 900 mbar. Afterwards, the leaves were washed with ice-cold sterile H_2O four times, dried, weighed and snap-frozen in liquid nitrogen.

Due to the nature of formaldehyde to not only crosslink RNA-protein complexes but also DNA-protein as well as multiprotein complexes, overcrosslinking would result in protein loss due to the formation of insoluble aggregates that are subsequently removed during lysate clearing (Sutherland et al., 2008; Klockenbusch and Kast, 2010). After application of 1% formaldehyde as used for RIP performed in Arabidopsis (Köster et al, 2014), protein recovery after IP was drastically reduced (not shown). The determination of optimal formaldehyde concentration was by assessing the recovery of large rRNAs extracted with and without reverse crosslinking, thus using the recovery of large rRNAs as a crosslink marker. For this, crosslinking was performed using 100 mg leaf material in formaldehyde solution of different concentration, followed by RNA extraction with and without reverse crosslinking. Since there was no difference in rRNA recovery between 0.5% and 1% formaldehyde (Supplemental Fig. 2A), overcrosslinking was avoided by using 0.5% formaldehyde instead.

3.29.2 Lysis

RIP-qPCR and RIP-Seq experiments were performed in four and three biological replicates, respectively. For each replicate, 1 g crosslinked plant material per genotype was ground using the tissue lyser (2 x 30 seconds, 1/30). Subsequently, the ground crosslinked leaf material was lysed, whereby the optimal lysis buffer composition was determined empirically and based on the commonly used RIPA buffer, resulting in the addition of 10% glycerol to aid protein stability. Furthermore, high salt proved to be necessary for the efficiently extraction SR proteins (Supplemental Fig. 2B). To lyse the cells, the metal ball was kept inside the tube and 2 vol C2 lysis buffer (50 mM Tris-HCl pH 7.6, 4 mM $MgCl_2$, 500 mM NaCl, 1% NP40 substitute, 1% Sodium deoxycholate, 10% glycerol, 0.1% SDS, 1 mM NaF, 5 mM DTT, 1x EDTA-free Protease inhibitor cocktail (1 tablet/10 ml buffer, Roche), Ribolock [100 U/ml]) were added, followed by incubation at 40°C and 1,400 rpm for approximately 30 seconds to facilitate rapid mixture of the ground leaf material and the buffer. Subsequently, the lysates were incubated on ice for 5 min, during which they were vortexed thoroughly several times, followed by lysate clearing by centrifugation at max. speed for 10 min at 4°C. Supernatants were pooled per genotype, further cleared by filtration through a syringe filter (Filtropur S. 0.45 µm) and collected in 15 ml falcon tubes. The total lysate volume was adjusted to 2 ml if necessary, using C2 buffer, followed by addition of 2 vol dilution buffer (50 mM Tris-HCl pH 7.6, 4 mM $MgCl_2$, 10% glycerol, 1 mM NaF, 5 mM DTT, 1x EDTA-free Protease inhibitor cocktail (1 tablet/10 ml buffer, Roche), Ribolock [100 U/ml]) to reduce the salt content to 167 mM. 1.17 % of the lysate (70 µl) was mixed with 750 µl TRIZol for RNA extraction (see below).

Establishing of a lysis buffer that allowed efficient recovery of nuclei and GFP-RS2Z proteins as well as maintained GFP-RS2Z protein integrity was performed empirically by performing lysis of 100 mg ground leaf material in buffers of different composition followed by immunoblot analysis.

3.29.3 Nanobody-bead preparation

45 µl PureCube Ni-NTA Magbeads (15 µl per sample) (Cube biotech, Monheim, Germany) were equilibrated using protein storage buffer (50 mM HEPES pH 7.6, 150 mM NaCl, 10% glycerol) and then mixed with 150 µg purified His-tagged GFP-nanobody (50 µg per sample) in 1 ml Nanobody binding buffer (50 mM HEPES pH 7.6, 150 mM NaCl, 10% glycerol, Heparin [500 ng/µl], Ribolock [40 U/µl]).

Ni-NTA Magbeads were incubated with GFP-nanobodies for 1 h at 4°C on a rotation wheel. Afterwards, beads were washed two times with 400 µl Nanobody wash buffer (50 mM HEPES pH 7.6, 150 mM NaCl, 10% glycerol, Heparin [200 ng/µl], Ribolock [40 U/µl]). Finally, the beads were resuspended in 320 µl last wash buffer (50 mM Tris-HCl pH 7.6, 4 mM $MgCl_2$, 150 mM NaCl, 1 mM NaF, 5 mM DTT, 1x EDTA-free Protease inhibitor cocktail (1 tablet/10 ml buffer, Roche), Ribolock [50 U/ml]) and distributed into three 1.5 ml-tubes for equal distribution between the three samples.

3.29.4 RIP

The diluted lysate (6 ml) was mixed with 100 µl Nanobody-bound Ni-NTA magnetic beads in last wash buffer in 15 ml falcon tubes and incubated on a rotation shaker for 1 h at 4°C. Afterwards, the samples were distributed into 2 ml Eppendorf tubes in a magnetic separator. Following removal of the supernatant, the magnetic beads were resuspended in a total of 400 µl wash buffer (50 mM Tris-HCl pH 7.6, 4 mM $MgCl_2$, 500 mM NaCl, 2 M Urea, 1% NP40 substitute, 1% Sodium deoxycholate, 10% glycerol, 0.1% SDS, 1 mM NaF, 5 mM DTT, 1x EDTA-free Protease inhibitor cocktail (1 tablet/10 ml buffer, Roche), Ribolock [50 U/ml]), transferred into a new tube and washed three times with 400 µl wash buffer for 10 min on a rotation wheel at 4°C. Afterwards, the magnetic beads were again transferred to a new tube and washed twice. Finally, the beads were washed for 5 min using 400 µl last wash buffer.

Recovery of non-specifically bound RNAs to the Ni-NTA magnetic beads was avoided by elution using imidazole-containing elution buffer followed by RNA extraction, instead of direct incubation of the beads in TRIZol. Nanobodies and bound RNA-protein complexes were eluted by 5 min incubation in 40 µl elution buffer (25 mM Tris-HCl pH 7.6, 150 mM NaCl, 5 mM EDTA, 400 mM Imidazole, 1x EDTA-free Protease inhibitor cocktail (1 tablet/10 ml buffer, Roche), Ribolock [100 U/ml]) including repeated vortexing. The beads were collected on a magnetic separator and the supernatant was mixed with 750 µl TRIZol. Afterwards, a second elution using 30 µl elution buffer was performed. The second elution was then added to the TRIZol mixture.

3.29.5 RNA extraction

The whole elution fraction and the input aliquot (1.17%) were mixed with 750 µl TRIZol, followed by incubation for 7 min at 65°C and 1,400 rpm to reverse the formaldehyde crosslinking. The RNA was then extracted using either the standard TRIZol procedure (RIP-qPCR) or the Direct-zol MiniPrep kit (Zymo Research, Irvine, California, USA) (RIP-Seq).

3.29.6 RIP-qPCR

Following reverse crosslinking, the RNA was extracted using the standard TRIZol procedure (section 3.16) using 600 µl TRIZol per sample and adding 2 µl glycogen [5 mg/ml] as carrier prior to RNA precipitation. The RNA was eluted in 25 µl RNase-free ddH_2O. RNA concentration was determined using the NanoDrop spectrophotometer.

20 µl input and elution RNA, respectively, were used for cDNA synthesis using oligo(dT) primer in a total volume of 40 µl each (section 3.17). The cDNAs were diluted 1:2 for qRT-PCR (section 3.18.3). Relative enrichment was calculated using the $2^{-\Delta\Delta Ct}$ method by Livak and Schmittgen (2001) by

normalising the elution of each genotype to its corresponding input [ΔCt = Ct (IP) - Ct(Input)] and subsequent normalisation of RS2Z samples against GFP [ΔΔCt = ΔCt (RS2Z) - ΔCt(GFP)]. Fold changes were calculated by FC = $2^{-\Delta\Delta Ct}$ and subsequently log2-transformed (log2foldchange, LFC). Statistical analysis was performed using student's t-test on LFC values. Enrichment calculation based on % Input involving an adjustment of the 1% Input to 100% will give the same result for fold enrichments. In order to determine fold enrichments for genes that were not present in all samples, undetermined ΔCt values were set to 40 (observed in the case of *RS2Z* and *EF1α* transcripts but not *HSFA2*).

Since formaldehyde crosslinking not only crosslinks protein and RNA but also protein-protein interactions, enriched RNAs do not necessarily represent direct targets but also include indirect targets in which SR proteins could reside in the same complex or in close proximity. Therefore, enriched RNAs are further referred to as RS2Z-associated RNAs or RIP genes rather than direct targets.

3.29.7 RIP-Seq

Following reverse crosslinking, the RNA was extracted using DirectZol to ensure high quality and purity for subsequent library preparation. The procedure was performed according to the manufacturer's instructions, including 15 min DNaseI digestion which further allowed to omit any additional purification steps. The RNA was finally eluted from the columns in 25 µl RNase-free ddH_2O.

DirectZol extracted RNAs were quality assessed with the Agilent Bioanalyzer using the plant assay settings. Library preparation and high-throughput sequencing were performed by Admera Health, LLC (New Jersey, USA). Input RNA (RIN 6.6 - 7.1) was subjected to rRNA depletion using the QIAseq FastSelect kit, followed by library construction using the NEBNext Ultra II non-directional RNA Library Kit and subsequent paired-end RNA-sequencing (150 nt each direction, 60M total reads) on the Illumina NovaSeq 6000 platform. For IP samples, rRNA depletion was omitted. The library for replicate 1 was prepared using the same kit as for the input samples. For replicate 2 and 3, due to low RNA abundance, the SMARTer stranded Total RNA-seq kit V2 (TAKARA BIO INC.) was used.

Raw paired reads of 2x150 nt length were quality-evaluated using FastQC. Instead of adapter trimming and removal of low quality reads, reads were mapped against the tomato reference genome (*S. lycopersicum cv*. Heinz 1706, genome build 4.0) in a splice-aware manner (Fernandez-Pozo et al., 2014) using Star (Galaxy version 2.7.8a) (Dobin et al., 2012) with default settings, except for the following changes: --genomeSAindexNbases 14, --sjdbGTFfile ITAG4.0_gene_models.gff, --sjdbOverhang 149, --chimOutType don't report, --outFilterType yes, --outFilterMultimapNmax 1, --outFilterMismatchNmax 999, --outFilterMismatchNoverLmax 0.05.

The identity of unmapped reads was examined by mapping against eight representative rRNA databases using SortMeRNA (Kopylova and Touzet, 2012). Additionally, the unmapped reads were mapped against the tomato chloroplast (RefSeq accession: NC_007898.3) and mitochondrion full genomes (RefSeq assembly accession: GCA_000325825) as well as the human (GRCg38/hg38, Dec 2013) and *E. coli B*L21 genome (RefSeq assembly accession: GCF_013166975.1) using Star (Dobin et al., 2012).

Reads per gene were counted using htseq-count (Galaxy version 0.9.1) (Anders et al., 2015) with the following settings: --mode union. –stranded no, --minaqual 10, --type gene, --idattr ID.

Further, R (www.r-project.org) and the environment RStudio (www.rstudio.com) were used to analyse and visualise count data. Batch effects resulting from non-simultaneous library preparation and use of different library preparation kits were removed as follows: Read counts for input and IP samples were batch adjusted individually using ComBat-seq (sva package) (Zhang et al., 2020b; Leek et al., 2021). Exemplified code as follows:

```
batch <- colData(dds)$replicate

dds_adjusted <- ComBat_seq(counts = as.matrix(counts(dds)), batch = batch)
```

Batch-corrected read counts of input and IP samples were then merged to a count matrix. Subsequently, significant enrichment of transcripts in GFP-RS2Z samples relative to GFP was assessed as ratio over ratio ((IP for GFP-RS2Z / Input for GFP-RS2Z) / (IP for GFP / Input for GFP)). An assay identifier was assigned to input and IP datasets, respectively. Then, ratio over ratio calculation was performed individually for GFP-RS2Z35 over GFP and GFP-RS2Z36 over GFP. For each combination, the following code was used, following the description of DESeq2 developer Dr. Love: https://support.bioconductor.org/p/61509/ (accessed on 28.12.2021), employing a likelyhood test (LRT) to identify significantly different ratios in GFP-RS2Z against GFP. Hereby, a reduced model without the interaction term (assay:genotype) that represents the ratio over ratio is compared to the full model (genotype + assay + assay:genotype).

```
dds <- DESeqDataSetFromHTSeqCount(sampleTable = sampleTable, directory = mydir, design = ~ genotype + assay + assay:genotype)

ddsf <- DESeq(dds, test="LRT", reduced = ~ assay + genotype)

results(ddsf)
```

For each gene, an adjusted p-value (padj) was calculated based on the false discovery rate (FDR) determined using the Benjamini-Hochberg procedure (implemented in DESeq2). Subsequently, overestimation of LFC enrichment for low abundant transcripts was compensated by LFC shrinkage performed using the apeglm package (Zhu et al., 2019). Since transcripts are only scarcely annotated for tomato, enrichment analysis was performed for genes instead of individual transcripts. Finally, significantly enriched transcripts with shrunken LFCs > 2 and padj < 0.01 were referred to as RIP genes. As the RIP procedure is prone to high background noise, more stringent criteria were applied for RIP-Seq in contrast to differential expression (DE) analysis in order to minimise the detection of false positives.

Heatmaps were generated with the ComplexHeatmap package (Gu et al., 2016) depicting enrichment in *GFP-RS2Z35* or *GFP-RS2Z36* as shrunken LFC values relative to *GFP*.

To investigate whether RIP-enriched genes were primarily intron-containing, multiexon genes were determined as follows: Each gene with at least one transcript composed of two exons (multiexon gene) was determined as intron-containing. One-exon genes where therefore determined as intronless.

3.29.8 Immunoprecipitation (IP)

Validation of successful pulldown and establishing of IP-conditions for RIP were performed similar to the RIP protocol, but with less starting material (100 mg instead of 1 g) and instead of RNA, proteins were evaluated via immunoblot analysis. Changes compared to the RIP protocol (section 3.29.4) are as followed: Ribolock was omitted from all buffers. 10 µl PureCube Ni-NTA MagBeads and 25 µg purified nanobody were used. Lysate was cleared by centrifugation at 20,000 x g for 10 min twice instead of filtration. Samples were eluted in 42 µl elution buffer. Elutions and aliquots taken from input, flowthrough and the last wash fraction were supplemented with 4x Laemmli buffer and subsequently evaluated via immunoblot analysis, whereby the samples were loaded in amounts respective to their total volume.

The specificity of the RIP setup was validated by performing IP with and without addition of nanobody. The elution of RS2Z proteins was observed only when GFP-V_HH nanobody binding to the magnetic beads was performed, indicating that there was no substantial unspecific binding of RS2Z proteins to the beads (Supplemental Fig. 2C)

3.30 RNA sequencing

Excised leaves from six 6-week-old wild type and mutant plants were exposed to 1 h 40°C in sealed petri dishes in a water bath (control: 1 h 25°C). Total RNA was extracted using TRIZol as described in section 3.16. Subsequently, RNAs from two plants were pooled. Thereby, RNA-Seq was performed in 3 biological replicates for each condition and genotype. RNA integrity was evaluated on agarose gels as well as by using the Qubit IQ Assay kit (Thermo Fisher Scientific, Waltham, Massachusetts, USA), whereby all RNAs were of good integrity with IQ scores between 8.3 and 10.0. Genomic DNA was removed by performing additional RNA purification via DirectZol including 15 min DNaseI digestion. Library construction (NEBNext Ultra II non-directional RNA Library Kit with polyA selection) and subsequent paired-end RNA-sequencing (150 nt each direction, 40M reads in total, Illumina NovaSeq 6000) were performed by Admera Health, LLC (New Jersey, USA). Raw read in FASTQ format were quality-evaluated using FastQC. Instead of adapter trimming and removal of low-quality reads, reads were mapped against the tomato reference genome (Heinz genome build 4.0) using Star (Galaxy version 2.7.8a) (Dobin et al., 2012), as described for RIP-Seq in section 3.29.7. Uniquely aligned reads were subsequently used for downstream DE and DAS analysis (sections 3.30.1-2).

3.30.1 Differential expression (DE) analysis

For each sample, gene expression was quantified as absolute read count for each coding gene using htseq count (Anders et al., 2015), following the same approach as described for RIP-Seq (section 3.29.7).

Batch effects in the HS samples were identified by principal component analysis (PCA) performed in R and consequently removed using ComBat-Seq (Leek et al., 2021 and Zhang et al., 2020; Supplemental

Fig. 3). For this, batch removal was performed for HS samples only whereby replicates were defined as batches. A final count matrix was then assembled using the read counts of control samples and the batch-adjusted read counts for HS. Prior to DE analysis, low abundance transcripts with a read sum across all samples < 10 were considered as noise and therefore removed. DE analysis was then performed using DESeq2 (Love et al, 2014) and statistically different LFCs between the datasets were determined by using the Wald test (DESeq2 default), thereby obtaining DE between all possible combinations of datasets. The design for DESeq2 analysis was set as "genotype", whereby the genotype term contained both the genotype and the condition, e. g. "*rs2z35*_C" and "*rs2z35*_HS".

dds <- DESeqDataSetFromHTSeqCount(sampleTable = sampleTable, directory = mydir, design = ~genotype)

To compensate for the overestimation of fold changes for low expressed genes or those with high dispersion, LFC shrinkage was performed using the apeglm package (Zhu et al., 2019). Similarity of the datasets was visualised by PCA analysis included in the DESeq2 package.

Transcripts were assigned as significantly differently expressed when their expression levels relative to the control were I $\log_2$FC I > 0.5849 (foldchange of 1.5) with padj < 0.05. Statistical analysis on the distribution of p-values was performed using two-tailed paired Wilcoxon test with a significance threshold of 0.05.

For visualisation in heat maps, count data was log-transformed and subsequently Z-score normalised. All heat maps were generated using ComplexHeatmap in R (Gu et al., 2016). Clustering was performed by partition clustering (k-means), whereby hierarchical clustering (pearson) was applied to each slice (children); the parent dendrogram was then generated based on the mean values of each slice (Gu et al., 2016). Due to the large number of genes depicted in heat maps, dendrograms were not displayed.

3.30.2 Differential alternative splicing (DAS) analysis

For analysis of differential AS (DAS) relative to WT, mapped reads were analysed for usage of SS based on local splice variants (LSVs) using Majiq (version 2.2) (Vaquero-Garcia et al., 2016) with default settings, based on splice junction counts. LSV quantification was expressed as percent selected index (PSI, Ψ) for each splice junction, whereby relative changes between samples (e. g. WT HS vs *rs2z36* HS) were expressed as ΔPSI (ΔΨ). AS events with IΔPSII > 0.05 (--threshold 0.05; --non-changing-threshold 0.02) and a changing probability > 0.5 were considered significant. Majiq output was kindly provided by Dr. Mario Keller.

Identification of AS types based on the Majiq output was performed by Dr. Mario Keller (unpublished R package). In short, AS events were reduced to binary events, whereby splicing change in one junction must be met by inverse change of another junction by at least 50%. Complex events and those that did not meet the 50% criteria were filtered out. The output was kindly provided by Dr. Mario Keller.

Due to their low number, alternative first (AFE) and last exon events (ALE) were merged with simple cassette exons (SCE) and summarized as ES. Splicing changes were expressed for each splice junction as ΔPSI relative to the reference group (e. g. WT). For heatmap visualisation of ΔPSI values using the complex heatmap package (Gu et al., 2016), the direction of regulation was depicted relative to a

reference junction: the intron served as reference for IR events and the 5' inclusion junction of retained exons served as reference for ES events. For A5'SS and A3'SS events, the most 5' located splice (= upstream located) site served as reference. Any events that could not be identified in at least one dataset were excluded from the heatmap to avoid missing values that would otherwise have interfered with k-means clustering (8.4-14.1% of all events were filtered out).

3.30.3 Identification of gene classes of interest

Genes involved in RNA biosynthesis, RNA processing and protein homeostasis were identified by three combined methods: Mapman v4.0 (Schwacke et al., 2019), a classification and annotation framework; PANTHER v16.0 (Mi et al., 2021), a protein classification system that incorporates evolutionary relationships, and manual inspection of the ITAG 4.0 gene description (Fernandez-Poco et al., 2014). Genes identified by the three methods were then merged to a final set.

3.30.4 Singular GO term enrichment analysis (SEA)

Gene ontologies (GO) were used to describe global trends in the functional properties of regulated genes. Identification of enriched GO terms was performed by comparing the list of regulated genes to the appropriate background from which the list of regulated genes derived from. For DE genes (section 3.30.1), all expressed genes with a read sum > 10 across all datasets (WT and *rs2z* mutants under control and HS conditions) were defined as background. For DAS genes (section 3.30.2), the background consisted of those expressed genes that were identified to be alternatively spliced in the WT under control or HS conditions. For RIP genes (section 3.29.7), the background included all expressed genes with a read sum > 10 across all RIP input datasets (*GFP, GFP-RS2Z35, GFP-RS2Z36*).

First, gene IDs were converted into transcript IDs (ITAG 4.0 version) (Fernandez-Poco et al., 2014) using R and were subsequently passed to agriGO v2.0, a tool focused on agricultural species (Tian et al., 2017). Singular enrichment analysis (SEA) of GO terms in agriGO v2.0 was performed using default settings, including Fisher statistical analysis and Yekutieli FDR-correction with a significance level of 0.05, and a minimum number of mapping entries of 5. agriGO v2.0 employed the completed GO version 2016.

Due to the high number of significantly enriched GO terms, identified terms were clustered based on their similarity and thus reducing their redundancy using the rrvgo package (v1.8.0) in R (Sayols 2020). The similarity matrix was built using default settings (Resnik distance method). The *Arabidopsis thaliana* TAIR10 OrgDb object (v3.15.1) was used as database for GO terms (Carlson 2019). Clustered terms were then visualised as treemap plots with box sizes proportionate to significance levels.

3.31 Amino acid sequence alignment

Pairwise sequence alignments of RS2Z35 and RS2Z36 were performed using EMBOSS Needle with default settings (matrix: EBLOSUM62, Gap_penalty: 10.0, Extend_penalty: 0.5), employing the Needleman-Wunsch alignment algorithm (Rice et al., 2000).

4. Results

4.1 Regulation of *HSFA2* splicing by SR proteins

In the past decade, the long-underestimated extent of AS has been reported as an important layer for rapid stress regulation. AS reshapes the transcriptome in response to stress, impacting both the coding potential and transcript abundance. The HS-dependent AS of *HSFA2* (section 1.5.3), a core regulator of the HSR and thermotolerance, represents an example for stress-regulated transcript diversification through AS (Hu et al., 2020a). Furthermore, the splicing efficiency of *HSFA2* intron 2 correlates with HS adaption in wild and modern tomato species (Hu et al., 2020a).

As IR of *HSFA2* intron 2 is crucial for its function for ATT, splicing silencers represent ideal candidates for its regulation. SR proteins are considered as core regulators of AS. In the tomato genome, 17 canonical and 2 non-canonical SR proteins were identified (Rosenkranz et al., 2021). To assess whether SR proteins are responsible for the AS regulation of *HSFA2* intron 2, a PCaMV35S:GFP-HSFA2 minigene was transiently co-expressed in tomato mesophyll protoplasts with each of the 17 SR or the two SR-like proteins (Fig. 6A). The expression of HA-tagged SR proteins in protoplasts was confirmed via immunoblot analysis shown in Supplemental Figure 4. The minigene is composed of a GFP-tag N-terminally fused to a *HSFA2* fragment encompassing intron 2 flanked by part of exon 2 and part of exon 3 (Hu et al., 2020a, Fig. 6B). After 4.5 hours of expression at 25°C, the protoplasts were either exposed to 1 h HS (37.5°C) or kept at 25°C (Fig. 6A). GFP-HSFA2 isoform ratios were then quantified following immunoblot analysis in which translation products of the minigene were used as readout for splicing regulation (Fig. 6A-B). The splicing efficiency is thereby expressed as the fraction of GFP-HSFA2-II.

Based on the immunoblot analysis, the expression of 9 out of 17 tomato SR proteins (RS30, RS42, SC30b as well as the entire SCL, RSZ and RS2Z subfamilies) shifted GFP-HSFA2-II ratios towards GPF-HSFA2-I, therefore potentially acting as splicing silencers (Fig. 6C-D). In contrast, the SR-like protein SR46a enhanced the fraction of GFP-HsfA2-II, potentially acting as splicing enhancer of *HSFA2* (Fig. 6C-D). The regulation of GFP-HSFA2 was generally independent from HS as indicated by similar impact on the HSFA2-minigene under both control and HS conditions, except for RS29, that only upon HS significantly enhanced the fraction of GFP-HSFA2-II but, however, showed similar trends under control conditions (Fig. 6C-D). This suggests that neither SR protein required heat to regulate *HSFA2* splicing.

RT-PCR was conducted to investigate whether the HSFA2 protein isoform ratio changes were indeed a consequence of AS. For this, HA-SR proteins were transiently expressed in protoplasts followed by exposure to 37.5°C for 1 h (Fig. 6E). Endogenous *HSFA2* transcripts were subsequently amplified using primers flanking intron 2 which allows the investigation of the *HSFA2* splicing pattern (Fig. 6F). The splicing efficiency was expressed as the fraction of *HSFA2-II* (Fig. 6G). In line with the minigene assay, RS30, SC30b, SCL29, RS2Z35 and RS2Z36 reduced the splicing efficiency of endogenous *HSFA2*, while splicing changes by RS29, SCL31, RSZ21a, RSZ21b and SR46a could not be observed, suggesting

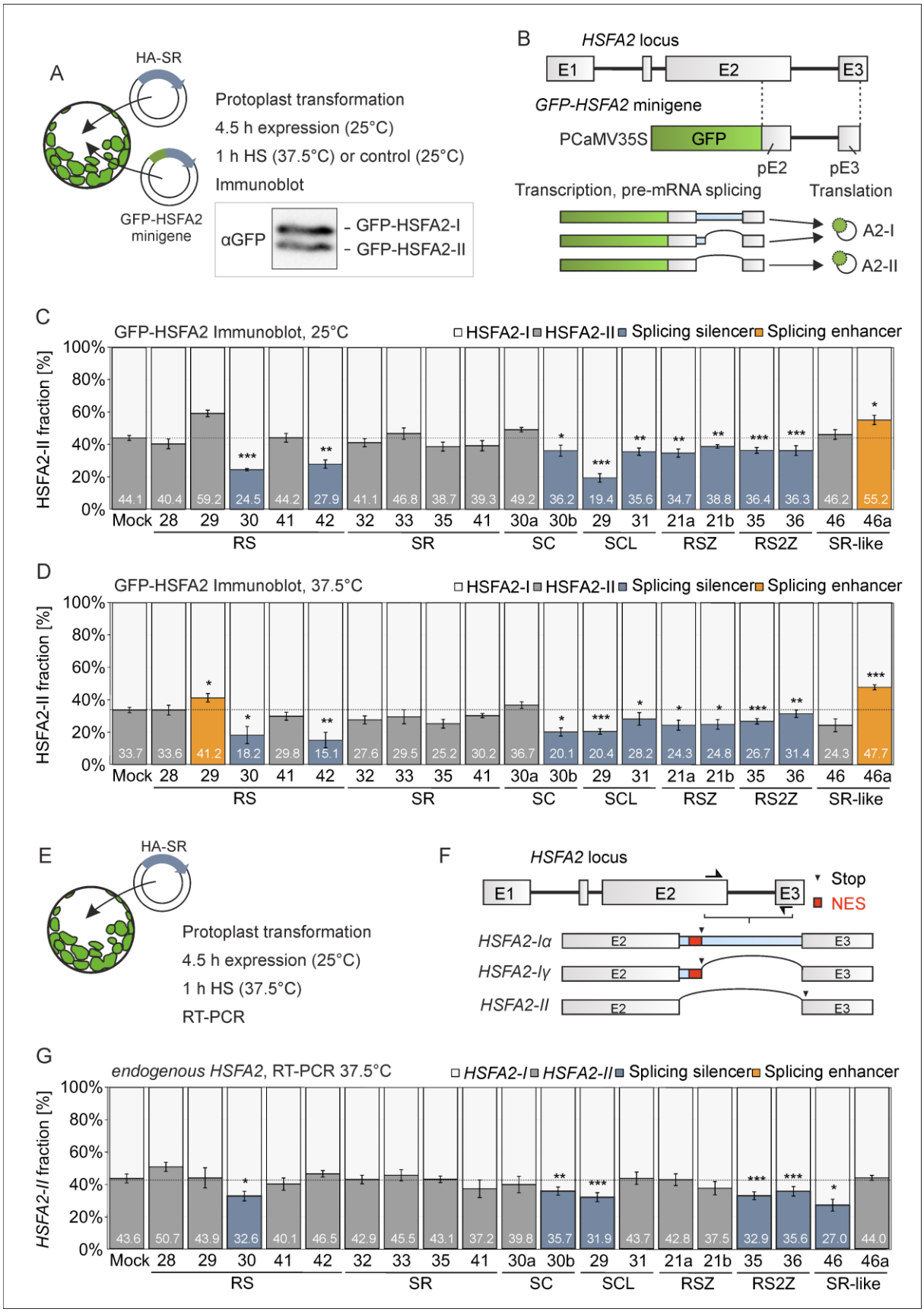
A
HA-SR
GFP-HSFA2 minigene
Protoplast transformation
4.5 h expression (25°C)
1 h HS (37.5°C) or control (25°C)
Immunoblot
αGFP
- GFP-HSFA2-I
- GFP-HSFA2-II
B
HSFA2 locus
E1
E2
E3
GFP-HSFA2 minigene
PCaMV35S
GFP
pE2
pE3
Transcription, pre-mRNA splicing
Translation
A2-I
A2-II
C
GFP-HSFA2 Immunoblot, 25°C
HSFA2-I HSFA2-II Splicing silencer Splicing enhancer
HSFA2-II fraction [%]
100%
80%
60%
40%
20%
0%
44.1 40.4 59.2 24.5 44.2 27.9 41.1 46.8 38.7 39.3 49.2 36.2 19.4 35.6 34.7 38.8 36.4 36.3 46.2 55.2
Mock 28 29 30 41 42 32 33 35 41 30a 30b 29 31 21a 21b 35 36 46 46a
RS SR SC SCL RSZ RS2Z SR-like
D
GFP-HSFA2 Immunoblot, 37.5°C
HSFA2-I HSFA2-II Splicing silencer Splicing enhancer
HSFA2-II fraction [%]
100%
80%
60%
40%
20%
0%
33.7 33.6 41.2 18.2 29.8 15.1 27.6 29.5 25.2 30.2 36.7 20.1 20.4 28.2 24.3 24.8 26.7 31.4 24.3 47.7
Mock 28 29 30 41 42 32 33 35 41 30a 30b 29 31 21a 21b 35 36 46 46a
RS SR SC SCL RSZ RS2Z SR-like
E
HA-SR
Protoplast transformation
4.5 h expression (25°C)
1 h HS (37.5°C)
RT-PCR
F
HSFA2 locus
E1
E2
E3
Stop
NES
HSFA2-Iα
HSFA2-Iγ
HSFA2-II
G
endogenous HSFA2, RT-PCR 37.5°C
HSFA2-I HSFA2-II Splicing silencer Splicing enhancer
HSFA2-II fraction [%]
100%
80%
60%
40%
20%
0%
43.6 50.7 43.9 32.6 40.1 46.5 42.9 45.5 43.1 37.2 39.8 35.7 31.9 43.7 42.8 37.5 32.9 35.6 27.0 44.0
Mock 28 29 30 41 42 32 33 35 41 30a 30b 29 31 21a 21b 35 36 46 46a
RS SR SC SCL RSZ RS2Z SR-like

Figure 6. Regulation of *HSFA2* splicing by SR proteins. **(A)** Schematic workflow to assess *HSFA2* splicing regulation by SR proteins via minigene reporter assay followed by immunoblot. **(B)** GFP-HSFA2 minigene structure encompassing an N-terminal GFP-tag fused to *HSFA2* intron 2 flanked by part of exon 2 and part of exon 3 (grey box: exon; black line: intron; thin blue box: retained intron sequence; Hu et al., 2020a). The processed minigene mRNA is translated into the respective protein isoforms, GFP-HSFA2-I and GFP-HSFA2-II, and is used as indicative outcome of splicing. GFP-HSFA2 splicing efficiency in the presence of tomato HA-tagged SR proteins without (25°C) **(C)** and with HS application (1 h 37.5°C) **(D)**. The splicing efficiency is expressed as the fraction of GFP-HSFA2-II relative to all isoforms. The respective fractions were calculated from signal intensities after immunoblotting. Values represent the average of at least four independent biological replicates. **(E)** Workflow of the assessment of endogenous *HSFA2* splicing in the presence of HA-SR proteins. **(F)** *HSFA2* gene locus and main transcript variants obtained by RT-PCR. Primer positions are depicted as arrows. Black triangles represent stop codons. Red boxes indicate the NES specific to HSFA2-I encoding transcripts. **(G)** Quantification of splicing efficiency as fraction of *HSFA2-II* relative to all transcript variants in protoplasts expressing HA-SR proteins followed by subsequent exposure to 1 h 37.5°C. The *HSFA2-II* fraction was calculated from band intensities on EtBr-stained agarose gels. Values represent the average of three independent biological replicates. In (C), (D), and (G), asterisks indicate statistical significance based on paired student's t-test against the mock control: * $p < 0.05$, ** $p < 0.01$, *** $p < 0.001$. Error bars represent standard error (SE).

additional layers of regulation beyond splicing in these cases (Fig. 6G). SR46 significantly reduced the splicing efficiency of endogenous *HSFA2* (Fig 6G*)* but not of the GFP-HSFA2 minigene (Fig. 6C-D). However, a similar trend could be observed for the minigene at 37.5°C (Fig. 6D), suggesting that *HSFA2* regulation by SR46 likely depends on the temperature stimulus.

As transcriptional induction of specific factors points towards their potential role under HS conditions, the tomato SR protein family was characterised under elevated temperatures (Rosenkranz et al., 2021). qRT-PCR analysis of the levels of the protein-coding transcripts of SR genes in leaves exposed to 37.5°C for 1 hour or kept at 25°C, revealed the HS-induction of 5 canonical (RS28, SR32, SR33, SC30b and RS2Z36) and 1 non-canonical (SR46a) SR protein (Fig. 7A). These genes have thus potential roles as splicing regulators under HS. Therefore, the *HSFA2* intron 2 splicing profile in the presence of HS-induced SR proteins was observed further (Fig. 7B). Similar to the impact of increasing temperatures (Fig. 3), transient expression of the HS-induced SR proteins SC30b and RS2Z36 inhibited the splicing of *HSFA2* intron 2, reducing the splicing efficiency by approximately 8% (Fig. 7B), while the transient expression of other HS-induced SR proteins did not alter the *HSFA2* splicing profile (Fig. 7B). Both SC30b and RS2Z36 belong to SR protein subfamilies with two members each (Fig. 4). While expression of SC30a did not impact the *HSFA2* splicing profile, RS2Z35 had a similar inhibitory effect like RS2Z36 (Fig. 7C). However, it cannot be excluded that differences in *HSFA2* AS-regulation between SR proteins could have arisen from differences in SR protein turnover, as observed for SC30a and SC30b. The protein signal obtained for SC30a was substantially weaker compared to SC30b although they were expressed under the same conditions and driven by the same promoter (Supplemental Fig. 4).

Taken together, 6 out of 17 SR-proteins were shown to act as splicing silencers of *HSFA2* intron 2. While the regulation of *HSFA2* splicing by many SR proteins suggest potential redundancy between tomato SR proteins, only *SC30b* and *RS2Z36* were transcriptionally induced by HS, which reflects potential specific functions for these proteins under HS conditions.

4.2 Regulation of *HSFA2* variants by SR proteins

Natural variations occurring during tomato domestication correlate with *HSFA2* intron 2 splicing efficiency, which is mediated through the presence of three SNPs in intron 2: GGG in modern tomato cultivars such as *S. lycopersicum* (*HSFA2*^{GGG}) and AAA in wild tomato cultivars such as *S. peruvianum* (*HSFA2*^{AAA}) (Hu et al., 2020a). The minigene assay was utilized to investigate whether the change in splicing efficiency between tomato species could be attributed to SR proteins and whether the regulation of *HSFA2* splicing by SR proteins described in section 4.1 occurred in a polymorphism-dependent manner. Translation products of the constitutively expressed GFP-HSFA2 minigene were again used as readout for splicing regulation, but in this case, the minigene sequence harboured the intronic polymorphisms of the AAA haplotype (*GFP-HSFA2*^{AAA}) (Fig. 8A). Thereby, splicing silencers specific for *HSFA2*^{GGG} or splicing enhancers specific for *HSFA2*^{AAA} would be ideal candidates for the differences in splicing efficiency among tomato cultivars.

Again, for the majority of SR proteins, the impact on *HSFA2* AS was not specific for HS, as regulation of *GFP-HSFA2*^{AAA} was similar in minigene assays performed at 25°C and 37.5°C (Fig. 8B-C). RS42 and SR46a however impacted *HSFA2* isoform ratios only when HS was applied, suggesting HS-dependent

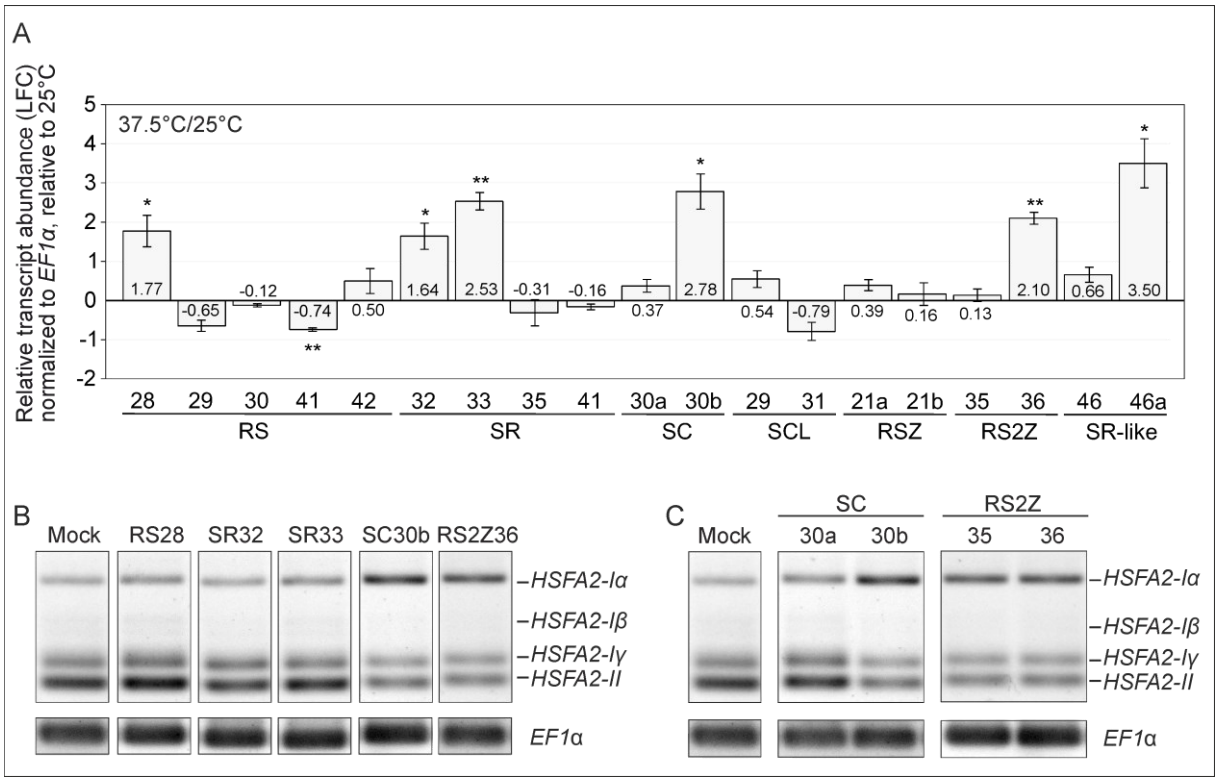

Figure 7. Regulation of *HSFA2* splicing by HS-induced SR proteins. (A) Full-length protein-coding transcript levels of tomato SR proteins exposed to 37.5°C for 1 h, relative to control conditions. Transcript levels are normalised to the housekeeping gene *EF1α* as internal standard and expressed as log_2foldchange (LFC) relative to control (25°C), using the 2^(-ΔΔCt) method (Livak and Schmittgen, 2001). Values represent the average of three independent biological replicates. Asterisks indicate statistical significance based on paired student's t-test against 25°C: * $p < 0.05$, ** $p < 0.01$. Error bars represent standard errors (SE). **(B)** Representative agarose gels depicting the *HSFA2* splicing pattern in heat stressed protoplasts transiently overexpressing heat-induced SR proteins as described in Fig. 6E-F. **(C)** Representative agarose gels depicting the *HSFA2* splicing pattern in heat stressed protoplasts transiently overexpressing SR proteins of the SC and RS2Z subfamily, as described in Fig. 6E-F. To avoid saturation, RT-PCRs were conducted with 28 cycles for *EF1α* and 25 cycles for *HSFA2*, respectively.

regulation in these cases. RS30, RS42, SCL29, SCL31, RSZ21a, RSZ21b and SR46a that were shown to regulate *GFP-HSFA2*^{GGG} (Fig. 6C-D), similarly impacted *GFP-HSFA2*^{AAA} (Fig. 8B-C). Transient expression of *RS28,* however, reduced the fraction of *GFP-HSFA2-II* of the AAA haplotype (Fig. 8B-C) but did not impact *HSFA2*^{GGG} (Fig. 6C-D).

The members of the RS2Z subfamily, RS2Z35 and RS2Z36, were the only SR proteins impacting *HSFA2*^{GGG} and *HSFA2*^{AAA} in contrasting directions depending on the haplotype. While RS2Z proteins

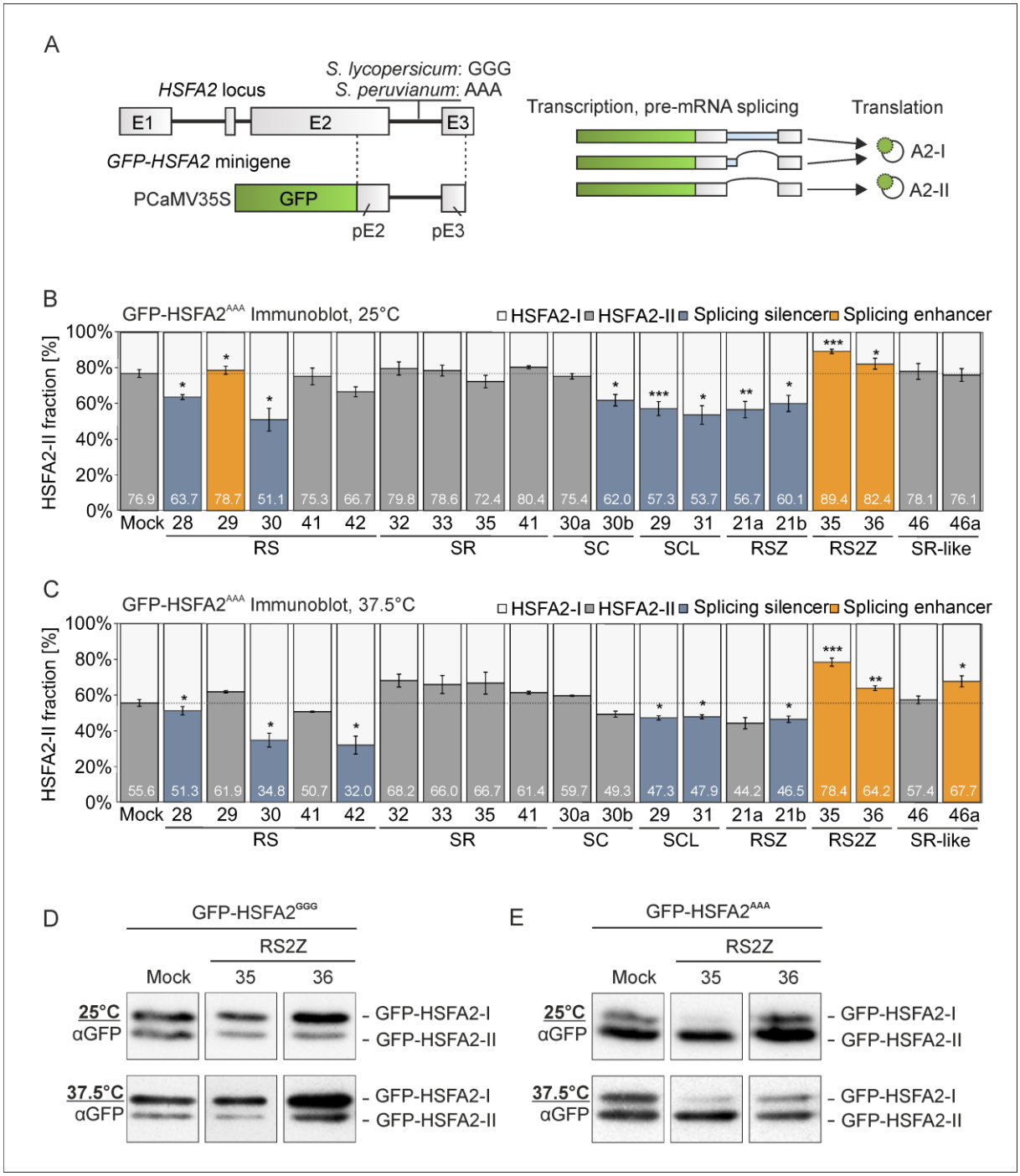

Figure 8. Regulation of natural *HSFA2* variations by SR proteins. (A) Overview of the GFP-HSFA2 minigene assay reflecting intronic variants between tomato cultivars (*S. lycopersicum*: *HSFA2*^{GGG}, *S. peruvianum*: *HSFA2*^{AAA}). The workflow is the same as in Fig. 6A. Splicing efficiency of the *GFP-HSFA2*^{AAA} minigene in the presence of SR proteins without **(B)** and with **(C)** application of 1 h HS at 37.5°C as described for Fig. 6C-D. Representative immunoblots for GFP-HSFS2^{GGG} **(D)** and GFP-HSFA2^{AAA} **(E)** in the presence of RS2Z proteins.

reduced the fraction of GFP-HsfA2-II^{GGG} (Fig. 8D), the fraction of GFP-HsfA2-II^{AAA} was enhanced further (Fig. 8B-C & E), suggesting RS2Z proteins as splicing enhancers of *HSFA2* from the AAA haplotype. The regulation of both GFP-HsfA2-II^{GGG} and GFP-HsfA2-II^{AAA} could be observed at both temperature conditions, 25°C and 37.5°C (Fig. 8D-E, see also Fig. 6C-D and Fig.8B-C), indicating that their impact on splicing was generally independent from HS.

As the minigene assay suggests that RS2Z proteins act as splicing silencers or enhancers, depending on naturally occurring polymorphisms in *HSFA2* intron 2 (Fig. 6-8), RT-PCR was conducted to verify that observed changes were indeed attributed to AS. For this, a heat-stress inducible PHSP21.5:GFP-HSFA2 minigene was utilized in order to mimic natural *HSFA2* HS-induction (Fig. 9A-B). It was confirmed that RT-PCR using constitutively expressed GFP-HSFA2 minigene yielded the same splicing pattern

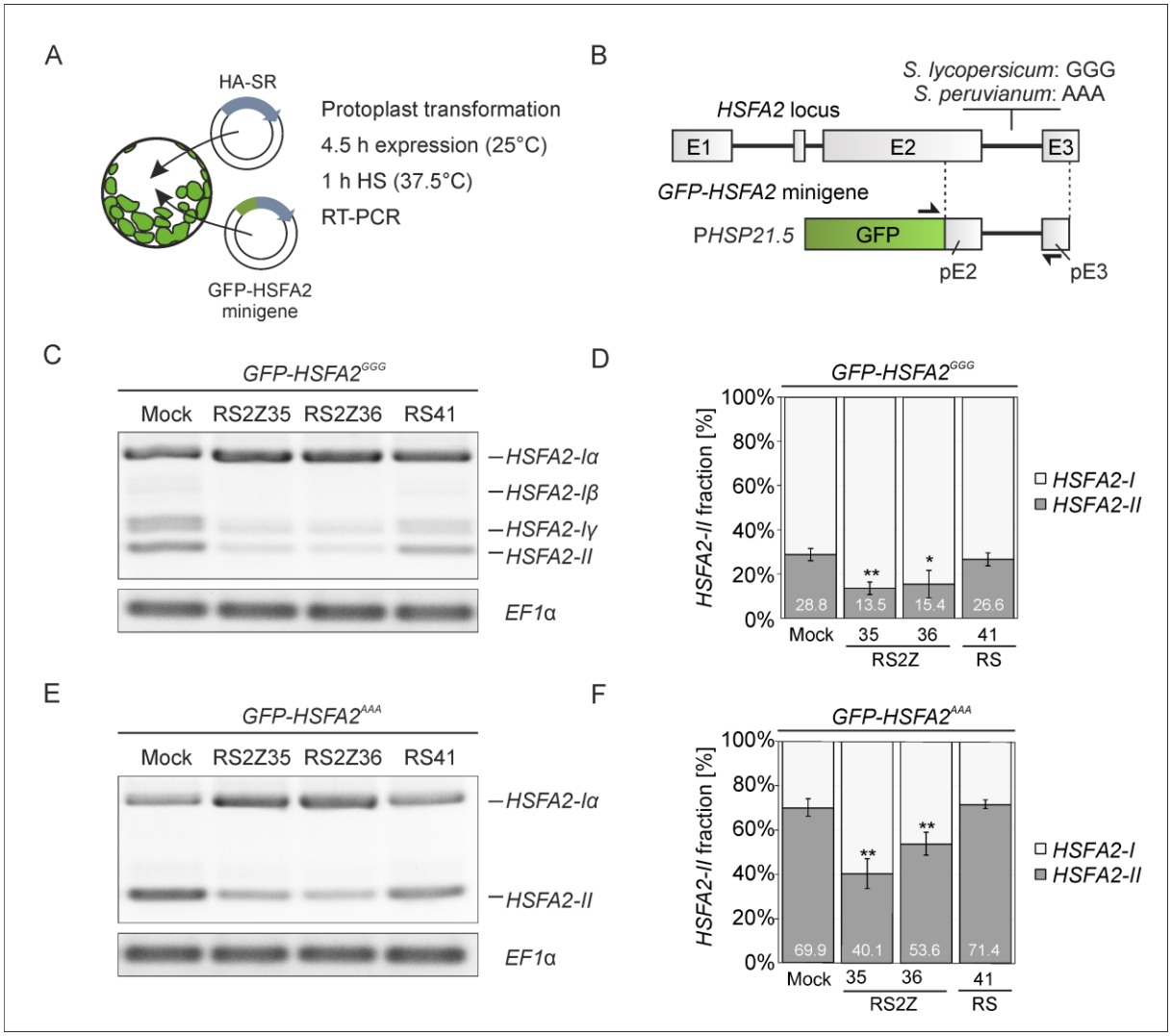

Figure 9. RT-PCR analysis of the regulation of natural *HSFA2* variations by RS2Z proteins. (A) Schematic workflow to assess *HSFA2* splicing regulation by SR proteins via minigene reporter assay followed by RT-PCR. **(B)** GFP-HSFA2 minigene structure as in Fig. 6B. Arrows indicate primer positions for RT-PCR, similar to Fig. 6F. Splicing pattern of *GFP-HSFA2^{GGG}* **(C)** or *GFP-HSFA2^{AAA}* **(E)** co-expressed with HA-RS2Z proteins or HA-RS41 as negative control. **(D)&(F)** depict the quantification of splicing efficiency as *GFP-HSFA2-II* fraction in protoplasts coexpressing HA-RS2Z or HA-RS41 as depicted in (C) & (E) and described for Fig. 6G. Values represent the average of at least three independent biological replicates. Asterisks indicate statistical significance based on paired student's t-test against mock control: * $p < 0.05$, ** $p < 0.01$, *** $p < 0.001$.

(Supplemental Fig. 5). Protoplasts were co-transformed with the PHSP21.5:GFP-HSFA2 minigene (Fig. 8A-B) and either HA-RS2Z35, HA-RS2Z36 or HA-RS41, whereby HA-RS41 served as negative control. Following expression at 25°C for 4.5 hours and subsequent exposure to 37.5° for 1 h hour, RT-PCR was carried out using primers flanking *HSFA2* intron 2 (Fig. 9A). In contrast to the immunoblot assay, RS2Z proteins inhibited intron 2 splicing in both *GFP-HSFA2*^{GGG} and *GFP-HSFA2*^{AAA} (Fig. 9C-F), therefore acting as splicing inhibitors of *HSFA2* irrespective of the intronic polymorphisms. This however suggests, that RS2Z proteins impact *HSFA2* transcripts beyond splicing regulation in a haplotype-specific manner. Although the contrasting ratio changes of the GFP-HSFA2 minigene translation products could not be attributed to similar changes in AS, and therefore likely stem from regulation beyond splicing, e. g. nuclear retention of specific transcripts or regulation of translation efficiency, these results highlight a special role of RS2Z proteins in *HSFA2* regulation. Additionally, RS2Z proteins represent a plant-specific subfamily of SR proteins with additional features compared to canonical SR proteins present in other eukaryotes (Fig. 4). Due to this, and their observed impact on *HSFA2*, the study primarily focusses on the RS2Z proteins further on and aims to characterise its two members, RS2Z35 and RS2Z36, and their involvement in the tomato HSR.

4.3 Contrasting regulation by a HS-induced hnRNP

Apart from SR proteins, hnRNPs play a major role in SS recognition, often antagonizing SR proteins (Cáceres et al., 1994; Eperon et al., 2000). Since most tomato SR proteins inhibited *HSFA2* intron 2 splicing, the impact of the only HS-induced hnRNP was investigated to get a more detailed understanding on *HSFA2* AS regulation. Expression analysis of splicing-related genes (Wang and Brendel, 2004) in tomato seedlings exposed to 39°C compared to control conditions using massive analysis of cDNA ends (MACE) (data obtained from Hu et al., 2020b) revealed that a single hnRNP, *Solyc02g088790*, orthologous to Arabidopsis *GLYCIN-RICH RNA-BINDING PROTEIN 3* (*GR-RBP3)*, was transcriptionally induced by HS by 2.7-fold (LFC 1.43) (Fig. 10A). Transient expression of the *GR-RBP3* coding sequence (CDS) fused to an N-terminal HA tag in protoplasts showed that similar to SR proteins (Supplemental Fig. 4 and section 4.6), GR-RBP3 likely undergoes post-translational modification in response to HS (Fig. 10B), indicated by the loss of a higher MW protein signal, likely representing a shift towards reduced phosphorylation under HS. Furthermore, upon transient overexpression of *GR-RBP3* in protoplasts subjected to 1 h HS (37.5°C), the splicing profile of endogenous *HSFA2* was altered in favour of the fully spliced transcript *HSFA2-II* (Fig. 10C), suggesting *GR-RBP3* as a HS-regulated splicing enhancer of *HSFA2* and thus acting as potential antagonist of SR proteins for this particular AS event.

4.4 The requirement of individual domains for splicing repression

SR proteins are RNA-binding proteins composed of N-terminal RNA binding components as well as a C-terminal RS domain (Fig. 11A). The RNA binding components of the RS2Z subfamily are comprised of an N-terminal RRM followed by two zinc finger motifs of the CCHC-type (zinc knuckles, ZnK) that are separated from the RRM by a short glycine-rich region (Fig. 11A, see Supplemental Fig. 6 for the detailed aa sequences). To investigate which of the domains would be essential for their splicing repressor function, HA-RS2Z domain mutant constructs were created (Fig. 11A). Protoplasts were

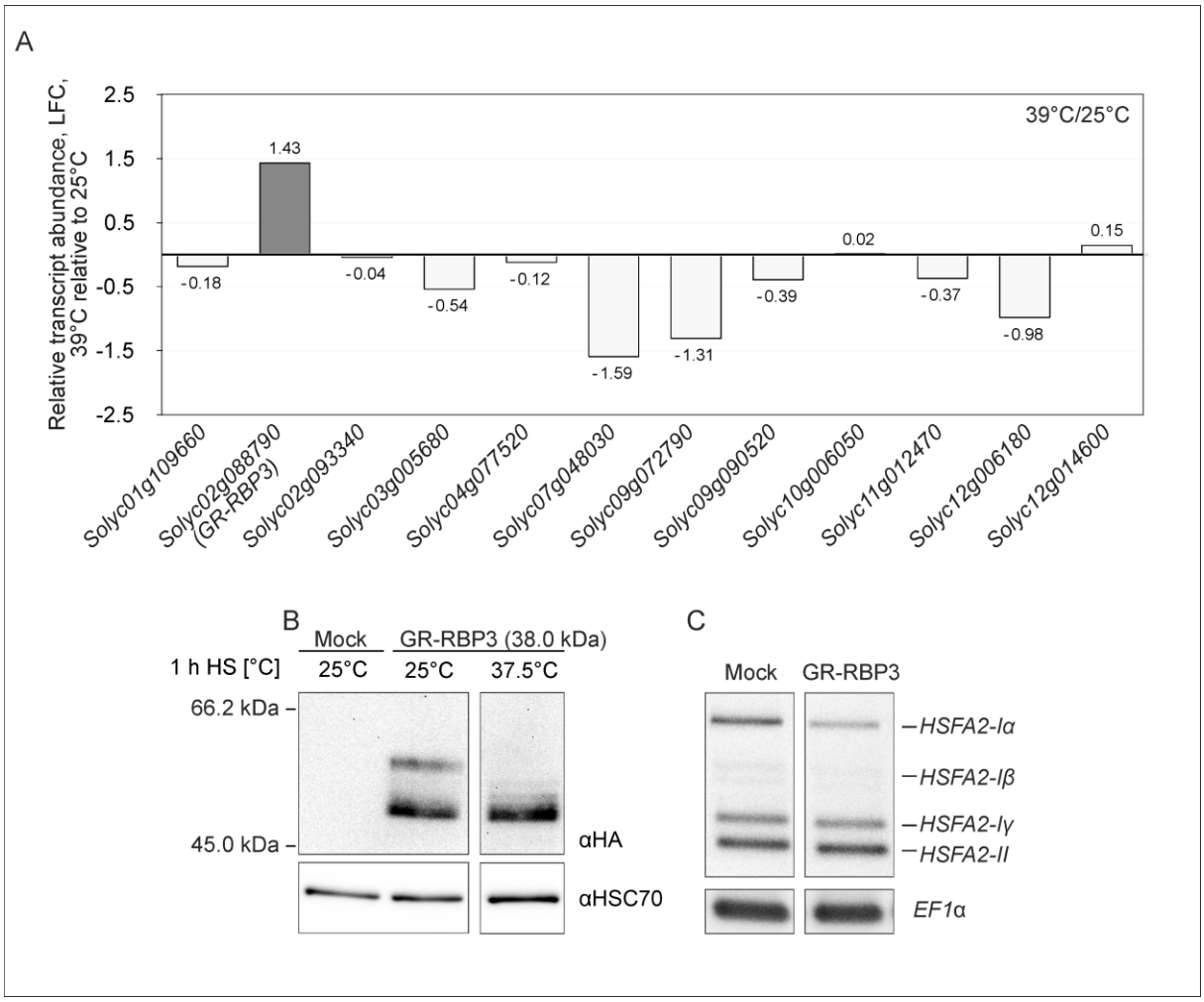

Figure 10. HS-induction of hnRNP *GR-RBP3* and regulation of *HSFA2* splicing. **(A)** Relative transcript levels of tomato hnRNPs in seedlings exposed to 39°C for 1.5 h, followed by 1.5 h recovery at 25°C. Transcript levels were obtained from massive amplification of cDNA ends (MACE) performed by Hu et al. (2020b) and expressed as LFC relative to control (25°C). **(B)** Immunoblot of HA-tagged GR-RBP3 transiently expressed in tomato mesophyll protoplasts for 4.5 h at 25°C and exposed to 1 h 37.5°C or kept at control (25°C). **(C)** *HSFA2* splicing pattern in heat stressed protoplasts (1 h 37.5°C) transiently HA-tagged GR-RBP3.

co-transformed with the GFP-HSFA2 minigene described earlier (section 4.2; Fig. 8A) and WT or mutant HA-RS2Z constructs, whereby either the RRM, both ZnKs, or the RS-rich region (the part of the RS domain with the highest RS/SR content) were deleted (Fig. 11A, see Supplemental Fig. 7 for the detailed aa sequences). The expression of the constructs was validated by immunoblot analysis (Fig. 11B). All constructs showed a higher than calculated apparent MW, likely due to phosphorylation of the RS domain (Fig. 11B). The ratio of *GFP-HSFA2* translation products were analysed by immunoblot analysis (Fig. 11C). While the fraction of GFP-HSFA2-II in the presence of HA-RS2Z constructs lacking either the RRM or the RS-rich region did not differ compared to the expression of the WT constructs, the fraction of GFP-HSFA2-II was enhanced in the presence of the HA-RS2ZΔZnK construct (Fig. 11C). The same results were obtained when the minigene assay was performed at 37.5°C (not shown).

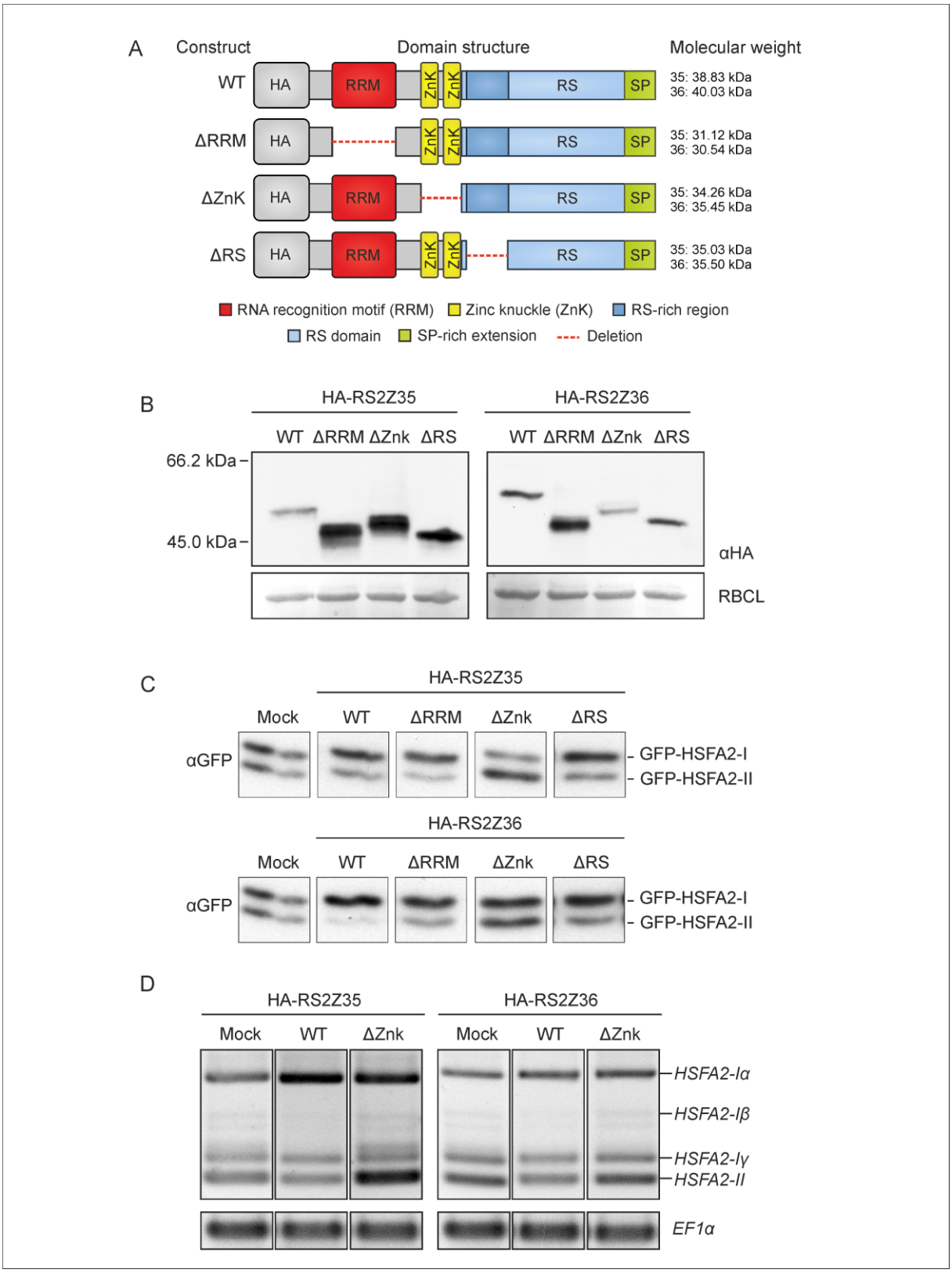

Figure 11. Requirement of RS2Z domains for *RS2Z*-mediated regulation of *HSFA2* AS. (A) Scheme representing domain structures of HA-RS2Z constructs. Deleted regions are indicated by red dotted lines. The calculated molecular weight is depicted on the right side for RS2Z35 (35) and RS2Z36 (36) constructs. **(B)** Immunoblot analysis of HA-RS2Z domain mutant constructs in tomato protoplasts. **(C)** Analysis of *HSFA2* splicing efficiency via GFP-HSFA2 minigene assay by co-expressing the minigene with HA-RS2Z domain mutants in tomato protoplasts at constant 25°C for 5.5 hours. **(D)** Analysis of *HSFA2* splicing by transient expression of HA-RS2Z domain mutants in protoplasts for 4.5 hours followed by 1 h 37.5°C. *HSFA2* intron 2 splicing patterns were analysed by RT-PCR with primers flanking intron 2 as shown in Fig. 6F.

RT-PCR amplifying endogenous *HSFA2* in protoplasts (as described for Fig. 6F) upon transient expression of the WT or HA-RS2Z deletion mutant constructs and subsequent HS exposure (1 h 37.5°C) was used to verify the requirement of the ZnK for splicing repression by RS2Z. In line with the minigene assay, on RNA level, the fraction of *HSFA2-II* was enhanced in the presence of the HA-RS2ZΔZnK construct compared to the WT construct and was similar to mock control (Fig. 11D). Therefore, the ZnKs are the essential components of *RS2Z35* and *RS2Z36* to repress *HSFA2* intron 2 removal, whereby the RRM and the RS-rich region are dispensable.

4.5 Regulation of *RS2Z* genes under elevated temperatures

To further characterise the plant-specific tomato RS2Z subfamily shown to be involved in *HSFA2* splicing regulation, transcriptional and post-transcriptional regulation of tomato RS2Z proteins was investigated with focus on elevated temperatures (see Rosenkranz et al., 2021 for the regulation of the entire tomato SR protein family).

RS2Z35 and RS2Z36, the two members of the RS2Z subfamily of SR proteins, share an equal domain structure consisting of an N-terminal RRM, followed by two ZnKs, an RS domain with 28.8% and 56.9% RS/SR content, respectively, and a C-terminal extension rich in SP (see Supplemental Fig. 6 for a pairwise aa alignment). The RNA binding components of the two proteins are very similar, while there are differences in their RS domains (Supplemental Fig. 6). SR proteins often emerged as sets of paralogs in which one member is the dominantly expressed member over the other (Richardson et al., 2011). This is also true for many tomato SR proteins, whereby RS2Z35 was shown to be the dominantly expressed member over RS2Z36 (Rosenkranz et al., 2021).

Generally, the temperature treatment for protoplast experiments was set to 37.5°C and those employing leaves were performed at 40°C. This was done to accommodate for the difference in heat sensitivity of the two tissue types, whereby the peak induction of *HSFA2* and approximately equal ratio of HSFA2-I and HSFA2-II encoding transcripts were observed at 40°C in leaves and thus correspond to 37.5°C in protoplasts (Supplemental Fig. 8). Therefore, further on, protoplast experiments were performed at 37.5°C, while experiments using tomato leaves were performed at 40°C.

In line with previous results reporting induction of *RS2Z36* at 37.5°C (Fig. 7A), *RS2Z36* was as well transcriptionally induced in detached leaves exposed to 1 h HS at 40°C relative to control conditions (3.2-fold), while *RS2Z35* transcript levels remained unchanged (Fig. 12A), suggesting a role for RS2Z36 in response to elevated temperatures.

To examine whether *RS2Z* genes are transcriptionally regulated in response to both cold and heat, 1 h cold stress of 7°C was applied to detached leaves, whereby transcript levels of both RS2Z members were not impacted relative to control conditions (Fig. 12A), indicating that *RS2Z36* is not induced upon general temperature stimulus but specifically in response to HS. Following *RS2Z* transcript levels during 40°C HS, *RS2Z36* levels peak after 1 h HS (Fig. 12B, bottom panel) similarly to *HSFA2* (Fig. 21A), thus following the general pattern of many HS-induced genes that peak in expression after 1 h HS (Lohmann et al., 2004), while *RS2Z35* levels were not significantly altered throughout 3 h of HS at 40°C (Fig. 12B, top panel).

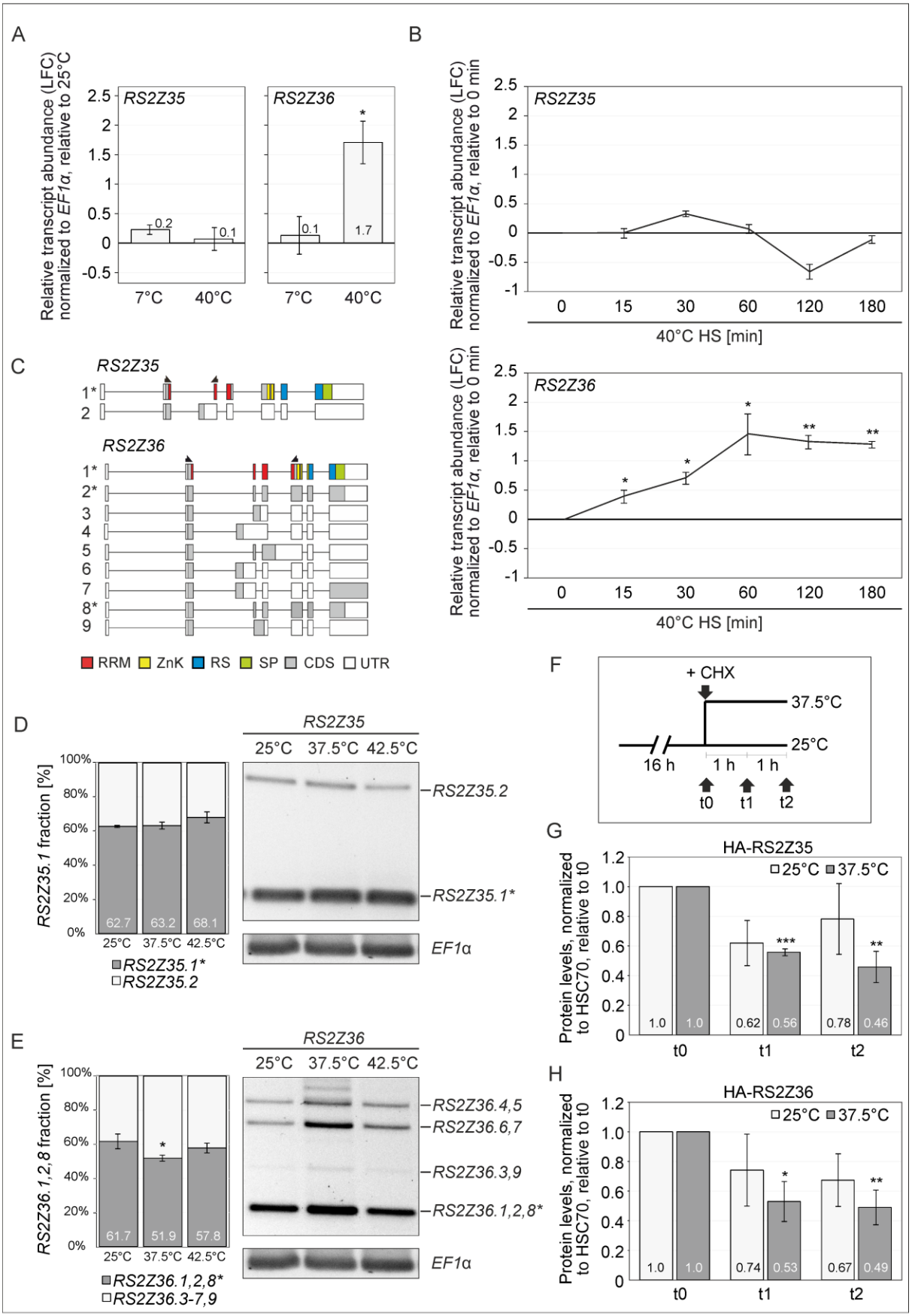
A
Relative transcript abundance (LFC) normalized to EF1α, relative to 25°C
RS2Z35
RS2Z36
7°C
40°C
B
Relative transcript abundance (LFC) normalized to EF1α, relative to 0 min
RS2Z35
RS2Z36
40°C HS [min]
C
RS2Z35
RS2Z36
RRM ZnK RS SP CDS UTR
D
RS2Z35
25°C 37.5°C 42.5°C
RS2Z35.2
RS2Z35.1*
EF1α
RS2Z35.1 fraction [%]
RS2Z35.1*
RS2Z35.2
E
RS2Z36
RS2Z36.4,5
RS2Z36.6,7
RS2Z36.3,9
RS2Z36.1,2,8*
RS2Z36.1,2,8 fraction [%]
RS2Z36.3-7,9
F
+ CHX
37.5°C
25°C
16 h
1 h
1 h
t0
t1
t2
G
HA-RS2Z35
Protein levels, normalized to HSC70, relative to t0
H
HA-RS2Z36

Figure 12. Regulation of *RS2Z* genes under HS. (A) Expression analysis of *RS2Z* genes in response to 1 h heat (40°C) or 1 h cold stress (7°C) relative to control (25°C). qRT-PCR was performed and analysed as described in Fig. 7A. Values represent the average of three independent biological replicates. Asterisks indicate statistically significant differences to control (paired student's t-test): * $p < 0.05$, ** $p < 0.01$; *** $p < 0.001$. **(B)** Expression analysis of *RS2Z* genes over time during HS (40°C) application from 0 (control) up to 3 hours, relative to t0 (0 min HS). Values represent the average of at least three independent biological replicates. Asterisks indicate statistically significant differences to t0 (student's t-test: * $p < 0.05$, ** $p < 0.01$; *** $p < 0.001$). **(C)** Schematic representation of *RS2Z* transcript variants described in Rosenkranz et al. (2021). Boxes and lines indicate exons and introns, respectively. Box colours indicate coding (grey) and noncoding (white) sequences as well as domain-coding regions (red: RRM, yellow: ZnK, blue: RS domain (RS), light green: SP-rich region (SP)). Arrows indicate primer positions for RT-PCR depicted in (D) and (E). **(D)** Analysis of *RS2Z3*5 splicing patterns by RT-PCR using primers depicted in (C) with a representative gel on the left and quantified splicing efficiency on the right side. Splicing efficiency was expressed as the fraction of properly spliced full-length RS2Z35 protein encoding fraction (*RS2Z25.1*), indicated by transcript name followed by an asterisk, quantified by band intensities on EtBr-stained agarose gels. Values represent the average of six independent biological replicates and statistically significant differences under HS compared to 25°C are indicated by asterisks (paired student's t-test): * $p < 0.05$, ** $p < 0.01$; *** $p < 0.001$. **(E)** Analysis of *RS2Z36* splicing patterns by RT-PCR as described for (D). Full-length RS2Z36 encoding fractions are composed of transcripts *RS2Z36.1,2,8*. **(F)** Schematic presentation of CHX application for assessment of protein stability. Following 16 h of transient expression of HA-RS2Z proteins in tomato protoplasts, CHX was added (40 µM). Protoplasts were then either kept at 25°C to assess stability under control conditions or exposed to 37.5°C. Samples were taken after 0, 1, 2 h following addition of CHX. **(G)** HA-RS2Z35 protein stability following translational arrest by CHX application, expressed as protein levels normalised to internal control (HSC70) and relative to t0. Values represent the average of three independent biological replicates. Asterisks indicate statistically significant differences to t0 (paired student's t-test): * $p < 0.05$, ** $p < 0.01$; *** $p < 0.001$ **(H)** HA-RS2Z36 protein stability as described for (G). RT-PCRs were conducted with 30 cycles for *RS2Z* and 28 cycles for *EF1α*.

Not only do SR proteins regulate the splicing of other genes, they also undergo extensive AS themselves as reported for example for Arabidopsis (Palusa et al., 2007) and Cassava (Gu et al., 2020) SR proteins. Identification and description of splicing profiles for all tomato SR proteins were described in Rosenkranz et al. (2021). Alternative 3'SS selection introduces a PTC in *RS2Z35* exon 2, thereby producing two variants, whereby only *RS2Z35.1* encodes for the full-length protein (Fig. 12C). AS of *RS2Z36* is more complex, leading to the production of nine transcript variants, whereby *RS2Z36.3-7* and *RS2Z36.9* have a PTC within the RRM encoding region, leading to a long 3' untranslated region (UTR) which likely targets these transcripts for degradation via the NMD pathway (Fig. 12C). *RS2Z36.1,2,8* encode for the full-length protein (Fig. 12C). AS at a NAGNAG acceptor motif, a common mechanism found among SR proteins (Schindler et al., 2008; Yan et al., 2015), leads to the production of a putative protein isoform lacking a single serine (RS2Z36.2, 8) compared to the canonical isoform (RS2Z36.1). Compared to RS2Z36.1 and RS2Z36.2, RS2Z36.8 is missing the last three nucleotides of the 3'UTR, not affecting the CDS further and was thereby also considered coding for the full-length RS2Z protein (Rosenkranz et al, 2021). *RS2Z25* and *RS2Z36* both are alternatively spliced under control conditions (62.7 and 61.7%, respectively; Fig. 12D-E), whereby splicing efficiency of *RS2Z36* was slightly reduced upon 1 h HS at 37.5°C (51.9%, Fig. 12E).

Since heat negatively impacts the stability of many proteins, the degradation of HA-RS2Z35 and HA-RS2Z36 were monitored by chasing the proteins after inhibition of translation (Fig. 12F). HA-SR proteins were transiently expressed in protoplasts overnight. Subsequently, translation was stalled by addition of CHX. The protoplasts were either kept at 25°C to assess general SR protein stability or exposed to 37.5°C to assess protein stability during HS. At constant 25°C, both HA-RS2Z35 and HA-

RS2Z36 protein levels were not significantly reduced upon addition of CHX (Fig. 12G-H), indicating that both remain stable for at least two hours following inhibition of translation. Under HS however, both HA-RS2Z35 and HA-RS2Z36 showed a significantly higher turnover whereby protein levels were reduced to almost 50% already after one hour (56% and 53%, respectively) (Fig. 12G-H).

SR proteins are post-translationally modified through phosphorylation of the RS domain that determines their activity and localisation (section 1.8.3). Subcellular localisation was analysed by transient expression of GFP-tagged SR proteins in protoplasts for 4.5 hours, along with ENP1-mCherry as a nuclear marker, followed by CLSM imaging directly (control) or following 1 h 38°C (HS). GFP showed a nucleocytoplasmic distribution in line with previous reports (Wu et al., 2017; Fig. 13A). To investigate whether RS2Z protein localisation differs from that of other HS-induced SR proteins, the localisation of GFP-SC30b was observed in addition to GFP-RS2Z proteins. Both GFP-RS2Z and GFP-SC30b proteins were solely nuclear localised and accumulated in subnuclear structures embedded in an otherwise ubiquitous nuclear distribution, with no visible differences between control and HS conditions (Fig. 13A). These subnuclear structures, however, did not resemble the generally strong speckled pattern shown for Arabidopsis SR proteins obtained under similar experimental conditions, including At-RS2Z33 (Lorkovic et al., 2008). Furthermore, under the HS conditions applied here, a clear preferential localisation in speckles upon HS as reported for At-RS45 (Ali et al., 2003) was not observed either.

Since phosphorylation of the RS domain determines not only SR protein localisation but also activity, the occurrence of different phosphorylation states upon HS was examined by transient expression of HA-RS2Z proteins in protoplasts including 1 h 37.5°C (or continuous 25°C as control). For each RS2Z protein, an aliquot of the protein extract was incubated with alkaline phosphatase to obtain a dephosphorylated sample that served as reference for the degree of phosphorylation. Both HA-RS2Z35 and HA-RS2Z36 showed a lower apparent MW upon dephosphorylation compared to the untreated samples, which was closer to the calculated MW (38.83 kDa and 40.03 kDa, respectively) (Fig. 13B). Not only RS2Z members, but many tomato SR proteins, showed higher than calculated apparent MW, indicating that tomato SR proteins in general are heavily phosphorylated (Supplemental Fig. 4). In samples not treated with phosphatase, both RS2Z proteins showed three detectable phosphorylation states that, however, did not differ between control and HS conditions (Fig. 13B). The most prominent protein signal for HA-RS2Z was the one closest to the dephosphorylated state with an approximate MW of 50-55 kDa. A fully dephosphorylated protein as observed upon phosphatase treatment could not be detected in untreated samples, indicating that RS2Z proteins possess at least some degree of basal phosphorylation (Fig. 13B). The phosphorylation states were further analysed by Phos-tag PAGE. The Phos-tag compound binds to phosphate groups and thus reduces the migration pace of phosphorylated proteins through a Phos-tag containing polyacrylamide gel (Kinoshita et al., 2006), which allows a more detailed analysis of different phosphorylation states. Again, both HA-RS2Z35 and HA-RS2Z36 showed three phosphorylation states in total with no entirely dephosphorylated state visible neither under control nor HS conditions (Fig. 13C). Furthermore, no changes in the ratio of

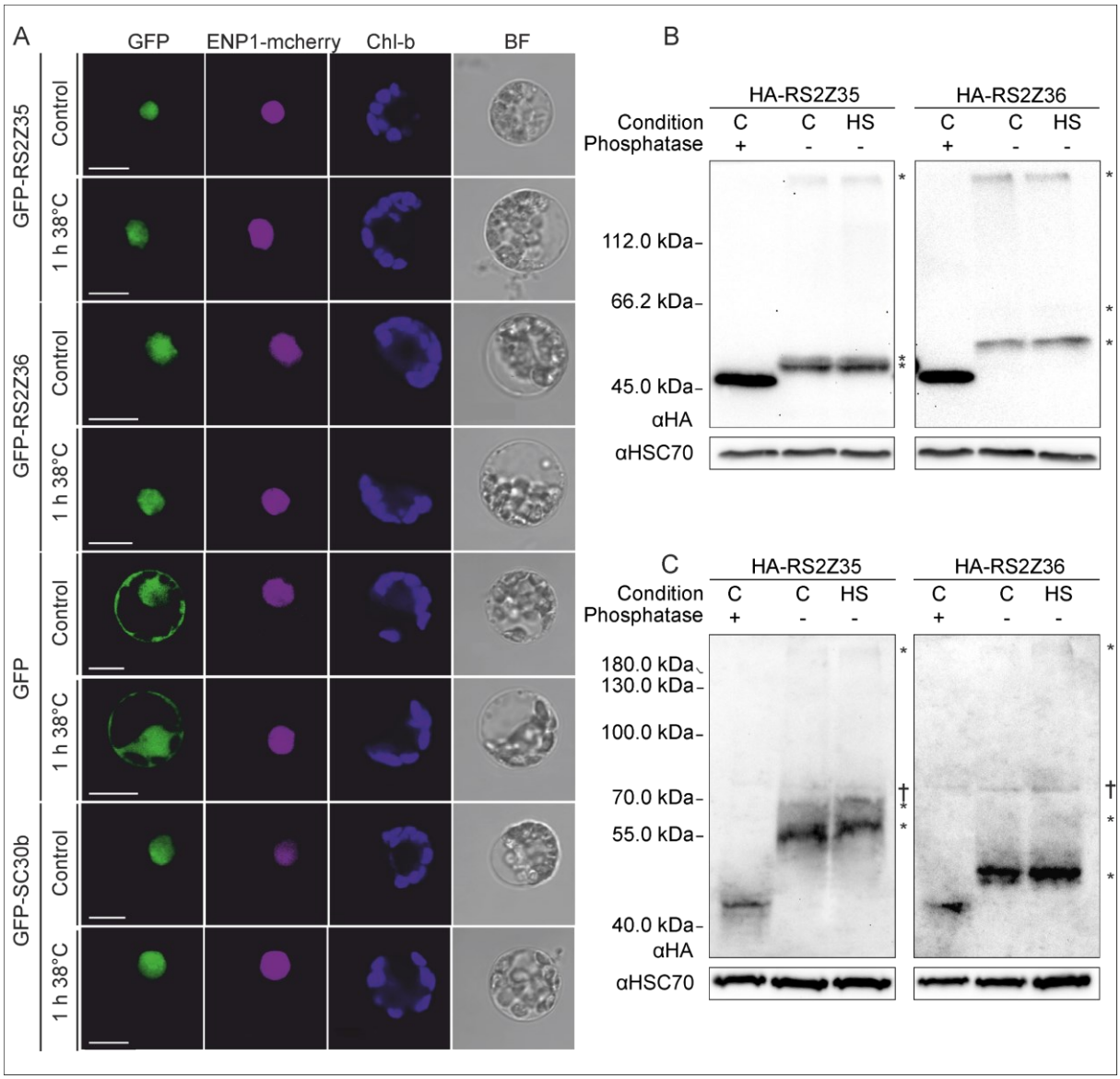

Figure 13. Subcellular localisation and phosphorylation of RS2Z proteins. (A) CLSM images of tomato protoplasts transiently expressing *GFP-RS2Z*, *GFP-SC30b* or *GFP* following overnight expression at 25°C followed by exposure to 1 h HS (38°C) or kept at control conditions (25°C). Scale bars indicate 10 µm. Co-expression of *ENP1-mCherry* served as nuclear marker. Chl-b: Chlorophyll b autofluorescence. BF: brightfield. **(B)** Phosphorylation status of HA-RS2Z proteins, visualised by immunoblot analysis following 4.5 h expression at 25°C and 1 h HS (37.5°C, HS) or continuous 25°C (control, C). Protein extracts were left untreated (-) or were dephosphorylated using alkaline phosphatase (+). **(C)** Detailed analysis of phosphorylation status by immunoblot analysis following Phos-tag PAGE of HA-RS2Z proteins as described in (B). Asterisks indicate different phosphorylation states. Crosses indicate unspecific signal from antibody cross-reactivity.

phosphorylation states between control and HS conditions could be observed (Fig. 13C). Comparing the migration behaviour of HA-RS2Z proteins in Phos-tag PAGE, untreated HA-RS2Z35 showed a higher apparent MW than HA-RS2Z36, indicating that it employed a generally higher degree of phosphorylation than HA-RS2Z36.

4.6 Generation of mutant and transgenic plant lines

To further characterise tomato RS2Z proteins and their role in the tomato HSR, knockout mutants were generated by employing a CRISPR/Cas9 cassette integrated into the tomato genome via *Agrobacterium tumefaciens*-mediated plant transformation. Two sgRNAs were selected for each gene, aiming to create mutations in two different regions for each gene. By this, it was aimed for an increase in mutation success and the possibility for a larger deletion. Two mutations were identified in each gene, Del1383A and Ins3944A in *rs2z35*, and Ins79T and Del1402T in *rs2z36* (Fig. 14A) (mutation sites are indicated as nucleotide position based on the ITAG 2.5 gene annotation). Del1383A in *rs2z35* and Ins79T in *rs2z36* are positioned in the RRM in proximity to the start codon and create a frame-shift downstream that results in a PTC, thus preventing the translation of the full-length protein (Fig. 14A; see Supplemental Fig. 9 for the aa sequences). As no specific antibody for RS2Z proteins was available, WT and mutant mimic constructs were generated, harbouring the genomic sequence of *RS2Z* fused to an N-terminal 3xHA-tag in-frame with the translation start of the protein (PCaMV35S:HA-g*RS2Z35*, PCaMV35S-HA-g*RS2Z36*). The WT and mutant mimic constructs were then transiently expressed in protoplasts, whereby a protein signal of the expected molecular weight could only be observed for the WT constructs (the calculated molecular weight for full-length HA-RS2Z35 and HA-RS2Z36 is 43.05 kDa and 42.31 kDa, respectively. The apparent molecular weight is at approximately 50 and 55 kDa, respectively). This indicates that the mutations indeed prevent the expression of the full-length SR protein (Fig. 14B). The mutants were thus considered to be functional knockouts and are referred to as knockout mutants further on. In this study, homozygous T-DNA-free knockout lines for the individual RS2Z proteins were generated, *rs2z35* and *rs2z36*. Accounting for the potential functional redundancy of *RS2Z35* and *RS2Z36*, a T-DNA-free homozygous double mutant was obtained by crossing of the *rs2z* single mutants and subsequent screening of the T2 generation via Sanger sequencing. The double mutant is further referred to as *rs2z35 rs2z36*.

Under both control and HS conditions, transcripts coding for RS2Z35 and RS2Z36 were reduced in leaves of single and double mutant plants compared to the WT, indicating that mutant transcripts were potentially targeted for NMD (Fig. 14C). Since translation is negatively impacted by HS, the induction of *RS2Z36* transcripts by HS may outrun NMD activity, thus resulting in less reduction of *RS2Z36* transcript levels in the *rs2z36* and *rs2z35 rs2z36* mutant under HS (Fig. 14C).

Additionally, stable plant lines overexpressing PCaMV35S-driven N-terminal GFP fusions (*GFP-RS2Z35*, *GFP-RS2Z36,* or *GFP* alone) were created using *Agrobacterium tumefaciens*-mediated plant transformation. The absence of kanamycin-sensitive plants in the T2 generation in two rounds of screening (10-15 plants each) indicates, that the *GFP* expressing lines generated in this study were likely homozygous. T0 generations of *GFP-RS2Z35* and *GFP-RS2Z36* lines were created by Löchli (2020). However, for *GFP-RS2Z* lines, no homozygous plant could be obtained in several rounds of screening in the T2 and T3 generation, suggesting that a high degree of *RS2Z* overexpression may negatively

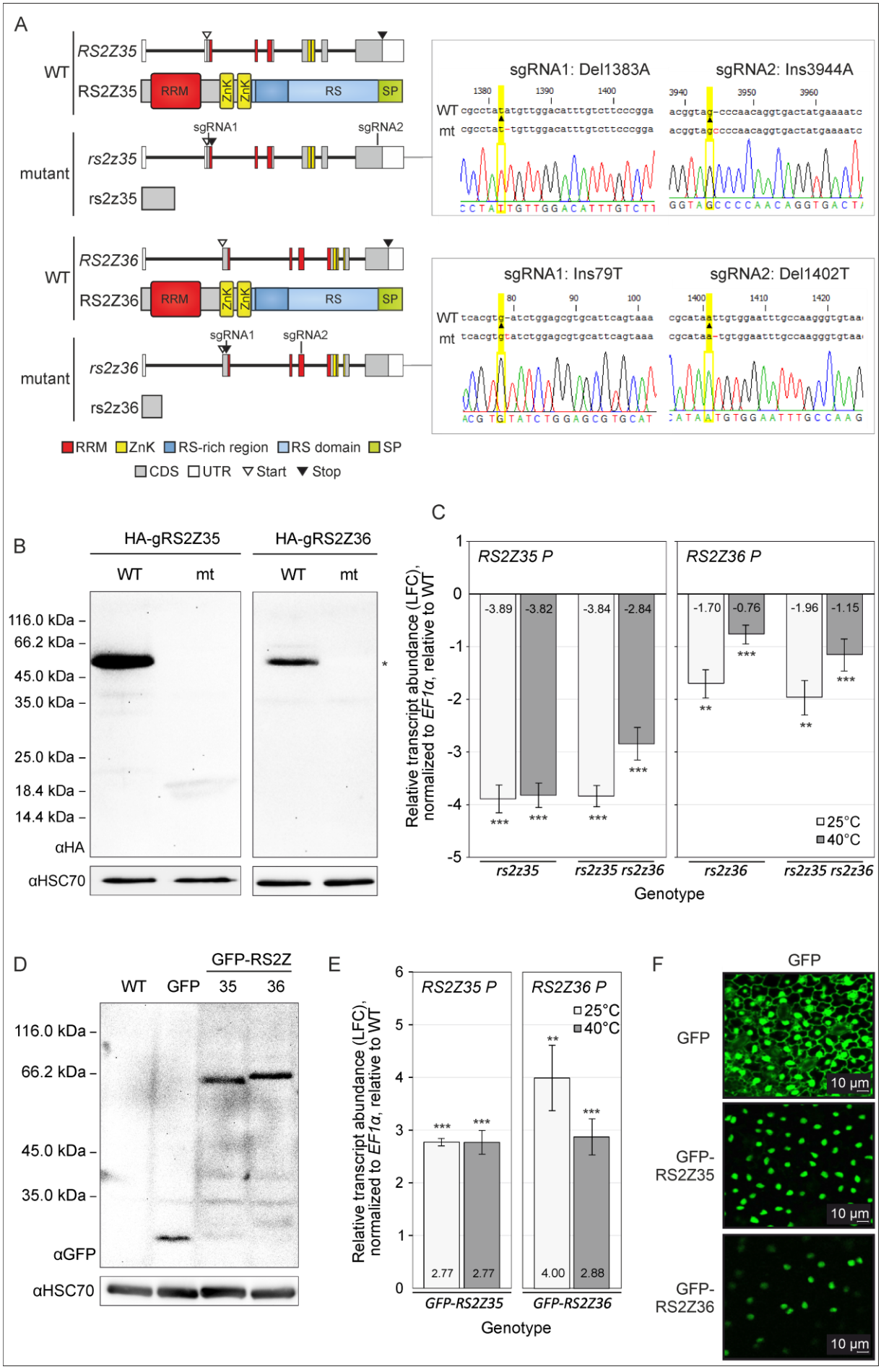
A
WT
RS2Z35
RS2Z35
RRM
ZnK
ZnK
RS
SP
mutant
rs2z35
sgRNA1
sgRNA2
rs2z35
sgRNA1: Del1383A
sgRNA2: Ins3944A
WT cgcctatatgttggacatttgtcttcccgga
mt cgcctat-tgttggacatttgtcttcccgga
acggtag-cccaacaggtgactatgaaaatc
acggtagccccaacaggtgactatgaaaatc
WT
RS2Z36
RS2Z36
mutant
rs2z36
rs2z36
sgRNA1: Ins79T
sgRNA2: Del1402T
WT tcacgtg-atctggagcgtgcattcagtaaa
mt tcacgtgtatctggagcgtgcattcagtaaa
cgcataattgtggaatttgccaagggtgtaa
cgcataa-tgtggaatttgccaagggtgtaa
RRM ZnK RS-rich region RS domain SP
CDS UTR Start Stop
B
HA-gRS2Z35
HA-gRS2Z36
WT
mt
WT
mt
116.0 kDa
66.2 kDa
45.0 kDa
35.0 kDa
25.0 kDa
18.4 kDa
14.4 kDa
αHA
αHSC70
C
RS2Z35 P
RS2Z36 P
Relative transcript abundance (LFC), normalized to EF1α, relative to WT
-3.89
-3.82
-3.84
-2.84
-1.70
-0.76
-1.96
-1.15
25°C
40°C
rs2z35
rs2z35 rs2z36
rs2z36
rs2z35 rs2z36
Genotype
D
GFP-RS2Z
WT
GFP
35
36
116.0 kDa
66.2 kDa
45.0 kDa
35.0 kDa
αGFP
αHSC70
E
RS2Z35 P
RS2Z36 P
25°C
40°C
Relative transcript abundance (LFC), normalized to EF1α, relative to WT
2.77
2.77
4.00
2.88
GFP-RS2Z35
GFP-RS2Z36
Genotype
F
GFP
GFP
GFP-RS2Z35
GFP-RS2Z36
10 µm

Figure 14. Generation of *rs2z* mutant and *GFP-RS2Z* overexpression plants. (A) Schematic representation of WT and mutant *RS2Z* gene structure and coding sequence (left side). Exons and introns are depicted by boxes and lines, respectively. Coloured boxes indicate regions coding for protein domains. Red: RRM, yellow: ZnK, dark blue: RS-rich region with RS domain, light blue: RS domain, light green: SP-rich region, grey: coding sequence (CDS), white: untranslated region (UTR). Arrow heads indicate start (white) and stop codons (black). sgRNA1 and sgRNA2 indicate the positioning of mutations introduced by CRISPR/Cas9. Corresponding electropherograms of WT and mutant (mt) sequences for each sgRNA region are depicted on the right side. **(B)** Immunoblot analysis of transient expression of HA-gRS2Z constructs containing the genomic sequence of WT or mutant *RS2Z* genes in protoplasts. The asterisk indicates the expected size for the WT construct. **(C)** Verification of *rs2z* knockout in tomato leaves in WT and mutant plants by expression analysis of full-length protein-coding *RS2Z5* (*RS2Z35.1*) and *RS2Z36* (*RS2Z36.1,2,8*) (see Fig. 12C) by qRT-PCR. Expression levels are normalised to *EF1α* as internal control and depicted as LFC relative to WT under control or HS conditions (1 h 40°C). Values represent the average of at least three independent biological replicates. Statistically significant differences (paired student's t-test against WT) are indicated by asterisks: * $p < 0.05$; ** $p < 0.01$; *** $p < 0.001$. Error bars: SE. **(D)** Representative immunoblot depicting the expression of GFP and GFP-RS2Z proteins in non-stressed leaves from transgenic tomato plants overexpressing the indicated construct driven by the CaMV35S promoter. **(E)** Verification of *RS2Z* overexpression in transgenic lines by qRT-PCR analysis of full-length protein-coding *RS2Z35* and *RS2Z36* transcripts relative to WT as described for (C); $n \geq 3$. **(F)** CLSM imaging of leaf epidermal cells from WT and transgenic plants (Bachiri, 2021).

impacted reproduction (see also section 4.7). The expression of the transgene was confirmed via immunoblot for each plant used in this study (Fig. 14D). While GFP (26.75 kDa) showed a protein signal at the expected MW, GFP-RS2Z35 (61.50 kDa) and GFP-RS2Z36 (62.77 kDa) showed slightly higher apparent MW of approximately 66-70 kDa, potentially attributed to phosphorylation of the RS domain. Overexpression of *GFP* and *GFP-RS2Z* was further verified by qRT-PCR relative to the WT, whereby both genes were overexpressed 7 to 16-fold (Fig. 14E). In contrast to the generally high level of PCaMV35S-driven overexpression of > 100-fold reported in other SR protein overexpression studies, e. g. At-SR30 (Lopato et al., 1999) and Os-SCL30 (Zhang et al., 2022), the overexpression of less than 20-fold in this study lies within the physiological range. The nuclear localisation of GFP-RS2Z in transgenic plants was confirmed by CLSM using leaf epidermal cells from the adaxial side (Bachiri, 2021; Fig. 14F).

4.7 Involvement of RS2Z proteins in fruit morphology and reproduction

As both RS2Z proteins are expressed under control conditions, the impact of the mutations on the morphology, development and growth was characterized in non-stressed plants. Under control conditions, *rs2z* mutant plants did not show vegetative growth phenotypes compared to the WT, except for a slightly reduced growth of the *rs2z35 rs2z36* mutant (Fig. 15A). Pulse-amplitude-modulation (PAM) fluorometry measurements in WT and *rs2z* single mutants did not show any significant differences compared to the WT, indicating that *rs2z35* or *rs2z36* knockout did not impact photosynthesis, neither under control nor HS conditions (Bachiri, 2021). Furthermore, the impact of *rs2z* knockout on reproduction was assessed. Since the *rs2z35 rs2z36* mutant line was established at a later stage, fruit-related analysis was performed with single mutants and overexpression lines only. Thereby, knockout as well as overexpression of *RS2Z* genes impacted reproduction. Compared to the WT, the average fruit weight was reduced in *rs2z35* and *rs2z36* lines (Fig. 15B) and was reduced even further in *GFP-RS2Z35* and *GFP-RS2Z36* transgene lines (Fig. 15B). These results indicate that misregulation of RS2Z proteins negatively impacts fruit size. *rs2z36* fruits produced 36% less seeds per fruit compared to WT (Fig. 15C). The overexpression of *GFP-RS2Z35* and *GFP-RS2Z36* reduced the

number of seeds to approximately 1/3 the amount of WT plants (Fig. 15C). Additionally, the fruits from *rs2z36* plants were more elongated compared to WT, with a fruit shape index of 0.92 in *rs2z36* compared to 0.85 in the WT (Fig. 15D-E).

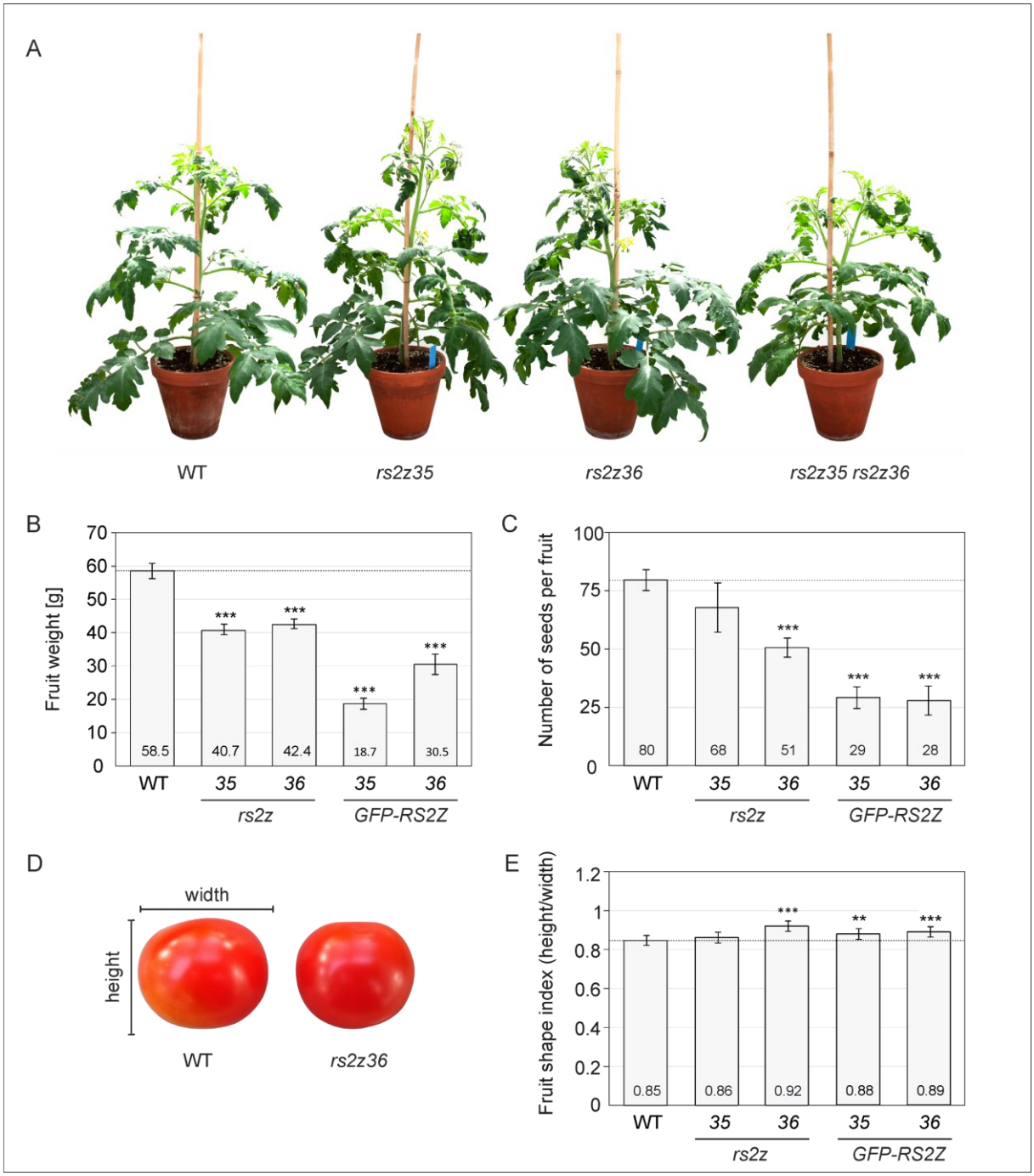

Figure 15. Phenotypes of *rs2z* mutant plants. (A) Representative images of approximately 12 week-old tomato plants. Fruit weight **(B)** and number of seeds per fruit **(C)**. **(D)** Schematic depiction of measurements used for fruit shape index calculation. **(E)** fruit shape index. Statistical analysis was performed using unpaired student's t-test against WT. Values represent averages of 15 **(B)**, 6 **(C)** and 15 **(E)** independent biological replicates. Error bars: SE. Asterisks depict statistically significant differences to WT: * $p < 0.05$; ** $p < 0.01$; *** $p < 0.001$.

4.8 Auto- and cross regulation between RS2Z protein members

Auto- and cross regulation is a common phenomenon among plant SR proteins, reported for example for At-RS2Z33 (Kalyna et al., 2003) and At-RS30 (Lopato et al., 1999). Auto- and cross regulation among the two members of the tomato RS2Z subfamily was investigated by qRT-PCR and RT-PCR. For qRT-PCR analysis, full-length protein-coding transcripts (*RS2Z35.1* referred to as *RS2Z35 P*, and *RS2Z36.1,2,8,* referred to as *RS2Z36 P*) were amplified with transcript-specific primers (Fig. 16A-B). While full-length

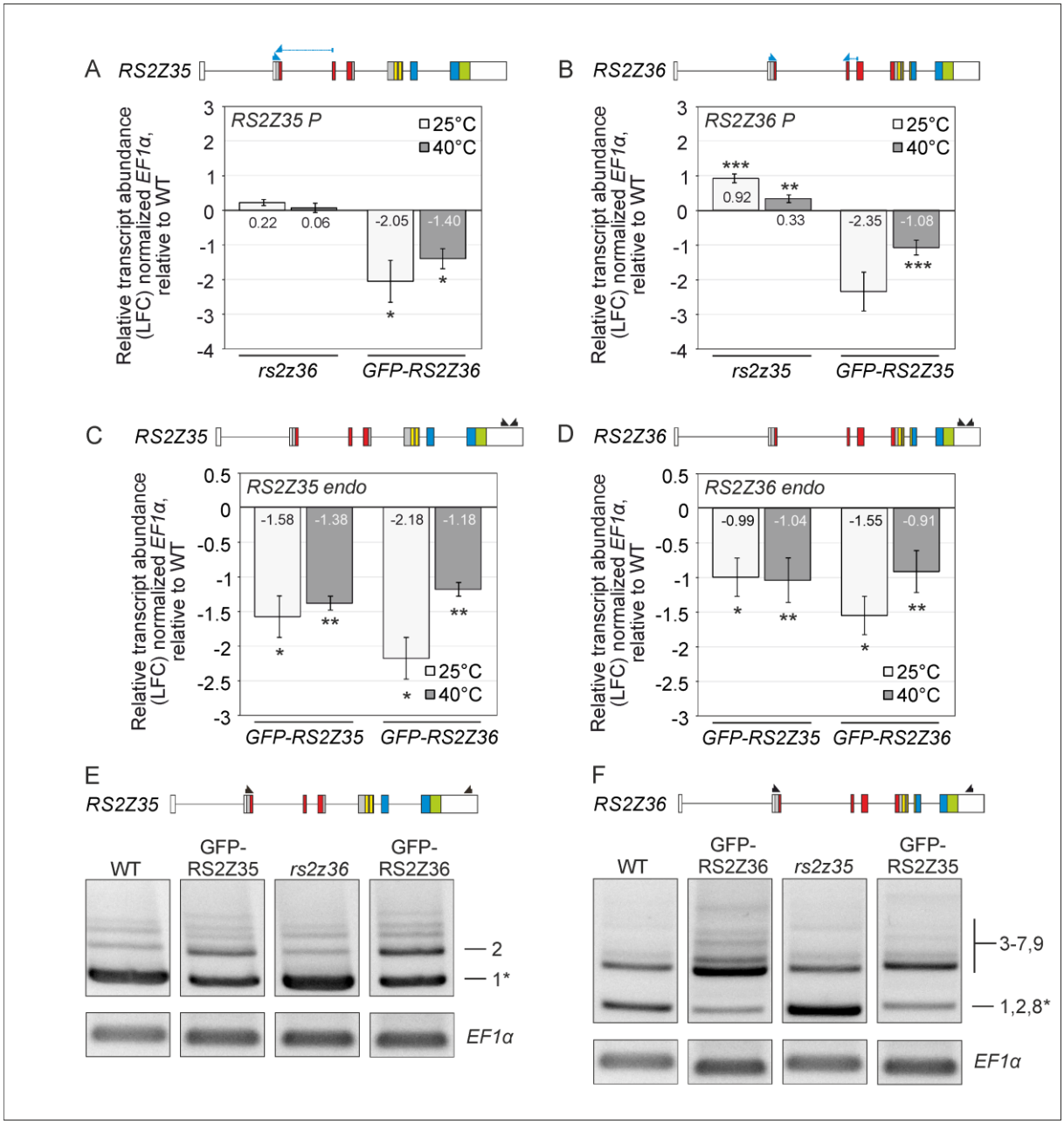

Figure 16. Auto- and cross-regulation among RS2Z proteins. Primer positions and transcript levels of full-length protein-coding *RS2Z35* **(A)** and *RS2Z36* **(B)** (see Fig. 12C for transcript variants) as well as transcript levels of endogenous *RS2Z35* **(C)** and *RS2Z36* **(D).** Leaves from WT, *rs2z* mutant and *GFP-RS2Z* overexpression plants were exposed to 1 h 40°C or kept under control conditions (25°C). Primer positions and RT-PCR depicting splicing patterns of endogenous *RS2Z35* **(E)** and *RS2Z36* **(F)** in leaves from indicated genotypes exposed to 1 h 40°C. Exons and introns are depicted by boxes and lines, respectively. Coloured boxes indicate domain sequences (as described for see Fig. 12C). Arrows indicate primer positions. Transcript levels are expressed as averages from three independent biological replicates as LFC relative to WT as described for Fig. 7A. RT-PCRs were conducted with 30 cycles for *RS2Z* and 28 cycles for *EF1α*.

protein coding *RS2Z35* transcripts were not altered in *rs2z36* mutant plants, full-length *RS2Z35* transcripts were reduced in plants overexpressing *GFP-RS2Z36* (Fig. 16C). Similarly, full-length protein coding *RS2Z36* transcripts were reduced in *GFP-RS2Z35* plants (Fig. 16B). Additionally, full-length protein coding *RS2Z36* levels were elevated in *rs2z35* plants by 1.9-fold under control and by 1.3-fold under HS conditions (Fig. 16B), suggesting negative cross-regulation of *RS2Z36* by *RS2Z35*.

For investigation of AS regulation of the endogenous *RS2Z* transcripts (referred to as *RS2Z35 endo* and *RS2Z36 endo*) in overexpression plants, endogenous transcripts were amplified using a reverse primer annealing in the 3'UTR, thus not amplifying transcripts that stem from the *GFP-RS2Z* transgene (Fig. 16 C-D). Overexpression of *GFP-RS2Z35* or *GFP-RS2Z36* led to a reduction of their own endogenous transcripts (Fig. 16C-D), suggesting autoregulation for both RS2Z proteins. Similarly, overexpression of one member caused a reduction of the endogenous transcript levels of the respective other member, suggesting additional cross-regulation between *RS2Z35* and *RS2Z36* (Fig. 16C-D). RT-PCR analysis in leaves exposed to 1 h 40°C demonstrated, that the cross- and autoregulation in *GFP-RS2Z* overexpression plants by reduction of functional transcripts observed in Figure 16A-B was caused by AS (Fig. 16E-F). RT-PCR performed at 25°C, however, showed the same trends (not shown). Overexpression of either *GFP-RS2Z35* or *GFP-RS2Z36* impacted AS of both endogenous *RS2Z35* and *RS2Z36*, whereby splicing was changed in favour of non-productive variants in all cases (Fig. 16E-F, lane 2 & 4). *rs2z36* knockout did not impact the *RS2Z35* splicing profile (Fig. 16E, lane 3). Elevated levels of full-length protein coding *RS2Z36* in the *rs2z35* mutant, however, could be attributed to enhanced splicing efficiency of *RS2Z36* in favour of the full-length protein-coding variant (Fig. 16F, lane 3).

In summary, overexpression of *RS2Z* genes was partially compensated by the downregulation of endogenous *RS2Z* through AS favouring non-productive variants. *rs2z35* knockout led to an increase in full-length protein-coding *RS2Z36* levels through AS, suggesting that *RS2Z35* attenuates *RS2Z36* levels in the WT. *rs2z36* knockout, however, did not impact *RS2Z35* levels, suggesting that *RS2Z36* does not cross regulate *RS2Z35* transcripts under physiological conditions. Overexpression of either member impacted splicing and functional levels of both *RS2Z35* and *RS2Z36*, suggesting a regulatory mechanism for maintaining the two proteins at homeostatic levels.

4.9 Redundancy of RS2Z proteins in *HSFA2* splicing regulation

HSFA2 splicing profiles in transgenic and mutant plants were assessed by RT-PCR in detached leaves exposed to 40°C for 1 hour, as described in section 4.1 (Fig. 6F). In line with transient overexpression of HA-RS2Z proteins in tomato protoplasts (Fig. 6G & Fig. 7C), stable overexpression of *GFP-RS2Z* in transgenic tomato plants reduced the splicing efficiency of *HSFA2* intron 2 by approximately 10 % (Fig. 17A-B). Interestingly, the *HSFA2* splicing profile was not altered in *rs2z35* and *rs2z36* single mutants, neither after 1, nor 2 h HS (40°C) (Fig. 17C & E). However, *HSFA2* intron 2 splicing efficiency was enhanced in the *rs2z35 rs2z36* mutant by approximately 10% after 1 h HS and by 7% after 2 h HS (Fig. 17D-E), therefore confirming that RS2Z proteins are indeed acting as splicing silencers in *HSFA2* AS. The absence of an effect on *HSFA2* splicing in the *rs2z* single mutants thus indicates a redundancy in splicing regulation, at least for *HSFA2*.

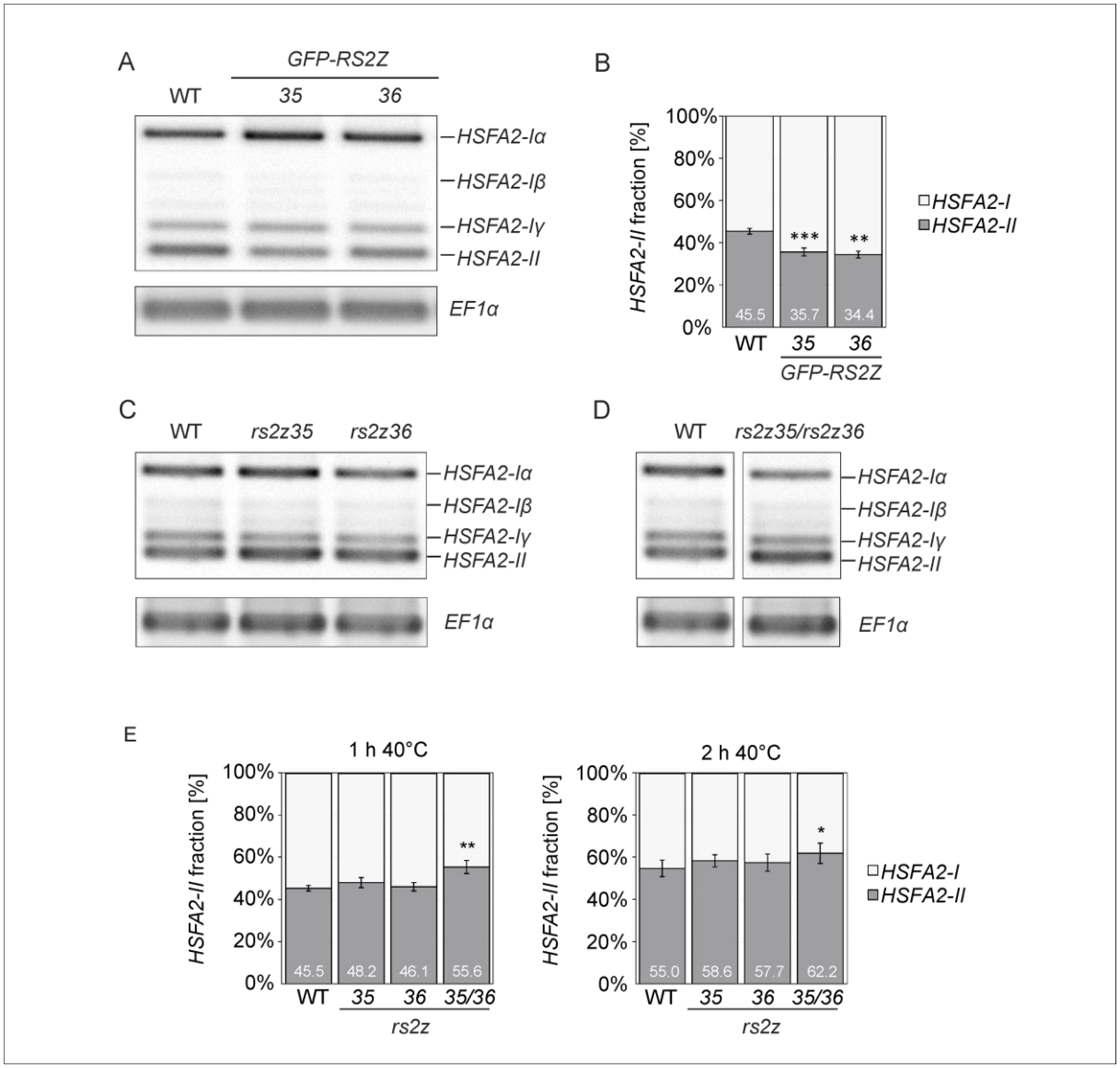

Figure 17. Regulation of *HSFA2* intron 2 splicing in *rs2z* mutants and *GFP-RS2Z* overexpression plants. (A) *HSFA2* intron 2 splicing profile in leaves of WT and *GFP-RS2Z* plants exposed to 1 h 40°C as described in Fig. 6F. **(B)** Quantification of *HSFA2* intron 2 splicing efficiency in *GFP-RS2Z* plants exposed to 1 h 40°C as depicted in (A) and as described in Fig 6G. *HSFA2* intron 2 splicing profile in leaves from the WT, *rs2z* single mutants **(C)** and the *rs2z35 rs2z36* double mutant **(D)** exposed to 1 h 40°C. Quantification of *HSFA2* intron 2 splicing efficiency in *rs2z* mutant plants exposed to 1 h 40°C (**E**, left side) as depicted in (C) and (D) or exposed to 2 h 40°C (**E**, right side). Values represent the average of at least six independent biological replicates. RT-PCRs were conducted with 25 cycles for *HSFA2* and 28 cycles for *EF1α*. Asterisks indicate statistical significance based on paired student's t-test against the WT: * $p < 0.05$, ** $p < 0.01$, *** $p < 0.001$. Error bars represent standard error (SE).

4.10 Interaction of RS2Z proteins with *HSFA2* pre-mRNA

As both RS2Z35 and RS2Z36 were shown to regulate *HSFA2* intron 2 AS, further investigations were targeted towards the interaction of RS2Z proteins with the *HSFA2* pre-mRNA *in vitro* by EMSA and *in vivo* by RIP.

4.11.1 Expression and purification of recombinant RS2Z proteins

To study *in vitro* binding of RS2Z35 and RS2Z36 towards *HSFA2* intron 2, recombinant GB1-His-RS2Z(RBD) proteins were expressed in and purified from bacterial cells. Full length SR proteins could not be obtained in *E. coli*, likely due to insufficient protein phosphorylation, resulting in poor solubility (not shown). Similar obstacles were also reported for other splicing factors like SF1 (Lee et al., 2020). Although stable and phosphorylated full-length SR proteins were successfully expressed in a cell-free translation system using Tobacco BY-2 lysate (Buntru et al., 2014), the yield was not sufficient for subsequent purification (not shown). Therefore, expression constructs were composed of the RNA binding components (RRM and ZnKs, further referred to as RNA binding domain (RBD)) (Fig. 18B, see Supplemental Fig. 10 for the aa sequences). The solubility of the recombinant proteins was aided by the addition of an N-terminal solubility tag, the immunoglobulin G-binding domain 1 of

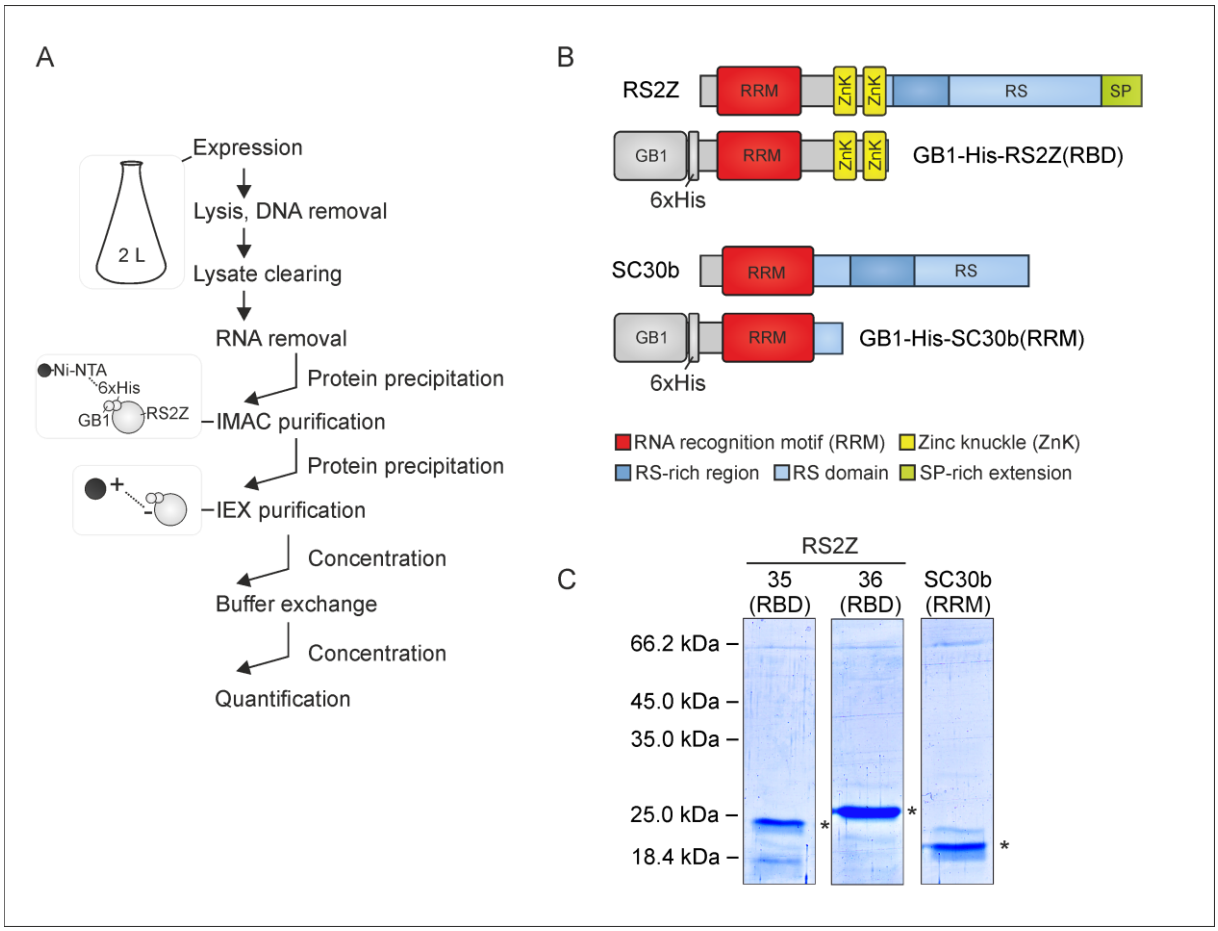

Figure 18. Expression and purification of recombinant SR proteins. (A) Schematic workflow. **(B)** Domain structure of expression constructs for recombinant RS2Z proteins (GB1-His-RS2Z35(RBD), GB1-His-RS2Z36(RBD)) and SC30b (GB1-His-SC30b(RRM)). **(C)** Representative Coomassie-stained 12% polyacrylamide gel following SDS-PAGE of elution fractions after cation exchange chromatography. Asterisks indicate the expected MW for the respective recombinant protein.

Streptococcal protein G (GB1) (Zhou et al., 2001; Cheng and Patel, 2004) which was previously used in studies involving the expression of SR protein RRMs without impacting their structure (Phelan et al., 2012). The solubility tag was followed by a 6xHis tag for affinity purification (Fig. 18A-B). The detailed purification procedure is described in section 3.28 and an overview of the workflow is provided in Figure 18A. Recombinant GB1-His-RS2Z35(RBD), GB1-His-RS2Z36(RBD) and GB1-His-SC30b(RRM) were expressed in *E. coli* and purified by IMAC (Supplemental Fig. 11A-C) followed by IEX (Supplemental Fig. 11D-F). Figure 18C shows a representative polyacrylamide gel of the purified recombinant SR proteins after IEX purification. For GB1-His-RS2Z35(RBD) with a MW of 23.75 kDa, a second protein signal at lower MW (approximately 18 kDa) emerged during purification, likely resulting from partial protein degradation. This, however, could not be observed for GB1-His-RS2Z36(RBD) to that extend, indicating that recombinant RS2Z35 was less stable than RS2Z36 and SC30b (Fig 18.C). Additionally, the overall yield of stable purified recombinant RS2Z35 was lower than RS2Z36 and SC30b, thus preventing the coverage of a broader range of RS2Z35 protein concentration in EMSA.

4.11.2 RNA Electromobility shift assay

To assess *in vitro* binding of RS2Z proteins to *HSFA2* intron 2, three intronic regions of the *HSFA2* pre-mRNA were transcribed *in vitro*. This followed the assumption that due to intron definition in plants and their function as splicing repressors, RS2Z proteins would preferentially bind to intronic sequences. The transcribed RNAs include the entire intron 2 of 300 nt, the 5'SS region including 40 nt of exon 2 and 56 nt of intron 2, and the 3'SS region including 50 nt of intron 2 and 46 nt of exon 3 (Fig. 19A. See Supplemental Fig. 1 for the nt sequences). All RNAs were transcribed with a 3' extension coding for the SP6 promoter sequence. Thereby, subsequent annealing of the RNA with a Cy5-labelled oligonucleotide complementary to the SP6 sequence allowed indirect RNA labeling (Fig. 19B).

For RS2Z35(RBD) and RS2Z36(RBD), binding towards the entire *HSFA2* intron 2 was established with increasing amounts of protein, causing a band shift (Fig. 19C). While the affinity towards the intron was higher for RS2Z35(RBD) with a dissociation constant (K_D) of approximately 100-125 nM (Fig. 19C), RS2Z36(RBD) showed lower affinity with a K_D of approximately 600 nM (Fig. 19D). In addition, SC30b which also acts as splicing inhibitor of *HSFA2* pre-mRNA (section 4.1), was able to bind to the RNA probe with a K_D of > 1 µM (Fig. 19E). In all cases, but preferentially for RS2Z36(RBD), binding of the entire intron caused a smear instead of a clear band shift, suggesting the presence of more than a single binding site for these proteins.

The specificity of the binding was assessed by a competitor assay in which the binding reaction was carried out in the presence of either non-specific (tRNA, N) or specific (unlabelled *in vitro* transcribed intron 2, S) competitor RNA in 28-fold excess (Fig. 19F). For RS2Z proteins as well as for SC30b, binding of labelled intron 2 was abolished in the presence of excess unlabelled intron 2, but not in the presence of excess tRNA, indicating that the binding of all three SR proteins for intron 2 was indeed specific (Fig. 19F).

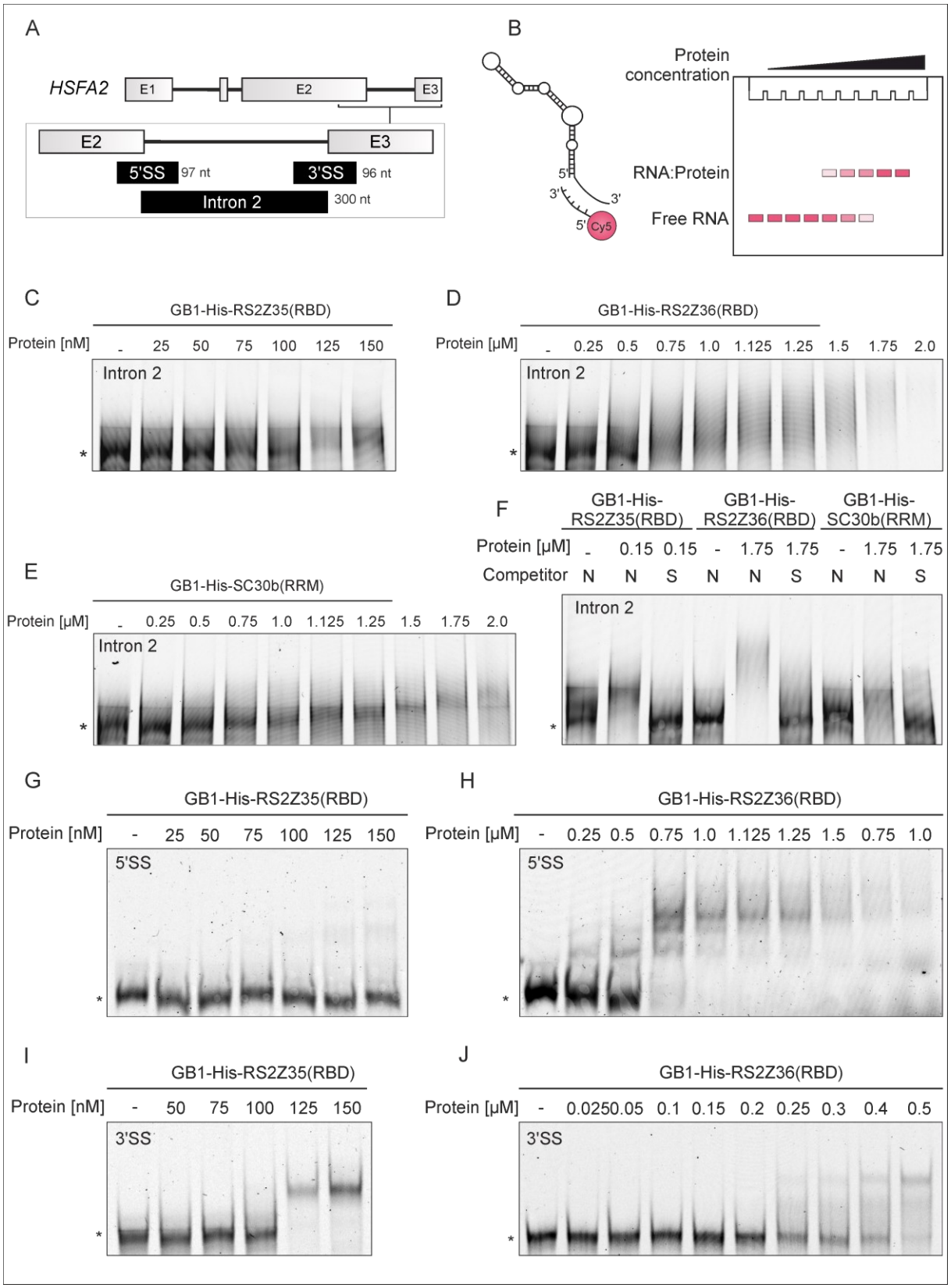
A
HSFA2
E1
E2
E3
E2
E3
5'SS
97 nt
3'SS
96 nt
Intron 2
300 nt
B
Protein concentration
RNA:Protein
Free RNA
5'
3'
3'
5'
Cy5
C
GB1-His-RS2Z35(RBD)
Protein [nM]
- 25 50 75 100 125 150
Intron 2
*
D
GB1-His-RS2Z36(RBD)
Protein [µM]
- 0.25 0.5 0.75 1.0 1.125 1.25 1.5 1.75 2.0
Intron 2
*
E
GB1-His-SC30b(RRM)
Protein [µM]
- 0.25 0.5 0.75 1.0 1.125 1.25 1.5 1.75 2.0
Intron 2
*
F
GB1-His-RS2Z35(RBD)
GB1-His-RS2Z36(RBD)
GB1-His-SC30b(RRM)
Protein [µM]
- 0.15 0.15 - 1.75 1.75 - 1.75 1.75
Competitor
N N S N N S N N S
Intron 2
*
G
GB1-His-RS2Z35(RBD)
Protein [nM]
- 25 50 75 100 125 150
5'SS
*
H
GB1-His-RS2Z36(RBD)
Protein [µM]
- 0.25 0.5 0.75 1.0 1.125 1.25 1.5 0.75 1.0
5'SS
*
I
GB1-His-RS2Z35(RBD)
Protein [nM]
- 50 75 100 125 150
3'SS
*
J
GB1-His-RS2Z36(RBD)
Protein [µM]
- 0.0250.05 0.1 0.15 0.2 0.25 0.3 0.4 0.5
3'SS
*

Figure 19. *In vitro* binding of recombinant RS2Z35, RS2Z36 and SC30b to *HSFA2* intron 2. (A) Representation of the *HSFA2* gene locus with indicated position and length of the *in vitro* transcribed RNAs. **(B)** Schematic representation of the workflow. *In vitro* transcribed RNA was indirectly fluorescently labelled by annealing to a Cy5-labelled oligonucleotide complementary to an extension of the RNA of interest. RNA and purified protein were incubated, and complexes were subsequently separated on 5% native polyacrylamide gels, followed by imaging of fluorescent signals. EMSA gels of the entire *HSFA2* intron 2 with purified recombinant GB1-His-RS2Z35(RBD) **(C)**, GB1-His-RS2Z36(RBD) **(D)** and GB1-His-SC30b(RRM) **(E)**. **(F)** Competitor assay by performing EMSA using the entire *HSFA2* intron 2 along with non-specific (tRNA, N) or specific (unlabelled intron 2, S) RNA in 28x molar excess. EMSA gels of the *HSFA2* 5'SS region with purified recombinant GB1-His-RS2Z35(RBD) **(G)** and GB1-His-RS2Z36(RBD) **(H)**. EMSA gels of the *HSFA2* 3'SS region with purified recombinant GB1-His-RS2Z35(RBD) **(I)** and GB1-His-RS2Z36(RBD) **(J)**. All EMSA experiments were performed using 30 nM RNA and 28x excess tRNA (with the exception for the competitor assay as described above).

Since both RS2Z proteins were able to bind to intron 2, it was investigated further whether RS2Z proteins were able to bind to both the 5'SS and 3'SS region and whether there would be preferences towards one region, potentially giving insight into the mechanism behind their splicing regulation.

RS2Z35-RBD was able to bind both the 5'SS and 3'SS region with a K_D of >150 nM and 100-125 nM, respectively, showing a higher affinity towards the 3'SS region (Fig. 19G & I). RS2Z36-RBD again showed lower affinity towards the RNA compared to RS2Z35-RBD, with a K_D of approximately 600 nM towards the 5'SS and 450 nM towards the 3'SS (Fig. 19H & J).

Collectively, the RNA binding elements of SC30b, RS2Z35 and RS2Z36 were able to bind to the *HSFA2* intron 2 *in vitro*, whereby RS2Z35(RBD) and RS2Z36(RBD) were able to bind at least two different regions, the 5'SS and the 3'SS region. Both RS2Z35(RBD) and RS2Z36(RBD) showed a higher affinity towards the 3'SS, whereby the overall affinity towards intron 2 was higher for RS2Z35(RBD) than for RS2Z36(RBD).

4.11.3 RNA Immunoprecipitation

To investigate whether RS2Z proteins bind to *HSFA2* RNA *in-vivo*, RNA immunoprecipitation (RIP) previously established for *Arabidopsis* (Köster et al., 2014) was adapted for tomato and performed using transgenic plant lines expressing *GFP* or *GFP-RS2Z*. The detailed workflow is described in section 3.29 and Figure 20A provides an overview. In brief, detached leaves from *GFP-RS2Z35*, *GFP-RS2Z36* and *GFP* expressing transgenic plants were exposed to 1 h 40°C to allow the synthesis of *HSFA2* pre-mRNA. Subsequently, RNA-protein complexes were crosslinked by formaldehyde fixation which allowed stringent washes and prevented unspecific binding after cell lysis. The optimal formaldehyde concentration was empirically determined by observing rRNA recovery after crosslinking (Supplemental Fig. 2A). GFP-RS2Z proteins and associated RNAs were then immunopurified by using His-tagged GFP-V_HH nanobodies that were purified from *E. coli* in this study (Supplemental Fig. 12). Successful recovery of GFP-RS2Z proteins and GFP after IP is depicted in Figure 20B. The levels of transcripts in the elution fraction (IP) were normalized to the input and expressed as relative enrichment to the GFP sample (described in detail in section 3.29.6).

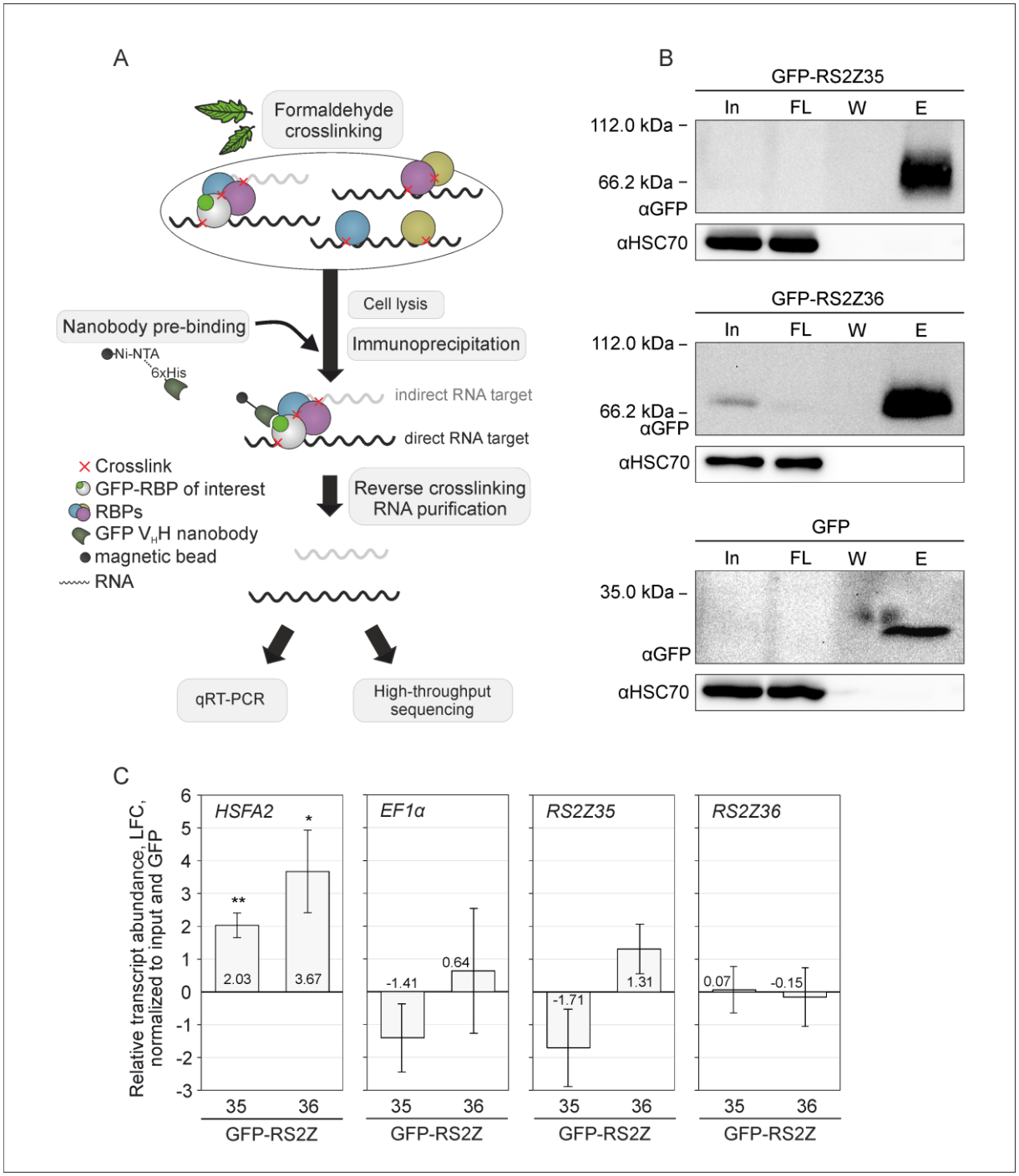

Figure 20. ***In vivo*** **binding of potential RNA targets by RS2Z35 and RS2Z36 using RNA immunoprecipitation (RIP). (A)** Representation of the general RIP workflow: Detached leaves from *GFP* and *GFP-RS2Z* overexpression plant are subjected to 1 h 40°C. RNA-protein complexes are subsequently crosslinked by formaldehyde fixation, followed by cell lysis. His-tagged GFP-V_HH nanobodies are prebound to Ni-NTA agarose coated magnetic beads. Cell lysates are mixed with the prebound nanobodies (IP), followed by extensive washing and elution of GFP-fusion proteins along with associated RNAs. Crosslinking is reversed, RNAs extracted and either transcribed into cDNA and used for qRT-PCR or used for library preparation followed by RNA sequencing. **(B)** Validation of GFP and GFP-RS2Z IP using GFP- V_HH nanobodies as described in (A) by immunoblot analysis. In: Input (2%), FL: flowthrough (2%), W: last wash (2%), E: elution (40%). **(C)** Enrichment of *HSFA2, EF1α, RS2Z35* and *RS2Z36* transcripts obtained by qRT-PCR following RIP. Enrichment values represents the average of four independent biological replicates. Transcript levels of eluted RNAs (IP) were normalised to the input and expressed as LFC relative to GFP, using the $2^{-\Delta\Delta Ct}$ method (Livak and Schmittgen, 2001). Asterisks indicate statistical significance based on paired student's t-test against GFP: * $p < 0.05$, ** $p < 0.01$. Error bars: SE.

In both *GFP-RS2Z35* and *GFP-RS2Z36* samples, *HSFA2* transcripts were significantly enriched more than 4-fold compared to *GFP*, indicating that *HSFA2* pre-mRNA is associated with both RS2Z proteins *in-vivo* (Fig. 20C, panel 1). *EF1α* which served as negative control was indeed not enriched (Fig. 20C, panel 2). Surprisingly, transcripts coding for RS2Z35 or RS2Z36 were not significantly enriched in either *GFP-RS2Z35* or *GFP-RS2Z36* samples (Fig. 20C, panel 3 & 4), suggesting that cross- and autoregulation described in section 4.8 are likely not attributed to direct interaction with the impacted transcripts and may instead be mediated through other proteins.

4.11 Involvement of RS2Z proteins in acquired and basal thermotolerance

Further, the consequences of *HSFA2* splicing regulation by RS2Z proteins on HS gene expression and thermotolerance were assessed. *HSFA2* is a classical HS-induced gene with peak expression after 1 h HS at 40°C (Fig. 21A). Following AS of *HSFA2* intron 2 during application of 40°C HS, HSFA2-I encoding transcripts accumulated upon the onset of HS, but *HSFA2* splicing efficiency increased over time (Fig. 21B). Simultaneously, the induction of total *HSFA2* levels declined following 1 h HS (Fig. 21A-B). HSFA2-I protein levels however peaked at 2 h HS and remained stable for at least one hour, while HSFA2-II levels were scarcely detectable due to low protein stability (Fig. 21C). It is noteworthy, that there was a visible delay between transcription and translation whereby peak transcriptional induction of *HSFA2* was observed after 1 h HS, which however corresponds to peak protein levels observed after 2 h HS (Fig. 21A-C). In line with RT-PCR analyses showing a lack of *HSFA2* splicing changes in *rs2z* single mutants (Fig. 17C & E), HSFA2 protein levels were not changed either (Fig. 21D).

In line with RT-PCR analyses showing a ratio shift towards transcripts coding for the less stable isoform HSFA2-II in the *rs2z35 rs2z36* mutant (Fig. 17D-E), the HSFA2-I protein fraction was reduced relative to HSFA2-II (Fig. 21E). More prominently, overall HSFA2 protein levels were reduced in the *rs2z35 rs2z36* mutant compared to the WT in response to 1, 2 and 3 h 40°C (Fig. 21E). Congruent with the reduction in HSFA2 protein levels, transcript accumulation of known HSFA2 targets such as *HSP17.7A-CI* and *APX3* (Fragkostefanakis et al., 2016) obtained by RT-PCR were reduced upon 2 h 40°C only in *rs2z35 rs2z36*, but not in *rs2z* single mutants (Fig. 22A). Interestingly, *HSFA2* itself was transcriptionally reduced upon 2 h in *rs2z35 rs2z36* (Fig. 22B). In line with the reduction in transcript abundance (Fig. 22A), HSP17-CI protein levels were reduced in the *rs2z35 rs2z36* mutant, whereby the reduction was more subtle after 1 and 2 h 40°C and more prominently after 3 h HS (Fig. 22D). In *rs2z* single mutants, HSP17-CI protein levels were not affected (Fig. 22C).

Since HSFA2 is a key factor involved in ATT (Hu et al, 2020a) and its levels were affected in the *rs2z35 rs2z36* mutant as described above, thermotolerance of *rs2z* mutant plants was investigated to understand their role in physiological responses to HS, using the hypocotyl elongation assay (Fig. 23A). In brief, ATT was assessed by priming young seedlings with a nonlethal HS of 40°C for 1 h, followed by a 3 h recovery period to allow synthesis of HS gene products, and subsequent exposure to a severe HS of 47.5°C for 1.5 hours, thus employing a common regime to assess short-term ATT (Fig. 23A).

An *hsfa2* knockout mutant was used as an ATT-sensitive genotype. Under control conditions, all genotypes showed a similar hypocotyl elongation (growth rate), except for *rs2z35 rs2z36* which had a 0.01 cm/day reduced elongation compared to the WT (Fig. 23B). Interestingly, after exposure to the ATT regime, all mutants showed reduced growth relative to their own controls (Fig. 23C). Considering that *HSFA2* was only impacted in the *rs2z35 rs2z36* mutant (demonstrated in Fig. 17 and Fig. 21), these results indicate that *RS2Z35* and *RS2Z36* regulate ATT in an HSFA2-independent manner.

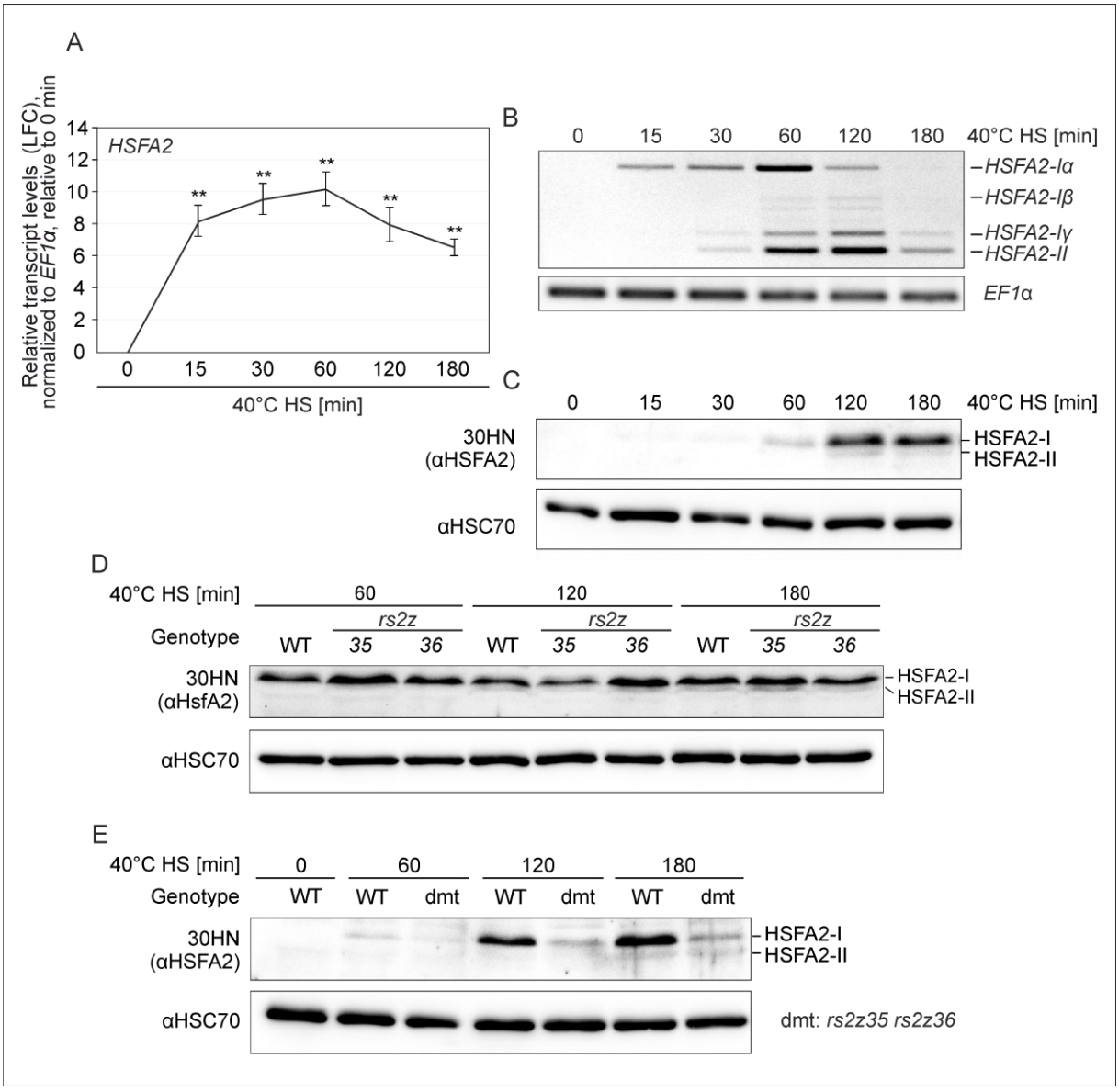

Figure 21. Regulation of *HSFA2* levels by heat and in *rs2z* mutants. (A) HS-induced expression of *HSFA2* in tomato leaves over 3 h HS at 40°C, starting from the onset of HS application (0 min). Transcript levels are normalised to the housekeeping gene *EF1α* as internal standard and expressed as LFC relative to 0 min HS, using the $2^{-\Delta\Delta Ct}$ method (Livak and Schmittgen, 2001). Values represent the average of four independent biological replicates. Asterisks indicate statistical significance based on paired student's t-test against 0 min: * $p < 0.05$, ** $p < 0.01$. Error bars: SE. **(B)** *HSFA2* intron 2 splicing profile over 3 h HS at 40°C obtained as described in Fig. 6F. **(C)** HSFA2 protein accumulation over 3 h HS at 40°C obtained by immunoblot analysis employing an antibody detecting both HSFA2-I and HSFA2-II. HSC70 served as internal control. **(D)** Immunoblot analysis in WT and *rs2z* single mutants as described for (C). **(E)** Immunoblot analysis in WT and *rs2z35 rs2z36* double mutant (dmt) as described for (C).

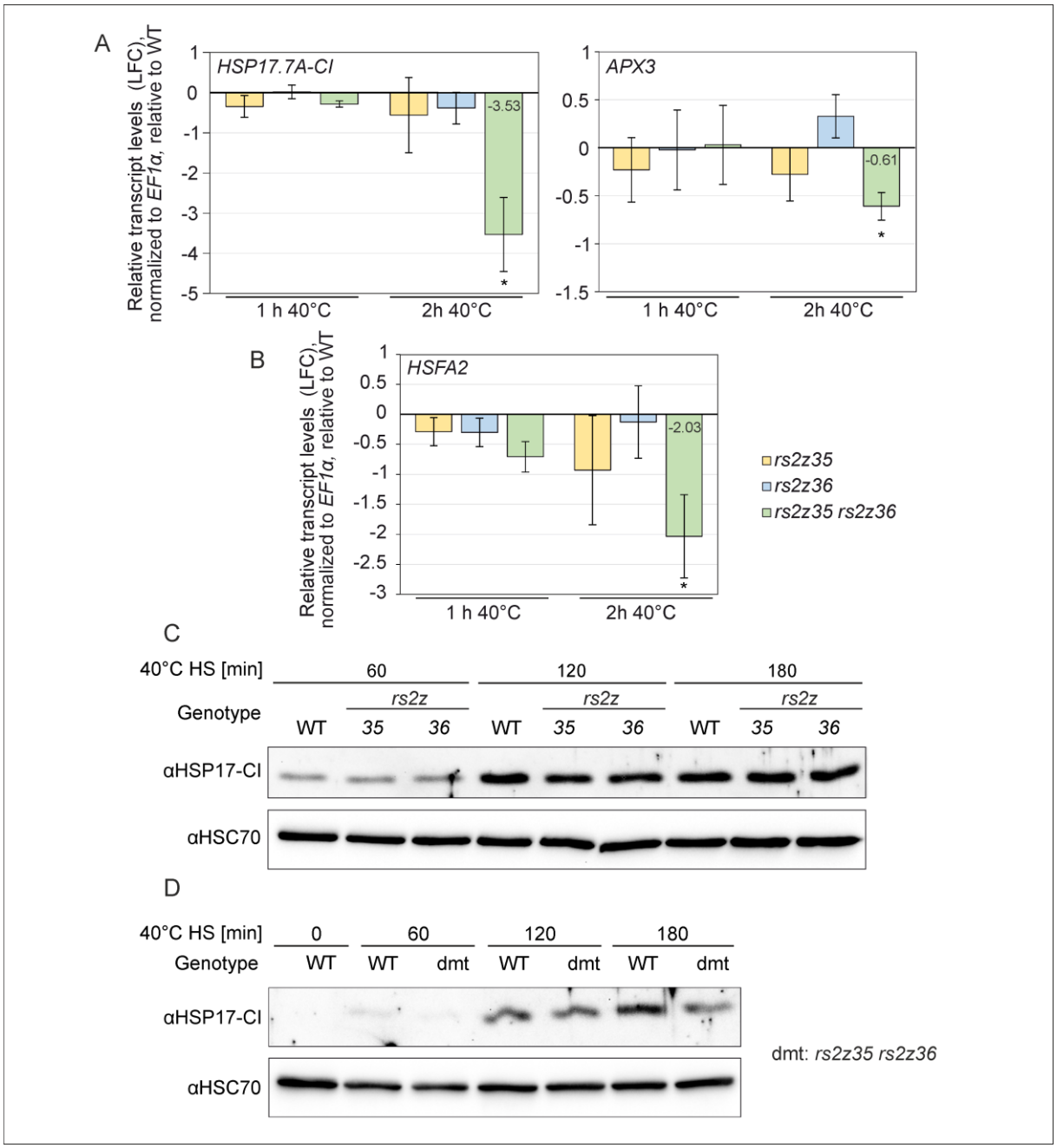

Figure 22. E**xpression of HS-responsive genes in *rs2z* mutants.** Expression of HS-genes, *HSP17.7A-CI*, *APX3* **(A)** and *HSFA2* **(B)** in response to 1 and 2 h 40°C in leaves from *rs2z* mutants relative to WT. Transcript levels are normalised to the housekeeping gene *EF1α* as internal standard and expressed as LFC relative to WT, using the $2^{-\Delta\Delta Ct}$ method (Livak and Schmittgen, 2001). Values represent the average of at least four independent biological replicates. Asterisks indicate statistical significance based on paired student's t-test against WT: * $p < 0.05$, ** $p < 0.01$. Error bars: SE. **(C)** HSP17-CI protein levels after 1,2 and 3 h HS at 40°C obtained by immunoblot analysis in leaves of WT and *rs2z* single mutants. HSC70 (non-HS responsive HSP) served as control. **(E)** Immunoblot analysis of HSP17-CI protein levels in WT and *rs2z35 rs2z36* double mutant as described for (C). The HSP17-CI antibody may recognize several HSP17-CI proteins, but the extent to which individual HSP17-CI proteins contribute to the immunoblot signal is not known.

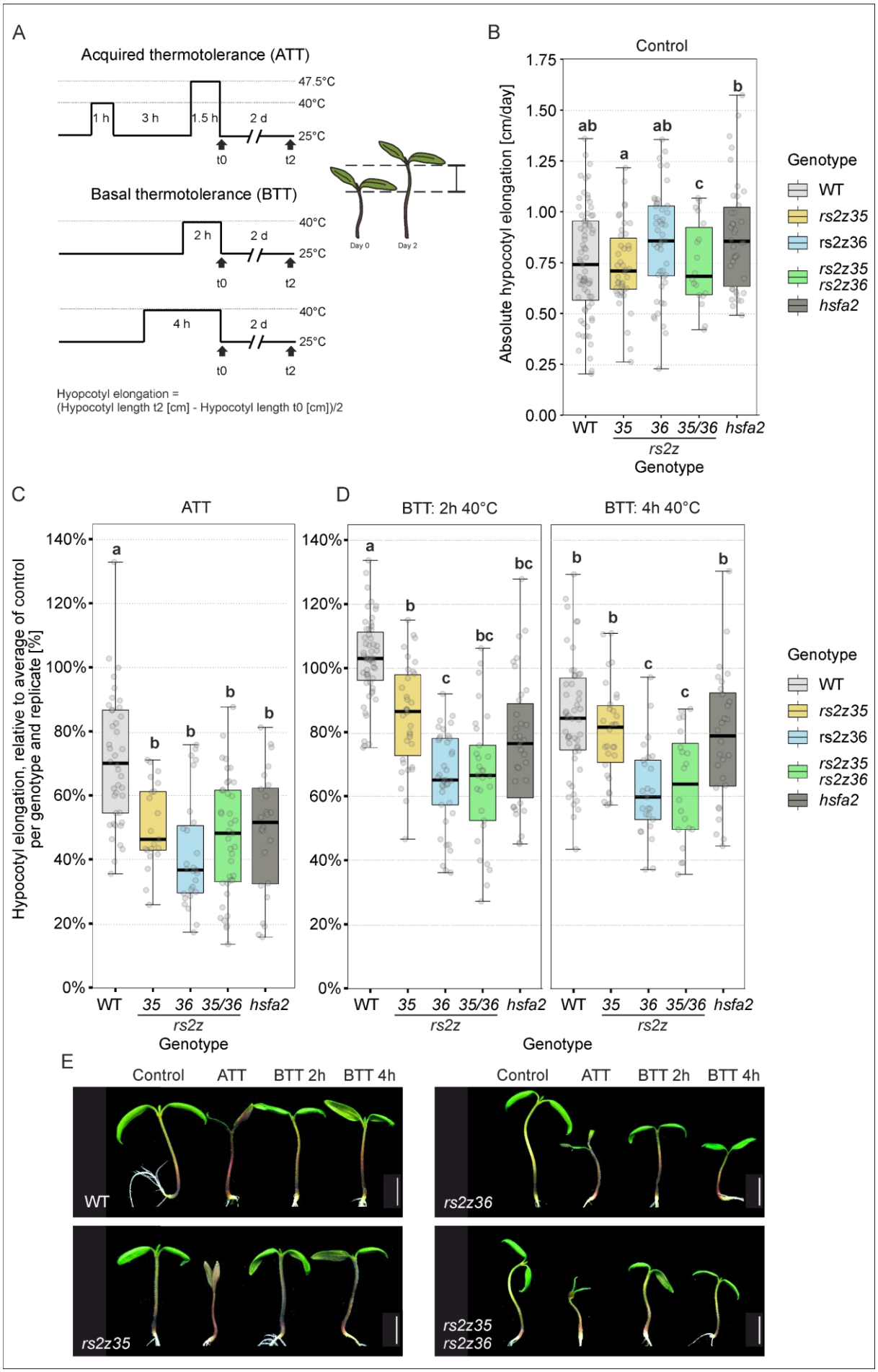
A
Acquired thermotolerance (ATT)
47.5°C
40°C
1 h
3 h
1.5 h
2 d
25°C
t0
t2
Basal thermotolerance (BTT)
2 h
4 h
Day 0
Day 2
Hyopcotyl elongation =
(Hypocotyl length t2 [cm] - Hypocotyl length t0 [cm])/2
B
Control
Absolute hypocotyl elongation [cm/day]
WT
35
36
35/36
hsfa2
rs2z
Genotype
rs2z35
rs2z36
rs2z35 rs2z36
C
ATT
D
BTT: 2h 40°C
BTT: 4h 40°C
Hypocotyl elongation, relative to average of control per genotype and replicate [%]
E
Control
ATT
BTT 2h
BTT 4h
WT
rs2z36
rs2z35
rs2z35 rs2z36

Figure 23. Acquired and basal thermotolerance of *rs2z* mutant plants. (A) Schematic representation of temperature regimes applied to tomato WT and *rs2z* mutant seedlings. **(B)** Absolute growth of WT and *rs2z* mutant plants under control conditions, depicted as hypocotyl elongation [cm/day]. Relative growth rate after ATT **(C)** or BTT **(D)** stress treatments were calculated as hypocotyl elongation relative to the average of control plants of the same genotype and replicate. Individual datapoints are shown as dots. At least 18 seedlings were used in total across four independent replicates. Boxplots show the interquartile range, lines represent the median. Statistical analysis was performed by one-way ANOVA and Duncan post-hoc test with a significance threshold of 0.05 **(E)** Composite representative photographs of seedlings two days after stress. The images were assembled digitally without alterations in their proportional scale by including a ruler in each picture. White lines indicate 1 cm.

The assessment of thermotolerance was extended to BTT, further investigating the thermotolerance capacity of the mutants by exposure to 40°C for 2 or 4 hours (Fig. 23A). Exposure to 40°C is considered a mild stress treatment as indicated by unaltered growth rates of etiolated wild type seedlings exposed to increasing temperatures for 1.5 h (Hu et al., 2020b). Additionally, in a preliminary experiment conducted by Bachiri, the exposure to 1 h 40°C did not impact *rs2z* single mutants (Supplemental Fig. 13). Therefore, the HS exposure to 40°C was prolonged to 2 or 4 hours. While *hsfa2* was more sensitive than the WT after 2 h HS treatment, the growth rate was indifferent after 4 h HS (Fig. 23D-E). *rs2z36* and the *rs2z35 rs2z36* double mutant were more sensitive than the WT upon both HS treatments, while *rs2z35* showed higher sensitivity only in response to the 2 h treatment (Fig. 23D-E).

In summary, *HSFA2* itself as well as HS-genes downstream of *HSFA2* were negatively affected in the *rs2z35 rs2z36* mutant, but not in the *rs2z* single mutants, suggesting regulation of HS genes in a redundant manner, which can at least in part be attributed to *HSFA2* splicing. Surprisingly, relative hypocotyl elongation after exposure to direct HS was reduced not only in the *rs2z35 rs2z36* and *hsfa2* mutants, but also in the *rs2z36* single mutant. Upon exposure to repeated HS after HS priming (ATT regime), all mutants including *rs2z35* showed reduced relative growth compared to the WT. These results suggest additional roles for RS2Z protein in ATT and an additional role for RS2Z36 in BTT through mechanisms beyond *HSFA2.*

4.12 *RS2Z*-mediated transcriptome changes

Since thermotolerance to a mild HS of 40°C was impacted not only in the *rs2z35 rs2z36* mutant, but also in the *rs2z36* mutant, global transcriptome analysis was performed utilizing RNA-Seq after 1 h 40°C, the time at which most HS-genes reach peak expression. Detached tomato leaves (WT, *rs2z35*, *rs2z36*, *rs2z35 rs2z36*) were exposed to 1 h HS (40°C) or kept under control conditions (25°C) with three biological replicates for each condition and genotype. (Fig. 24A)

Following RNA-Seq, raw reads of all 24 samples were of generally good quality with mean Phred quality scores >34 over the entire read length. Raw paired reads were mapped to the tomato genome in a splice-aware manner. 21,566,983 to 34,072,407 paired reads were obtained per sample, whereby 75.38% to 79.08% uniquely mapped to the tomato genome. Aligned reads were then counted per gene and batch effects were removed. The adjusted count data was then prefiltered for low abundant transcripts and used for differential expression (DE) analysis in the mutants against the WT for each condition (Fig. 24A). Additionally, DE in response to HS was obtained by comparing gene counts in the WT under HS conditions relative to control. To compensate for the overestimation of changes in low

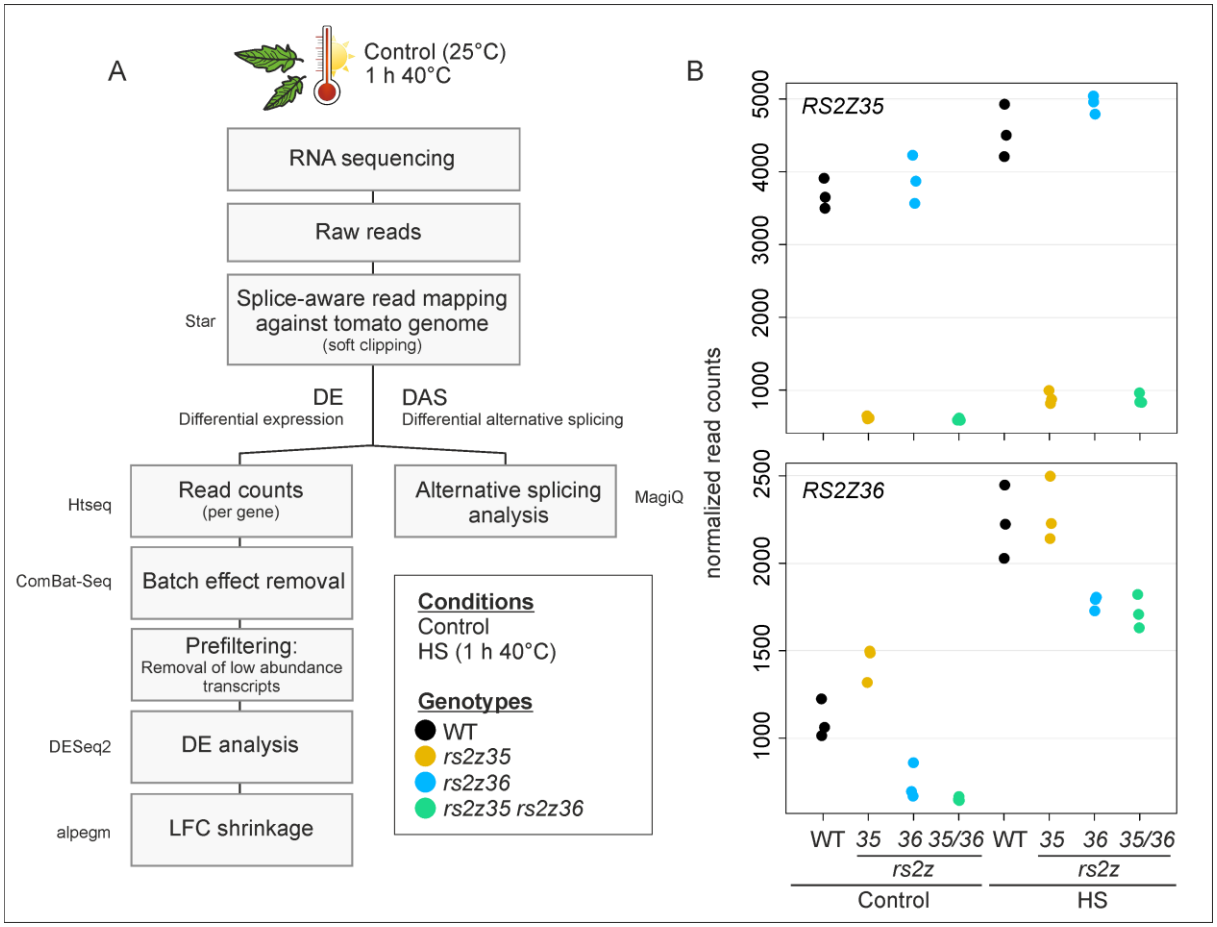

Figure 24. RNA sequencing in WT and *rs2z* mutant plants. (A) Overview of the workflow following RNA-Seq with indicated tools used. **(B)** Confirmation of *rs2z* mutants by RNA-Seq depicted by library size normalised read counts for *RS2Z35* (top) and *RS2Z36* (bottom) for both control and HS conditions in all genotypes.

expressed genes, the obtained LFCs were shrunken. All LFCs obtained from RNA-Seq further mentioned therefore refer to shrunken LFCs.

In line with qRT-PCR analysis earlier (Fig. 14C), the *RS2Z* transcripts were reduced in the respective single mutant, and both were reduced in the *rs2z35 rs2z36* double mutant (Fig. 24B).

The similarity of the samples was investigated by PCA analyses based on the top 500 genes with highest variance among all datasets (all genotypes and conditions simultaneously = row variance), showing the great impact of HS on the transcriptome by complete separation of the control and HS samples in PC1 (Fig. 25A). Further, the genotypes separated in PC2, whereby *rs2z36* and *rs2z35 rs2z36* separated from the WT and *rs2z35* under both conditions, with a more distinct separation under HS (Fig. 25A). In WT leaves, 4,581 genes were down- and 4,963 genes were upregulated in response to HS compared to control conditions (Fig. 25B). The putative functions of the proteins coded by these genes was investigated by singular gene ontology (GO) enrichment analysis of up- and downregulated genes, respectively, against all expressed genes. Due to the high number of enriched terms (37 terms for up- and 143 terms for downregulated genes in the biological process category, respectively), the GO terms were further summarized to parent terms. For HS-induced genes, the most significantly

overrepresented GO terms were those involved in response to unfolded proteins, protein folding and response to heat (Fig. 25C). The HS-reduced genes were represented by a larger number of enriched GO terms, which portrayed a broad spectrum of biological processes including shoot system

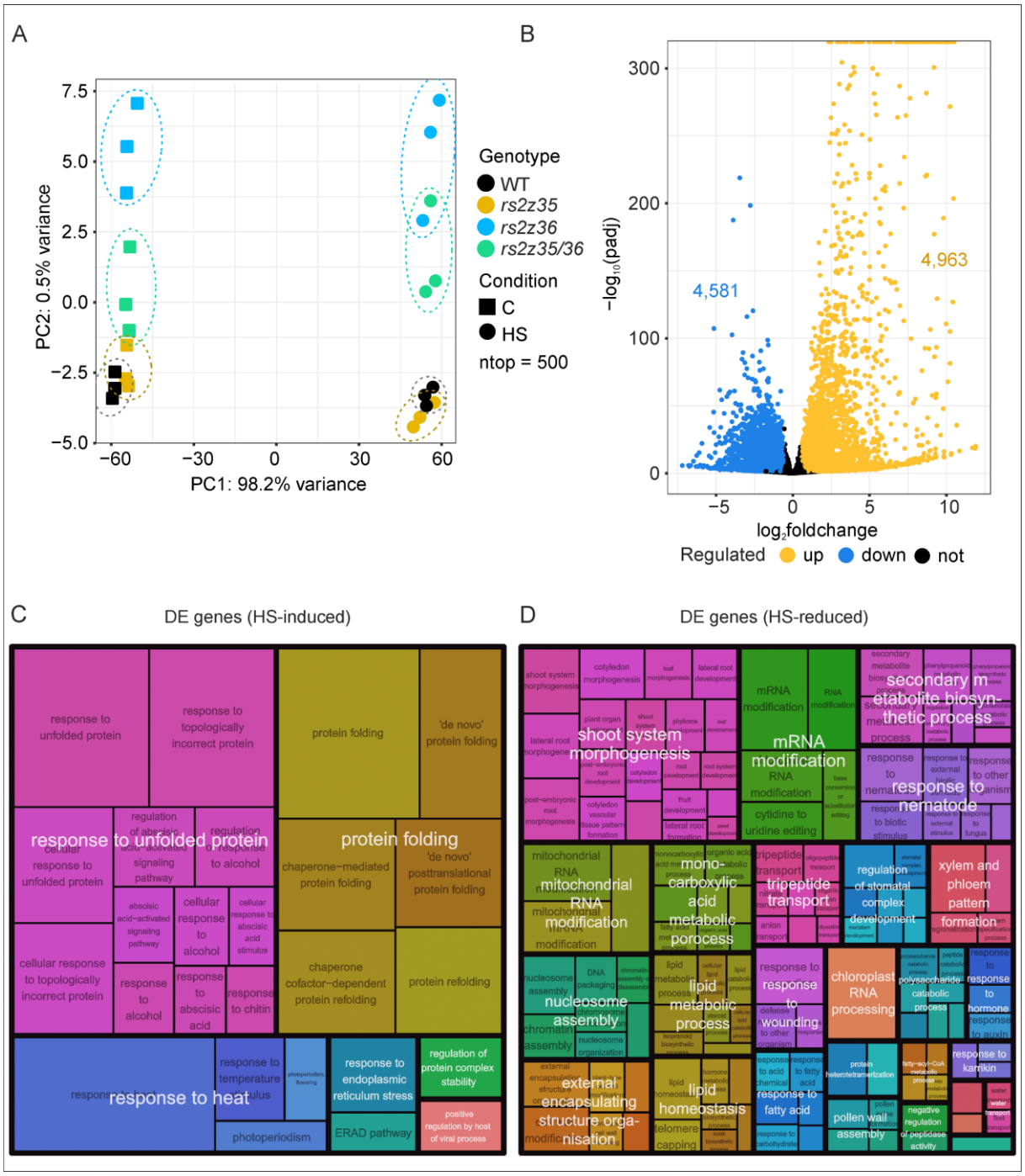

Figure 25. Differential expression analysis in response to heat stress. **(A)** Two-dimensional principal component analysis (PCA) plot depicting similarities between control and HS (1 h 40°C) samples for WT and *rs2z* mutants based on the 500 genes with the greatest row variance. Ellipses were drawn manually in to highlight clustering. **(B)** Volcano plot depicting up- and downregulated genes in the WT in response to HS compared to control. Colours indicate significant up- (yellow) and downregulated (blue) genes. Alterations in expression were considered significant with I LFC I > 0.5849 and padj < 0.05. Summarized parent terms for significantly enriched GO terms in HS-induced **(C)** or HS-reduced **(D)** genes compared to all expressed genes. Colours indicate terms belonging to the same cluster. Box sizes are proportional to significance level (-log10(FDR)).

morphogenesis, mRNA modification, secondary metabolite biosynthesis process and many others, indicating the repression of a large subset of cellular functions upon HS (Fig. 25D).

A comparison between the WT and the *rs2z* mutant HS samples revealed that a total of 452 genes was differentially regulated. 13, 100 and 153 genes were upregulated and 21, 132 and 114 genes were downregulated in *rs2z35*, *rs2z36* and *rs2z35 rs2z36*, respectively (Fig 26A, left side (set size)). Similar numbers were observed under control conditions (not shown). Since *rs2z36* and *rs2z35 rs2z36* both showed HS-sensitive phenotypes earlier (section 4.11), it was of particular interest to not only globally describe which genes were affected in *rs2z* mutants under HS conditions, but especially whether there would be any overlap between the *rs2z36* single mutant and the *rs2z35 rs2z36* double mutant. The overlap of significant DE genes in *rs2z* mutants under HS is depicted as upset plot in Figure 26A (top part, intersection size). Only intersections with more than 10 genes are depicted. 28 genes were upregulated in both *rs2z36* and *rs2z35 rs2z36*, while 27 genes were downregulated in both genotypes. The small number of regulated genes in *rs2z35* did not primarily overlap with *rs2z35 rs2z36* (Fig. 26A).

Further on, all genes regulated in any *rs2z* mutant under HS were summarized as *RS2Z*-regulated genes. The analysis of intersections between the *RS2Z*-regulated genes under HS with those regulated under control conditions and those regulated by heat (DE genes in WT HS vs C) revealed, that 300 genes (67% of all *RS2Z*-regulated genes under HS) were regulated by *RS2Z* and as well HS-responsive (Fig. 26B). The majority (243 genes) of these genes was regulated by *RS2Z* specifically under HS but not under control conditions. 57 HS-responsive genes (13%) were simultaneously regulated in *rs2z* mutants under HS and control conditions. The remaining *RS2Z*-regulated genes under HS were heat unresponsive (33%). These were primarily regulated under HS (111 genes, 24%), and only 42 HS-unresponsive genes (9%) were regulated by *RS2Z* under both HS and control conditions (Fig. 26B).

To evaluate global trends of DE genes in the *rs2z* mutants, normalised log-transformed read counts of *RS2Z*-regulated genes under HS were depicted in a heatmap including read counts for all genotypes under control and HS conditions (Fig. 26C). This way, genes that were identified to be regulated by *RS2Z* were analysed for global trends among all mutants. This revealed trends that would potentially be missed when previously defined cutoffs (LFC > 0.5849, padj < 0.05) were not met in all genotypes. Comparing the read counts for the WT under control and HS conditions, it was again evident that many *RS2Z*-regulated genes were also regulated by HS, in a positive (Fig. 26C, cluster 1 & 2) or a negative way (Fig. 26, cluster 5 & 6), whereby the regulation in *rs2z* mutants was shifted either in the same direction (“up-up”, “down-down”), e. g. further upregulation of HS-induced genes in *rs2z36* and

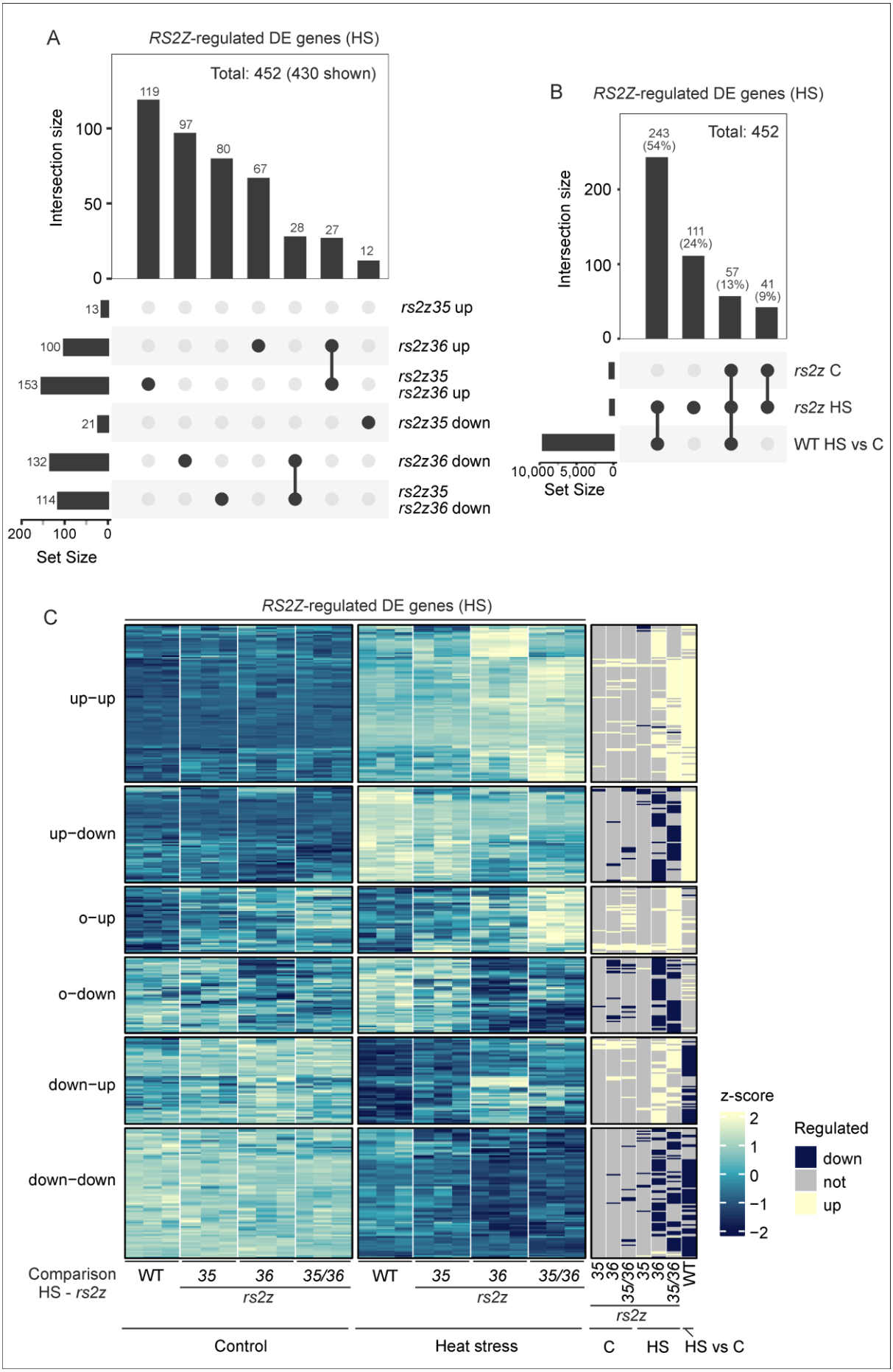
A
RS2Z-regulated DE genes (HS)
Total: 452 (430 shown)
Intersection size
119
97
80
67
28
27
12
13
100
153
21
132
114
rs2z35 up
rs2z36 up
rs2z35
rs2z36 up
rs2z35 down
rs2z36 down
rs2z35
rs2z36 down
200 100 0
Set Size
B
RS2Z-regulated DE genes (HS)
Total: 452
Intersection size
243 (54%)
111 (24%)
57 (13%)
41 (9%)
rs2z C
rs2z HS
WT HS vs C
10,000 5,000 0
Set Size
C
RS2Z-regulated DE genes (HS)
up−up
up−down
o−up
o−down
down−up
down−down
z-score
2
1
0
−1
−2
Regulated
down
not
up
Comparison
HS - rs2z
WT
35
36
35/36
rs2z
WT
35
36
35/36
rs2z
35
36
35/36
35
36
35/36
WT
rs2z
Control
Heat stress
C
HS
HS vs C

Figure 26. Differentially expressed genes in *rs2z* mutants under HS. (A) Upset plot depicting overlaps (intersections) between up- and downregulated genes in *rs2z* mutants under HS. Intersections with less than 10 genes were excluded. **(B)** Upset plot depicting overlaps between genes DE-regulated in *rs2z* mutants under control (*rs2z* C) or HS (*rs2z* HS) conditions, and genes DE-regulated in the WT in response to HS (WT HS vs C). (C) Heatmap depicting read counts for all conditions and genotypes for *RS2Z*-regulated genes under HS. Library size normalised read counts were log-transformed and z-score normalised with colours reflecting z-scores (yellow: high expression, blue: low expression). Expressions on the left side indicate trends in response to HS compared to trends as consequence of *rs2z* knockout (e. g. up-up). Right-side columns indicate statistically significant changes in the respective mutant compared to WT (or WT HS vs. C), whereby expression changes of ILFCI > 0.5849 and padj > 0.05 were considered significant. Dark blue colour indicates significant down-, light yellow colour indicates significant upregulation, respectively.

rs2z35 rs2z36 (Fig. 26C, cluster 1) or in the opposite direction ("down-up", "up-down"), e. g. downregulation of HS-induced genes as shown in Figure 26C (cluster 2). Additionally, HS-unresponsive genes were regulated in *rs2z* mutants as well, as depicted in Fig. 26C (cluster 3 & 4) ("o-up", "o-down").

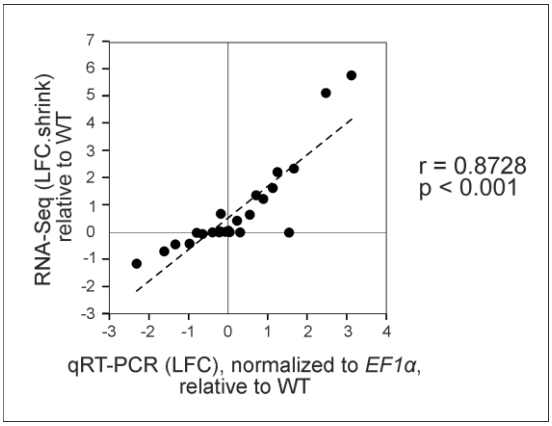

Figure 27. Correlation between RNA-Seq and qRT-PCR. LFCs were obtained from 8 genes in *rs2z35*, *rs2z36* and *rs2z35 rs2z36* relative to the WT. r: pearson correlation coefficient. The cDNA was prepared from the same RNA that was sequenced.

To confirm the reliability of the RNA-Seq approach, the DE of eight genes regulated in *rs2z35 rs2z36* was validated by qRT-PCR. Shrunken LFC values after RNA-Seq significantly correlated with LFC values obtained by qRT-PCR with a high Pearson correlation coefficient of 0.87 (Fig. 27).

RS2Z-regulated genes were characterised by GO enrichment analysis. Due to the low amount of enriched GO terms, the terms were not reduced to broader parent terms. Among the significantly enriched GO terms for biological processes, "response to external stimulus" was the most prevalent with 155 genes represented by this term, followed by response to biotic stimulus, response to other organism and response to external biotic stimulus, suggesting that RS2Z proteins take part in those response mechanisms (Fig. 28A). Enriched GO terms for molecular functions exclusively involved terms representing peptidase regulation (Fig. 28A). GO terms related to response to heat or protein folding were absent, indicating that after 1 h 40°C, RS2Z proteins largely do not regulate the transcript abundance of core HSR genes. Thereby, DE of genes reported as main actors of heat tolerance was likely not the primary cause for HS sensitivity of *rs2z36* and *rs2z35 rs2z36*.

Interestingly, 37 of *RS2Z*-regulated genes were found to code for proteins involved in RNA biosynthesis, 13 in RNA processing and 27 in protein homeostasis. These categories contain proteins with putatively important functions for the regulation of stress response and thermotolerance. The identification of genes coding for proteins present in these three classes, however, can only serve as an attempt to understand the molecular basis for the observed HS phenotypes of *rs2z* mutants and does not rule out that other classes contributed to said phenotypes to a substantial degree.

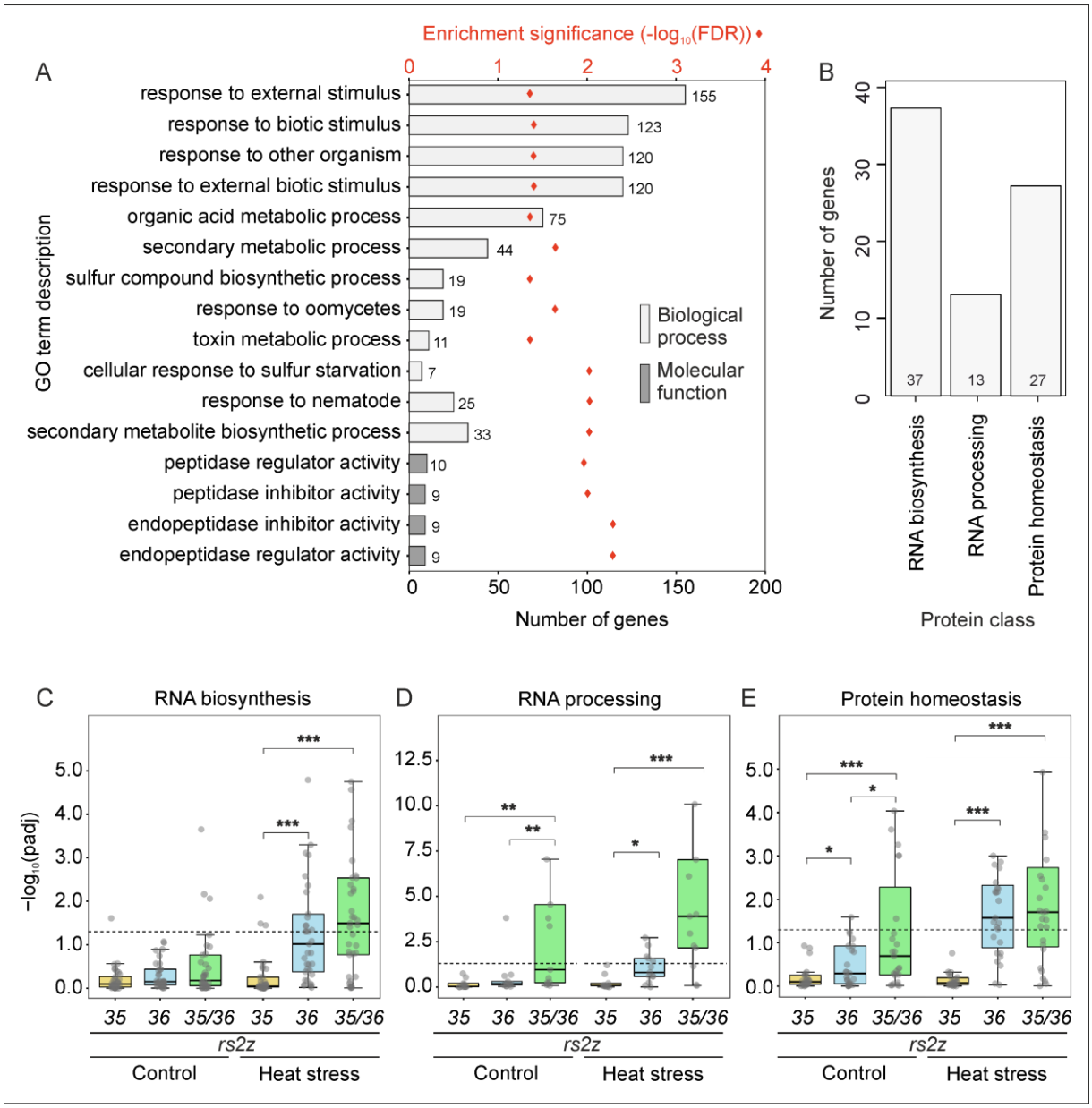

Figure 28. Characterisation of differentially expressed genes in *rs2z* mutants under HS. (A) GO term enrichment analysis of DE genes in *rs2z* mutants under HS compared to all expressed genes. Bars represent the number of genes reflected by the respective GO term. Diamonds indicate significance level. **(B)** Number of identified genes coding for proteins involved in RNA biosynthesis, RNA processing, and protein homeostasis among *RS2Z*-regulated DE genes. **(C)** Distribution of adjusted p-values for DE genes coding for proteins involved in RNA biosynthesis **(C),** RNA processing **(D)**, and protein homeostasis **(E)** among *rs2z* mutants under control and HS, depicted as boxplots. Boxplots show the interquartile range, lines represent the median. Asterisks indicate significant differences between the mutants under either control or HS conditions (paired Wilcoxon test. * $p < 0.05$; ** $p < 0.01$; *** $p < 0.001$).

The proteins involved in RNA biosynthesis are further referred to as TFs, as most genes in this class were indeed coding for TFs. Attributing to the fact that most *RS2Z*-regulated DE genes were found in *rs2z36* and *rs2z35 rs2z36*, the distribution of p-values for the three classes were observed to evaluate whether these genes were regulated in both *rs2z36* and *rs2z35 rs2z36* or were specific for one (Fig. 28C-E). Indeed, regulation of these three classes was similar for both *rs2z36* and *rs2z35 rs2z36* for which the p-value distribution was significantly different compared to *rs2z35* (Fig. 28C-E). Additionally, RNA biosynthesis genes were predominantly *RS2Z*-regulated under HS, but not under control

conditions (Fig. 28C). RNA processing and protein homeostasis genes were regulated as well under control conditions in *rs2z35 rs2z36* (Fig. 28D-E).

To get a closer impression of how the genes attributed to the three classes were regulated in the individual *rs2z* mutants under HS, heat maps were generated using log-transformed normalised count data of the HS samples (Fig. 29). In addition to the gene ID, ITAG 4.0 gene descriptions were provided for genes of particular interest due to similar regulation in either all mutants or in *rs2z36* and *rs2z35 rs2z36*. In the RNA biosynthesis gene class, approximately half were downregulated in both *rs2z36* and *rs2z35 rs2z36*, for example *CRF2-like* (Solyc07g054630) which was significantly downregulated in both *rs2z36* and *rs2z35 rs2z36*, and *WRKY9* (Solyc01g104550) which was significantly downregulated in *rs2z36* and shows a similar trend in *rs2z35 rs2z36* (Fig. 29A, cluster a). Many genes were upregulated primarily in *rs2z35 rs2z36* and showed trends towards slight upregulation in *rs2z36*, for example in the case of ethylene responsive factors (ERF) *ERF.B5* (Solyc03g093550), *ERF.B2* (Solyc03g093560) and *ERF.B4* (Solyc03g093540) (Fig. 29A, cluster b). A third group of TFs was upregulated primarily in *rs2z36* (Fig. 29A, cluster c). *CRF1* (Solyc06g009810) is one example of a TF upregulated in all *rs2z* mutants, representing a case of regulation by both *RS2Z35* and *RS2Z36* in a non-redundant fashion.

Among the genes coding for proteins involved in RNA processing, most were regulated in *rs2z35 rs2z36* only (Fig. 29B, cluster a) and some in *rs2z36* only (Fig. 29B, cluster b). A third cluster represented genes that showed a trend towards downregulation in all mutants, with some being involved in the RNA interference (RNAi pathway), for example *DICER-LIKE 2c* (Solyc11g008520) (Fig. 29B, cluster c).

Most genes coding for proteins involved in protein homeostasis were proteases or protease regulators. Roughly 1/3 were up-regulated in *rs2z35 rs2z36* or *rs2z36* with a similar trend in the respective other mutant, for example in the case of Solyc12g015800, coding for a putative RING/U-box superfamily protein (Fig. 29C, cluster a). Another set of genes was significantly downregulated in *rs2z35 rs2z36* with a similar trend in *rs2z36* (Fig. 29C, cluster b). The third cluster was significantly regulated in *rs2z36* with trends towards slight downregulation in *rs2z35* and *rs2z35 rs2z36* (Fig. 29C, cluster c).

Since genes coding for proteins involved in the response to biotic stimulus (pathogen response) were significantly enriched among DE genes in *rs2z* mutants (Fig. 28A), the regulation of these 123 genes was further inspected by heatmap visualisation in the individual mutants (Fig. 30). This group of genes was primarily composed of disease resistant (R) genes and TFs, some of which were described previously. Approximately 40% of the pathogen response genes were regulated primarily in *rs2z36* and *rs2z35 rs2z36* (e. g. TF *WRKY 9*), or in all mutants with higher impact in *rs2z35 rs2z36* (e. g. *DICER-LIKE 2c*) (Fig. 30, cluster a). Many genes were regulated primarily in *rs2z35 rs2z36* with milder effects in *rs2z36*, including *ETHYLENE-INDUCING XYLANASE (EIX) RECEPTOR 1*, *DICER-LIKE 2d,* TFs *WRKY 55* and *R2R3MYB* 52 as well as several members of the ERF family (Fig. 30, cluster b).

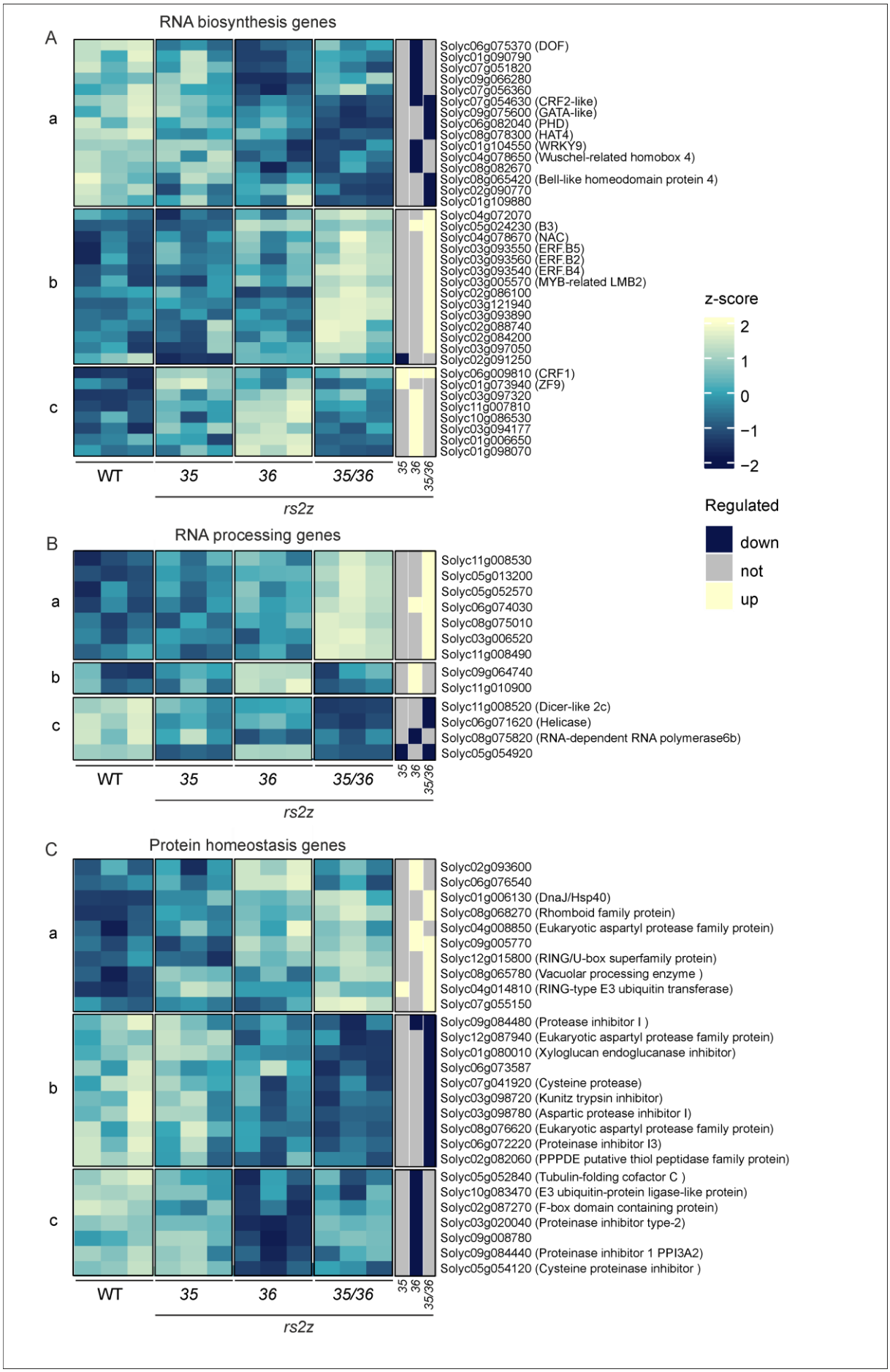
A
RNA biosynthesis genes
a
Solyc06g075370 (DOF)
Solyc01g090790
Solyc07g051820
Solyc09g066280
Solyc07g056360
Solyc07g054630 (CRF2-like)
Solyc09g075600 (GATA-like)
Solyc06g082040 (PHD)
Solyc08g078300 (HAT4)
Solyc01g104550 (WRKY9)
Solyc04g078650 (Wuschel-related homobox 4)
Solyc08g082670
Solyc08g065420 (Bell-like homeodomain protein 4)
Solyc02g090770
Solyc01g109880
b
Solyc04g072070
Solyc05g024230 (B3)
Solyc04g078670 (NAC)
Solyc03g093550 (ERF.B5)
Solyc03g093560 (ERF.B2)
Solyc03g093540 (ERF.B4)
Solyc03g005570 (MYB-related LMB2)
Solyc02g086100
Solyc03g121940
Solyc03g093890
Solyc02g088740
Solyc02g084200
Solyc03g097050
Solyc02g091250
c
Solyc06g009810 (CRF1)
Solyc01g073940 (ZF9)
Solyc03g097320
Solyc11g007810
Solyc10g086530
Solyc03g094177
Solyc01g006650
Solyc01g098070
WT
35
36
35/36
rs2z
z-score
2
1
0
−1
−2
Regulated
down
not
up
B
RNA processing genes
a
Solyc11g008530
Solyc05g013200
Solyc05g052570
Solyc06g074030
Solyc08g075010
Solyc03g006520
Solyc11g008490
b
Solyc09g064740
Solyc11g010900
c
Solyc11g008520 (Dicer-like 2c)
Solyc06g071620 (Helicase)
Solyc08g075820 (RNA-dependent RNA polymerase6b)
Solyc05g054920
WT
35
36
35/36
rs2z
C
Protein homeostasis genes
a
Solyc02g093600
Solyc06g076540
Solyc01g006130 (DnaJ/Hsp40)
Solyc08g068270 (Rhomboid family protein)
Solyc04g008850 (Eukaryotic aspartyl protease family protein)
Solyc09g005770
Solyc12g015800 (RING/U-box superfamily protein)
Solyc08g065780 (Vacuolar processing enzyme)
Solyc04g014810 (RING-type E3 ubiquitin transferase)
Solyc07g055150
b
Solyc09g084480 (Protease inhibitor I)
Solyc12g087940 (Eukaryotic aspartyl protease family protein)
Solyc01g080010 (Xyloglucan endoglucanase inhibitor)
Solyc06g073587
Solyc07g041920 (Cysteine protease)
Solyc03g098720 (Kunitz trypsin inhibitor)
Solyc03g098780 (Aspartic protease inhibitor I)
Solyc08g076620 (Eukaryotic aspartyl protease family protein)
Solyc06g072220 (Proteinase inhibitor I3)
Solyc02g082060 (PPPDE putative thiol peptidase family protein)
c
Solyc05g052840 (Tubulin-folding cofactor C)
Solyc10g083470 (E3 ubiquitin-protein ligase-like protein)
Solyc02g087270 (F-box domain containing protein)
Solyc03g020040 (Proteinase inhibitor type-2)
Solyc09g008780
Solyc09g084440 (Proteinase inhibitor 1 PPI3A2)
Solyc05g054120 (Cysteine proteinase inhibitor)
WT
35
36
35/36
rs2z

Figure 29. Heatmaps depicting a subset of *RS2Z*-regulated DE genes. Heatmaps as described for Fig. 26C for *RS2Z*-regulated genes under HS coding for proteins involved in RNA biosynthesis **(A)**, RNA processing **(B)**, and protein homeostasis **(C)**. Gene annotations were added to genes with similar trends under HS, either in *rs2z36* and *rs2z35 rs2z36*, or all mutants.

Additionally, two TFs involved in the cytokinin response pathway stood out that were not included in the 'response to biotic stimulus' GO term: *CYTOKININ RESPONSE FACTOR 1 (CRF1)* and *CYTOKININ RESPONSE FACTOR 2-LIKE* (*CRF2-like)* (Fig. 31). *CRF1* was significantly HS-induced in the WT by 2-fold and further upregulated in all *rs2z* mutants by 4.9-fold (*rs2z35*), 2.7-fold (*rs2z36*) and 4.1-fold (*rs2z35 rs2z36*) which was reflected by normalised read counts as shown in Figure 31 (left panel). *CRF2-like* was strongly upregulated only in *rs2z36* (HS: 54.8-fold) and *rs2z35 rs2z36* (HS: 35.0-fold), but not in *rs2z35* (Fig. 31B, right panel). The DE of both *CRF1* and *CRF2-like* was observed under control conditions to a similar extent (Fig. 31A-B).

Collectively, RS2Z proteins are involved in the transcriptional regulation of many HS-responsive genes, mostly in a redundant fashion. RS2Z36, however, played a dominant role over RS2Z35 as indicated by greater impact of *rs2z36* on gene expression. While genes involved in the HSF/HSP system were not impacted in their expression, genes involved in metabolite synthesis and response to pathogens were DE, suggesting that RS2Z proteins may regulate heat tolerance through other biological processes or interconnections of stress pathways.

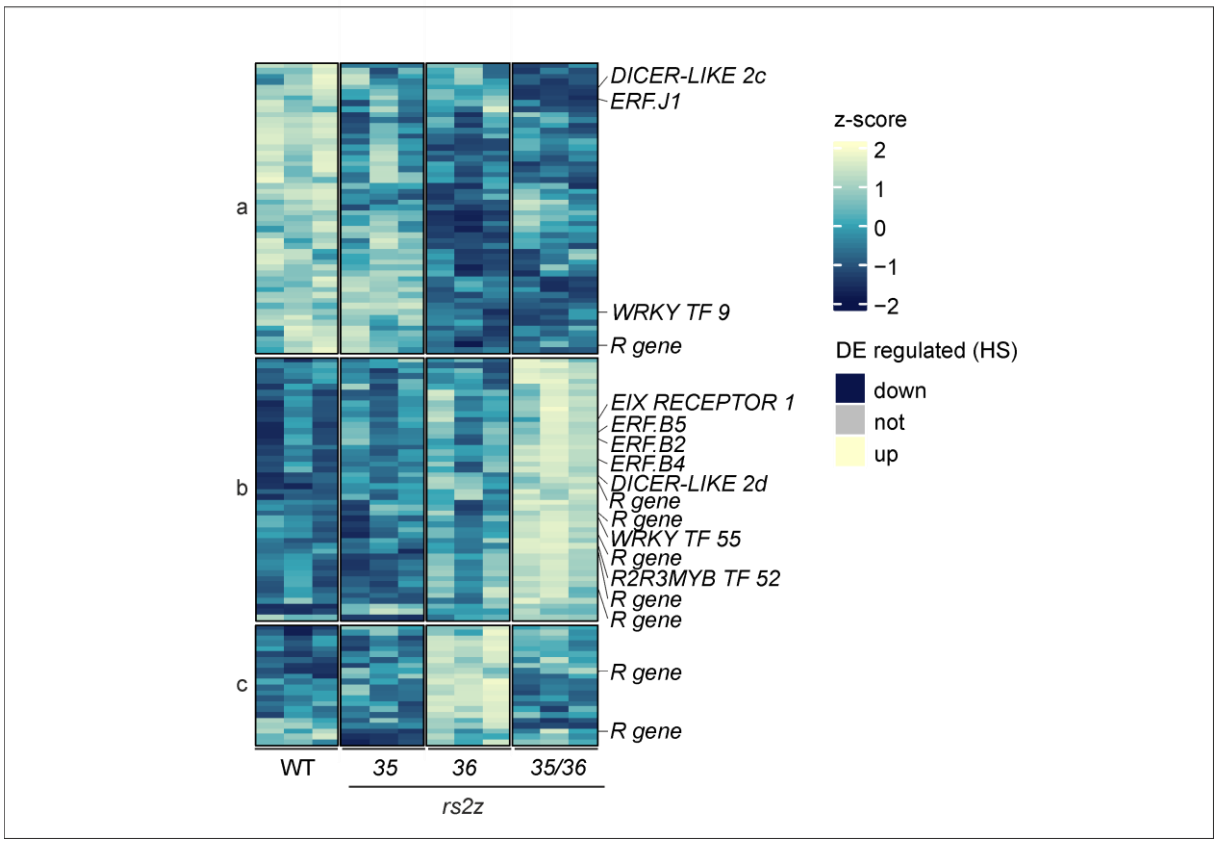

Figure 30. Differential expression of genes involved in pathogen response. Heatmaps depicting normalised read counts in HS samples for *RS2Z*-regulated genes coding for proteins involved in the response to biotic stimulus. Gene annotations were added to genes of interest (transcription factors (TF), disease resistance (R) genes and genes involved in the ethylene response pathway). ERF: ethylene response factor.

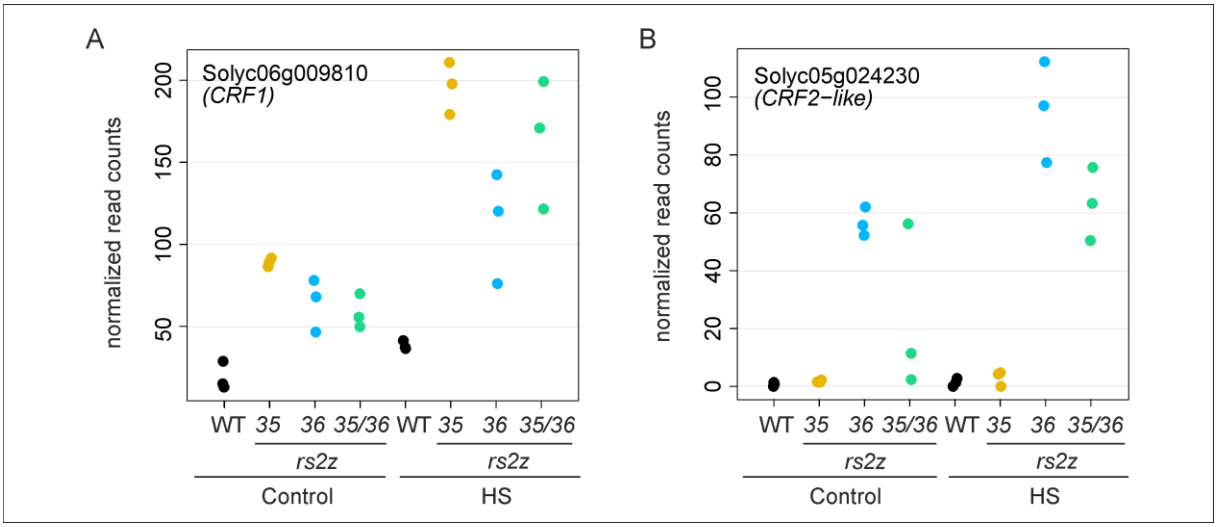

Figure 31. Read counts for differential expressed CRF genes in *rs2z* mutants. Library size normalised read counts for Solyc06g009810 *(CRF1)* **(A)**, Solyc07g054630 *(CRF2-like)* **(B)** in control and HS (1 h 40°C) samples from WT and *rs2z* mutants.

4.13 The effect of *rs2z* knockout on the alternative splicing profile of tomato genes

The RNA-Seq datasets were further used to identify the effect of *rs2z* knockout on the splicing of tomato genes under control (C) and HS conditions (HS). Differential AS (DAS) analysis was performed in response to HS (WT HS vs. C) and in the mutants compared to the WT under both conditions (HS, control) (Fig. 24A). Out of 20,202 expressed multiexon genes, 7,809 (39%) were identified to be alternatively spliced (under either control or HS conditions, or both) (Fig. 32A, left side). 29% of these alternatively spliced genes (2,258 genes) were DAS in response to HS (Fig. 32A, right side). From these, 37% were simultaneously DE in response to HS, whereby 575 DAS-genes were up- and 271 were downregulated (Fig. 32B). The identified splicing events were classified into four groups: A3'SS, A5'SS, ES and IR, whereby non-binary complex events were excluded. Among the 2,258 HS-regulated DAS genes, 2,780 DAS events were identified, indicating the occurrence of multiple AS events in one gene (Fig. 32C). A3'SS was the most prevalent type, making up for 40% of all events identified, followed by A5'SS, ES and IR.

An attempt to identify enriched GO terms among the DAS genes yielded 171 significantly enriched terms for the biological processes category which were further summarised to broader parent terms (Fig. 32D). It was evident that the enriched GO terms reflected a broad range of biological processes, indicating that AS impacts not only a specific subset of genes with particular functions, but represents a more global regulation impacting different processes, including genes involved in the establishment of molecule localisation, RNA processing, organelle organization and macromolecule modification (Fig. 32D). Among the RNA processing parent term, genes involved in RNA splicing were shown to be significantly enriched, highlighting that splicing of splicing regulators themselves is regulated in response to HS (Fig. 32D).

A total of 1,950 genes were DAS under HS in at least one *rs2z* mutant compared relative to the WT, further referred to as *RS2Z*-regulated DAS genes (Fig. 33A). The highest number of DAS genes were observed in *rs2z35 rs2z36* (1,190 genes), but a slightly lower number was identified in the single mutants as well (906 in *rs2z35* and 919 in *rs2z36*) (Fig. 33A, set size). 241 genes (12.4%) were significantly DAS in all mutants and 796 genes (40.8%) were significantly DAS in more than one mutant (Fig. 33A, intersection size). 1,263 (64.8%) of the *RS2Z*-regulated DAS genes under HS were specifically regulated under HS but not under control conditions (Fig. 33B). Interestingly, 1,279 genes (65.6%) were also DAS in response to HS (WT HS vs. C) (Fig. 33B). Observing this intersection from the

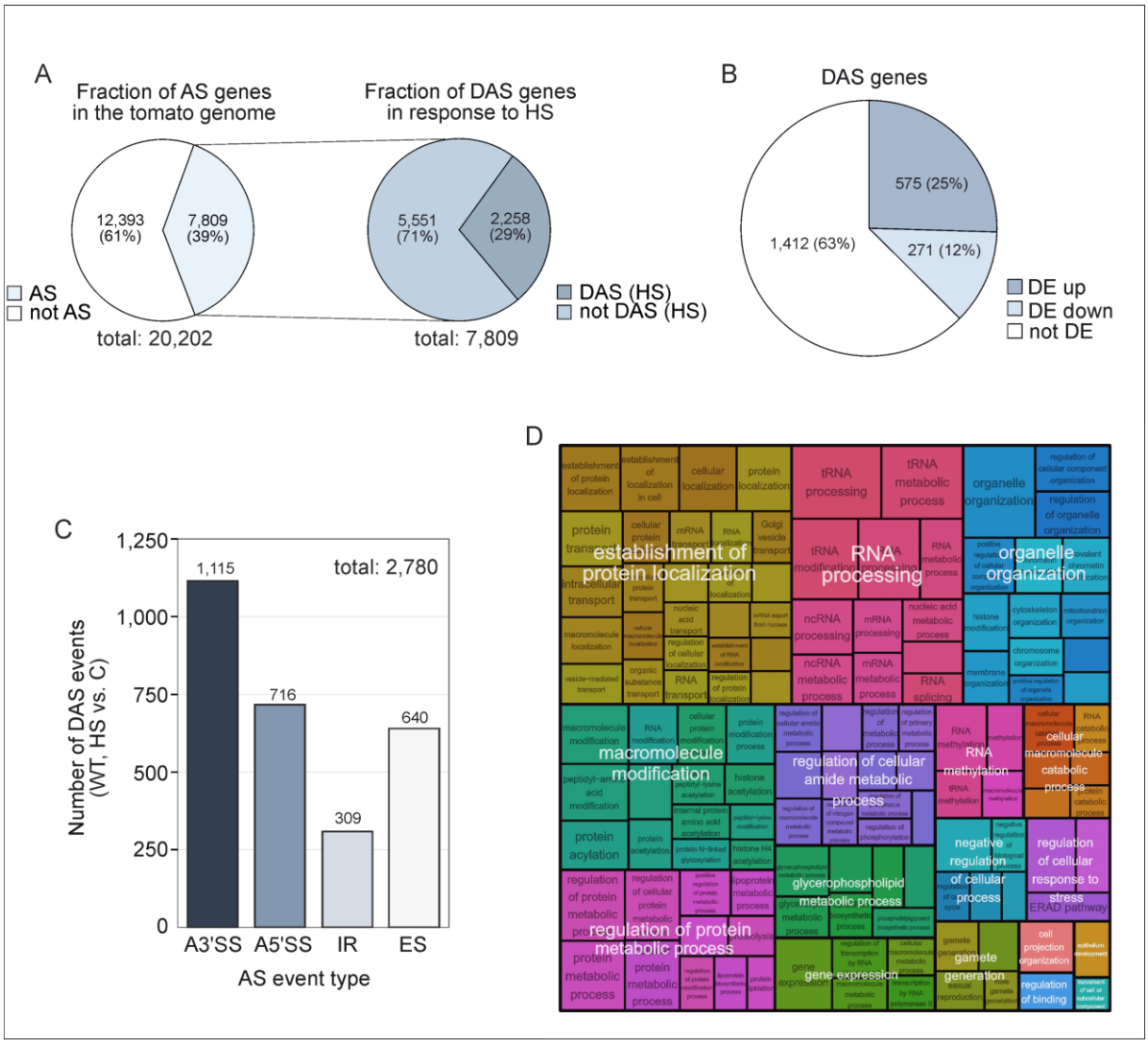

Figure 32. Alternative splicing in response to heat stress. (A) Fraction of alternatively spliced genes in the tomato genome and differentially alternatively spliced (DAS) genes in response to HS relative to control. **(B)** Overlaps between DE genes and DAS genes in response to HS relative to control. **(C)** Frequency of changed AS evens in response to HS by event type. A3'SS: alternative 3' splice site, A5'SS: alternative 5' splice site; IR: intron retention; ES: exon skipping. **(D)** Summarized parent terms for significantly enriched GO terms among DAS genes in response to HS. Colours indicate terms belonging to the same cluster. Box sizes are proportional to significance level (-log10(FDR)).

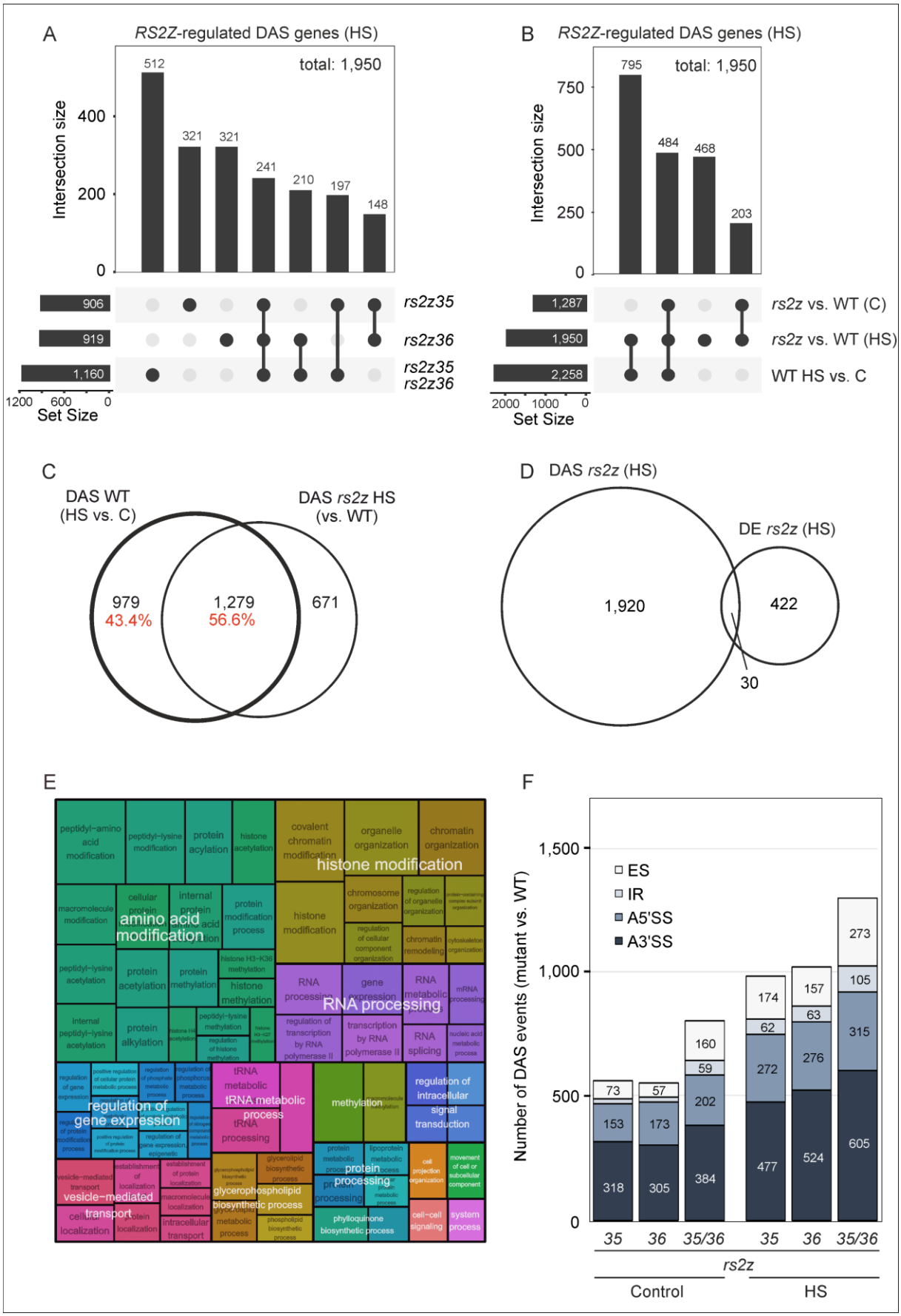
A
RS2Z-regulated DAS genes (HS)
total: 1,950
Intersection size
512
321
321
241
210
197
148
906
919
1,160
rs2z35
rs2z36
rs2z35
rs2z36
Set Size
B
RS2Z-regulated DAS genes (HS)
total: 1,950
Intersection size
795
484
468
203
1,287
1,950
2,258
rs2z vs. WT (C)
rs2z vs. WT (HS)
WT HS vs. C
Set Size
C
DAS WT
(HS vs. C)
DAS rs2z HS
(vs. WT)
979
43.4%
1,279
56.6%
671
D
DAS rs2z (HS)
DE rs2z (HS)
1,920
422
30
E
histone modification
amino acid modification
RNA processing
regulation of gene expression
tRNA metabolic process
protein processing
glycerophospholipid biosynthetic process
vesicle-mediated transport
regulation of intracellular signal transduction
F
Number of DAS events (mutant vs. WT)
ES
IR
A5'SS
A3'SS
73
153
318
57
173
305
160
59
202
384
174
62
272
477
157
63
276
524
273
105
315
605
35
36
35/36
35
36
35/36
rs2z
Control
HS

Figure 33. Differential alternative splicing in *rs2z* mutants. (A) Upset plot depicting the number and overlaps of DAS genes among *rs2z* mutants under HS, relative to the WT. **(B)** Overlaps between DAS genes in *rs2z* mutants under HS conditions with those regulated in *rs2z* mutants under control conditions and those DAS in response to HS (WT HS vs C). Only intersections involving *RS2Z*-regulated genes under HS are shown. **(C)** Venn diagram depicting the overlap between DAS genes in response to heat (DSA WT, HS vs C) and DAS genes in *rs2z* mutants relative to WT under HS conditions (DAS *rs2z* HS vs WT). **(D)** Overlap between DAS and DE genes in *rs2z* mutants under HS. **(E)** Summarized parent terms for significantly enriched GO terms among DAS genes in *rs2z* mutants relative to WT (under HS conditions). Colours indicate terms belonging to the same cluster. Box sizes are proportional to significance level ($-\log_{10}$(FDR)). **(F)** Frequency DAS evens in *rs2z* mutants compared to WT under control and HS conditions. A3'SS: alternative 3' splice site, A5'SS: alternative 5' splice site; IR: intron retention; ES: exon skipping.

opposite direction, more than half (56.6%) of all HS-dependent DAS genes were impacted in at least one *rs2z* mutant (Fig. 33C), indicating an important role for RS2Z proteins in HS-induced AS events. This regulation could either be direct, in which RS2Z proteins directly take part in the regulation of an AS event, or indirect, in which RS2Z proteins regulate another factor that in turn regulates AS. Since AS potentially influences RNA abundance through coupling with the NMD pathway (Neumann et al., 2020), an overlap between DE and DAS genes was expected. However, only 30 DAS genes were simultaneously DE in the *rs2z* mutants under HS, suggesting that *RS2Z*-regulated DE and DAS genes represent independent modes of regulation by *RS2Z* (Fig. 33D).

Global assessment of the putative functions of *RS2Z*-regulated DAS genes under HS by GO-term enrichment analysis yielded 123 terms enriched for the biological processes category (Fig. 33E), hence indicating that rather than a specific set of genes, a broad range of genes were impacted, similar to the findings of HS-responsive DAS genes in the WT (Fig. 32D). The most abundant parent terms were aa modification, histone modification and RNA processing, followed by regulation of gene expression and vesicle-mediated transport (Fig. 33E).

The comparison between AS type frequencies in the mutants compared to the WT under control and HS conditions revealed, that under HS, the total number of DAS genes increased (Fig. 33F). Under both control and HS conditions, A3'SS events made up the majority of regulated genes, followed by A5'SS, ES and IR, suggesting that A3'SS events are the primary event type regulated by RS2Z proteins (Fig. 33F). To inspect trends among the *rs2z* mutants for the regulation of DAS genes, *RS2Z*-regulated AS events under HS were depicted as heat maps for each AS type, whereby each event is represented by ΔPSI values relative to the WT (for WT HS vs. C, ΔPSI depict the splicing change relative to control conditions), and subsequently clustered based on the ΔPSI values (Fig. 34A-D). ΔPSI values thereby represent the splicing change relative to a reference: the retained intron for IR events, the retained exon for ES events and the upstream-located SS for A3'SS and A5'SS events. For all AS types, there was no preferential regulation in any direction, e. g. for IR events, both IR and intron splicing (IS) could be observed to a similar extend (Fig. 34D), suggesting that RS2Z proteins may not have a preferential mode of action and rather act as neutral splicing regulators in a context-dependent manner. In many cases, splicing changes observed under HS conditions were specific for HS (e. g. Fig. 34D, cluster d) or

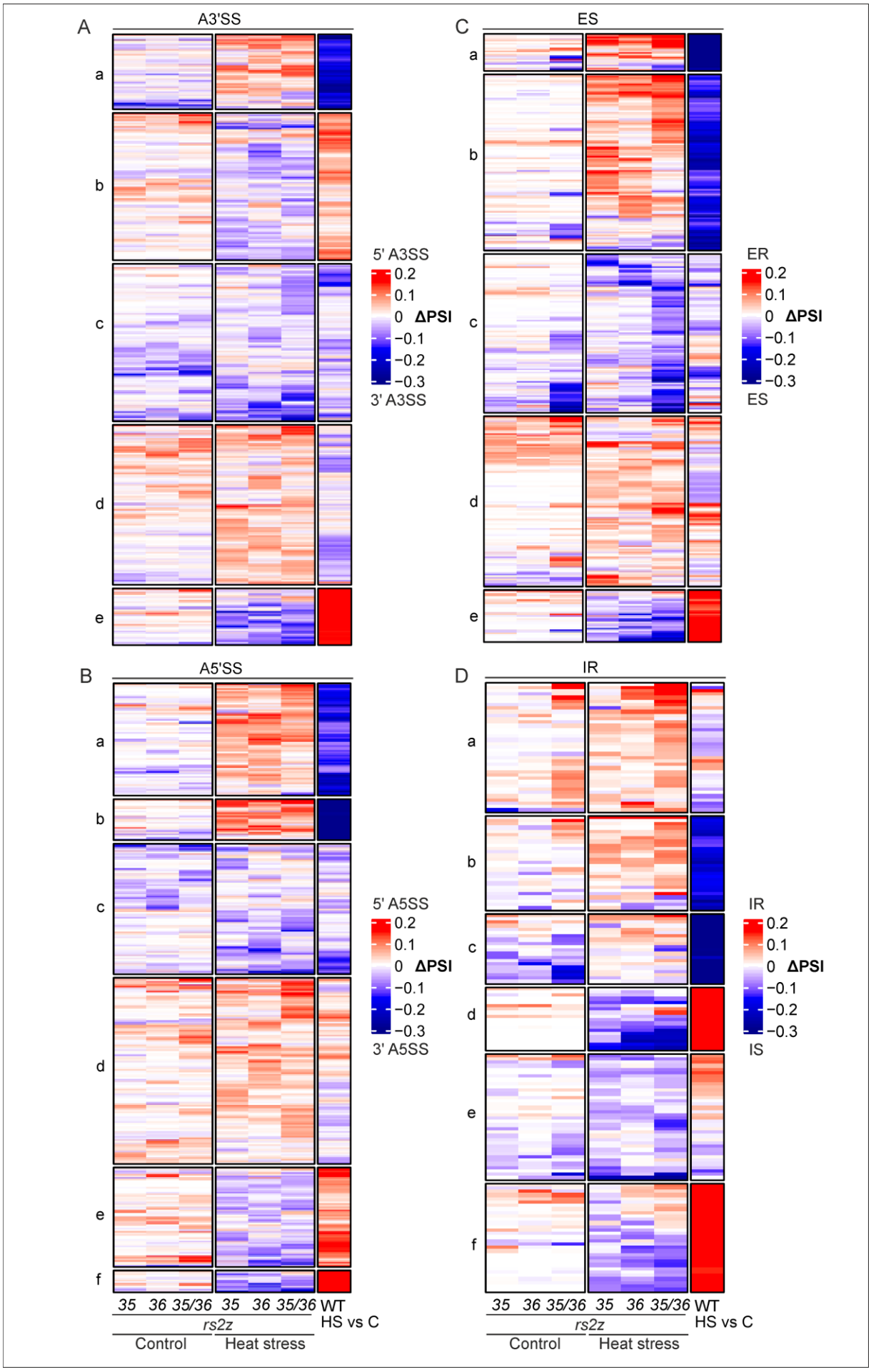
A
A3'SS
a
b
c
d
e
5' A3SS
0.2
0.1
0 ΔPSI
−0.1
−0.2
−0.3
3' A3SS
C
ES
a
b
c
d
e
ER
0.2
0.1
0 ΔPSI
−0.1
−0.2
−0.3
ES
B
A5'SS
a
b
c
d
e
f
5' A5SS
0.2
0.1
0 ΔPSI
−0.1
−0.2
−0.3
3' A5SS
D
IR
a
b
c
d
e
f
IR
0.2
0.1
0 ΔPSI
−0.1
−0.2
−0.3
IS
35 36 35/36 35 36 35/36 WT
rs2z
HS vs C
Control
Heat stress
35 36 35/36 35 36 35/36 WT
rs2z
HS vs C
Control
Heat stress

Figure 34. Global trends in *RS2Z*-regulated AS events under HS. Heatmaps depicting AS changes splicing in *rs2z* mutants relative to WT or in WT HS relative to WT control (WT HS vs C). Colours reflect the direction of ΔPSI (percent selected index) values for each splice event relative to the retained intron for IR events, the retained exon for ES events and the more 5'-located splice site for A3'SS and A5'SS events. Only genes regulated in *rs2z* mutants under HS were included. Each heatmap represents one splice type: **(A)** A3'SS, **(B)** A5'SS, **(C)** ES, **(D)** IR.

more prominent under HS compared to control (e. g. Fig. 34C, cluster c). Strikingly, many *RS2Z*-regulated events were also identified as HS-regulated events (Fig. 34A-D, WT HS vs. C), whereby the direction of regulation was often contrasted between WT HS vs C and *rs2z* vs WT. This is indicated by positive ΔPSI values in one case and negative values in another (e. g. Fig. 34B, cluster a-b). This suggests the involvement of RS2Z proteins in the HS-dependent regulation of many AS events.

The putative function of the proteins coded by the *RS2Z*-regulated DAS genes was further examined by the identification of genes coding for three protein classes: RNA biosynthesis (163 genes), RNA processing (139 genes) and protein homeostasis (165 genes) (Fig. 35A). For each gene class, heat maps were generated depicting *RS2Z*-regulated AS events under HS for each AS type individually, whereby genes with similar trends in either all mutants or in *rs2z36* and *rs2z35 rs2z36* were further annotated with the ITAG 4.0 gene description (Supplemental Fig. 14-16). TFs that were DAS-regulated in *rs2z* were represented by diverse classes of TFs, among them several genes coding for transcription initiation factors and members of the nuclear factor Y (NF-Y) family (Supplemental Fig. 14).

However, the scarce annotation of tomato genes based on automatic annotation by large, hindered the description of most *RS2Z*-regulated genes on a global scale. Due to the diverse nature of *RS2Z*-regulated genes, it was beyond the scope of this study to narrow down the most interesting events as well as to describe all AS events identified, hence why for each class, a few examples are presented in which the AS event resided within the CDS of the target gene, potentially impacting the coding potential. These examples could thus reflect candidates for the HS-phenotypes described earlier. An example of a gene coding for a protein involved in RNA biosynthesis regulated in all mutants is Solyc01g080200 which encodes for a mediator of transcription (mediator of RNA polymerase II transcription subunit 33A-like). This gene was alternatively spliced by A3'SS intron 4, whereby all *rs2z* mutants promoted the usage of the 3'-located SS (Fig. 35B). Another example is Solyc01g005440, coding for a member of the TIFY family of TFs (JASMONATE ZIM-DOMAIN PROTEIN 2) (Fig. 35C). In *rs2z35* and *rs2z36*, the usage of the 3'SS was promoted by 5 and 6%, respectively, and by 25% in *rs2z35 rs2z36* (Fig. 35C). AS analysis for this gene was verified by RT-PCR employing cDNA generated from the same RNA that was sent for RNA-Seq. For this, oligonucleotide primers were used that flanked

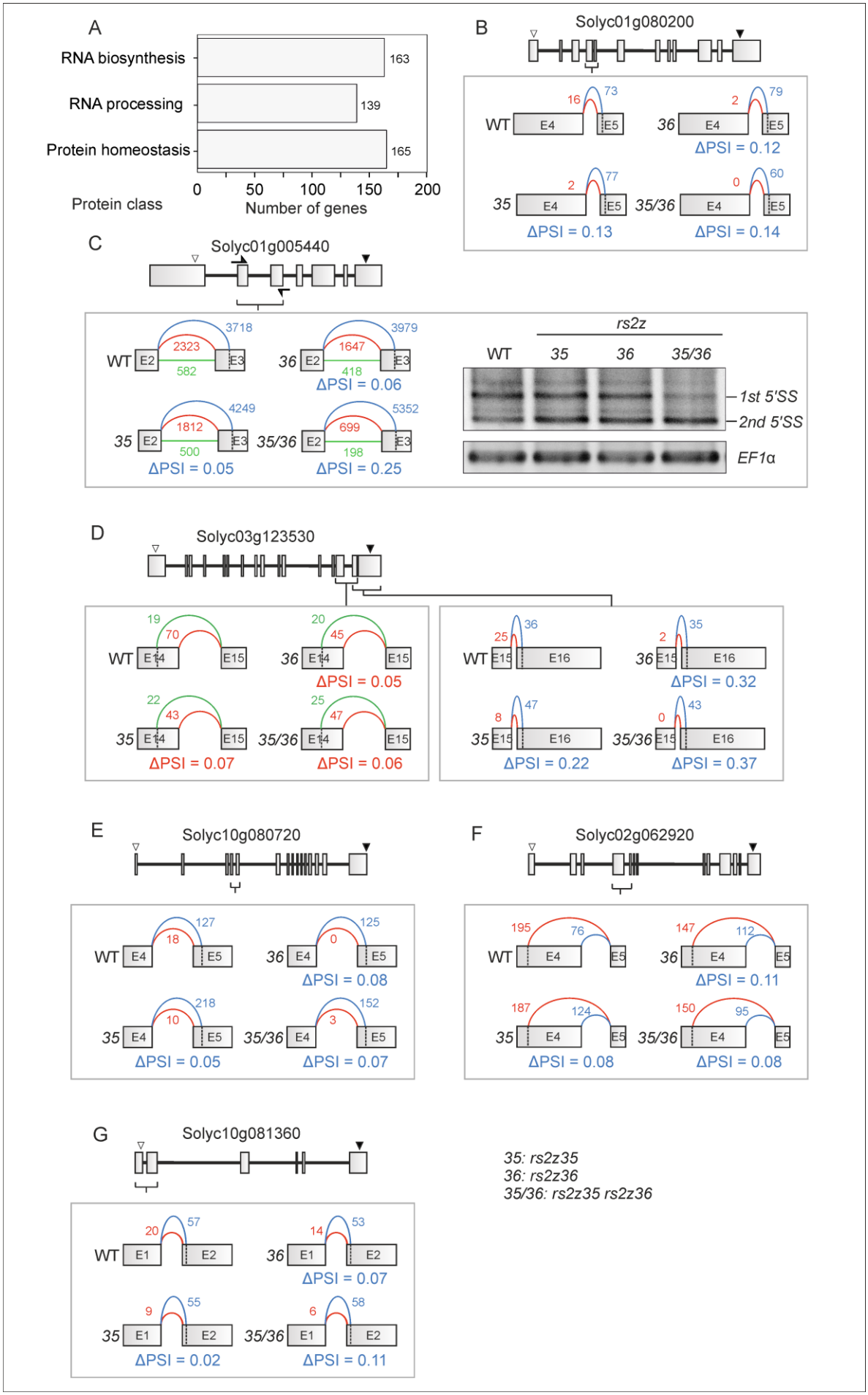
A
RNA biosynthesis
RNA processing
Protein homeostasis
163
139
165
0
50
100
150
200
Protein class
Number of genes
B
Solyc01g080200
WT
36
35
35/36
ΔPSI = 0.12
ΔPSI = 0.13
ΔPSI = 0.14
C
Solyc01g005440
ΔPSI = 0.06
ΔPSI = 0.05
ΔPSI = 0.25
rs2z
1st 5'SS
2nd 5'SS
EF1α
D
Solyc03g123530
ΔPSI = 0.05
ΔPSI = 0.07
ΔPSI = 0.06
ΔPSI = 0.32
ΔPSI = 0.22
ΔPSI = 0.37
E
Solyc10g080720
ΔPSI = 0.08
ΔPSI = 0.05
ΔPSI = 0.07
F
Solyc02g062920
ΔPSI = 0.11
ΔPSI = 0.08
ΔPSI = 0.08
G
Solyc10g081360
ΔPSI = 0.07
ΔPSI = 0.02
ΔPSI = 0.11
35: rs2z35
36: rs2z36
35/36: rs2z35 rs2z36

Figure 35. Visualisation of DAS-regulated genes coding for proteins involved in RNA biosynthesis, RNA processing and protein homeostasis in rs2z mutants relative to WT under HS. (A) Number of *RS2Z*-regulated DAS genes under HS coding for proteins involved in RNA biosynthesis, RNA processing and protein homeostasis. Splice graphs depict DAS events in *rs2z* mutants relative to WT for exemplified genes: **(B)** Solyc01g080200 (*MEDIATOR OF RNA POL II TRANSCRIPTION SUBUNIT 33A*-like), **(C)** Solyc01g005440 (*JASMONATE ZIM-DOMAIN PROTEIN 2*) with representative RT-PCR obtained from cDNA synthesized from the same RNA that was sequenced, **(D)** Solyc03g123530 (*CCAAT/ENHANCER-BINDING PROTEIN ZETA*), **(E)** Solyc10g080720 (*POLYPYRIMIDINE TRACT-BINDING PROTEIN HOMOLOG 3*), **(F)** Solyc02g062920 (*U2 SNRNP AUXILIARY FACTOR LARGE SUBUNIT*), **(G)** Solyc10g081360 (*HSP20-like*). ΔPSI is given for the splice site corresponding to the direction of change in the mutants compared to WT and the colour indicates the respective splice site. Mutants are abbreviated as follows: *35: rs2z35; 36: rs2z36; 35/36: rs2z35 rs2z36.* Gene structures are depicted as boxes and lines representing exons and introns, respectively. Arrowheads indicate start (white) and stop (black) codons.

the AS event, giving rise to two distinguishable signals depending on which 3'SS was utilized (Fig. 35C). The regulation of an AS event in all mutants with a stronger impact in *rs2z35 rs2z36* suggested that the loss of both RS2Z members had an additive impact on the AS-regulation, indicating that the RS2Z members share the same function and can partially compensate for each other in these cases. Another example for DAS-regulated TFs in *rs2z* mutants is Solyc03g123530 (*CCAAT/ENHANCER-BINDING PROTEIN ZETA*), whereby two AS events were regulated in *rs2z* mutants compared to the WT (Fig. 35D). All mutants altered the A5'SS of intron 14 and the A3'SS of intron 15 in favour of the respective downstream-located SS (Fig. 35D). Splicing of *HSFA2* intron 2 shown to be more efficient in *rs2z35 rs2z36* previously (Fig. 17D-E) was reflected by only 3.8% preferential intron excision in RNA-Seq AS analysis (not shown), which likely is attributed to the complexity of *HSFA2* splicing with six A5'SS junctions identified and the variability in *HSFA2* splicing efficiency among the replicates, even for the WT. However, RT-PCR amplifying the intron 2 flanking region as described in Fig. 6F using cDNA synthesized from the same RNA that was used for RNA-Seq, showed a trend towards more efficient intron 2 splicing in *rs2z35 rs2z36* compared to the WT in each replicate (Supplemental Fig. 17).

The genes coding for proteins involved in RNA processing show diverse functions, including RNA methylation and tRNA modification (Supplemetal Fig. 15). Among the DAS-regulated RNA processing genes, there were two genes coding for SR proteins, *SC30b* (Solyc01g105140) and *SR33* (Solyc01g099810). DAS in *SC30b* and *SR33,* however, impacted the UTR and not the CDS (not shown). An example for a DAS gene in which the AS event potentially impacts the CDS is Solyc10g080720, coding for a polypyrimidine-rich tract binding protein (PTBP), in which A3'SS in intron 4 was shifted towards the downstream-located SS in all mutants (Fig. 35E). Another example is Solyc02g062920, coding for the large subunit of U2AF. In this case, A5'SS of intron 4 was shifted towards the 3'SS in all mutants (Fig. 35F). This indicates that other splicing-related genes are impacted in their AS profile in *rs2z* mutants and could thus contribute to downstream effects.

RS2Z-regulated DAS genes involved in protein homeostasis represented different aspects of this process, whereby many were involved in ubiquitination. While the most well-known HSPs involved in the HSR like *HSP70* and *HSP90* were not impacted, *RS2Z*-regulated DAS genes included *HSP40* (DnaJ) and *HSP20-like* (Supplemental Fig. 16). The splicing profile of Solyc10g081360 (*HSP20-like*) for example was significantly altered in *rs2z36* and *rs2z35 rs2z36*, but not in *rs2z35* (Fig. 35G).

4.14 Identification of RS2Z-associated RNA targets

RNA-Seq revealed differences in DE and DAS regulation of a plethora of genes in *rs2z* mutants, suggesting that RS2Z proteins are directly or indirectly involved in their regulation under HS. To assess which RNAs are associated with RS2Z proteins, RNA immunoprecipitation followed by RNA-Seq (RIP-Seq) was employed, following the RIP workflow depicted in Fig. 20A. Here, following RIP, the RNA obtained from input and IP fractions was subjected to high-throughput sequencing. To include the capture of non-poly(A)-tail containing RNAs and those in the process of transcription, as well as to account for expected reduced integrity of captured RNAs (IP RNAs), poly(A) selection was not performed for RIP samples. Due to low recovery of IP RNAs, however, rRNA depletion could not be performed for IP samples either (Supplemental Fig. 2E). This, however, led to a substantial amount of residual rRNA contamination, reflected in a reduced fraction of reads uniquely mapping to the tomato genome (29.16-60.67% for input and 6.21-11.3% for IP). Unmapped reads in the IP datasets were further mapped against rRNA databases as well as against tomato plastid, human and bacteria genomes, confirming that the low number of uniquely mapped reads was indeed a consequence of mainly rRNA contamination (not shown). Collectively, 10.9-21.9 Million input and 3.6-8.6 Million IP reads of a generally good quality with mean Phred quality scores >34 over the entire read length uniquely mapped to the tomato genome.

Fig. 36A depicts a brief overview of the workflow following RNA-Seq. After splice-aware mapping against the tomato genome, reads per gene were counted. Subsequently, for both Input and IP samples, batch effects likely resulting from differences in library preparation were removed. Input and IP read counts were assembled in a count matrix, prefiltered for low abundance genes and subsequently subjected to enrichment analysis, calculating relative enrichment as $\log_2$foldchange (LFC) in the IP over Input and in *GFP-RS2Z* over *GFP* (ratio over ratio). Overestimation of enrichment of low abundant transcripts was met by LFC shrinkage. Analysis of sample similarity by PCA showed that both Input and IP samples of the *GFP* samples were different from *GFP-RS2Z* samples, whereby *GFP-RS2Z* input samples clustered together, but the IP samples were different from one another (Fig. 36B). This indicates that DE caused by *RS2Z* overexpression was likely similar for *GFP-RS2Z35* and *GFP-RS2Z36,* while there were differences between RS2Z35 and RS2Z36-associated transcripts (Fig. 36B). Transcripts associated with either GFP-RS2Z35, GFP-RS2Z36 or both are further referred to as RIP genes. Library-size normalised read counts in input samples confirmed the overexpression of both *RS2Z35* and *RS2Z36* in the respective line (Fig. 36C).

Since RIP is prone to a high signal to noise ratio, stringent criteria were applied for the enrichment of RNA targets to avoid false positives. Only transcripts with a relative enrichment of LFC > 2 and padj < 0.01 were considered as significantly enriched (Fig. 36D). 617 and 848 genes were significantly enriched in *GFP-RS2Z35* and *GFP-RS2Z36*, respectively (Fig. 36D). Among the total of 1,227 RIP genes, 130, 90 and 94 genes were identified as coding for proteins involved in RNA biosynthesis, RNA processing and protein homeostasis, respectively (Fig. 36E). GO term enrichment analysis revealed

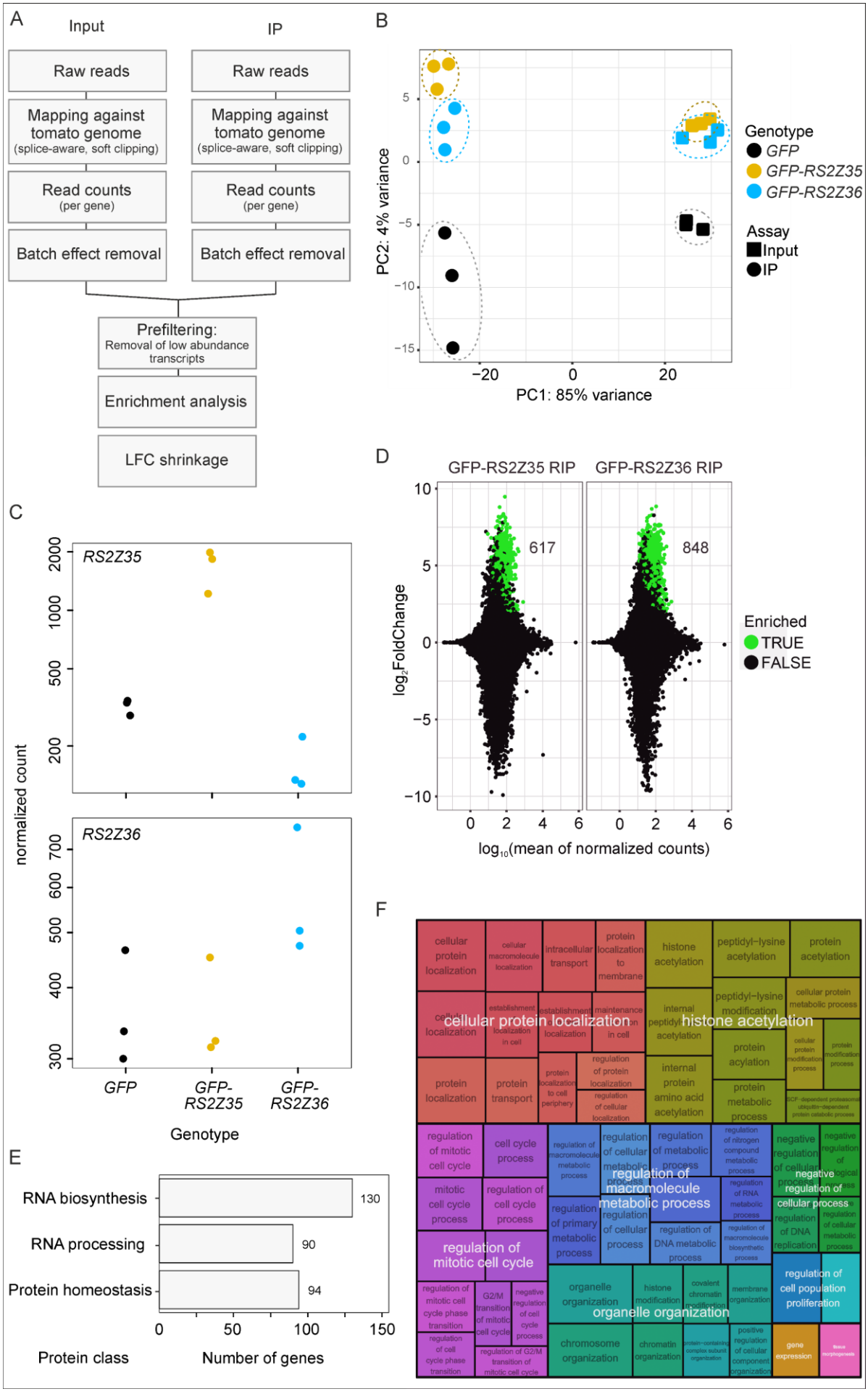
A
Input
IP
Raw reads
Raw reads
Mapping against tomato genome (splice-aware, soft clipping)
Mapping against tomato genome (splice-aware, soft clipping)
Read counts (per gene)
Read counts (per gene)
Batch effect removal
Batch effect removal
Prefiltering: Removal of low abundance transcripts
Enrichment analysis
LFC shrinkage
B
PC2: 4% variance
PC1: 85% variance
Genotype
GFP
GFP-RS2Z35
GFP-RS2Z36
Assay
Input
IP
C
RS2Z35
RS2Z36
normalized count
GFP
GFP-RS2Z35
GFP-RS2Z36
Genotype
D
GFP-RS2Z35 RIP
GFP-RS2Z36 RIP
617
848
log2FoldChange
log10(mean of normalized counts)
Enriched
TRUE
FALSE
E
RNA biosynthesis
RNA processing
Protein homeostasis
130
90
94
Protein class
Number of genes
F
cellular protein localization
histone acetylation
regulation of macromolecule metabolic process
organelle organization
regulation of mitotic cell cycle
negative regulation of cellular process
regulation of cell population proliferation

Figure 36. Identification of RS2Z-associated transcripts (RIP genes) by RNA immunoprecipitation followed by RNA-Seq (RIP-Seq). (A) Schematic workflow of read processing following RIP. Raw reads were mapped against the tomato genome in a splice-aware manner with soft clipping followed by read counting per gene. Read counts were then adjusted for batch effects and combined to a count matrix containing both input and elution (IP) samples. After prefiltering, enrichment of transcripts in the IP over Input and in *GFP-RS2Z* over *GFP* was assessed and expressed as LFC. LFC shrinkage was conducted to compensate the overestimation of changes in low abundant transcripts. **(B)** PCA plot depicting similarities between Genotypes (*GFP*, *GFP-RS2Z*) and assay type (Input, IP) based on the 100 genes with the greatest row variance. Ellipses were manually drawn to highlight clustering. **(C)** Confirmation of *RS2Z* overexpression in RIP Input samples depicted by library size normalised read counts for *RS2Z35* (top) and *RS2Z36* (bottom). **(D)** MA plot depicting enriched transcripts in *GFP-RS2Z35* and *GFP-RS2Z36* over *GFP*. Significantly enriched transcripts (LFC > 2, padj < 0.01) are indicated by green colour. **(E)** Number of genes coding for proteins involved in RNA biosynthesis, RNA processing and protein homeostasis among RIP genes. **(F)** Summarized parent terms for significantly enriched GO terms among RIP genes. Colours indicate terms belonging to the same cluster. Box sizes are proportional to significance level ($-\log_{10}$(FDR)).

that proteins encoded by RIP genes were of diverse nature with 73 terms significantly enriched for the biological process category. Proteins encoded by RIP genes are thus involved in several cellular processes, including protein localisation, epigenetic regulation, macromolecule metabolism, cell cycle regulation, organelle organization, and others (Fig. 36F).

While approximately 50% of all RIP-enriched targets were uniquely associated with GFP-RS2Z36, approximately 20% of RIP-enriched targets were shared among GFP-RS2Z35 and GFP-RS2Z36 (Fig. 37A-B). As SR proteins are involved in both canonical and alternative splicing (Shepard and Hertel, 2009), RS2Z proteins were expected to be associated with multiexon and alternatively spliced genes. Multiexon genes made up 77% of all genes expressed in the input samples (Fig. 37C). Among the RIP genes, this fraction increased to 88% (Fig. 37C), indicating preferential association with multiexon transcripts. Similarly, RS2Z proteins largely associated with transcripts that were shown to be alternatively spliced under control and/or HS conditions in the WT (72%) (Fig. 37D). 20% of the RIP genes were shown to be DAS in *rs2z* mutants (RIPxDAS) (see Supplemental Fig. 18-19 for heat map depiction), whereby 58% of these genes were associated specifically with RS2Z36 and 39% were associated with both RS2Z proteins (Fig. 38A). Among the RIPxDAS genes were for example the *POLYPYRIMIDINE TRACT-BINDING PROTEIN HOMOLOG 3* (Solyc10g080720), *CCAAT/ENHANCER-BINDING PROTEIN ZETA* (Solyc03g123530) as well as the *MEDIATOR OF RNA POL II SUBUNIT 33A*-like gene (Solyc01g080200) described earlier (Supplemental Fig. 18, Fig. 35). Other RIP genes that stood out due to their strong AS-regulation were for example Solyc04g072510, coding for a mitochondrial transcription termination factor family protein, in which A5'SS of intron 1 was impacted *rs2z36* and *rs2z35 rs2z36* (Supplemental Fig. 18). ES in Solyc06g054650, coding for an integral membrane metal-binding family protein (DUF2296), was promoted by approximately 20% in *rs2z36* and *rs2z35 rs2z36* (Supplemental Fig. 19). Solyc06g082150, coding for a 6-phosphofructo-2-kinase/fructose-2, 6-bisphosphatase, and Solyc02g091340, coding for a pyridoxal kinase, were impacted by A3'SS in *rs2z36* and *rs2z35 rs2z36* (Supplemental Fig. 18). Excision of intron 4, 5 and 6 as well as A3'SS of intron 8 of Solyc06g060310, coding for a chlorophyllide a oxygenase, was impacted in both *rs2z36* and *rs2z35 rs2z36* (Supplemental Fig. 18-19). A3'SS events in Solyc09g005300, coding for a mRNA cap guanine-N7 methyltransferase, and Solyc03g118070, coding for a sucrose nonfermenting 4-like protein, were both regulated in all mutants by more than 12% (Supplemental Fig. 18). Lastly, Solyc01g104720, coding for

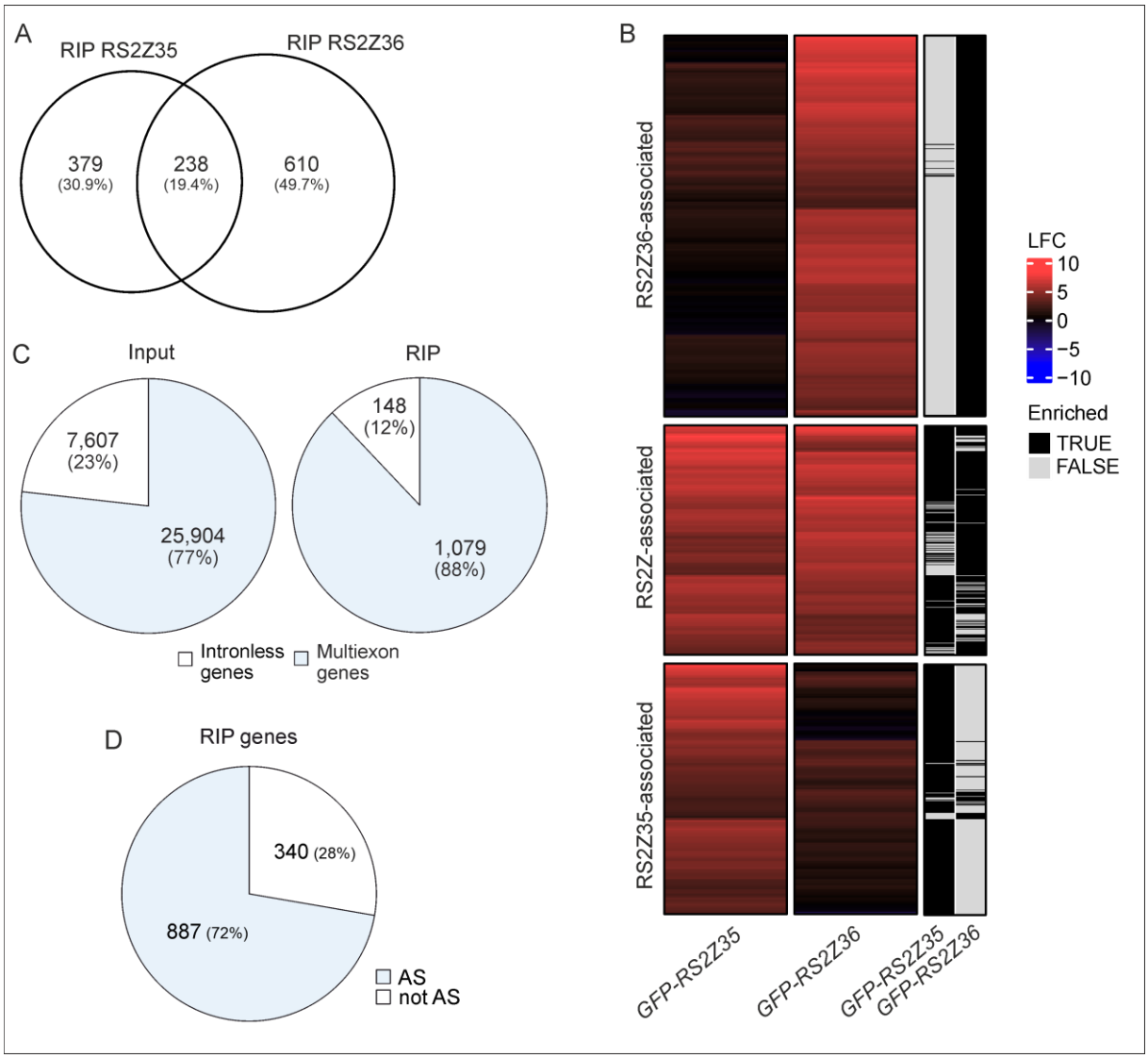

Figure 37. Shared and common RS2Z-associated transcripts. (A) Overlap of RS2Z35- and RS2Z36-asociated genes. **(B)** Heatmap depicting enrichment levels of RS2Z35- and RS2Z36-asociated genes. Colour indicates LFC enrichment over GFP: red: positive enrichment. Blue: negative enrichment. Black: not enriched. Right-side columns indicate significant enrichment (black) with LFC > 2 and padj < 0.01. **(C)** Venn diagrams depicting the fraction of intronless and multiexon genes among all genes expressed in the RIP input (left) and among RIP genes (transcripts associated with any GFP-RS2Z protein) (right). **(D)** Fraction of RIP genes shown to be alternatively spliced in the WT based on RNA-Seq in leaves under control and HS (1 h 40°C) conditions as shown in Fig. 32.

a thionin-like protein, showed preferential excision of intron 1 and 2 by at least 9% in *rs2z36* and *rs2z35 rs2z36* (Supplemental Fig. 19). In this case, AS likely caused alterations in transcript abundance, as this gene was shown to be DE with reduced levels in *rs2z36* and *rs2z35 rs2z36* compared to WT under HS (Supplemental Fig. 20). Similarly, the transcript levels of Solyc03g123530 (*CCAAT/ENHANCER-BINDING PROTEIN ZETA*), a RIP gene shown to be DAS in *rs2z* mutants (Fig. 34E, Supplemental Fig. 18-19), were reduced in all mutants by 1.27-fold in *rs2z35* and 1.44 in *rs2z36* and *rs2z35 rs2z36* (not included in heatmaps as it did not pass the LFC > 0.5849 threshold, Supplemental Fig. 21). In total, 20 RIP genes were shown to be DE in *rs2z* mutants under HS, 5 of them were intronless (Fig. 37A and Supplemental Fig. 20). Solyc07g008620 (*EIX RECEPTOR 1*) is yet another RIP gene shown to be DE with elevated levels in *rs2z36* and *rs2z35 rs2z36* compared to WT and *rs2z35* (Supplemental Fig. 20), representing a gene in which association with RS2Z proteins impacted transcript levels through means other than AS.

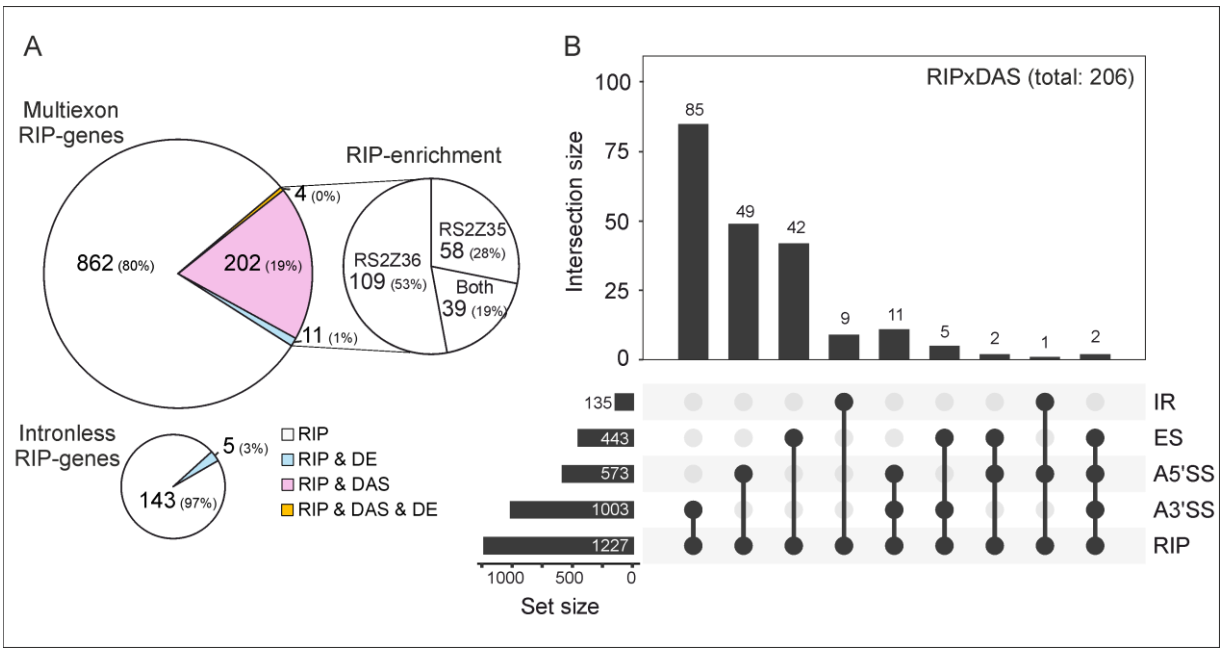

Figure 38. Alternative splicing of RS2Z-associated transcripts. (A) Overlaps RIP genes with genes shown to be DE or DAS in *rs2z* mutants under HS (left). For DAS genes associated with any RS2Z protein (RIPxDAS genes) it is further indicated with which RS2Z protein the corresponding transcripts were associated in RIP-Seq (right). **(B)** Upset plot depicting the frequency of AS types among RIPxDAS genes as overlaps of DAS genes (in any *rs2z* mutant under HS) by type with genes associated with any RS2Z protein (RIP genes).

Among the RIPxDAS genes, A3'SS events were the most prevalent AS type, following similar frequencies observed in all DAS genes in *rs2z* mutants under HS (Fig. 38B), indicating that A3'SS likely is the primary AS type regulated by *RS2Z35* and *RS2Z36*. Furthermore, it is noteworthy that regardless of the AS type, RIPxDAS RNAs were not differentially spliced in a particular direction (Supplemental Fig. 18-19), further suggesting a context-dependent regulation by RS2Z proteins.

Considering that 20% of DAS genes were associated with RS2Z proteins, the possibility of missed RS2Z-association not only by the application of stringent cutoffs, but also by low abundance of the respective transcripts in RNA-Seq of *rs2z* mutants, was evaluated. Thereby, a large portion of genes that were enriched in RIP but not identified as DAS in *rs2z* mutants was indeed low abundant in the mutant dataset and therefore potentially prevented the evaluation of local splice variants due to low coverage of splice junctions (Supplemental Fig. 2D). This however indicates that the overlaps of RIP and DAS genes are potentially greater than reported here. Additionally, the enrichment of *HSFA2,* previously reported by RIP-qPCR (Fig. 20C), was not observed in RIP-Seq. Observing the read coverage across the *HSFA2* gene locus, it can be noted that read counts in the 3'end of intron 2 in a region specific for *HSFA2-Iα* (Supplemental Fig. 22A, red box) were underrepresented, while a slight enrichment in this region could be seen in RIP elution fractions in GFP-RS2Z35 and GFP-RS2Z36 samples compared to GFP (Supplemental Fig. 22A), indicating that rather than total *HSFA2*, *HSFA2-Iα* transcripts may be associated with RS2Z proteins. Similarly, the coverage in the RIP input did not reflect the shift towards IR previously observed upon *RS2Z* overexpression (Fig. 17A; Supplemental Fig. 22A). Lower coverage of the 3' end of intron 2 specific for *HSFA2-Iα* was as well observed in RNA-Seq of the WT (Supplemental Fig. 22B) although *HSFA2-Iα* transcripts show high abundance based on RT-PCR (Supplemental Fig. 22C), suggesting reduced mappability of this region, potentially due to the high AU-content of 81%

compared to the higher coverage 5’ region of the intron (60% AU), which ultimately might be the underlying cause for the lack of *HSFA2* enrichment in RIP-Seq.

In summary, a large number of transcripts were identified to be associated with GFP-RS2Z35 and/or GFP-RS2Z36 and coding for proteins with diverse functions. 206 RIP-enriched transcripts were also reported to be DAS in *rs2z* mutants, suggesting that AS of these genes is regulated by *RS2Z* through interaction with the RNA in a direct (directly binding to the RNA) or indirect (e. g. residing in the same complex) manner. Half of the RS2Z-associated transcripts were specifically associated with GFP-RS2Z36 but not GFP-RS2Z35, further suggesting a prevalent role of RS2Z36 in response to HS.

5. Discussion

Understanding the molecular details of the HS response is crucial for the development of stress-resistant crops. While the regulation of transcription has been the focus of studies regarding HS response and thermotolerance, little is known about the downstream regulatory mechanisms that control mRNA abundance and diversity as well. The impact of HS on AS of many genes had been described in several plant species, but the mechanisms underlying are largely unknown. In this study, it is shown that two splicing regulators, RS2Z35 and RS2Z36, are essential for ATT by regulating the AS profile of *HSFA2*, an important key factor of the ATT, and their involvement in the AS of a broad range of genes as neutral splicing regulators. Additionally, this work demonstrates the involvement of the HS-induced member RS2Z36 in BTT. Thus, this study expands the knowledge on the relevance of splicing factors and demonstrates their importance for thermotolerance.

5.1 Regulation of the *HSFA2* pre-mRNA splicing by RS2Z proteins

TFs are the key factors of stress responses, mediating the transduction of stress signals into adaptive cellular output (section 1.3). HSFA2, the main regulator of ATT, is a prominent example for TF regulation on a co-transcriptional level, in which AS determines the ratio of two distinct protein isoforms, thereby regulating the acclimation capacity of the cell (section 1.5.3; Hu et al., 2020a). In this study, the expression of several SR proteins alters the splicing profile of *HSFA2*, namely RS30, SC30b, SCL29 as well as both members of the RS2Z subfamily, RS2Z35 and RS2Z36 (Fig. 6G; Fig. 17). Other SR proteins, namely RS29, RS42, SCL31 and the two entire RSZ subfamily, regulate HSFA2 on post-splicing level (Fig. 6C-D), which could reflect SR-protein-mediated and transcript-specific regulation of nuclear export or translation efficiency. SC30b and RS2Z36 were identified as the only HS-induced splicing repressors of *HSFA2* (Fig. 7B). Knockout of the two members of the RS2Z subfamily, but not of single RS2Z members, improved *HSFA2* splicing efficiency, but was not sufficient to shift the ratio entirely in favour of *HSFA2-II* (Fig. 17C-E). Thus, the mild impact of RS2Z knockout and the occurrence of IR even in the absence of RS2Z proteins indicates functional redundancy not only between RS2Z subfamily members, but also with SR proteins of different subfamilies or other splicing regulators. This, however, does not exclude the possibility that temperature inhibits splicing due to direct effects on the spliceosome, which could likewise contribute to IR. The retention of intron 2 ensures the accumulation of HSFA2-I upon the onset of HS (Fig.3A; Fig.39A), whereby the splicing efficiency increases with prolonged HS duration, favouring the less stable isoform HSFA2-II over time and thus representing a possible mechanism for HSR attenuation (Fig. 21B). Retention of intron 2 is thereby likely mediated by the activity of constitutively expressed SR proteins and further maintained by HS-induction of SC30b and RS2Z36, opposing the influence of an HS-induced hnRNP acting as splicing enhancer, GR-RBP3, that may overcome the impact of SR proteins during prolonged HS (Fig. 10C; Fig. 39A).

Furthermore, RS2Z35 and RS2Z36, both repressors of *HSFA2* splicing, were shown to interact with *HSFA2* RNA both *in vitro* (Fig. 19) and *in vivo* (Fig. 20) with preferential binding to the AU-rich 3' region of the intron as observed in EMSA using different regions of the intron (Fig. 19G-J), suggesting a preference for RS2Z for AU-rich sequences. The phosphorylation status of SR proteins could be indicative for a preferential activity under HS. However, neither RS2Z35 nor RS2Z36 showed

HS-dependent differential regulation in their phosphorylation status (Fig. 13B-C). Additionally, the RS-rich region in their RS domains proved to be dispensable for their repressor function in *HSFA2* splicing regulation (Fig. 11). The requirement for an RS domain may thus be substrate-specific, similarly as for human SR protein SRSF1 (Zhu and Krainer, 2000). Thus, RS2Z proteins may not inhibit *HSFA2* splicing through mechanisms that require an RS domain, including direct interaction with spliceosomal components or the modulation of their activity via phosphorylation. This, however, does not exclude that the RS domain takes part in the splicing regulation of other RNA targets. While the RS-rich region was dispensable for *HSFA2* splicing repression, the ZnKs were required (Fig. 11), although it cannot be excluded that the deletion of the ZnKs may have disturbed protein folding or altered subcellular localization. RS2Z proteins thus likely block binding sites for splicing enhancers in *HSFA2*, like GR-RBP3, or disturb the interaction between components of the U2 snRNP and the *HSFA2* pre-mRNA (Fig. 39A), but further evidence would be needed to validate these hypotheses. Furthermore, while phosphorylation is the major and well described posttranslational modification of SR proteins, other modifications including acetylation (Choudhary et al., 2009) and arginine methylation (Sinha et al., 2010) could likewise modulate SR protein activity.

Recently, the 3' region of *HSFA2* intron 2 has been shown to form temperature-dependent secondary structures, suggested to modulate accessibility of the pre-mRNA for splicing factors or the U2 snRNP during HS (Broft et al., 2022). However, most SR proteins were able to impact *HSFA2* splicing in a minigene reporter assay conducted under control conditions (Fig. 6 & 8), indicating that the binding of SR protein to *HSFA2* pre-mRNA is not strictly HS-dependent and rather reflects an additional, concentration-dependent regulation. Thereby, regulation of *HSFA2* splicing is likely mediated by a combination of HS-dependent structure alterations, as well as by splicing regulators acting in an antagonistic and combinatorial fashion.

Expanding from the initial assessment of *HSFA2* AS, the study further focused on the role of the plant specific RS2Z subfamily. Indeed, RS2Z36 was specifically upregulated by HS (Fig. 12A), which may compensate for its reduced protein stability under HS as observed in chase experiments (Fig. 12H) and thus likely ensures its abundance under HS, further indicating a functional relevance for this splicing factor in response to elevated temperatures.

The regulation of *HSFA2* splicing in favour of the less stable isoform HSFA2-II upon *rs2z* knockout correlated with reduced expression levels of known HSFA2 downstream targets, *APX3* and *HSP17.7A-CI* (Fig. 22A & D), highlighting the importance of RS2Z proteins for the HSFA2-dependent HSR. This is further supported by the lower ATT of the *rs2z35 rs2z36* double mutant (Fig. 23C). Thereby, RS2Z proteins are directly involved in the HSR through the regulation of HSFA2.

Interestingly, despite the absence of *HSFA2* intron 2 splicing alteration in *rs2z* single mutants, both *rs2z35* and *rs2z36* mutants were less tolerant in the ATT regime (Fig. 23C). Additionally, *rs2z* single mutants, primarily *rs2z36*, were more thermosensitive in response to a direct HS incident, a condition that does not require HSFA2 for thermotolerance (Fig. 23D). This suggests non-redundant functions of

RS2Z members in ATT, but also highlights the important role of RS2Z36 in BTT, indicating a role for RS2Z proteins in the HSR beyond the regulation of HSFA2.

5.2 Regulation of HS-dependent alternative splicing by RS2Z proteins

Most HS-genes display peak expression after 1 h HS (Lohmann et al., 2004) which enables HS acclimation further on. Thereby, the differential regulation of genes in *rs2z* mutants after 1 h HS serves as a basis to understand HSFA2-independent regulation of the HSR and allows the identification of regulated genes potentially causing reduced thermotolerance of *rs2z* mutants.

In the WT, HS impacted the splicing profile of more than 2,000 genes coding for various metabolic processes, including RNA processing and the regulation of gene expression (Fig. 33E). This result agrees with other reports on the widespread effect of high temperatures on AS (Jiang et al., 2017; Keller et al., 2017; Ling et al., 2018; Lee and Adams, 2020). AS contributes directly to the transcriptome reshaping either by impacting the transcript abundance or the coding potential. In addition, the effect of HS on the splicing profile of many regulatory upstream factors, namely transcription and splicing factors, (Fig. 32D) indicates indirect effects as well, which further amplifies the impact of heat on the transcriptome. Furthermore, HS-induced AS does not only impact the transcripts of HS-related genes, but also of genes that are not altered in their expression (Fig. 32B). While many genes are downregulated in response to HS (Fig. 25B), which likely reflects a shift in transcription in favour of HS-genes, others are still required for basic cellular mechanisms, for example those encoding for proteins involved in protein localisation, organelle organisation or macromolecule modification (Fig. 32D). AS of non-HS-responsive genes could thus aid in maintaining steady state levels of housekeeping genes under HS. Additionally, PTC-inducing AS has been reported to enhance the fraction of nuclear sequestered transcripts upon HS (Göhring et al., 2014). This in turn protects them from the NMD pathway and may immediately reduce the pool of translatable transcripts, while simultaneously serving as a reservoir of splicing-competent transcripts that can be processed once the stress subsides (Göhring et al., 2014; Chaudhary et al., 2019).

Interestingly, more than half of these HS-regulated genes were also differentially regulated in *rs2z* mutants (Fig. 33B-C), in which the impact of HS and the impact of *rs2z* mutation led to opposing effects in many cases (Fig. 34). This suggests, that RS2Z proteins play a broad and major role in thermotolerance by regulating both HS-dependent and HS-independent AS events.

While the large number of regulated genes and the fragmented annotation of the tomato genome prevented a thorough investigation of each regulated AS event, at least 163 genes coding for proteins involved in RNA biosynthesis were identified among the *RS2Z*-regulated DAS genes (Fig. 35A), potentially contributing to ATT. One interesting *RS2Z*-regulated factor is the CCAAT/ENHANCER-BINDING PROTEIN ZETA (Fig. 35D), a protein so far uncharacterised in tomato. Human CCAAT/ENHANCER-BINDING PROTEIN ZETA has been reported to bind to the *HSP70* promoter (Lum et al., 1990), rendering this factor a potential candidate for *RS2Z*-mediated HSR-regulation. While its splicing pattern was altered in all *rs2z* mutants, *rs2z35* and *rs2z36* impacted different AS events in the same gene, suggesting additive instead of redundant functions in this case (Fig. 35D). Furthermore,

CCAAT/ENHANCER-BINDING PROTEIN ZETA transcript levels were reduced in all mutants (Supplemental Fig. 21), representing regulation of transcript abundance through AS. Moreover, NF-Y TFs also belong to the CCAAT-binding factor family and many members respond to abiotic stress in plants (Xu et al., 2014). Upon *rs2z* knockout, at least two NF-Y factors, *NF-YB8* and *NF-YC2* were AS-regulated (Supplemental Fig. 14), which could therefore–among many others–represent additional candidates for the *RS2Z*-mediated thermotolerance. Furthermore, AS-regulation of genes coding for proteins involved in protein homeostasis could directly contribute to HSR, for example *HSP20-like* (Fig. 35G) or genes coding for E3 ubiquitin protein ligases (Supplemental Fig. 16).

Furthermore, since the AS analysis is based in local splice variants following short-read sequencing and thus the identity of the whole transcripts is not known, it could not be deduced whether AS alteration in *rs2z* mutants provoke changes in the coding potential or lead to the formation of potential PTC. Therefore, it can only be speculated whether RS2Z proteins mediate the production of isoforms of important regulatory factors or whether they may contribute to the reduction of translatable transcripts, and thus reduce the burden on the chaperone system under HS (section 1.5.2).

While almost 2,000 genes showed DAS events upon *rs2z* knockout (Fig. 33A), only 206 of these transcripts were associated with RS2Z proteins *in vivo* (Fig. 38A), suggesting that a large portion of DAS events could have arisen from indirect effects in which RS2Z proteins regulate another splicing factor. Only a small number of DE genes were coding for proteins involved in RNA processing (Fig. 28B), which were predominantly regulated in the *rs2z35 rs2z36* double mutant and code for proteins involved in the RNAi pathway (Fig. 29B), and thus could not explain the potential downstream effects per se. However, 139 genes coding for RNA processing factors were DAS in *rs2z* mutants (Fig. 35A), which potentially impacted the levels of functional isoforms and thereby shifted AS patterns of downstream targets. Such candidates could be PTBs (Fig. 35E) or spliceosomal components like U2AF (Fig. 35F).

Splicing regulation was observed predominantly in *rs2z35 rs2z36*, but with a substantial overlap with both *rs2z35* and *rs2z36* (Fig. 33A). Hereby, non-redundant functions of RS2Z35 and RS2Z36 were indicated by AS events regulated in the single mutants (Fig. 33A). In many cases, however, the knockout of one RS2Z member had a subtle impact on AS while the consequences of the double knockout were more pronounced (Fig. 34-35), suggesting largely redundant functions of RS2Z proteins in splicing regulation as observed for *HSFA2* intron 2 regulation (Fig. 17).

Strikingly, only a minor fraction of *RS2Z*-regulated DAS genes was simultaneously DE (Fig. 33D), indicating that DAS and DE-regulation could represent two separate levels of regulation. Similarly low overlaps have been reported upon knockout of At-*SR45-1* (Zhang et al., 2017). *RS2Z*-regulated DE genes that are not DAS could thus represent indirect effects caused by DAS-regulated TFs, attributed to the large number of 163 RS2Z-regulated DAS genes encoding for TFs (Fig. 35A). Similarly, 37 TFs are DE-regulated in *rs2z* mutants which, although they do not include well-known HSR-related factors, could likewise contribute to thermotolerance. The sensitivity of the *rs2z36* single mutant to a direct HS incident may thus be attributed to the DE of TFs belonging to classes with roles in abiotic stress responses, including WRKY (Li et al. 2011), NAC (Shahnejat-Bushehri et al., 2012) and hormone-

responsive TFs such as ERFs (Mizoi et al., 2012) or cytokinin response factors (CRF) (Shi et al., 2014; Fig. 29A). *RS2Z*-regulated DAS genes that are not DE suggest that for many DAS genes, AS-regulation did not manifest in altered transcript abundance. AS may thereby protect transcripts from NMD by nuclear retention and thus reduce the pool of translatable transcripts (Göhring et al., 2014; Chaudhary et al., 2019).

5.3 Proposed functions of RS2Z proteins in splicing and beyond

Out of over 1,000 RS2Z-associated transcripts, 206 were shown to be DAS in *rs2z* mutants (Fig. 38A; RIPxDAS genes), providing evidence that RS2Z proteins take part in their splicing regulation, either by direct interaction or by residing in the same complex. Furthermore, A3'SS was the most prevalent AS type among all *RS2Z*-regulated DAS genes as well as among the 206 RIPxDAS genes, suggesting the regulation of 3'SS recognition as primary mode of action for RS2Z proteins (Fig. 38B). In this notion, RS2Z proteins, while able to bind to several regions within *HSFA2* intron 2, preferentially bind to the 3' region of this intron (Fig. 19G-J). This suggests that RS2Z proteins may preferentially bind to AU-rich-sequences present in the 3'region of the intron. Since RIP-Seq does not provide information about the binding sites within the associated transcripts, the detailed binding motifs could not be identified. Moreover, DAS events in *rs2z* mutants were not regulated in a particular direction (Fig. 34, Supplemental Fig. 18-19), which suggests that RS2Z proteins act as neutral splicing regulators and consequently, their impact may depend on the molecular context in a gene-specific fashion. Furthermore, DAS genes in *rs2z* mutants reflected a broad spectrum of genes (Fig. 33E), which suggests that RS2Z proteins exhibit broader roles in AS regulation and may not only regulate specific AS events, but aid in the reduction of translatable transcripts on a larger scale.

Additionally, RS2Z proteins associate with a large number of transcripts that were not identified as DAS genes in the *rs2z* mutants. There are three potential reasons for this observation. The first reason is the limitation of the methods, in which for example a number of false negatives for DAS genes underestimated their total number. While low coverage in RNA-Seq could have prevented the detection of their AS events (Supplemental Fig. 2D), it is likely also the underestimation of IR events that contributed to a number of false negatives. In fact, the prevalence of IR that is often reported as a mechanism in response to HS (section 1.5.2) was not reported in this study (Fig. 32C). Attributed to the insufficiently annotated tomato transcriptome and since IR events are the most challenging to detect and to quantify (Broseus and Ritchie, 2020), the frequency of IR events was likely underestimated both in response to HS and in *rs2z* mutants compared to the WT. Employing additional software dedicated to IR prediction such as IRFinder-S (Lorenzi et al., 2021), could thus complement the identified AS events and complete the picture. It is therefore possible that at least some RS2Z-associated genes were falsely identified as not DAS.

Furthermore, upon *RS2Z* overexpression, transcript levels of the endogenous gene as well as of the respective other RS2Z member were observed to be downregulated (Fig. 16C-D). This, however, was not reflected by read counts for the RS2Z genes in the RIP input (Fig. 36C). Therefore, it cannot be excluded that the endogenous RS2Z protein or the respective other member interfered by competing for RNA targets with GFP-RS2Z.

The second option considers that although the majority of RS2Z-associated transcripts derived from multiexon genes, 148 intronless transcripts were identified as well (Fig. 37C). Many mammalian SR proteins, including the ZnK containing SRSF7, display nucleocytoplasmic shuttling and were reported to engage in other aspects of RNA metabolism besides splicing (section 1.8.3), for example in nuclear RNA export by acting as adaptors of the nuclear export factor NXF1 (Müller-McNicoll et al., 2016). In Arabidopsis, a role for SR-like protein SR45 in RNA export was suggested based on its association with a substantial number of intronless genes in RIP-Seq (Xing et al., 2015). At-SR45 thereby fulfils many roles in RNA metabolism and was further suggested to sequester IR transcripts in the nucleus and thus delay their splicing (Filichkin et al., 2015). Tomato RS2Z proteins did not display cytoplasmic localisation (Fig. 13A), which could either indicate strict nuclear localisation or that their presence in the cytoplasm is short-lived, resulting in a net nuclear signal. However, although there is no plant ortholog of human nuclear export NXF1, a component of the Transcription-Export (TREX) complex that coordinates mRNA export in both metazoans and plants has been shown to directly interact with SR proteins in Arabidopsis and co-localises with ZnK-containing SR proteins At-RSZ22 and At-RS2Z33 in nuclear speckles (Sørensen et al., 2017). Consequently, a role for tomato RS2Z proteins in nuclear export can be envisioned in which they hand over export-ready mRNAs to the export machinery without translocating to the cytoplasm themselves and could thus contribute to nuclear export or retention of their associated transcripts. Since RNA-Seq performed in this study did not follow cell fractionation into cytoplasmic and nuclear fractions, the residency of RS2Z-associated transcripts in RNA-Seq could not be determined. It is thereby possible, although speculative, that RS2Z proteins play a role in nuclear retention and/or nuclear export of transcripts (Fig. 39B).

Thirdly, 72% of RIP genes were identified as AS (Fig. 37D) but only 20% were identified to be DAS in *rs2z* mutants (Fig. 38A). The association of transcripts with RS2Z proteins could thus reflect their existing but dispensable role in canonical and alternative splicing of many of their associated transcripts, in which other SR proteins compensated the loss of RS2Z proteins in the *rs2z* mutants. This suggests that while RS2Z proteins may not be essential for the AS of their associated transcripts, they could nevertheless represent a link between splicing and nuclear retention and/or nuclear export. However, this is beyond the scope of this study and experimental evidence is needed to support this hypothesis. A potential role for RS2Z proteins beyond splicing, however, is further indicated by the regulation of HSFA2 from wild tomato species, harbouring three intronic polymorphisms compared to modern species (section 1.5.3; Hu et al., 2020a). While RS2Z proteins acted as splicing repressors of both $HSFA2^{GGG}$ and $HSFA2^{AAA}$, resulting in the preferential accumulation of HSFA2-I-encoding transcripts (Fig. 9), the ratio of HSFA2 protein isoforms was shifted towards HSFA2-II in the wild variant (Fig. 8B-E). Astonishingly, members of the RS2Z subfamily were the only SR proteins that impacted the two HSFA2 variants in opposing fashion, suggesting an exceptional role of those among the tomato SR proteins.

5.4 Redundancy and specificity of RS2Z proteins

RS2Z35 and RS2Z36 bind to unique and overlapping sets of RNA targets, in which half of all identified targets were specifically associated with RS2Z36, further highlighting the dominant role of the HS-induced member RS2Z36 over RS2Z35 (Fig. 37A-B). In contrast, although RS2Z35 is not HS-induced (Fig. 12A), it was able to compensate for the loss of RS2Z36 in the *rs2z36* single mutant in *HSFA2* intron 2 splicing regulation (Fig. 17C & E) and consequently in the downstream impact on HSP expression (Fig. 22A-C). However, DE analysis revealed that over 200 genes were differentially regulated in the *rs2z36* single mutant, in which RS2Z35 was not able to compensate, highlighting a specialised function of RS2Z36 in many cases. Furthermore, RS2Z36 was able to compensate the loss of RS2Z35 in the *rs2z35* single mutant almost fully as indicated by the absence of thermosensitivity towards a direct stress of 40°C (Fig. 23D) and the low number of DE genes in *rs2z35 (*Fig. 26A). This could partially be attributed to the cross-regulation of *RS2Z36* by RS2Z35, in which the absence of RS2Z35 positively impacted full-length protein-coding *RS2Z36* levels and thus likely aided a proper compensation. While RS2Z35 and RS2Z36 are members of the same subfamily and possess the same domain structure, they mostly differ in their RS domains, in which RS2Z36 displayed a higher RS/SR content than RS2Z35 (Supplemental Fig. 6), which likely modulates different interactions of the RS2Z members with other RS-domain containing proteins. Furthermore, the interaction of Arabidopsis RS2Z protein RS2Z33 with other SR proteins relies not only on the RS domain, but also on the presence of the RNA binding components (Lopato et al., 2002), suggesting that differences between RS2Z members in the ZnKs, as well as the RS domains, potentially modulate their specific interaction with other factors.

Additionally, the *in vitro* binding affinity of recombinant RS2Z proteins lacking the RS domains towards *HSFA2* intron 2 differed between RS2Z members, with the affinity of RS2Z35(RBD) being about five times higher than that of RS2Z36(RBD) (Fig. 19). In contrast to the two RS2Z members in Arabidopsis with 100% shared identity in their RNA binding components (Lopato et al., 2002), tomato RS2Z differ slightly in their ZnKs, which could be the underlying cause for the difference in affinity (Supplemental Fig. 6). The requirement of the ZnKs for *HSFA2* splicing regulation indicates that the ZnKs are indeed involved in determining target specificity (Fig. 11C), similar as reported for ZnK containing human SR protein SRSF7 (former 9G8) (Cavaloc et al., 1999). While the RRM of RS2Z35 and RS2Z36 was dispensable for *HSFA2* intron 2 AS regulation (Fig. 11C), the presence of three RNA binding components (RRM and two ZnKs) likely contributes to the diverse landscape of associated transcripts (Fig. 36F) in which the three components may have combined and specific target sequences. Therefore, in addition to the differences in their RS domains, differences in their RNA binding components could very well contribute to the association of specific transcripts with one RS2Z member or the other.

Furthermore, RS2Z35 was shown to cross-regulate *RS2Z36* via AS (Fig. 16), reflecting a need to tightly regulate functional RS2Z36 levels. The elevated levels of *RS2Z36* in the *rs2z35* mutant thus likely further compensated its loss, demonstrated by the absence of most phenotypes in *rs2z35*, including *HSFA2* splicing alteration, BTT as well as reproduction. Collectively, the results obtained in this study suggest that tomato RS2Z proteins act redundantly in many ways but also have distinct functions with a specialised role of RS2Z36 in response to heat.

RS2Z proteins were further shown to impact tomato reproduction (Fig. 15B-E). While fruit weight was similarly reduced in *rs2z35* and *rs2z36*, the number of seeds and fruit morphology were only impacted in *rs2z36* (Fig. 15B-E), highlighting a specialised role of RS2Z36 not only in stress response but also in reproduction. Furthermore, overexpression of either *RS2Z* member drastically reduced the number of seeds (Fig. 15C), suggesting that elevated levels of RS2Z proteins beyond a certain threshold are detrimental for the plant and need to be attenuated accordingly. An increase in non-productive splicing in *RS2Z* genes upon *RS2Z* overexpression, representing auto- as well as cross regulation between RS2Z proteins (Fig. 16), further supports the notion that RS2Z genes are tightly regulated and thus that HS-induction of *RS2Z36* reflects a requirement for this particular SR protein during HS. The impact of *rs2z36* knockout on reproduction and fruit morphology further indicates broader and additional roles for RS2Z36 beyond stress responses. RS2Z36 is the generally low expressed member of the RS2Z subfamily and similarly, other HS-induced tomato SR proteins, SR33 and SC30b, represent the generally low expressed member of their subfamilies as well (Rosenkranz et al., 2021). This suggests that the low expressed members may be induced under certain conditions or tissue types in which they fulfil specialized functions, as indicated for RS2Z36 in this study.

5.5 Regulation of thermotolerance on crossroads of stress responses

Interestingly, while for DAS regulation, the numbers of genes regulated by *rs2z35* and *rs2z36* were similar, DE genes were more prevalent for the *rs2z36* single and the *rs2z35 rs2z36* double mutant over *rs2z35* (Fig. 26A, Fig. 29). Therefore, the *rs2z36*-specific DE genes could potentially account for its reduced BTT. Surprisingly, *RS2Z*-regulated DE genes, by large, did not represent well-known HSR components like those involved in protein folding or response to heat (Fig. 25), but rather genes involved in pathogen response pathways (Fig. 28A, Fig. 30), including the pathogen response factor *EIX RECEPTOR 1* (Ron and Avni, 2004), and several disease resistance (R) genes (Fig. 30). R proteins act as receptors of pathogen-derived signals and mediate the downstream response pathway (Tör et al., 2003). Interestingly, R genes are not only transcriptionally induced in response to pathogen infection, but also in response to environmental conditions including heat, hinting towards partially common or overlapping mechanisms (MacQueen and Bergelson, 2016). Consistent with this notion, seven R genes were downregulated in *rs2z* plants. On top of that, DE genes involved in protein homeostasis primarily consisted of those involved in protein degradation rather than protein folding (Fig. 29C), which could as well be attributed to a role of RS2Z proteins in both HSR and plant immunity (Tör et al., 2003). Recently, it has been reported that a pre-exposure to pathogens could positively impact recovery (Liu et al., 2022b), and tomato HSFA1a has been found to be essential for R-gene mediated nematode resistance (Zhou et al., 2018), pointing towards interlinked mechanisms between the two response pathways.

Phytohormones, such as cytokinin (CK), ethylene (ET), salicylic acid (SA) or jasmonic acid (JA), among others, play important parts in both biotic and abiotic stresses, in which different types of phytohormones cross pathways in antagonistic and cooperative ways (Mur et al., 2006; Love et al., 2008; Dodds and Rathjen, 2010; Zwack and Rashotte, 2015; Yang et al., 2019; Chen et al., 2021). For example, SA signalling, although being a main component of the pathogen response pathway, plays a

role in BTT as well (Clarke et al., 2004; Feng et al., 2020). ET, acting as balancing coordinator of plant growth and stress response by cooperation with other hormones, particularly with SA and JA in pathogen response pathways (Chen et al., 2021), is likewise involved in BTT (Larkindale et al., 2005). Indeed, many tomato ERFs are transcriptionally induced by HS (Klay et al., 2018). Furthermore, two Arabidopsis ERFs, ERF95 and ERF97, were recently reported to regulate BTT through the regulation of HS-genes, including *HSFA2* (Huang et al., 2021), thereby further establishing the involvement of ET signalling in the HSR (Huang et al., 2021). Interestingly, expression levels of *HSFA2* (Fig. 22B), as well as several members of the ERF family (Fig. 30), were reduced upon *rs2z* knockout. Consequently, there is potential for the existence of hormone-related *RS2Z*-regulated pathways upstream of *HSFA2*. As Arabidopsis mutants defective in ET and JA signalling were impaired in ATT (Larkindale et al., 2005), it is therein feasible to consider that reduced ATT in any *rs2z* mutant may be caused by a disturbance in phytohormone signalling and its downstream pathways.

Several TFs were differentially regulated primarily in *rs2z36* and *rs2z35 rs2z36*, but not *rs2z35* (Fig. 28C; Fig. 39B), rendering them potential candidates for the observed RS2Z36-specific reduction of BTT in hypocotyl elongation assays (Fig. 23D). These include TFs such as WRKY, MYB as well as several ERFs (Fig. 30) which play diverse and overlapping roles in both abiotic and biotic stress responses with a special role for WRKY TFs in conferring plant immunity (Pandey and Somssich, 2009; Pandey et al., 2015; Chen et al., 2021). Several WRKY TFs have been reported to regulate both BTT and pathogen response, for example *Capsicum annuum* (pepper) WRKY27 as a positive regulator of pathogen and a negative regulator of HS response (Dang et al. 2014; Dang et al., 2018). In contrast, pepper WRKY40 (Dang et al., 2013) and Arabidopsis WRKY33 and WRKY39 are required for both pathogen defence, as well as thermotolerance (Zheng et al., 2006; Li et al., 2011). In this notion, WRKY40, a mediator of pathogen and HS response in pepper, is induced by signalling mechanisms mediated by ET, SA, and JA (Dang et al., 2013), representing an important factor for pathways downstream of hormonal networks. Although several tomato WRKY TFs have been reported to be involved in biotic and/or abiotic stress pathways in tomato (Bai et al., 2018b), the *RS2Z*-regulated factors WRKY9 and WRKY55 have not been studied in detail so far. Collectively, *RS2Z36*-regulated TFs may act as mediators of pathogen and heat response (Fig. 39B). Consequently, RS2Z proteins could thus play a role in phytohormone signal transduction through the regulation of WRKY or ERF TFs. Although the HS-induction of *RS2Z36* was drastically reduced upon HSFA1a co-suppression and thus indicating dependence on the HSF-system (Rosenkranz et al., 2021), the induction of *RS2Z36* was not abolished entirely and could likewise be dependent on HS-related WRKY, MYB or ERF factors in addition, as indicated by the presence of the respective elements in the *RS2Z36* promoter (Rosenkranz et al., 2021).

Furthermore, two CRFs, *CRF1* and *CRF2-like*, stood out among *RS2Z*-regulated DE genes (Fig. 31). CRFs represent a cytokinin-responsive ERF subgroup but despite their name do not only respond to CK, but also to other hormones and stresses (Shi et al., 2012; Shi et al., 2014), and were suggested as integrators of hormonal and stress responses in plant adaptation (Kim, 2016), making them additional candidates for thermotolerance regulation beyond the HSF system. However, neither the gene annotated as *CRF1* in this study nor *CRF2-like* were listed among tomato CRF genes (Shi et al., 2012)

and are therefore entirely uncharacterised. Since the *CRF1* gene in this study was as well shown to respond to heat (Fig. 31A), it would be an interesting candidate for further thermotolerance studies.

Both stress signalling and expression of protective genes need to be synchronised for efficient stress responses to maintain cellular homeostasis. This is crucial, especially when a plant is exposed to multiple stress conditions simultaneously. Although some studies imply a positive relation between pathogen defence and HSR (MacQueen and Bergelson, 2016; Liu et al., 2022b), heat-stressed plants are more susceptible to pathogen attacks, attributed to a temperature-dependent inhibition of pathogen response pathways (Wang et al., 2009; Marques de Carvalho et al., 2015). The need to suppress pathogen defence mechanisms for a proper HSR could in part result from contrasting pathways. For example, plants respond to local infections with the so-called hypersensitive response, causing local apoptosis of the infected tissue through a burst of ROS species, which results in the confinement of pathogens (Love et al., 2008). This however contrasts the efforts of heat stressed plants to avoid cell death, among others by avoiding the overaccumulation of ROS through the induction of ROS scavengers (Love et al., 2008; Suzuki and Katano, 2018).

Yet, although exposure to a multitude of co-occurring stresses reflects the real-world situation more accurately, the crossroads of stress responses are difficult to investigate due to the complexity of the individual stress responses. In that regard, it has been reported that salt and pathogen responses share downstream pathways, including involvement of the same TFs (Bai et al., 2018a), highlighting the prevalence of interconnected pathways in response to biotic and abiotic stresses and allowing the conclusion that similar overlapping pathways may exist for the HSR as well. Moreover, plants prioritise abiotic stress response over biotic stress response if exposed to stress combinations, suggesting that the plant indeed represses some aspects of pathogen defence pathways in favour of the HSR (Suzuki and Katano, 2018a). This is further indicated by the enrichment of GO terms involving response to biotic stimuli in the downregulated genes response to HS in this study (Fig. 25D). RS2Z proteins thereby likely influence the synchronization of signalling and response to pathogens and heat to ensure a functional HSR. Although the specific mode of action could not be uncovered due to missing characterisation of the impacted factors, RS2Z proteins likely impact thermotolerance through the regulation of factors shared or antagonized by pathogen and heat response pathways (Fig. 39B). Thereby, they would act on crossroads of response pathways between the response to pathogens and the response to HS, with RS2Z36 dominating over RS2Z35 (Fig. 39B), causing a BTT phenotype upon *rs2z36* knockout (Fig. 23D). While some of the DE genes were also impacted under control conditions (Fig. 26 & 31), *rs2z36* did not show growth phenotypes in the absence of heat (Fig. 15A), suggesting that the regulation of pathogen response genes may inflict the HSR but not vegetative growth and indeed pose HS-dependent regulation.

However, only a minor fraction of DE gene-encoded transcripts was associated with RS2Z proteins in RIP-Seq, one being *EIX RECEPTOR 1* (Supplemental Fig. 20), whereas the vast majority of DE genes identified in *rs2z* mutants were neither DAS (Fig. 33D), nor directly associated with RS2Z proteins (Fig. 38A). Therefore, the regulation of pathogen response factors likely represents downstream effects, resulting from an upstream factor regulated by RS2Z proteins, potentially through AS (Fig. 39B). One

candidate is the JASMONATE ZIM-DOMAIN (JAZ) PROTEIN 2 (Fig. 35C). JAZ proteins play roles in biotic and abiotic pathways by acting as hubs for integrating ET and JA signals (Kazan, 2015; Chini et al., 2017) and could thus be one of the upstream factors leading to *RS2Z*-mediated DE genes involved in crossroads of HSR and pathogen defence (Fig. 39B).

The diverse nature of *RS2Z*-regulated DAS genes and the large overlap of *RS2Z*-regulated with HS-regulated DAS genes strongly suggests that RS2Z proteins play an important and potentially broader role in HS-dependent AS regulation (Fig. 39B). Attributed to their involvement in the expression of pathogen response genes, the DAS genes in *rs2z* mutants likely reflect AS events that are at least partially shared by the HSR and pathogen response pathway. Thereby, plant SR proteins seem to be at

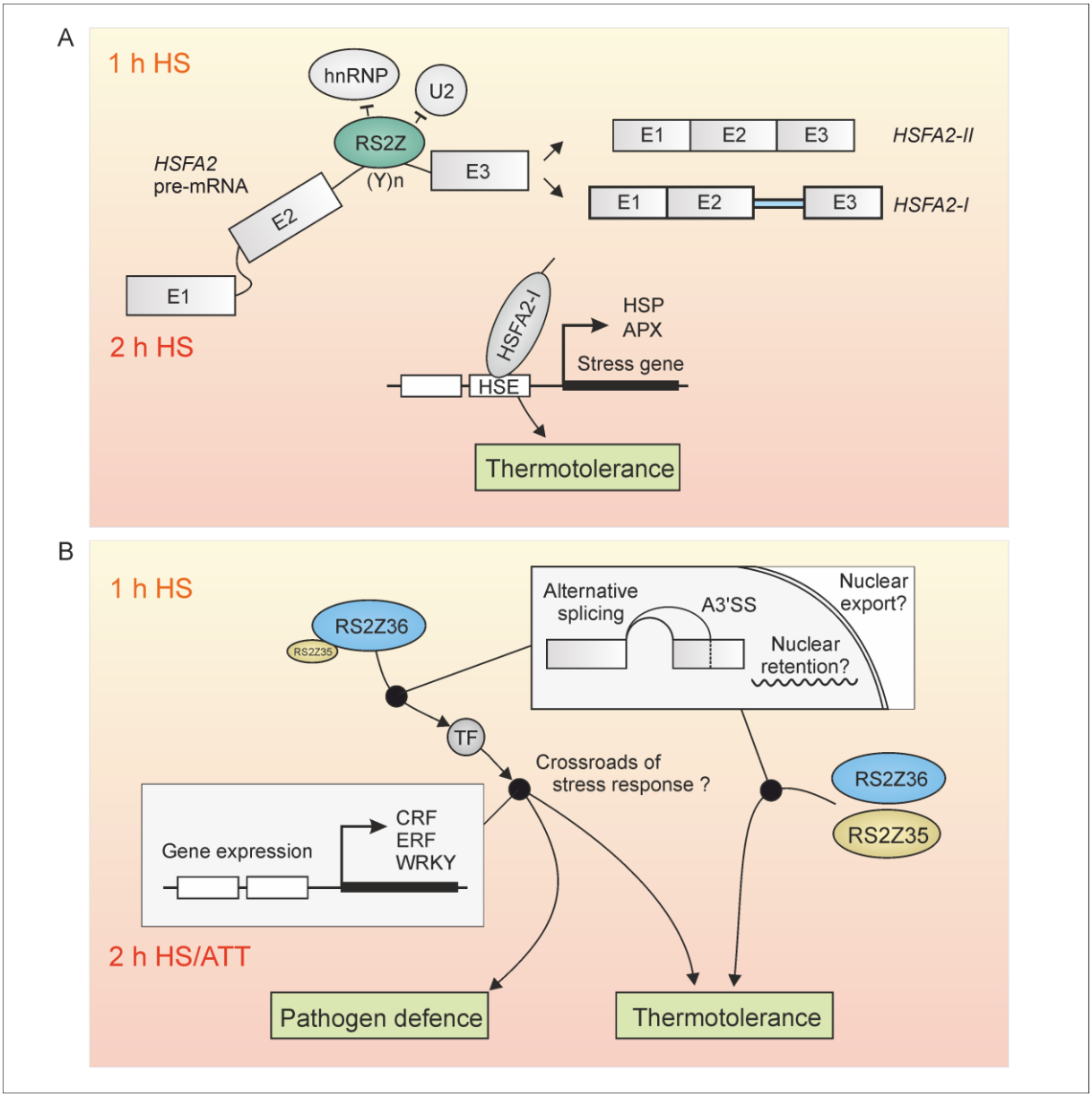

Figure 39. Working model on the functional role of RS2Z proteins in the tomato thermotolerance. (A) RS2Z proteins redundantly inhibit *HSFA2* intron 2 removal and thereby promote the production of protein isoform HSFA2-I. **(B)** Right side: RS2Z proteins impact HS-responsive AS events primarily via A3'SS and contribute to thermotolerance potentially through control of transcript abundance or localisation. Left side: RS2Z36 regulates the expression of pathogen response genes, potentially through the AS-regulation of upstream TFs. These likely act on crossroads between pathogen defense and thermotolerance.

least as versatile in their functions as their mammalian counterparts, as for example demonstrated for Arabidopsis SR-like protein SR45 involved in both salt stress (Albaqami et al., 2019) and plant immunity (Zhang et al., 2017), and likewise as suggested for tomato RS2Z proteins in this study.

5.6 Conclusion and outlook

This study provides experimental evidence for the involvement of SR proteins in tomato thermotolerance through regulation of the key regulator of ATT, HSFA2. Furthermore, RS2Z proteins take part in more than half of HS-induced AS events and thus likely play a broader role in the HSR. On top of this, RS2Z proteins, especially RS2Z36, regulate the expression of pathogen response-related genes in response to HS, thereby likely modulating crossroads of pathogen and HS response pathways. Thereby, this study provides further evidence for the broad and important role of splicing factors in plant stress response pathways. However, the detailed role of RS2Z proteins in acclimation remains largely unknown.

Since RS2Z proteins, surprisingly, were not only involved in the HSR through the regulation of HSFA2 but impacted the expression of genes involved in pathogen response as well, future studies should investigate their role in other abiotic and biotic stress regimes besides HS. This could provide insights into whether RS2Z proteins regulate genes on crossroads of general stress response or whether they confer elevated thermotolerance to the expense of plant immunity. As the application of a single stress differs significantly from the situation in the field in which plants are exposed to a variety of co-occurring biotic and abiotic stresses, it would be of interest to study the role of RS2Z proteins in combined stress responses as well, e. g. simultaneous pathogen infection and HS exposure.

In this notion, it is crucial to investigate whether *RS2Z* overexpression lines indeed possess enhanced thermotolerance and/or pathogen resistance, as genes conferring tolerance to both biotic and abiotic stresses would be valuable candidates for the development of robust crops. Due to the lack of homozygous *GFP-RS2Z* overexpression lines and the negative impact on reproduction and thus low number of seeds, thermotolerance assays of *GFP-RS2Z* overexpression lines could not be conducted within this study. While disturbance of RS2Z proteins by either knockout or overexpression negatively impacted tomato reproduction, conditional *RS2Z* overexpression, confined to specific (vegetative) tissues or under certain (HS) conditions, could thereby serve as a means of generating thermotolerant crops.

Furthermore, while this study provided a general characterisation of RS2Z proteins under elevated temperatures and revealed a dominant role of RS2Z36, it did not focus on distinguishing RS2Z35- and RS2Z36-specific functions in detail, which is in part attributed to their largely redundant role in *HSFA2* splicing. Methods to identify RNA binding sites on a global scale other than RIP-Seq, such as individual-nucleotide resolution cross-linking and immunoprecipitation (iCLIP) (Huppertz et al., 2014) would identify directly bound target RNAs and thereby cross validate the findings in this study, and could further discriminate between direct and indirect targets. The generation of plant lines overexpressing *GFP-RS2Z* in a *rs2z* mutant background could thereby overcome potential competition between the tagged transgene with endogenous RS2Z proteins. Furthermore, iCLIP would help to overcome the

limitations of RIP by providing information about the binding sites, thereby allowing the identification of binding motifs specific for RS2Z35 and RS2Z36 and thus enable further conclusions on how they impact their specific target RNAs. This could also indicate whether RS2Z proteins do indeed preferentially bind to AU-rich sequences. Together with the information on DAS genes in this study, the binding to high-confidence targets of special interest could subsequently be analysed with RNA EMSA using identified target sequences in WT and mutant format to further elucidate their mode of action. Additionally, the particular role of the individual RNA binding components (RRM and ZnKs) in the binding of target transcripts could be investigated by deleting individual components in recombinant SR proteins and observing their binding affinity to specific target sequences.

Moreover, while short-read sequencing enables the quantification of local splice variants, it does not allow the prediction of entire transcripts and thus potential isoforms. While this study provided a general impression of the role of RS2Z proteins in HS-dependent AS, it is necessary to uncover the consequences of those events. Efforts to obtain entire transcripts using long-read sequencing, so-called isoform sequencing (Iso-Seq, Rhoads and Au, 2015) could provide insight into the precise exon-intron structure of existing RNA variants occurring under control and HS conditions, and thus allow reliable estimations on how *RS2Z*-regulated AS impacts their coding potential. This would consequently allow a more detailed analysis of the consequence of AS events caused by *rs2z* knockout in this study and could therefore further elucidate the role of RS2Z-mediated AS for thermotolerance. Additionally, cell fractionation followed by sequencing of nuclear and cytoplasmic fractions in WT and *rs2z* mutants could uncover whether transcripts identified as RS2Z-associated are altered in their nuclear export upon *rs2z* knockout, thus investigating a potential role for RS2Z proteins beyond splicing.

Additionally, while the 1 h HS time point investigated in this study is crucial for the establishment of the HSR and provided valuable insight into the immediate regulation by RS2Z proteins, further analyses of later time points (prolonged or re-occurring HS) are needed to fully understand the consequence of the mechanisms impacted by RS2Z, and particularly RS2Z36, that would manifest as downstream effects after the 1 h time point. Similar to the regulation of *APX3* and *HSP17* in *rs2z35 rs2z36* that were only evident after prolonged HS of 2-3 hours, downstream genes of other *RS2Z*-regulated TFs would likely emerge at a later time point as well and could thereby contribute to deciphering which upstream factors play the major role in *RS2Z*-mediated thermotolerance. Additionally, while the exposure to 1 h 40°C did not impact growth rates of *rs2z* single mutants in preliminary results (Supplemental Figure 13), the impact of 2 h 40°C on the growth rates of the *rs2z36* and the *rs2z35 rs2z26* mutants demonstrate their sensitivity towards mild HS. Therefore, the physiological assessment of the acclimation capacity to 1 h 40°C should be thoroughly repeated in future studies including the *rs2z35 rs2z36* double mutant.

Moreover, despite the RS domain being dispensable for their splicing repressor function in *HSFA2* intron 2, the RS domains of RS2Z proteins likely mediate their interaction with other factors, such as other SR proteins and spliceosomal components. While there is evidence for the interaction between RS2Z proteins and other SR proteins, such as SCL29 and SC30b, as obtained by yeast two-hybrid assay and bimolecular fluorescence complementation (Vraggalas, 2022), uncovering a global RS2Z protein

interaction network by co-immunoprecipitation followed by tandem mass spectrometry ((Co-IP)/MS) would provide further information on their mode of action during splicing by interaction with spliceosomal components and other splicing-related factors. Additionally, interaction with export complexes would indicate a potential role during RNA export. In that regard, while the results obtained by RIP-Seq were analysed for coding RNAs in this study, analyses of long non-coding RNAs (lncRNAs) would allow conclusions on whether RS2Z proteins engage in lncRNA-driven nuclear body formation and could as well elucidate their potential involvement in lncRNA metabolism.

Collectively, while this study demonstrated the importance of RS2Z proteins in tomato thermotolerance, we are only beginning to understand the detailed mechanisms on how they impact their specific targets and which diverse roles they may play in plant RNA metabolism and stress responses.

References

Abràmoff MD, Magalhães PJ, Ram SJ (2004) Image Processing with Image J. *Biophotonics Int* 11 (7): 36–41

Albaqami MK, Laluk K, Reddy ASN (2019) The Arabidopsis Splicing Regulator SR45 Confers Salt Tolerance in a Splice Isoform-Dependent Manner. *Plant Mol Biol.* 100 (4–5): 379–90. https://doi.org/10.1007/s11103-019-00864-4

Ali GS, Golovkin M, Reddy ASN (2003) Nuclear Localization and in Vivo Dynamics of a Plant-Specific Serine/Arginine-Rich Protein. *Plant J.* 36 (6): 883–93. https://doi.org/10.1046/j.1365-313X.2003.01932.x

Ali GS, Palusa SG, Golovkin M, Prasad J, Manley JL, Reddy ASN (2007) Regulation of Plant Developmental Processes by a Novel Splicing Factor. *PLoS One.* 2 (5): e471. https://doi.org/10.1371/journal.pone.0000471

Anduaga M, Evantal N, Patop IL, Bartok O, Weiss R, Kadener S (2019) Thermosensitive Alternative Splicing Senses and Mediates Temperature Adaptation in Drosophila. *ELife.* 8: e44642. https://doi.org/10.7554/eLife.44642

Anders, S., Pyl PT, Huber W (2015) HTSeq--a Python Framework to Work with High-Throughput Sequencing Data. *Bioinformatics.* 31 (2): 166–69. https://doi.org/10.1093/bioinformatics/btu638

Andrási N, Norbert, Pettkó-Szandtner A, Szabados L (2021) Diversity of Plant Heat Shock Factors: Regulation, Interactions, and Functions. *J Exp Bot.* 72 (5): 1558–75. https://doi.org/10.1093/jxb/eraa576

Ausubel FM, Brent R, Kingston RE, Moore DD, Seidman JG, Smith JA, Struhl K (2003). Current Protocols in Molecular Biology. John Wiley & Sons Inc, Ringbou Edition

Bachiri S (2021) Regulation and Functions of RS2Z Genes in Tomato. Master thesis. Goethe-University, Frankfurt am Main

Bai Y, Yuling, Kissoudis C, Zhe Yan Z, Visser RGF, van der Linden CG (2018a) Plant Behaviour under Combined Stress: Tomato Responses to Combined Salinity and Pathogen Stress. *Plant J.* 93 (4): 781–93. https://doi.org/10.1111/tpj.13800

Bai Y, Sunarti S, Kissoudis C, Visser RGF, van der Linden CG (2018b) The Role of Tomato WRKY Genes in Plant Responses to Combined Abiotic and Biotic Stresses. *Front Plant Sci.* 9: 801. https://doi.org/10.3389/fpls.2018.00801

Balazadeh S (2022) A “Hot” Cocktail: The Multiple Layers of Thermomemory in Plants. *Curr Opin Plant Biol.* 65: 102147. https://doi.org/10.1016/j.pbi.2021.102147.

Baniwal SK, Bharti K, Chan KY, Fauth M, Ganguli A, Kotak S, Mishra SK, Nover L, Port M, Scharf KD, Tripp J, Weber C, Zielinski D, von Koskull-Döring P (2004) Heat Stress Response in Plants: A Complex Game with Chaperones and More than Twenty Heat Stress Transcription Factors. *J Biosci.* 29 (4): 471–87. https://doi.org/10.1007/BF02712120

Barta A, Kalyna M, Reddy ASN (2010) Implementing a Rational and Consistent Nomenclature for Serine/Arginine-Rich Protein Splicing Factors (SR Proteins) in Plants. *Plant Cell.* 22 (9): 2926-29. https://doi.org/10.1105/tpc.110.078352

Battisti DS, Naylor RL. (2009) Historical Warnings of Future Food Insecurity with Unprecedented Seasonal Heat. *Science.* 323 (5911): 240–44. https://doi.org/10.1126/science.1164363

Bokszczanin K (2013) Perspectives on Deciphering Mechanisms Underlying Plant Heat Stress Response and Thermotolerance. *Front Plant Sci.* 4. https://doi.org/10.3389/fpls.2013.00315

Bradford MM (1976) A Rapid and Sensitive Method for the Quantitation of Microgram Quantities of Protein Utilizing the Principle of Protein-Dye Binding. *Anal. Biochem.* 72 (1–2): 248–54. https://doi.org/10.1016/0003-2697(76)90527-3

Broft P, Rosenkranz RRE, Schleiff E, Hengesbach M, Schwalbe H (2022) Structural Analysis of Temperature-Dependent Alternative Splicing of HsfA2 Pre-MRNA from Tomato Plants. *RNA Biol.* 19 (1): 266–78. https://doi.org/10.1080/15476286.2021.2024034

Broseus L, Ritchie W (2020) Challenges in Detecting and Quantifying Intron Retention from next Generation Sequencing Data. *Comput Struct Biotechnol J.* 18: 501–8. https://doi.org/10.1016/j.csbj.2020.02.010

Buntru M, Vogel S, Spiegel H, Schillberg S (2014) Tobacco BY-2 Cell-Free Lysate: An Alternative and Highly-Productive Plant-Based in Vitro Translation System. *BMC Biotechnol.* 14 (1): 37. https://doi.org/10.1186/1472-6750-14-37

Busch W, Wunderlich M, Schöffl F (2004) Identification of Novel Heat Shock Factor-Dependent Genes and Biochemical Pathways in Arabidopsis Thaliana: Novel HSF Target Genes. *Plant J.* 41 (1): 1–14. https://doi.org/10.1111/j.1365-313X.2004.02272.x

Butt H, Piatek A, Li L, Reddy ASN, Mahfouz MM (2019) Multiplex CRISPR Mutagenesis of the Serine/Arginine-Rich (SR) Gene Family in Rice. *Genes.* 10 (8): 596. https://doi.org/10.3390/genes10080596

Cáceres JF, Stamm S, Helfman DM, Krainer AR (1994) Regulation of Alternative Splicing in Vivo by Overexpression of Antagonistic Splicing Factors. *Science.* 265 (5179): 1706–9. https://doi.org/10.1126/science.8085156.

Cáceres JF, Screaton GR, Krainer AR (1998) A Specific Subset of SR Proteins Shuttles Continuously between the Nucleus and the Cytoplasm. *Genes Dev*. 12 (1): 55–66. https://doi.org/10.1101/gad.12.1.55

Capovilla G, Pajoro A, Immink RGH, Schmid M (2015) Role of Alternative Pre-MRNA Splicing in Temperature Signaling. *Curr Opin Plant Biol.* 27 (October): 97–103. https://doi.org/10.1016/j.pbi.2015.06.016

Carlson M (2017) Org.At.Tair.Db. *Bioconductor*. https://doi.org/10.18129/B9.BIOC.ORG.AT.TAIR.DB

Cavallari N, Nibau C, Fuchs A, Dadarou D, Barta A, Doonan JH (2018) The Cyclin-Dependent Kinase G Group Defines a Thermo-Sensitive Alternative Splicing Circuit Modulating the Expression of Arabidopsis ATU2AF65A. *Plant J.* 94 (6): 1010–22. https://doi.org/10.1111/tpj.13914

Cavaloc Y, Bourgeois CF, Kister L, Stévenin J (1999) The Splicing Factors 9G8 and SRp20 Transactivate Splicing through Different and Specific Enhancers. *RNA.* 5 (3): 468–83. https://doi.org/10.1017/S1355838299981967

Chamala S, Feng G, Chavarro C, Barbazuk WB (2015) Genome-Wide Identification of Evolutionarily Conserved Alternative Splicing Events in Flowering Plants. *Frontiers Bioeng Biotechnol.* 3:33. https://doi.org/10.3389/fbioe.2015.00033

Chang CY, Lin WD, Tu SL (2014) Genome-Wide Analysis of Heat-Sensitive Alternative Splicing in Physcomitrella Patens. *Plant Physiol.* 165 (2): 826–40. https://doi.org/10.1104/pp.113.230540

Chan-Schaminet KY, Baniwal SK, Bublak D, Nover L, Scharf DK (2009) Specific Interaction between Tomato HsfA1 and HsfA2 Creates Hetero-Oligomeric Superactivator Complexes for Synergistic Activation of Heat Stress Gene Expression. *J Biol Chem.* 284 (31): 20848–57. https://doi.org/10.1074/jbc.M109.007336

Charng YY, Liu HC, Liu NY, Hsu FC, Ko SS (2006) Arabidopsis Hsa32, a Novel Heat Shock Protein, is Essential for Acquired Thermotolerance during Long Recovery after Acclimation. *Plant Physiol.* 140 (4): 1297–1305. https://doi.org/10.1104/pp.105.074898

Charng YY, Liu HC, Liu NY, Chi WT, Wang CN, Chang SH, Wang TT (2007) A Heat-Inducible Transcription Factor, HsfA2, Is Required for Extension of Acquired Thermotolerance in Arabidopsis. *Plant Physiol.* 143 (1): 251–62. https://doi.org/10.1104/pp.106.091322

Choudhary C, Kumar C, Gnad F, Nielsen ML, Rehman M, Walther TC, Olsen JV, Mann M (2009) Lysine Acetylation Targets Protein Complexes and Co-Regulates Major Cellular Functions. *Science.* 325 (5942): 834–40. https://doi.org/10.1126/science.1175371

Chaudhary S, Jabre I, Reddy ASN, Staiger D, Syed NH (2019) Perspective on Alternative Splicing and Proteome Complexity in Plants. *Trends Plant Sci.* 24 (6): 496–506. https://doi.org/10.1016/j.tplants.2019.02.006

Chen H, Bullock DA, Alonso JM, Stepanova AN (2021) To Fight or to Grow: The Balancing Role of Ethylene in Plant Abiotic Stress Responses. *Plants.* 11 (1): 33. https://doi.org/10.3390/plants11010033

Cheng Y, Patel DJ (2004) An Efficient System for Small Protein Expression and Refolding. *Biochem Biophys Res Commun.* 317 (2): 401–5. https://doi.org/10.1016/j.bbrc.2004.03.068

Chetelat R, Peacock S (2013) Guidelines for Emasculating and Pollinating Tomatoes. C.M. Rick Tomato Genetic Resources Center, Department of Vegetable Crops, University of California. https://tgrc.ucdavis.edu/Guidelines_Emasculating_and_Pollinating_Tomatoes.pdf.

Chini A, Ben-Romdhane W, Hassairi A, Aboul-Soud MAM (2017) Identification of TIFY/JAZ Family Genes in Solanum Lycopersicum and Their Regulation in Response to Abiotic Stresses. *PLOS One*. 12 (6): e0177381. https://doi.org/10.1371/journal.pone.0177381

Clark S, Yu F, Gu L, Min XJ (2019) Expanding Alternative Splicing Identification by Integrating Multiple Sources of Transcription Data in Tomato. *Front Plant Sci.* 10 (May): 689. https://doi.org/10.3389/fpls.2019.00689

Clarke SM, Mur LAJ, Wood JE, Scott IM (2004) Salicylic Acid Dependent Signaling Promotes Basal Thermotolerance but Is Not Essential for Acquired Thermotolerance in Arabidopsis Thaliana. *Plant J.* 38 (3): 432–47. https://doi.org/10.1111/j.1365-313X.2004.02054.x

Conway JR, Lex A, Gehlenborg N (2017) UpSetR: An R Package for the Visualization of Intersecting Sets and Their Properties. *Bioinformatics.* 33 (18): 2938–40. https://doi.org/10.1093/bioinformatics/btx364

Corell RA, Riordan JA, Gross RH (1994) Chemical Induction of Stress Proteins Does Not Induce Splicing Thermotolerance under Conditions Producing Survival Thermotolerance. *Exp Cell Res.* 211 (2): 189–96. https://doi.org/10.1006/excr.1994.1077

Cruz T, Carvalho R, Richardson D, Duque P (2014). Abscisic Acid (ABA) Regulation of Arabidopsis SR Protein Gene Expression. *Int J Mol Sci.* 15 (10): 17541–64. https://doi.org/10.3390/ijms151017541

Dagert M, Ehrlich SD (1979) Prolonged Incubation in Calcium Chloride Improves the Competence of Escherichia Coli Cells. *Gene*. 6 (1): 23–28. https://doi.org/10.1016/0378-1119(79)90082-9

Dang FF, Wang YN, Yu L, Eulgem T, Lai Y, Liu ZQ, Wang X, Qiu AL, Zhang TX, Lin J, Chen YS, Guan DY, Cai HY, Mou SL, He SL (2013) CaWRKY40, a WRKY protein of pepper, plays an important role in the regulation of tolerance to heat stress and resistance to Ralstonia solanacearum infection. *Plant Cell Environ*. 36 (4): 757–74. https://doi.org/10.1111/pce.12011

Dang FF, Wang Y, She J, Lei Y, Liu Z, Eulgem T, Lai Y, Lin J, Yu L, Lei D, Guan D, Li X, Yuan Q, He S (2014) Overexpression of CaWRKY27, a Subgroup IIe WRKY Transcription Factor of Capsicum Annuum, Positively Regulates Tobacco Resistance to Ralstonia Solanacearum Infection. *Physiol. Plant.* 150 (3): 397–411. https://doi.org/10.1111/ppl.12093

Dang, Fengfeng, Jinhui Lin, Baoping Xue, Yongping Chen, Deyi Guan, Yanfeng Wang, Shuilin He (2018) CaWRKY27 Negatively Regulates H2O2-Mediated Thermotolerance in Pepper (Capsicum Annuum). *Front Plant Sci.* 9: 1633. https://doi.org/10.3389/fpls.2018.01633

Das R, Dufu K, Romney B, Feldt M, Elenko M, Reed R (2006) Functional Coupling of RNAP II Transcription to Spliceosome Assembly. *Genes Dev.* 20 (9): 1100–1109. https://doi.org/10.1101/gad.1397406

Das R, Yu J, Zhang Z, Gygi MP, Krainer AR, Gygi SP, Reed R (2007) SR Proteins Function in Coupling RNAP II Transcription to Pre-MRNA Splicing. *Mol Cell.* 26 (6): 867–81. https://doi.org/10.1016/j.molcel.2007.05.036

Day IS, Golovkin M, Palusa SG, Link A, Ali GS, Thomas J, Richardson DN, Reddy ASN (2012) Interactions of SR45, an SR-like Protein, with Spliceosomal Proteins and an Intronic Sequence: Insights into Regulated Splicing: Interaction of SR45 with Spliceosomal Components. *Plant J.* 71 (6): 936–47. https://doi.org/10.1111/j.1365-313X.2012.05042.x

Deng H, Cheema J, Zhang H, Woolfenden H, Norris M, Liu Z, Liu Q, Yang X, Yang M, Deng X, Cao X, Ding Y (2018) Rice In Vivo RNA Structurome Reveals RNA Secondary Structure Conservation and Divergence in Plants. *Mol Plant.* 11 (4): 607–22. https://doi.org/10.1016/j.molp.2018.01.008

Ding F, Cui P, Wang Z, Zhang S, Ali S, Xiong L (2014) Genome-Wide Analysis of Alternative Splicing of Pre-MRNA under Salt Stress in Arabidopsis. *BMC Genomics.* 15 (1): 431. https://doi.org/10.1186/1471-2164-15-431

Dobin A, Davis CA, Schlesinger F, Drenkow J, Zaleski C, Jha S, Batut P, Chaisson M, Gingeras TR (2013) STAR: Ultrafast Universal RNA-Seq Aligner. *Bioinformatics.* 29 (1): 15–21. https://doi.org/10.1093/bioinformatics/bts635

Dodds PN, Rathjen JP (2010) Plant Immunity: Towards an Integrated View of Plant–Pathogen Interactions. *Nat Rev Genet.* 11 (8): 539–48. https://doi.org/10.1038/nrg2812

Döring P, Treuter E, Kistner C, Lyck R, Chen A, Nover L (2000) The Role of AHA Motifs in the Activator Function of Tomato Heat Stress Transcription Factors HsfA1 and HsfA2. *Plant Cell.* 12 (2): 265. https://doi.org/10.2307/3870927

Dujardin G, Lafaille C, de la Mata M, Marasco LE, Muñoz MJ, Le Jossic-Corcos C, Corcos L, Kornblihtt AR (2014) How Slow RNA Polymerase II Elongation Favors Alternative Exon Skipping. *Mol Cell.* 54 (4): 683–90. https://doi.org/10.1016/j.molcel.2014.03.044

Duque P (2011) A Role for SR Proteins in Plant Stress Responses. *Plant Signal Behav.* 6 (1): 49–54. https://doi.org/10.4161/psb.6.1.14063

Duvaud S, Gabella C, Lisacek F, Stockinger H, Ioannidis V, Durinx C (2021) Expasy, the Swiss Bioinformatics Resource Portal, as Designed by Its Users. *Nucleic Acids Res.* 49 (W1): W216-27. https://doi.org/10.1093/nar/gkab225

El-shershaby A, Ullrich S, Simm S, Scharf KD, Schleiff E, Fragkostefanakis S (2019) Functional Diversification of Tomato HsfA1 Factors Is Based on DNA Binding Domain Properties. *Gene.* 714 (September): 143985. https://doi.org/10.1016/j.gene.2019.143985

Engler C, Youles M, Gruetzner R, Ehnert TM, Werner S, Jones JDG, Patron NJ, Marillonnet S (2014) A Golden Gate Modular Cloning Toolbox for Plants. *ACS Synth Biol.* 3 (11): 839–43. https://doi.org/10.1021/sb4001504

Eperon IC, Makarova OV, Mayeda A, Munroe SH, Cáceres JF, Hayward DG, Krainer AR (2000) Selection of Alternative 5′ Splice Sites: Role of U1 SnRNP and Models for the Antagonistic Effects of SF2/ASF and HnRNP A1. *Mol Cell Biol.* 20 (22): 8303–18. https://doi.org/10.1128/MCB.20.22.8303-8318.2000

Fakan S (1994) Perichromatin Fibrils Are in Situ Forms of Nascent Transcripts. *Trend Cell Biol.* 4 (3): 86–90. https://doi.org/10.1016/0962-8924(94)90180-5

Fang Y, Hearn S, Spector DL (2004) Tissue-Specific Expression and Dynamic Organization of SR Splicing Factors in Arabidopsis. *Mol Biol Cell.* 15 (6): 2664–73. https://doi.org/10.1091/mbc.e04-02-0100

Feng J, Zhang M, Yang KN, Zheng CX (2020) Salicylic Acid-Primed Defence Response in Octoploid Strawberry “Benihoppe” Leaves Induces Resistance against Podosphaera Aphanis through Enhanced Accumulation of Proanthocyanidins and Upregulation of Pathogenesis-Related Genes. *BMC Plant Biol*. 20 (1): 149. https://doi.org/10.1186/s12870-020-02353-z

Fernandez-Pozo N, Menda N, Edwards JD, Saha S, Tecle IY, Strickler SR, Bombarely A, Fisher-York T, Pujar A, Foerster H, Yan A, Mueller LA (2015) The Sol Genomics Network (SGN)—from Genotype to Phenotype to Breeding. *Nucleic Acids Res.* 43 (D1): D1036–41. https://doi.org/10.1093/nar/gku1195

Filichkin SA, Priest HD, Givan SA, Shen R, Bryant DW, Fox SE, Wong WK, Mockler TC (2010) Genome-wide mapping of alternative splicing in Arabidopsis thaliana. *Genome Res.* 20 (1): 45–58. https://doi.org/10.1101/gr.093302.109

Filichkin SA, Cumbie JS, Dharmawardhana P, Jaiswal P, Chang JH, Palusa SG, Reddy ASN, Megraw M, Mockler TC (2015) Environmental stresses modulate abundance and timing of alternatively spliced circadian transcripts in Arabidopsis. *Mol Plant.* 8 (2) :207-227. https://doi.org/10.1016/j.molp.2014.10.011

Fragkostefanakis S, Röth S, Schleiff E, Scharf KD (2015) Prospects of Engineering Thermotolerance in Crops through Modulation of Heat Stress Transcription Factor and Heat Shock Protein Networks: Hsfs and Hsps for Improvement of Crop Thermotolerance. *Plant Cell Environ.* 38 (9): 1881–95. https://doi.org/10.1111/pce.12396

Fragkostefanakis S, Mesihovic A, Simm S, Paupière MJ, Hu Y, Paul P, Mishra SK, Tschiersch B, Theres K, Bovy A, Schleiff E, Scharf KD (2016) HsfA2 Controls the Activity of Developmentally and Stress-Regulated Heat Stress Protection Mechanisms in Tomato Male Reproductive Tissues. *Plant Physiol.* 170 (4): 2461–77. https://doi.org/10.1104/pp.15.01913

Fu XD (2004) Towards a Splicing Code. *Cell.* 119 (6): 736–38. https://doi.org/10.1016/j.cell.2004.11.039.

Fu XD, Ares M (2014) Context-Dependent Control of Alternative Splicing by RNA-Binding Proteins. *Nat Rev Genet.* 15 (10): 689–701. https://doi.org/10.1038/nrg3778

Fuente van Bentem S (2006) Phosphoproteomics Reveals Extensive in Vivo Phosphorylation of Arabidopsis Proteins Involved in RNA Metabolism. *Nucleic Acids Res.* 34 (11): 3267–78. https://doi.org/10.1093/nar/gkl429

Gao H, Gordon-Kamm WJ, Lyznik LA (2004) ASF/SF2-like Maize Pre-MRNA Splicing Factors Affect Splice Site Utilization and Their Transcripts Are Alternatively Spliced. *Gene.* 339: 25–37. https://doi.org/10.1016/j.gene.2004.06.047

Gerland P, Raftery AE, Ševčíková H, Li N, Gu D, Spoorenberg T, Alkema L, Fosdick BK, Chunn J, Lalic N, Bay G, Buettner T, Heilig GK, Wilmoth J (2014) World Population Stabilization Unlikely This Century. *Science.* 346 (6206): 234–37. https://doi.org/10.1126/science.1257469

Gibson DG, Young L, Chuang RY, Venter JC, Hutchison CA, Smith HO (2009) Enzymatic Assembly of DNA Molecules up to Several Hundred Kilobases. *Nat Methods.* 6 (5): 343–45. https://doi.org/10.1038/nmeth.1318

Godoy Herz MA, Kornblihtt AR (2019) Alternative Splicing and Transcription Elongation in Plants. *Front Plant Sci.* 10: 309. https://doi.org/10.3389/fpls.2019.00309

Godoy Herz, MA, Kubaczka MG, Brzyżek G, Servi L, Krzyszton M, Simpson C, Brown J, Swiezewski S, Petrillo E, Kornblihtt AR (2019) Light Regulates Plant Alternative Splicing through the Control of Transcriptional Elongation. *Mol Cell.* 73 (5): 1066-1074.e3. https://doi.org/10.1016/j.molcel.2018.12.005

Göhring J, Jacak J, Barta A (2014) Imaging of Endogenous Messenger RNA Splice Variants in Living Cells Reveals Nuclear Retention of Transcripts Inaccessible to Nonsense-Mediated Decay in Arabidopsis. *Plant Cell.* 26 (2): 754–64. https://doi.org/10.1105/tpc.113.118075

Golovkin M, Reddy ASN (1998) The Plant U1 Small Nuclear Ribonucleoprotein Particle 70K Protein Interacts with Two Novel Serine/Arginine–Rich Proteins. *Plant Cell* 10 (10): 1637–47. https://doi.org/10.1105/tpc.10.10.1637

Gray SB, Brady SM (2016) Plant Developmental Responses to Climate Change. *Dev Biol*. 419 (1): 64–77. https://doi.org/10.1016/j.ydbio.2016.07.023

Grossman AD, Erickson JW, Gross CA (1984) The HtpR Gene Product of E. Coli Is a Sigma Factor for Heat-Shock Promoters. *Cell.* 38 (2): 383–90. https://doi.org/10.1016/0092-8674(84)90493-8

Gu Z, Eils R, Schlesner M (2016) Complex Heatmaps Reveal Patterns and Correlations in Multidimensional Genomic Data. *Bioinformatics.* 32 (18): 2847–49. https://doi.org/10.1093/bioinformatics/btw313

Gu J, Ma S, Zhang Y, Wang D, Cao S, Wang ZY (2020) Genome-Wide Identification of Cassava Serine/Arginine-Rich Proteins: Insights into Alternative Splicing of Pre-MRNAs and Response to Abiotic Stress. *Plant Cell Physiol*. 61 (1): 178–91. https://doi.org/10.1093/pcp/pcz190

Hahn A, Bublak D, Schleiff E, Scharf KD (2011) Crosstalk between Hsp90 and Hsp70 Chaperones and Heat Stress Transcription Factors in Tomato. *Plant Cell.* 23 (2): 741–55. https://doi.org/10.1105/tpc.110.076018

Haltenhof T, Kotte A, De Bortoli F, Schiefer S, Meinke S, Emmerichs AK, Petermann KK, Timmermann B, Imhof P, Franz A, Loll B, Wahl MC, Preußner M, Heyd F (2020) A Conserved Kinase-Based Body-Temperature Sensor Globally Controls Alternative Splicing and Gene Expression. *Mol Cell.* 78 (1): 57-69.e4. https://doi.org/10.1016/j.molcel.2020.01.028

Hatfield JL, Boote KJ, Kimball BA, Ziska LH, Izaurralde RC, Ort D, Thomson AM, Wolfe D (2011) Climate Impacts on Agriculture: Implications for Crop Production. *J. Agron.* 103 (2): 351–70. https://doi.org/10.2134/agronj2010.0303

Hiller M, Zhang Z, Backofen R, Stamm S (2007) Pre-MRNA Secondary Structures Influence Exon Recognition. *PLoS Genet.* 3 (11): e204. https://doi.org/10.1371/journal.pgen.0030204

Hirsz D, Dixon LE (2021) The Roles of Temperature-Related Post-Transcriptional Regulation in Cereal Floral Development. *Plants.* 10 (11): 2230. https://doi.org/10.3390/plants10112230

Hong SW, Vierling E (2000) Mutants of Arabidopsis Thaliana Defective in the Acquisition of Tolerance to High Temperature Stress. *Proc Natl Acad Scie U S A*. 97 (8): 4392–97. https://doi.org/10.1073/pnas.97.8.4392

Hong HY, Yoo GS, Choi JK (2000) Direct Blue 71 Staining of Proteins Bound to Blotting Membranes. *Electrophoresis.* 21 (5): 841–45. https://doi.org/10.1002/(SICI)1522-2683(20000301)21:5<841::AID-ELPS841>3.0.CO;2-4

Hönig A, Auboeuf D, Parker MM, O'Malley BW, Berget SM (2002) Regulation of Alternative Splicing by the ATP-Dependent DEAD-Box RNA Helicase P72. *Mol Cell Biol.* 22 (16): 5698–5707. https://doi.org/10.1128/MCB.22.16.5698-5707.2002

Howard JM, Sanford JR (2015) The RNAissance Family: SR Proteins as Multifaceted Regulators of Gene Expression: The RNAissance Family. *Wiley Interdiscip Rev RNA.* 6 (1): 93–110. https://doi.org/10.1002/wrna.1260

Hu Y, Mesihovic A, Jiménez-Gómez JM, Röth S, Gebhardt P, Bublak D, Bovy A, Scharf KD, Schleiff E, Fragkostefanakis S (2020a) Natural Variation in HsfA2 Pre-mRNA Splicing Is Associated with Changes in Thermotolerance during Tomato Domestication. *New Phytol.* 225 (3): 1297–1310. https://doi.org/10.1111/nph.16221

Hu Y, Fragkostefanakis S, Schleiff E, Simm S (2020b) Transcriptional Basis for Differential Thermosensitivity of Seedlings of Various Tomato Genotypes. *Genes.* 11 (6): 655. https://doi.org/10.3390/genes11060655

Huang Y, Steitz JA (2001) Splicing Factors SRp20 and 9G8 Promote the Nucleocytoplasmic Export of MRNA. *Mol Cell.* 7 (4): 899–905. https://doi.org/10.1016/S1097-2765(01)00233-7

Huang Y, Steitz JA (2005) SRprises along a Messenger's Journey. *Mol Cell.* 17 (5): 613–15. https://doi.org/10.1016/j.molcel.2005.02.020

Huang J, Zhao X, Bürger M, Wang Y, Chory J (2021) Two Interacting Ethylene Response Factors Regulate Heat Stress Response. *Plant Cell.* 33 (2): 338–57. https://doi.org/10.1093/plcell/koaa026

Huppertz I, Attig J, D'Ambrogio A, Easton LE, Sibley CR, Sugimoto Y, Tajnik M, König J, Ule J (2014) ICLIP: Protein–RNA Interactions at Nucleotide Resolution. *Methods*. 65 (3): 274–87. https://doi.org/10.1016/j.ymeth.2013.10.011

Pörtner HO, Roberts DC, Tignor M, Poloczanska ES, Mintenbeck K, Alegría A, Craig M, Langsdorf S, Löschke S, Möller V, Okem A, Rama B (Eds.) (2022) Climate Change 2022: Impacts, Adaptation, and Vulnerability. Contribution of Working Group II to the Sixth Assessment Report of the Intergovernmental Panel on Climate Change Cambridge University Press. In Press. Cambridge University Press.

Ishigaki Y, Li X, Serin G, Maquat LE (2001) Evidence for a Pioneer Round of MRNA Translation. *Cell.* 106 (5): 607–17. https://doi.org/10.1016/S0092-8674(01)00475-5

Isken O, Maquat LE (2007) Quality Control of Eukaryotic MRNA: Safeguarding Cells from Abnormal MRNA Function. *Genes Dev.* 21 (15): 1833–3856. https://doi.org/10.1101/gad.1566807

Isshiki M, Tsumoto A, Shimamoto K (2006) The Serine/Arginine-Rich Protein Family in Rice Plays Important Roles in Constitutive and Alternative Splicing of Pre-MRNA. *Plant Cell.* 18 (1): 146-58. https://doi.org/10.1105/tpc.105.037069

Jabre I, Reddy ASN, Kalyna M, Chaudhary S, Khokhar W, Byrne LJ, Wilson CM, Syed NH (2019) Does Co-Transcriptional Regulation of Alternative Splicing Mediate Plant Stress Responses? *Nucleic Acids Res.* 47 (6): 2716–26. https://doi.org/10.1093/nar/gkz121

Jia J, Long Y, Zhang H, Li Z, Liu Z, Zhao Y, Lu D, Jin X, Deng X, Xia R, Cao X, Zhai J (2020) Post-Transcriptional Splicing of Nascent RNA Contributes to Widespread Intron Retention in Plants. *Nat Plants.* 6 (7): 780–88. https://doi.org/10.1038/s41477-020-0688-1

Jiang J, Liu X, Liu C, Liu G, Li S, Wang L (2017) Integrating Omics and Alternative Splicing Reveals Insights into Grape Response to High Temperature. *Plant Physiol.* 173 (2): 1502–18. https://doi.org/10.1104/pp.16.01305

Kalyna M, Lopato S, Barta A (2003) Ectopic Expression of AtRSZ33 Reveals Its Function in Splicing and Causes Pleiotropic Changes in Development. *Mol Biol Cell.* 14 (9): 3565–77. https://doi.org/10.1091/mbc.e03-02-0109

Kalyna M, Barta A (2004) A Plethora of Plant Serine/Arginine-Rich Proteins: Redundancy or Evolution of Novel Gene Functions? *Biochem Soc Trans.* 32 (4): 561–64. https://doi.org/10.1042/BST0320561

Kalyna M, Simpson CG, Syed NH, Lewandowska D, Marquez Y, Kusenda B, Marshall J, Fuller J, Cardle L, McNicol J, Dinh HQ, Barta A, Brown JW (2012) Alternative Splicing and Nonsense-Mediated Decay Modulate Expression of Important Regulatory Genes in Arabidopsis. *Nucleic Acids Res.* 40 (6): 2454–69. https://doi.org/10.1093/nar/gkr932

Kannan S, Halter G, Renner T, Waters ER (2018) Patterns of Alternative Splicing Vary between Species during Heat Stress. *AoB Plants.* 10 (2). https://doi.org/10.1093/aobpla/ply013

Löchli K (2020) Function and Regulation of Splicing Factors RS2Z35 and RS2Z36 in Tomato. Master thesis. Goethe-University, Frankfurt am Main

Kazan K (2015) Diverse Roles of Jasmonates and Ethylene in Abiotic Stress Tolerance. *Trends Plant Sci.* 20 (4): 219–29. https://doi.org/10.1016/j.tplants.2015.02.001

Keller M, Hu Y, Mesihovic A, Fragkostefanakis S, Schleiff E, Simm S (2017) Alternative Splicing in Tomato Pollen in Response to Heat Stress. *DNA Res.* 24 (2): 205-2017. https://doi.org/10.1093/dnares/dsw051

Kim J (2016) CYTOKININ RESPONSE FACTOR s Gating Environmental Signals and Hormones. *Trends Plant Sci.* 21 (12): 993–96. https://doi.org/10.1016/j.tplants.2016.10.004

Kim GD, Cho YH, Lee BH, Yoo SD (2017) STABILIZED1 Modulates Pre-MRNA Splicing for Thermotolerance. *Plant Physiol.* 173 (4): 2370–82. https://doi.org/10.1104/pp.16.01928

Kim GD, Yoo SD, Cho YH (2018) STABILIZED1 as a Heat Stress-Specific Splicing Factor in Arabidopsis Thaliana'. *Plant Signal Behav.* 13 (2): e1432955. https://doi.org/10.1080/15592324.2018.1432955

Kinoshita E, Kinoshita-Kikuta E, Takiyama K, Koike T (2006) Phosphate-Binding Tag, a New Tool to Visualize Phosphorylated Protein'. *Mol Cell Proteomics*. 5 (4): 749–57. https://doi.org/10.1074/mcp.T500024-MCP200

Kitsios G, Alexiou KG, Bush M, Shaw P, Doonan JH (2008) A Cyclin-Dependent Protein Kinase, CDKC2, Colocalizes with and Modulates the Distribution of Spliceosomal Components in Arabidopsis. *Plant J.* 54 (2): 220–35. https://doi.org/10.1111/j.1365-313X.2008.03414.x

Klay I, Gouia S, Liu M, Mila I, Khoudi H, Bernadac A, Bouzayen M, Pirrello J (2018) Ethylene Response Factors (ERF) Are Differentially Regulated by Different Abiotic Stress Types in Tomato Plants. *Plant Sci.* 274: 137–45. https://doi.org/10.1016/j.plantsci.2018.05.023

Klockenbusch C, Kast J (2010) Optimization of Formaldehyde Cross-Linking for Protein Interaction Analysis of Non-Tagged Integrin β 1. *J Biomed Biotechnol.* 2010: 1–13. https://doi.org/10.1155/2010/927585

Kopylova E, Noé L, Touzet H (2012) SortMeRNA: Fast and Accurate Filtering of Ribosomal RNAs in Metatranscriptomic Data. *Bioinformatics.* 28 (24): 3211–17. https://doi.org/10.1093/bioinformatics/bts611

Köster T, Haas M, Staiger D (2014) The RIPper Case: Identification of RNA-Binding Protein Targets by RNA Immunoprecipitation. *Methods Mol Biol.* New York, 1158: 107-21 https://doi.org/10.1007/978-1-4939-0700-7_7

Kotak S, Port M, Ganguli A, Bicker F, von Koskull-Döring P (2004) Characterization of C-Terminal Domains of Arabidopsis Heat Stress Transcription Factors (Hsfs) and Identification of a New Signature Combination of Plant Class A Hsfs with AHA and NES Motifs Essential for Activator Function and Intracellular Localization. *Plant J.* 39 (1): 98–112. https://doi.org/10.1111/j.1365-313X.2004.02111.x

Kumar SV, Wigge PA (2010) H2A.Z-Containing Nucleosomes Mediate the Thermosensory Response in Arabidopsis. *Cell*. 140 (1): 136–47. https://doi.org/10.1016/j.cell.2009.11.006

Laemmli UK (1970) Cleavage of Structural Proteins during the Assembly of the Head of Bacteriophage T4. *Nature.* 227 (5259): 680–85. https://doi.org/10.1038/227680a0

Lai MC, Lin RI, Tarn WY (2001) Transportin-SR2 Mediates Nuclear Import of Phosphorylated SR Proteins. *Proc Natl Acad Sci U S A.* 98 (18): 10154–59. https://doi.org/10.1073/pnas.181354098

Lambermon MHL (2000) UBP1, a Novel HnRNP-like Protein That Functions at Multiple Steps of Higher Plant Nuclear Pre-MRNA Maturation. *EMBO J.* 19 (7): 1638–49. https://doi.org/10.1093/emboj/19.7.1638

Lämke J, Brzezinka K, Altmann S, Bäurle I (2016) A Hit-and-run Heat Shock Factor Governs Sustained Histone Methylation and Transcriptional Stress Memory. *EMBO J.* 35 (2): 162–75. https://doi.org/10.15252/embj.201592593

Larkindale J, Hall JD, Knight MR, Vierling E (2005) Heat Stress Phenotypes of Arabidopsis Mutants Implicate Multiple Signaling Pathways in the Acquisition of Thermotolerance. *Plant Physiol.* 138 (2): 882–97. https://doi.org/10.1104/pp.105.062257

Lazar G, Goodman HM (2000) The Arabidopsis splicing factor SR1 is regulated by alternative splicing. *Plant Mol Biol.* 42 (4): 571–81. https://doi.org/10.1023/A:1006394207479

Lee KC, Jang YH, Kim SK, Park HY, Thu MP, Lee JH, Kim JK (2017) RRM Domain of Arabidopsis Splicing Factor SF1 Is Important for Pre-MRNA Splicing of a Specific Set of Genes. *Plant Cell Rep.* 36 (7): 1083–95. https://doi.org/10.1007/s00299-017-2140-1

Lee JS, Adams KL (2020) Global Insights into Duplicated Gene Expression and Alternative Splicing in Polyploid Brassica Napus under Heat, Cold, and Drought Stress. *Plant Genome.* 13 (3). https://doi.org/10.1002/tpg2.20057

Lee KC, Chung KS, Lee HT, Park JH, Lee JH, Kim JK (2020) Role of Arabidopsis Splicing Factor SF1 in Temperature-Responsive Alternative Splicing of FLM Pre-MRNA. *Front Plant Sci.* 11: 596354. https://doi.org/10.3389/fpls.2020.596354

Leek JT, Johnson WE, Parker HS, Fertig EJ, Jaffe AE, Zhang Y, Storey JD, Torres LC (2021). Sva: Surrogate Variable Analysis. R Package Version 3.42.0.

Li M, Berendzen KW, Schöffl F (2010) Promoter Specificity and Interactions between Early and Late Arabidopsis Heat Shock Factors. *Plant Mol Biol.* 73 (4–5): 559–67. https://doi.org/10.1007/s11103-010-9643-2

Li S, Fu Q,Chen L, Huang W, Yu D (2011) Arabidopsis Thaliana WRKY25, WRKY26, and WRKY33 Coordinate Induction of Plant Thermotolerance. *Planta.* 233 (6): 1237–52. https://doi.org/10.1007/s00425-011-1375-2

Li S, Wang Y, Zhao Y, Zhao X, Chen X, Gong Z (2020) Global Co-Transcriptional Splicing in Arabidopsis and the Correlation with Splicing Regulation in Mature RNAs. *Mol Plant*. 13 (2): 266–77. https://doi.org/10.1016/j.molp.2019.11.003

Li Z, Tang J, Bassham DC, Howell. SH (2021) Daily Temperature Cycles Promote Alternative Splicing of RNAs Encoding SR45a, a Splicing Regulator in Maize. *Plant Physiol.* 186 (2): 1318–35. https://doi.org/10.1093/plphys/kiab110

Lin J, Shi J, Zhang Z, Zhong B, Ziqiang Zhu Z (2022) Plant AFC2 Kinase Desensitizes Thermomorphogenesis through Modulation of Alternative Splicing. *iScience.* 25 (4): 104051. Https://doi.org/10.1016/j.isci.2022.104051

Ling Y, Serrano N, Gao G, Atia M, Mokhtar M, Woo YH, Bazin J, Veluchamy A, Benhamed M, Crespi M, Gehring C, Reddy A, Mahfouz MM (2018). Thermopriming Triggers Splicing Memory in Arabidopsis. *J Exp Bot.* 69 (10): 2659–75. https://doi.org/10.1093/jxb/ery062

Liu HC, Liao HT, Charng YY (2011) The Role of Class A1 Heat Shock Factors (HSFA1s) in Response to Heat and Other Stresses in Arabidopsis: Master Heat Shock Factors in Arabidopsis. *Plant Cell Environ.* 34 (5): 738–51. https://doi.org/10.1111/j.1365-3040.2011.02278.x

Liu HC, Charng YY (2012) Acquired Thermotolerance Independent of Heat Shock Factor A1 (HsfA1), the Master Regulator of the Heat Stress Response. *Plant Signal Behav.* 7 (5): 547–50. https://doi.org/10.4161/psb.19803

Liu J, Sun N, Liu M, Liu J, Du B, Wang X, Qi X (2013) An Autoregulatory Loop Controlling Arabidopsis HsfA2 Expression: Role of Heat Shock-Induced Alternative Splicing. *Plant Physiol.* 162 (1): 512–21. https://doi.org/10.1104/pp.112.205864

Liu N, Dai Q, Zheng G, He C, M, Pan T (2015) N6-Methyladenosine-Dependent RNA Structural Switches Regulate RNA–Protein Interactions. *Nature.* 518 (7540): 560–64. https://doi.org/10.1038/nature14234

Liu M, Gomes BL, Mila I, Purgatto E, Peres LEP, Frasse P, Maza E, Zouine M, Roustan JP, Bouzayen M, Pirrello J (2016) Comprehensive Profiling of Ethylene Response Factor Expression Identifies Ripening-Associated ERF Genes and Their Link to Key Regulators of Fruit Ripening in Tomato. *Plant Physiol.* 170 (3): 1732–44. https://doi.org/10.1104/pp.15.01859

Liu G, Wang J, Hou X (2020) Transcriptome-Wide N6-Methyladenosine (M6A) Methylome Profiling of Heat Stress in Pak-Choi (Brassica Rapa Ssp. Chinensis). *Plants.* 9 (9): 1080. https://doi.org/10.3390/plants9091080

Liu Z, Liu Q, Yang X, Zhang Y, Norris M, Chen X, Cheema J, Zhang H, Ding Y (2021) In Vivo Nuclear RNA Structurome Reveals RNA-Structure Regulation of MRNA Processing in Plants. *Genome Biol.* 22 (1): 11. https://doi.org/10.1186/s13059-020-02236-4

Liu XX, Guo QH, Xu WB, Liu P, Yan K (2022a) Rapid Regulation of Alternative Splicing in Response to Environmental Stresses. *Front Plant Sci.* 13 (March): 832177. https://doi.org/10.3389/fpls.2022.832177

Liu B, Kaurilind E, Zhang L, Okereke CN, Remmel T, Niinemets Ü (2022b) Improved Plant Heat Shock Resistance Is Introduced Differently by Heat and Insect Infestation: The Role of Volatile Emission Traits. *Oecologia.* 199 (1): 53–68. https://doi.org/10.1007/s00442-022-05168-x

Livak KJ, Schmittgen TD (2001) Analysis of Relative Gene Expression Data Using Real-Time Quantitative PCR and the 2−ΔΔCT Method. *Methods.* 25 (4): 402–8. https://doi.org/10.1006/meth.2001.1262

Lobell DB, Field CB (2007) Global Scale Climate–Crop Yield Relationships and the Impacts of Recent Warming. *Environ Res Lett.* 2 (1): 014002. https://doi.org/10.1088/1748-9326/2/1/014002

Lobell DB, Schlenker W, Costa-Roberts J (2011) Climate Trends and Global Crop Production Since 1980. *Science.* 333 (6042): 616–20. https://doi.org/10.1126/science.1204531

Lohmann C, Eggers-Schumacher G, Wunderlich M, Schöffl F (2004) Two Different Heat Shock Transcription Factors Regulate Immediate Early Expression of Stress Genes in Arabidopsis. *Mol Genet Genomics.* 271 (1): 11–21. https://doi.org/10.1007/s00438-003-0954-8

Loomis RJ, Naoe Y, Parker JB, Savic V, Bozovsky MR, Macfarlan T, Manley JL, Chakravarti D (2009) Chromatin Binding of SRp20 and ASF/SF2 and Dissociation from Mitotic Chromosomes Is Modulated by Histone H3 Serine 10 Phosphorylation. *Mol Cell.* 33 (4): 450–61. https://doi.org/10.1016/j.molcel.2009.02.003

Lopato S, Kalyna M, Dorner S, Kobayashi R, Krainer AR, Barta A (1999) AtSRp30, One of Two SF2/ASF-like Proteins from Arabidopsis Thaliana, Regulates Splicing of Specific Plant Genes'. *Genes Dev.* 13 (8): 987–1001. https://doi.org/10.1101/gad.13.8.987

Lopato S, Forstner C, Kalyna M, Hilscher J, Langhammer U, Indrapichate K, Lorković ZJ, Barta A (2002) Network of Interactions of a Novel Plant-Specific Arg/Ser-Rich Protein, AtRSZ33, with AtSC35-like Splicing Factors'. *J Biol Chem*. 277 (42): 39989–98. https://doi.org/10.1074/jbc.M206455200

Lorenzi C, Barriere S, Arnold K, Luco RF, Oldfield AJ, Ritchie W (2021). IRFinder-S: A Comprehensive Suite to Discover and Explore Intron Retention*. Genome Biol.* 22 (1): 307. https://doi.org/10.1186/s13059-021-02515-8

Lorković ZJ, Barta A (2004) Compartmentalization of the Splicing Machinery in Plant Cell Nuclei. *Trends Plant Sci.* 9 (12): 565–68. https://doi.org/10.1016/j.tplants.2004.10.003

Lorkovic Z, Hilscher J, Barta A (2008) Co-Localisation Studies of Arabidopsis SR Splicing Factors Reveal Different Types of Speckles in Plant Cell Nuclei. *Exp Cell Res*. 314 (17): 3175–86. https://doi.org/10.1016/j.yexcr.2008.06.020

Love AJ, Milner JJ, Sadanandom A (2008) Timing Is Everything: Regulatory Overlap in Plant Cell Death. *Trends Plant Sci.* 13 (11): 589–95. https://doi.org/10.1016/j.tplants.2008.08.006

Love MI, Huber W, Anders S (2014) Moderated Estimation of Fold Change and Dispersion for RNA-Seq Data with DESeq2. *Genome Biol.* 15 (12): 550. https://doi.org/10.1186/s13059-014-0550-8

Lum LS, Sultzman LA, Kaufman RJ, Linzer DI, Wu BJ (1990) A Cloned Human CCAAT-Box-Binding Factor Stimulates Transcription from the Human Hsp70 Promoter. *Mol Cell Biol*. 10 (12): 6709–17. https://doi.org/10.1128/mcb.10.12.6709-6717.1990

MacQueen A, Bergelson J (2016) Modulation of R -Gene Expression across Environments. *J Exp Bot.* 67 (7): 2093–2105. https://doi.org/10.1093/jxb/erv530

Manley JL, Krainer AR (2010) A Rational Nomenclature for Serine/Arginine-Rich Protein Splicing Factors (SR Proteins) *Genes Dev.* 24 (11): 1073–74. https://doi.org/10.1101/gad.1934910

Marques de Carvalho L, Benda ND, Vaughan MM, Cabrera AR, Hung K, Cox T, Abdo Z, Allen LH, PEA (2015) Mi-1-Mediated Nematode Resistance in Tomatoes Is Broken by Short-Term Heat Stress but Recovers Over Time. *J Nematol.* 47 (2): 133–40

Marquez Y, Brown JWS, Simpson C, Barta A, Kalyna M (2012) Transcriptome Survey Reveals Increased Complexity of the Alternative Splicing Landscape in Arabidopsis. *Genome Res.* 22 (6): 1184–95. https://doi.org/10.1101/gr.134106.111

Mastrangelo AM, Marone D, Laidò G, De Leonardis AM, De Vita P (2012) Alternative Splicing: Enhancing Ability to Cope with Stress via Transcriptome Plasticity. *Plant Sci.* 185–186 (April): 40–49. https://doi.org/10.1016/j.plantsci.2011.09.006

Matsukura S, Mizoi J, Yoshida T, Todaka D, Ito Y, Maruyama K, Shinozaki K, Yamaguchi-Shinozaki K (2010) Comprehensive Analysis of Rice DREB2-Type Genes That Encode Transcription Factors Involved in the Expression of Abiotic Stress-Responsive Genes. *Mol Genet Genomics.* 283 (2): 185–96. https://doi.org/10.1007/s00438-009-0506-y

McCormick S, Niedermeyer J, Fry J, Barnason A, Horsch R, Fraley R (1986) Leaf Disc Transformation of Cultivated Tomato (L. Esculentum) Using Agrobacterium Tumefaciens. *Plant Cell Rep*. 5 (2): 81–84. https://doi.org/10.1007/BF00269239

Mesihovic A, Ullrich S, Rosenkranz RRE, Gebhardt P, Bublak D, Eich H, Weber D, Berberich T, Scharf KD, Schleiff E (2022) 'HsfA7 Coordinates the Transition from Mild to Strong Heat Stress Response by Controlling the Activity of the Master Regulator HsfA1a in Tomato'. *Cell Rep.* 38 (2): 110224. https://doi.org/10.1016/j.celrep.2021.110224

Meyer M, Plass M, Pérez-Valle J, Eyras E, Vilardell J (2011) Deciphering 3'SS Selection in the Yeast Genome Reveals an RNA Thermosensor That Mediates Alternative Splicing. *Mol Cell.* 43 (6): 1033–39. https://doi.org/10.1016/j.molcel.2011.07.030

Mi H, Ebert D, Muruganujan A, Mills C, Albou LP, Mushayamaha T, Thomas PD (2021) PANTHER Version 16: A Revised Family Classification, Tree-Based Classification Tool, Enhancer Regions and Extensive API. *Nucleic Acids Res.* 49 (D1): D394–403. https://doi.org/10.1093/nar/gkaa1106

Mishra SK, Tripp J, Winkelhaus S, Tschiersch B, Theres K, Nover L, Scharf KD (2002) In the Complex Family of Heat Stress Transcription Factors, HsfA1 Has a Unique Role as Master Regulator of Thermotolerance in Tomato. *Genes Dev.* 16 (12): 1555–67. https://doi.org/10.1101/gad.228802

Mistry J, Chuguransky S, Williams L, Qureshi M, Salazar GA, Sonnhammer ELL, Tosatto SCE, Paladin L, Raj S, Richardson LJ, Finn RD, Bateman A (2021) Pfam: The Protein Families Database in 2021. *Nucleic Acids Res.* 49 (D1): D412–19. https://doi.org/10.1093/nar/gkaa913

Mittler R, Finka A, Goloubinoff P (2012) How Do Plants Feel the Heat? *Trends Biochem Sci.* 37 (3): 118–25. https://doi.org/10.1016/j.tibs.2011.11.007

Mizoi J, Shinozaki K, Yamaguchi-Shinozaki K (2012) AP2/ERF Family Transcription Factors in Plant Abiotic Stress Responses. *Biochim Biophys Acta.* 1819 (2): 86–96. https://doi.org/10.1016/j.bbagrm.2011.08.004.

Müller-McNicoll M, Botti V, de Jesus Domingues AM, Brandl H, Schwich OD, Steiner MC, Curk T, Poser I, Zarnack K, Neugebauer KM (2016) SR Proteins Are NXF1 Adaptors That Link Alternative RNA Processing to MRNA Export. *Genes Dev.* 30 (5): 553–66. https://doi.org/10.1101/gad.276477.115

Mullis K, Faloona F, Scharf S, Saiki R, Horn G, Erlich H (1986) Specific enzymatic amplification of DNA in vitro: the polymerase chain reaction. *Cold Spring Harb Symp Quant Biol*. 51 Pt 1: 263-73. https://doi.org/10.1101/sqb.1986.051.01.032

Muñoz MJ, de la Mata M, Kornblihtt AR (2010) The Carboxy Terminal Domain of RNA Polymerase II and Alternative Splicing. *Trends Biochem Sci.* 35 (9): 497–504. https://doi.org/10.1016/j.tibs.2010.03.010

Mur LAJ, Kenton P, Atzorn R, Miersch O, Wasternack C (2006) The Outcomes of Concentration-Specific Interactions between Salicylate and Jasmonate Signaling Include Synergy, Antagonism, and Oxidative Stress Leading to Cell Death. *Plant Physiol.* 140 (1): 249–62. https://doi.org/10.1104/pp.105.072348

Murashige T, Skoog F (1962) A Revised Medium for Rapid Growth and Bio Assays with Tobacco Tissue Cultures. *Physiol. Plant.* 15 (3): 473–97. https://doi.org/10.1111/j.1399-3054.1962.tb08052.x

Ner-Gaon H, Halachmi R, Savaldi-Goldstein S, Rubin E, Ophir R, Fluhr R (2004) Intron Retention Is a Major Phenomenon in Alternative Splicing in Arabidopsis. *Plant J.* 39 (6): 877–85. https://doi.org/10.1111/j.1365-313X.2004.02172.x

Neuhoff V, Arold N, Taube D, Ehrhardt W (1988) Improved Staining of Proteins in Polyacrylamide Gels Including Isoelectric Focusing Gels with Clear Background at Nanogram Sensitivity Using Coomassie Brilliant Blue G-250 and R-250. *Electrophoresis.* 9 (6): 255–62. https://doi.org/10.1002/elps.1150090603

Neumann A, Meinke S, Goldammer G, Strauch M, Schubert D, Timmermann B, Heyd F, Preußner M (2020) Alternative Splicing Coupled MRNA Decay Shapes the Temperature-dependent Transcriptome. *EMBO Rep.* 21 (12). https://doi.org/10.15252/embr.202051369

Nilsen TW (2003) The Spliceosome: The Most Complex Macromolecular Machine in the Cell? *Bioessays.* 25 (12): 1147–49. https://doi.org/10.1002/bies.10394

Nilsen TW, Graveley BR (2010) Expansion of the Eukaryotic Proteome by Alternative Splicing. *Nature.* 463 (7280): 457–63. https://doi.org/10.1038/nature08909

Ninomiya K, Kataoka N, Hagiwara M (2011) Stress-Responsive Maturation of Clk1/4 Pre-MRNAs Promotes Phosphorylation of SR Splicing Factor. *J Cell Biol.* 195 (1): 27–40. https://doi.org/10.1083/jcb.201107093

Ninomiya K, Adachi S, Natsume T, Iwakiri J, Terai G, Asai K, Hirose T (2020) LncRNA-dependent Nuclear Stress Bodies Promote Intron Retention through SR Protein Phosphorylation. *EMBO J*. 39 (3). https://doi.org/10.15252/embj.2019102729

Ninomiya K, Iwakiri J, Aly MK, Sakaguchi Y, Adachi S, Natsume T, Terai G, Asai K, Suzuki T, Hirose T (2021) M 6 A Modification of HSATIII LncRNAs Regulates Temperature-dependent Splicing. *EMBO J.* 40 (15). https://doi.org/10.15252/embj.2021107976

Nishizawa A, Yabuta Y, Yoshida E, Maruta T, Yoshimura K, Shigeoka S (2006) Arabidopsis Heat Shock Transcription Factor A2 as a Key Regulator in Response to Several Types of Environmental Stress. *Plant J.* 48 (4): 535–47. https://doi.org/10.1111/j.1365-313X.2006.02889.x

Nover L, Scharf KD, Gagliardi D, Vergne P, Czarnecka-Verner E, Gurley WB (1996) The Hsf World: Classification and Properties of Plant Heat Stress Transcription Factors. *Cell Stress Chaperones.* 1 (4): 215. https://doi.org/10.1379/1466-1268(1996)001<0215:THWCAP>2.3.CO;2

Nosaka Y, Nosaka AY (2017) Generation and Detection of Reactive Oxygen Species in Photocatalysis. *Chem Rev.* 117 (17): 11302–36. https://doi.org/10.1021/acs.chemrev.7b00161

Nover L, Bharti K, Döring P, Mishra SK, Ganguli A, Scharf KD (2001) Arabidopsis and the Heat Stress Transcription Factor World: How Many Heat Stress Transcription Factors Do We Need? *Cell Stress Chaperones.* 6 (3): 177. https://doi.org/10.1379/1466-1268(2001)006<0177:AATHST>2.0.CO;2

Ohama N, Kusakabe K, Mizoi J, Zhao H, Kidokoro S, Koizumi S, Takahashi F, Ishida T, Yanagisawa S, Shinozaki K, Yamaguchi-Shinozaki K (2016) The Transcriptional Cascade in the Heat Stress Response of Arabidopsis Is Strictly Regulated at the Level of Transcription Factor Expression'. *Plant Cell.* 28 (1): 181–201. https://doi.org/10.1105/tpc.15.00435

Oliveros JC (2007) Venny. An Interactive Tool for Comparing Lists with Venn's Diagrams. https://bioinfogp.cnb.csic.es/tools/venny/index.html

Palusa SG, Ali GS, Reddy AS (2007) Alternative Splicing of Pre-MRNAs of Arabidopsis Serine/Arginine-Rich Proteins: Regulation by Hormones and Stresses: Stress Regulation of Alternative Splicing of SR Genes. *Plant J.* 49 (6): 1091–1107. https://doi.org/10.1111/j.1365-313X.2006.03020.x

Palusa SG, Reddy ASN (2010) Extensive Coupling of Alternative Splicing of Pre-mRNAs of Serine/Arginine (SR) Genes with Nonsense-mediated Decay. *New Phytol.* 185 (1): 83–89. https://doi.org/10.1111/j.1469-8137.2009.03065.x.

Palusa SG, Reddy ASN (2015) Differential Recruitment of Splice Variants from SR Pre-MRNAs to Polysomes During Development and in Response to Stresses. *Plant Cell Physiol.* 56 (3): 421-27. https://doi.org/10.1093/pcp/pcv010

Pan Q, Shai O, Lee LJ, Frey BJ, Blencowe BJ (2008) Deep Surveying of Alternative Splicing Complexity in the Human Transcriptome by High-Throughput Sequencing. *Nat Genet.* 40 (12): 1413–15. https://doi.org/10.1038/ng.259

Panchuk II, Volkov RA, Schöffl F (2002) Heat Stress- and Heat Shock Transcription Factor-Dependent Expression and Activity of Ascorbate Peroxidase in Arabidopsis'. *Plant Physiol*. 129 (2): 838-53. https://doi.org/10.1104/pp.001362

Pandey SP, Somssich IE (2009) The Role of WRKY Transcription Factors in Plant Immunity. *Plant Physiol.* 150 (4): 1648–55. https://doi.org/10.1104/pp.109.138990

Pandey P, Ramegowda V, Senthil-Kumar M (2015) Shared and Unique Responses of Plants to Multiple Individual Stresses and Stress Combinations: Physiological and Molecular Mechanisms. Frontiers in Plant Science 6: 723. https://doi.org/10.3389/fpls.2015.00723.

Park MJ, Seo PJ, Park CM (2012) CCA1 Alternative Splicing as a Way of Linking the Circadian Clock to Temperature Response in Arabidopsis. *Plant Signal Behav.* 7 (9): 1194–96. https://doi.org/10.4161/psb.21300

Park HJ, You YN, Lee A, Jung H, Jo SH, Oh N, Kim HS, Lee HJ, Kim JK, Kim YS, Jung C, Cho HS (2020) OsFKBP20-1b Interacts with the Splicing Factor OsSR45 and Participates in the Environmental Stress Response at the Post-transcriptional Level in Rice. *Plant J.* 102 (5): 992–1007. https://doi.org/10.1111/tpj.14682.

Parsell DA, Lindquist S (1993) The function of heat-shock proteins in stress tolerance: degradation and reactivation of damaged proteins. *Annu Rev Genet*. 27 (1): 437–96. https://doi.org/10.1146/annurev.ge.27.120193.002253

Pelham HR, Bienz M (1982) A Synthetic Heat-Shock Promoter Element Confers Heat-Inducibility on the Herpes Simplex Virus Thymidine Kinase Gene. *EMBO J.* 1 (11): 1473–77

Peteranderl R, Rabenstein M, Shin YK, Liu CW, Wemmer DE, King DS, Nelson HC (1999) Biochemical and Biophysical Characterization of the Trimerization Domain from the Heat Shock Transcription Factor. *Biochemistry.* 38 (12): 3559–69. https://doi.org/10.1021/bi981774j

Phelan MM, Goult BT, Clayton JC, Hautbergue GM, Wilson SA, Lian LY (2012) The Structure and Selectivity of the SR Protein SRSF2 RRM Domain with RNA. *Nucleic Acids Res.* 40 (7): 3232–44. https://doi.org/10.1093/nar/gkr1164

Porath J, Carlsson J, Olsson I, Belfrage G (1975) Metal Chelate Affinity Chromatography, a New Approach to Protein Fractionation. *Nature.* 258 (5536): 598–99. https://doi.org/10.1038/258598a0

Port M, Tripp J, Zielinski D, Weber C, Heerklotz D, Winkelhaus S, Bublak D, Scharf KD (2004) Role of Hsp17.4-CII as Coregulator and Cytoplasmic retention factor of tomato heat stress transcription factor HsfA2. *Plant Physiol.* 135 (3): 1457-70. https://doi.org/10.1104/pp.104.042820

Prasad J, Colwill K, Pawson T, Manley JL (1999) The Protein Kinase Clk/Sty Directly Modulates SR Protein Activity: Both Hyper- and Hypophosphorylation Inhibit Splicing. *Mol Cell Biol.* 19 (10): 6991–7000. https://doi.org/10.1128/MCB.19.10.6991

Preußner M, Goldammer G, Neumann A, Haltenhof T, Rautenstrauch P, Müller-McNicoll M, Heyd F (2017) Body Temperature Cycles Control Rhythmic Alternative Splicing in Mammals. *Mol Cell.* 67 (3): 433-446.e4. https://doi.org/10.1016/j.molcel.2017.06.006

Punzo P, Grillo S, Batelli G (2020) Alternative Splicing in Plant Abiotic Stress Responses. *Biochem Soc Trans.* 48 (5): 2117–26. https://doi.org/10.1042/BST20200281

Pushpalatha P, Sharma-Natu P, Ghildiyal MC (2008) Photosynthetic Response of Wheat Cultivar to Long-Term Exposure to Elevated Temperature. *Photosynthetica.* 46 (4): 552–56. https://doi.org/10.1007/s11099-008-0093-x

Queitsch C, Hong SW, Vierling E, Lindquist S (2000) Heat Shock Protein 101 Plays a Crucial Role in Thermotolerance in Arabidopsis. *Plant Cell.* 12 (4): 479. https://doi.org/10.2307/3871063

Rahmstorf S, Dim Coumou D (2011) Increase of Extreme Events in a Warming World. *Proc Natl Acad Sci U S A.* 108 (44): 17905–9. https://doi.org/10.1073/pnas.1101766108

Rao S, Das JR, Mathur S (2021) Exploring the Master Regulator Heat Stress Transcription Factor HSFA1a-Mediated Transcriptional Cascade of HSFs in the Heat Stress Response of Tomato. *J. Plant Biochem. Biotechnol*. 30 (4): 878–88. https://doi.org/10.1007/s13562-021-00696-8

Rausin G, Tillemans V, Stankovic N, Hanikenne M, Motte P (2010) Dynamic Nucleocytoplasmic Shuttling of an Arabidopsis SR Splicing Factor: Role of the RNA-Binding Domains. *Plant Physiol.* 153 (1): 273–84. https://doi.org/10.1104/pp.110.154740.

Reddy ASN, Shad Ali GS (2011) Plant Serine/Arginine-Rich Proteins: Roles in Precursor Messenger RNA Splicing, Plant Development, and Stress Responses: Plant SR-Rich Proteins. *Wiley Interdiscip Rev RNA*. 2 (6): 875–89. https://doi.org/10.1002/wrna.98

Reddy ASN, Day IS, Göhring J Barta A (2012) Localization and Dynamics of Nuclear Speckles in Plants. *Plant Physiol.* 158 (1): 67–77. https://doi.org/10.1104/pp.111.186700

Reddy ASN, Marquez Y, Kalyna M, Barta A (2013) Complexity of the Alternative Splicing Landscape in Plants. *Plant Cell.* 25 (10): 3657–83. https://doi.org/10.1105/tpc.113.117523

Rhoads A, Au KF (2015) PacBio Sequencing and Its Applications. *Genomics Proteomics Bioinformatics.* 13 (5): 278–89. https://doi.org/10.1016/j.gpb.2015.08.002

Rice P, Longden I, Bleasby A (2000) EMBOSS: The European Molecular Biology Open Software Suite. *Trends Genet.* 16 (6): 276–77. https://doi.org/10.1016/S0168-9525(00)02024-2

Richardson DN, Rogers MF, Labadorf A, Ben-Hur A, Guo H, Paterson AH, Reddy ASN (2011) Comparative Analysis of Serine/Arginine-Rich Proteins across 27 Eukaryotes: Insights into Sub-Family Classification and Extent of Alternative Splicing. *PLoS One.* 6 (9): e24542. https://doi.org/10.1371/journal.pone.0024542.

Rio DC (2014) Electrophoretic Mobility Shift Assays for RNA–Protein Complexes. *Cold Spring Harb. Protoc.*2014 (4): pdb.prot080721. https://doi.org/10.1101/pdb.prot080721

Rizhsky L, Liang H, Mittler R (2002) The Combined Effect of Drought Stress and Heat Shock on Gene Expression in Tobacco. *Plant Physiol.* 130 (3): 1143–51. https://doi.org/10.1104/pp.006858

Robberson BL, Cote GJ, Berget SM (1990) Exon Definition May Facilitate Splice Site Selection in RNAs with Multiple Exons. *Mol Cell Biol.* 10 (1): 84–94. https://doi.org/10.1128/mcb.10.1.84-94.1990

Ron M, Avni A (2004) The Receptor for the Fungal Elicitor Ethylene-Inducing Xylanase Is a Member of a Resistance-Like Gene Family in Tomato. *Plant Cell.* 16 (6): 1604–15. https://doi.org/10.1105/tpc.022475

Roscigno RF, Garcia-Blanco MA (1995) SR Proteins Escort the U4/U6.U5 Tri-SnRNP to the Spliceosome. *RNA*. 1 (7): 692–706.

Rosenkranz RRE (2017) Involvement of Serine/Arginine-Rich Proteins in Plant Heat Stress Response. Master thesis. Goethe-University, Frankfurt am Main.

Rosenkranz RRE, Bachiri S, Vraggalas S, Keller M, Simm S, Schleiff E, Fragkostefanakis S (2021) Identification and Regulation of Tomato Serine/Arginine-Rich Proteins Under High Temperatures. *Front Plant Sci* 12: 645689. https://doi.org/10.3389/fpls.2021.645689

Rosenkranz RRE, Ullrich S, Löchli K, Simm S, Fragkostefanakis S (2022) Relevance and regulation of alternative splicing in plant heat stress response: current understanding and future directions. S. *Front Plant Sci.* (accepted for publication)

Röth S, Mirus O, Bublak D, Scharf KD, Schleiff E (2017) DNA-Binding and Repressor Function Are Prerequisites for the Turnover of the Tomato Heat Stress Transcription Factor HsfB1. *Plant J.* 89 (1): 31–44. https://doi.org/10.1111/tpj.13317

RStudio Team (2020) RStudio: Integrated Development for R. RStudio, PBC, Boston, MA URL Http://Www.Rstudio.Com/.

Saidi Y, Finka A, Goloubinoff P (2011) Heat Perception and Signalling in Plants: A Tortuous Path to Thermotolerance. *New Phytol.* 190 (3): 556–65. https://doi.org/10.1111/j.1469-8137.2010.03571.x

Sambrook J, Russell DW (2001). Molecular Cloning: A Laboratory Manual. 3rd ed. Cold Spring Harbor, N.Y: Cold Spring Harbor Laboratory Press.

Sanford JR, Gray NK, Beckmann K, Cáceres JF (2004) A Novel Role for Shuttling SR Proteins in MRNA Translation. *Genes Dev.* 18 (7): 755–68. https://doi.org/10.1101/gad.286404

Sayols S (2020). Rrvgo: A Bioconductor Package to Reduce and Visualize Gene Ontology Terms. https://ssayols.github.io/rrvgo.

Schaffner W, Weissmann C (1973) A Rapid, Sensitive, and Specific Method for the Determination of Protein in Dilute Solution. *Anal Biochem.* 56 (2): 502–14. https://doi.org/10.1016/0003-2697(73)90217-0

Scharf KD, Heider H, Höhfeld I, Lyck R, Schmidt E, Nover L (1998) The Tomato Hsf System: HsfA2 Needs Interaction with HsfA1 for Efficient Nuclear Import and May Be Localized in Cytoplasmic Heat Stress Granules. *Mol Cell Biol.* 18 (4): 2240–51. https://doi.org/10.1128/MCB.18.4.2240

Scharf KD, Berberich T, Ebersberger I, Nover L (2012) The Plant Heat Stress Transcription Factor (Hsf) Family: Structure, Function and Evolution. *Biochim Biophy Acta.* 1819 (2): 104–19. https://doi.org/10.1016/j.bbagrm.2011.10.002

Schindler S, Szafranski K, Hiller M, Ali G, Palusa SG, Backofen R, Platzer M, Reddy ASN (2008) Alternative Splicing at NAGNAG Acceptors in Arabidopsis Thaliana SR and SR-Related Protein-Coding Genes. *BMC Genomics.* 9 (1): 159. https://doi.org/10.1186/1471-2164-9-159

Schlegel S, Löfblom J, Lee C, Hjelm A, Klepsch M, Strous M, Drew D, Slotboom DJ, de Gier JW (2012) Optimizing Membrane Protein Overexpression in the Escherichia Coli Strain Lemo21(DE3). *J Mol Biol.* 423 (4): 648–59. https://doi.org/10.1016/j.jmb.2012.07.019.

Schneider CA, Rasband WS, Eliceiri KW (2012) NIH Image to ImageJ: 25 Years of Image Analysis. *Nat Methods.* 9 (7): 671–75. https://doi.org/10.1038/nmeth.2089

Schramm F, Ganguli A, Kiehlmann E, Englich G, Walch D, von Koskull-Döring P (2006) The Heat Stress Transcription Factor HsfA2 Serves as a Regulatory Amplifier of a Subset of Genes in the Heat Stress Response in Arabidopsis. *Plant Mol Biol.* 60 (5): 759–72. https://doi.org/10.1007/s11103-005-5750-x.

Schultheiss J, Kunert O, Gase U, Scharf KD, Nover L, Ruterjans H (1996) Solution Structure of the DNA-Binding Domain of the Tomato Heat-Stress Transcription Factor HSF24. *Eur J Biochem.* 236 (3): 911–21. https://doi.org/10.1111/j.1432-1033.1996.00911.x

Schwacke R, Ponce-Soto GY, Krause K, Bolger AM, Arsova B, Hallab A, Gruden K, Stitt M, Bolger ME, Usadel B (2019) MapMan4: A Refined Protein Classification and Annotation Framework Applicable to Multi-Omics Data Analysis. *Mol Plant.* 12 (6): 879–92. https://doi.org/10.1016/j.molp.2019.01.003

Schwartz R, Ting CS, King J (2001) Whole Proteome PI Values Correlate with Subcellular Localizations of Proteins for Organisms within the Three Domains of Life. *Genome Res.* 11 (5): 703–9. https://doi.org/10.1101/gr.158701

Shahnejat-Bushehri S, Mueller-Roeber B, Balazadeh S (2012) Arabidopsis NAC Transcription Factor JUNGBRUNNEN1 Affects Thermomemory-Associated Genes and Enhances Heat Stress Tolerance in Primed and Unprimed Conditions. *Plant Signal Behav.* 7 (12): 1518–21. https://doi.org/10.4161/psb.22092

Shalgi R, Hurt JA, Lindquist S, Burge CB (2014) Widespread Inhibition of Posttranscriptional Splicing Shapes the Cellular Transcriptome Following Heat Shock. *Cell Rep*. 7 (5): 1362–70. https://doi.org/10.1016/j.celrep.2014.04.044

Shepard PJ, Hertel KJ (2008) Conserved RNA Secondary Structures Promote Alternative Splicing. *RNA.* 14 (8): 1463–69. https://doi.org/10.1261/rna.1069408

Shepard PJ, Hertel KJ (2009) The SR Protein Family. *Genome Biol.* 10 (10): 242. https://doi.org/10.1186/gb-2009-10-10-242

Shi X, Gupta S, Rashotte AM (2012) Solanum Lycopersicum Cytokinin Response Factor (SlCRF) Genes: Characterization of CRF Domain-Containing ERF Genes in Tomato. *J Exp Bot.* 63 (2): 973–82. https://doi.org/10.1093/jxb/err325

Shi X, Gupta S, Rashotte, AM (2014) Characterization of Two Tomato AP2/ERF Genes, SlCRF1 and SlCRF2 in Hormone and Stress Responses. *Plant Cell Rep.* 33 (1): 35–45. https://doi.org/10.1007/s00299-013-1510-6

Shi Y, Manley JL (2007) A Complex Signaling Pathway Regulates SRp38 Phosphorylation and Pre-MRNA Splicing in Response to Heat Shock. *Mol Cell*. 28 (1): 79–90. https://doi.org/10.1016/j.molcel.2007.08.028

Shin C, Feng Y, Manley JL (2004) Dephosphorylated SRp38 Acts as a Splicing Repressor in Response to Heat Shock. *Nature.* 427 (6974): 553–58. https://doi.org/10.1038/nature02288.

Singh RP, Vara Prasad PV, Reddy KR (2013). Impacts of Changing Climate and Climate Variability on Seed Production and Seed Industry. In Advances in Agronomy, 118:49–110. Elsevier. https://doi.org/10.1016/B978-0-12-405942-9.00002-5

Sinha R, Allemand E, Zhang Z, Karni R, Myers MP, R. Krainer AR (2010) Arginine Methylation Controls the Subcellular Localization and Functions of the Oncoprotein Splicing Factor SF2/ASF. *Mol Cell Biol.* 30 (11): 2762–74. https://doi.org/10.1128/MCB.01270-09

Song L, Jiang Y, Zhao H, Hou M (2012) 'Acquired Thermotolerance in Plants. *Plant Cell Tissue Organ Cult.* 111 (3): 265–76. https://doi.org/10.1007/s11240-012-0198-6

Sørensen BB, Ehrnsberger HF, Esposito S, Pfab A, Bruckmann A, Hauptmann J, Meister G, Merkl R, Schubert T, Längst G, Melzer M, Grasser M, Grasser KD (2017) The Arabidopsis THO/TREX Component TEX1 Functionally Interacts with MOS11 and Modulates MRNA Export and Alternative Splicing Events. *Plant Mol Biol.* 93 (3): 283–98. https://doi.org/10.1007/s11103-016-0561-9

Spector DL, Lamond AI (2011) Nuclear Speckles. *Cold Spring Harb. Perspect. Biol.* 3 (2): a000646 https://doi.org/10.1101/cshperspect.a000646

Staiger D, Brown JWS (2013) Alternative Splicing at the Intersection of Biological Timing, Development, and Stress Responses. *Plant Cell.* 25 (10): 3640–56. https://doi.org/10.1105/tpc.113.113803

Steffen A, Elgner M, Staiger D (2019) Regulation of Flowering Time by the RNA-Binding Proteins AtGRP7 and AtGRP8. *Plant Cell Physiol*. 60 (9): 2040–50. https://doi.org/10.1093/pcp/pcz124

Stemmer M, Thumberger T, del Sol Keyer M, Wittbrodt J, Mateo JL (2015) CCTop: An Intuitive, Flexible and Reliable CRISPR/Cas9 Target Prediction Tool. *PLoS One.* 10 (4): e0124633. https://doi.org/10.1371/journal.pone.0124633

Streit D (2016) The Role of Serine/Arginine-Rich Proteins in Plant Heat Stress Response. Master thesis. Goethe-University, Frankfurt am Main.

Su Z, Tang Y, Ritchey LE, Tack DC, Zhu M, Bevilacqua PC, Assmann SM (2018) Genome-Wide RNA Structurome Reprogramming by Acute Heat Shock Globally Regulates MRNA Abundance. *Proc Natl Acad Sci U S A.* 115 (48): 12170–75. https://doi.org/10.1073/pnas.1807988115

Sutherland BW, Toews J, Kast J (2008) Utility of Formaldehyde Cross-Linking and Mass Spectrometry in the Study of Protein–Protein Interactions. *J Mass Spectrom.* 43 (6): 699–715. https://doi.org/10.1002/jms.1415

Suzuki N, Katano K (2018) Coordination Between ROS Regulatory Systems and Other Pathways Under Heat Stress and Pathogen Attack. *Front Plant Sci.* 9 (April): 490. https://doi.org/10.3389/fpls.2018.00490

Szádeczky-Kardoss I, Szaker HM, Verma R, Darkó É, Pettkó-Szandtner A, Silhavy D, Csorba T (2022) Elongation Factor TFIIS Is Essential for Heat Stress Adaptation in Plants. *Nucleic Acids Res*. 50 (4): 1927–50. https://doi.org/10.1093/nar/gkac020

Tanabe N, Kimura A, Yoshimura K, Shigeoka S (2009) Plant-Specific SR-Related Protein AtSR45a Interacts with Spliceosomal Proteins in Plant Nucleus. *Plant Mol Biol.* 70 (3): 241–52. https://doi.org/10.1007/s11103-009-9469-y

Tian T, Liu Y, Yan H, You Q, Yi X, Du Z, Xu W, Su Z (2017) AgriGO v2.0: A GO Analysis Toolkit for the Agricultural Community, 2017 Update. *Nucleic Acids Res.* 45 (W1): W122–29. https://doi.org/10.1093/nar/gkx382

Tillemans V, Leponce I, Rausin G, Dispa L, Motte P (2006) Insights into Nuclear Organization in Plants as Revealed by the Dynamic Distribution of Arabidopsis SR Splicing Factors. *Plant Cell.* 18 (11): 3218–34. https://doi.org/10.1105/tpc.106.044529

Töpfer R, Matzeit V, Gronenborn B, Schell J, Steinbiss HH (1987) A Set of Plant Expression Vectors for Transcriptional and Translational Fusions. *Nucleic Acids Res.* 15 (14): 5890–5890. https://doi.org/10.1093/nar/15.14.5890

Tör M, Yemm A, Holub E (2003) The Role of Proteolysis in R Gene Mediated Defence in Plants: Proteolysis in Defence Signalling. *Mol Plant Pathol.* 4 (4): 287–96. https://doi.org/10.1046/j.1364-3703.2003.00169.x

Towbin H, Staehelin T, Gordon J (1992) Electrophoretic transfer of proteins from polyacrylamide gels to nitrocellulose sheets: procedure and some applications. *Proc Natl Acad Sci U S A*. 76 (9): 4350-4. https://doi.org/10.1073/pnas.76.9.4350

Valencia P, Dias AP, Reed R (2008) Splicing Promotes Rapid and Efficient MRNA Export in Mammalian Cells. *Proc Natl Acad Sci U S A.* 105 (9): 3386–91. https://doi.org/10.1073/pnas.0800250105

Vaquero-Garcia J, Barrera A, Gazzara MR, González-Vallinas J, Lahens NF, Hogenesch JB, Lynch KW, Barash Y (2016) A New View of Transcriptome Complexity and Regulation through the Lens of Local Splicing Variations. *Elife.* 5: e11752. https://doi.org/10.7554/eLife.11752

Vara Prasad PV, Boote KJ, Allen L, Thomas JMG (2002) Effects of Elevated Temperature and Carbon Dioxide on Seed-Set and Yield of Kidney Bean (Phaseolus Vulgaris L.) *Glob Chang Biol.* 8 (8): 710–21. https://doi.org/10.1046/j.1365-2486.2002.00508.x

Verhage L, Severing EI, Bucher J, Lammers M, Busscher-Lange J, Bonnema G, Rodenburg N, Proveniers MC, Angenent GC, Immink RG (2017) Splicing-Related Genes Are Alternatively Spliced upon Changes in Ambient Temperatures in Plants. *PLoS One.* 12 (3): e0172950. https://doi.org/10.1371/journal.pone.0172950

Vierling E (1991) The Roles of Heat Shock Proteins in Plants'. *Annu Rev Plant Physiol Plant Mol Biol.* 42 (1): 579–620. https://doi.org/10.1146/annurev.pp.42.060191.003051

Vigh L, Nakamoto H, Landry J, Gomez-Munoz A, Harwood JL, Horvath I (2007) Membrane Regulation of the Stress Response from Prokaryotic Models to Mammalian Cells. *Ann N Y Acad Sci.* 1113 (1): 40–51. https://doi.org/10.1196/annals.1391.027.

Vraggalas V (2022) Functional Characterization of Serine/Arginine-Rich Proteins RS2Z35 and RS2Z36 in Tomato. Master thesis. Goethe-University, Frankfurt am Main.

Wagner S, Klepsch MM, Schlegel S, Appel A, Draheim R, Tarry M, Högbom M, van Wijk KJ, Slotboom DJ, Persson JO, de Gier JW (2008) Tuning Escherichia Coli for Membrane Protein Overexpression. *Proc Natl Acad Sci U S A.* 105 (38): 14371–76. https://doi.org/10.1073/pnas.0804090105

Wahid A, Gelani S, Ashraf M, Foolad M (2007) Heat Tolerance in Plants: An Overview. *Environ Exp Bot.* 61 (3): 199–223. https://doi.org/10.1016/j.envexpbot.2007.05.011

Wang BB, Brendel V (2004) The ASRG Database: Identification and Survey of Arabidopsis Thaliana Genes Involved in Pre-MRNA Splicing. *Genome Biol.* 5 (12): R102. https://doi.org/10.1186/gb-2004-5-12-r102

Wang Z, Burge CB (2008) Splicing Regulation: From a Parts List of Regulatory Elements to an Integrated Splicing Code. *RNA.* 14 (5): 802–13. https://doi.org/10.1261/rna.876308

Wang Y, Bao Z, Zhu Y, Hua J (2009) Analysis of Temperature Modulation of Plant Defense Against Biotrophic Microbes. *Mol Plant Microbe Interact.* 22 (5): 498–506. https://doi.org/10.1094/MPMI-22-5-0498

Wang K, Gao Y, Peng X, Yang G, Gao F, Li S, Zhu Y (2010) Using FAM Labeled DNA Oligos to Do RNA Electrophoretic Mobility Shift Assay. *Mol Biol Rep.* 37 (6): 2871–75. https://doi.org/10.1007/s11033-009-9841-7

Wang Y, Xiao X, Zhang J, Choudhury R, Robertson A, Li K, Ma M, Burge CB, Wang Z (2013) A Complex Network of Factors with Overlapping Affinities Represses Splicing through Intronic Elements. *Nat Struct Mol Biol.* 20 (1): 36–45. https://doi.org/10.1038/nsmb.2459

Warf MB, Diegel JV, von Hippel PH, Berglund JA (2009) The Protein Factors MBNL1 and U2AF65 Bind Alternative RNA Structures to Regulate Splicing. *Proc Natl Acad Sci U S A.* 106 (23): 9203–8. https://doi.org/10.1073/pnas.0900342106

Warf MB, Berglund JA (2010) Role of RNA Structure in Regulating Pre-MRNA Splicing. *Trends Biochem Sci.* 35 (3): 169–78. https://doi.org/10.1016/j.tibs.2009.10.004

Weide R, Koornneef M, Zabel P (1989) A Simple, Nondestructive Spraying Assay for the Detection of an Active Kanamycin Resistance Gene in Transgenic Tomato Plants. *Theor Appl Genet.* 78 (2): 169–72. https://doi.org/10.1007/BF00288794

Weis BLM (2015) Pre-rRNA Processing in A. Thaliana and the Role of 60S Ribosome Biogenesis Factors. PhD thesis. Goethe-University, Frankfurt am Main.

Wiebauer K, Herrero JJ, Filipowicz W (1988) Nuclear Pre-MRNA Processing in Plants: Distinct Modes of 3'-Splice-Site Selection in Plants and Animal. *Mol Cell Biol.* 8 (5): 2042–51. https://doi.org/10.1128/mcb.8.5.2042-2051.1988

Wilkinson ME, Charenton C, Nagai K (2020) RNA Splicing by the Spliceosome. *Ann Rev Biochem.* 89 (1): 359–88. https://doi.org/10.1146/annurev-biochem-091719-064225

Windgassen M, Sturm D, Cajigas IJ, González CI, Seedorf M, Bastians H, Krebber H (2004) Yeast Shuttling SR Proteins Npl3p, Gbp2p, and Hrb1p Are Part of the Translating MRNPs, and Npl3p Can Function as a Translational Repressor. *Mol Cell Biol.* 24 (23): 10479–91. https://doi.org/10.1128/MCB.24.23.10479-10491.2004

Wu JZ, Liu Q, Geng XS, Li KM, Luo LJ, Liu JP (2017) Highly Efficient Mesophyll Protoplast Isolation and PEG-Mediated Transient Gene Expression for Rapid and Large-Scale Gene Characterization in Cassava (Manihot Esculenta Crantz). *BMC Biotechnol.* 17 (1): 29. https://doi.org/10.1186/s12896-017-0349-2

Wu Z, Liang J, Wang C, Ding L, Zhao X, Cao X, Xu S, Teng N, Yi M (2019) Alternative Splicing Provides a Mechanism to Regulate LlHSFA3 Function in Response to Heat Stress in Lily. *Plant Physiol.* 181 (4): 1651–67. https://doi.org/10.1104/pp.19.00839

Xiao SH, Manley JL (1997) Phosphorylation of the ASF/SF2 RS Domain Affects Both Protein-Protein and Protein-RNA Interactions and Is Necessary for Splicing. *Genes Dev.* 11 (3): 334–44. https://doi.org/10.1101/gad.11.3.334

Xiao W, Adhikari S, Dahal U, Chen YS, Hao YJ, Sun BF, Sun HY, Li A, Ping XL, Lai WY, Wang X, Ma HL, Huang CM, Yang Y, Huang N, Jiang GB, Wang HL, Zhou Q, Wang XJ, Zhao YL, Yang YG (2016) Nuclear m 6 A Reader YTHDC1 Regulates MRNA Splicing. *Mol Cell.* 61 (4): 507–19. https://doi.org/10.1016/j.molcel.2016.01.012

Xing D, Wang Y, Hamilton M, Ben-Hur A, Reddy ASN (2015) Transcriptome-Wide Identification of RNA Targets of Arabidopsis SERINE/ARGININE-RICH45 Uncovers the Unexpected Roles of This RNA Binding Protein in RNA Processing. *Plant Cell.* 27 (12): 3294–3308. https://doi.org/10.1105/tpc.15.00641

Xu L, Lin Z, Tao Q, Liang M, Zhao G, Yin X, Fu R (2014) Multiple NUCLEAR FACTOR Y Transcription Factors Respond to Abiotic Stress in Brassica Napus L. Edited by Keqiang Wu. *PLoS One*. 9 (10): e111354. https://doi.org/10.1371/journal.pone.0111354

Yan X, Sablok G, Feng G, Ma J, Zhao H, Sun X (2015) Nagnag: Identification and Quantification of NAGNAG Alternative Splicing Using RNA-Seq Data. *FEBS Lett.* 589 (15): 1766–70. https://doi.org/10.1016/j.febslet.2015.05.029

Yang J, Duan G, Li C, Liu L, Han G, Zhang Y, Wang C (2019) The Crosstalks Between Jasmonic Acid and Other Plant Hormone Signaling Highlight the Involvement of Jasmonic Acid as a Core Component in Plant Response to Biotic and Abiotic Stresses. *Front Plant Sci.* 10: 1349. https://doi.org/10.3389/fpls.2019.01349

Yang Y, Li Y, Sancar A, Oztas O (2020) The Circadian Clock Shapes the Arabidopsis Transcriptome by Regulating Alternative Splicing and Alternative Polyadenylation. *J Biol Chem*. 295 (22): 7608-19. https://doi.org/10.1074/jbc.RA120.013513

Yángüez E, Castro-Sanz AB, Fernández-Bautista N, Oliveros JC, Castellano MM (2013) Analysis of Genome-Wide Changes in the Translatome of Arabidopsis Seedlings Subjected to Heat Stress. *PLoS One.* 8 (8): e71425. https://doi.org/10.1371/journal.pone.0071425

Yeakley JM, Tronchère H, Olesen J, Dyck JA, Wang HY, Fu XD (1999) Phosphorylation Regulates In Vivo Interaction and Molecular Targeting of Serine/Arginine-Rich Pre-MRNA Splicing Factors. *J Cell Biol.* 145 (3): 447–55. https://doi.org/10.1083/jcb.145.3.447

Yoshida T, Ohama N, Nakajima J, Kidokoro S, Mizoi J, Nakashima K, Maruyama K, Kim JM, Seki M, Todaka D, Osakabe Y, Sakuma Y, Schöffl F, Shinozaki K, Yamaguchi-Shinozaki K (2011) Arabidopsis HsfA1 Transcription Factors Function as the Main Positive Regulators in Heat Shock-Responsive Gene Expression. *Mol Genet Genomics.* 286 (5–6): 321–32. https://doi.org/10.1007/s00438-011-0647-7

Yost HJ, Lindquist S (1986) RNA Splicing Is Interrupted by Heat Shock and Is Rescued by Heat Shock Protein Synthesis. *Cell.* 45 (2): 185–93. https://doi.org/10.1016/0092-8674(86)90382-X

Zander G, Hackmann A, Bender L, Becker D, Lingner T, Salinas G, Krebber H (2016) mRNA Quality Control Is Bypassed for Immediate Export of Stress-Responsive Transcripts. *Nature.* 540 (7634): 593–96. https://doi.org/10.1038/nature20572

Zhang Z, Krainer AR (2004) Involvement of SR Proteins in MRNA Surveillance. *Mol Cell.* 16 (4): 597-607. https://doi.org/10.1016/j.molcel.2004.10.031

Zhang XN, Mount SM (2009) Two Alternatively Spliced Isoforms of the Arabidopsis SR45 Protein Have Distinct Roles during Normal Plant Development. *Plant Physiol.* 150 (3): 1450–58. https://doi.org/10.1104/pp.109.138180

Zhang XN, Shi Y, Powers JJ, Gowda NB, Zhang C, Ibrahim HMM, Ball HB, Chen SL, Lu H, Mount SM (2017) Transcriptome Analyses Reveal SR45 to Be a Neutral Splicing Regulator and a Suppressor of Innate Immunity in Arabidopsis Thaliana. *BMC Genomics.* 18 (1): 772. https://doi.org/10.1186/s12864-017-4183-7

Zhang H, Zhao Y, Zhu JK (2020a) Thriving under Stress: How Plants Balance Growth and the Stress Response. *Dev Cell*. 55 (5): 529–43. https://doi.org/10.1016/j.devcel.2020.10.012

Zhang Y, Parmigiani G, Johnson WE (2020b) ComBat-Seq: Batch Effect Adjustment for RNA-Seq Count Data. *NAR Genom Bioinform*. 2 (3): lqaa078. https://doi.org/10.1093/nargab/lqaa078

Zhang J, Sun Y, Zhou Z, Zhang Y, Yang Y, Zan X, Li X, Wan J, Gao X, Chen R, Huang Z, Li L, Xu Z (2022) OsSCL30 Overexpression Reduces the Tolerance of Rice Seedlings to Low Temperature, Drought and Salt. *Sci Rep.* 12 (1): 8385. https://doi.org/10.1038/s41598-022-12438-4

Zheng Z, Qamar SA, Chen Z, Mengiste T (2006) Arabidopsis WRKY33 Transcription Factor Is Required for Resistance to Necrotrophic Fungal Pathogens. *Plant J.* 48 (4): 592–605. https://doi.org/10.1111/j.1365-313X.2006.02901.x

Zhou P, Lugovskoy AA, Wagner G (2001) A Solubility-Enhancement Tag (SET) for NMR Studies of Poorly Behaving Proteins*. J Biomol NMR.* 20 (1): 11–14. https://doi.org/10.1023/A:1011258906244

Zhou Z, Fu XD (2013) Regulation of Splicing by SR Proteins and SR Protein-Specific Kinases. *Chromosoma.* 122 (3): 191–207. https://doi.org/10.1007/s00412-013-0407-z

Zhou J, Xu XC, Cao JJ, Yin LL, Xia XJ, Shi K, Zhou YH, Yu JQ (2018) Heat Shock Factor HsfA1a Is Essential for R Gene-Mediated Nematode Resistance and Triggers H_2O_2 Production. *Plant Physiol.* 176 (3): 2456–71. https://doi.org/10.1104/pp.17.01281

Zhu J, Krainer AR (2000) Pre-MRNA Splicing in the Absence of an SR Protein RS Domain. *Genes Dev.* 14 (24): 3166–78. https://doi.org/10.1101/gad.189500

Zhu G, Li W, Zhang F, Guo W (2018) RNA-Seq Analysis Reveals Alternative Splicing under Salt Stress in Cotton, Gossypium Davidsonii. *BMC Genomics.* 19 (1): 73. https://doi.org/10.1186/s12864-018-4449-8

Zhu A, Ibrahim JG, Love MI (2019) Heavy-Tailed Prior Distributions for Sequence Count Data: Removing the Noise and Preserving Large Differences. *Bioinformatics.* 35 (12): 2084–92. https://doi.org/10.1093/bioinformatics/bty895

Zinn KE, Tunc-Ozdemir M, Harper JF (2010) Temperature Stress and Plant Sexual Reproduction: Uncovering the Weakest Links. *J Exp Bot.* 61 (7): 1959–68. https://doi.org/10.1093/jxb/erq053

Zwack PJ, Rashotte AM (2015) Interactions between Cytokinin Signalling and Abiotic Stress Responses. *J Exp Bot.* 66 (16): 4863–71. https://doi.org/10.1093/jxb/erv172

Supplemental data

Supplemental datasets

The following datasets are deposited in xlsx format on the compact disc attached.

Dataset 1. DE genes. This dataset includes the gene ID, LFC and padj for each regulated gene.

1.1. WT HS relative to control

1.2. *rs2z* mutants relative to WT (control conditions)

1.3. *rs2z* mutants relative to WT (HS conditions)

Dataset 2. DAS genes. This dataset includes the gene ID and AS type for each regulated gene. Additionally, the processed Majiq output (classification of AS events by AS type) is included as additional data sheets.

2.1. WT HS relative to control

2.2. *rs2z35* (35mt) relative to WT (control conditions)

2.3. *rs2z35* (35mt) relative to WT (HS conditions)

2.4. *rs2z36* (36mt) relative to WT (control conditions)

2.5. *rs2z36* (36mt) relative to WT (HS conditions)

2.6. *rs2z35 rs2z36* (dmt) relative to WT (control conditions)

2.7. *rs2z35 rs2z36* (dmt) relative to WT (HS conditions)

Dataset 3. RIP genes. Enriched genes in *GFP-RS2Z* relative to *GFP*. This dataset includes the gene ID, LFC and padj for each enriched gene.

Dataset 4. Enriched GO terms. This dataset includes the significantly enriched GO terms among the regulated genes as indicated. P: biological process. M: molecular function. C: cellular compartment

4.1. DE genes, WT HS relative to control (up- and downregulated as separate sheets)

4.2. DE genes, *RS2Z*-regulated (regulated in any mutant) relative to WT (HS conditions)

4.3. DAS genes, WT HS relative to control (up- and downregulated as separate sheets)

4.4. DAS genes, *RS2Z*-regulated (regulated in any mutant) relative to WT (HS conditions)

4.5. RIP genes, *GFP-RS2Z* relative to *GFP*

Supplemental Figures

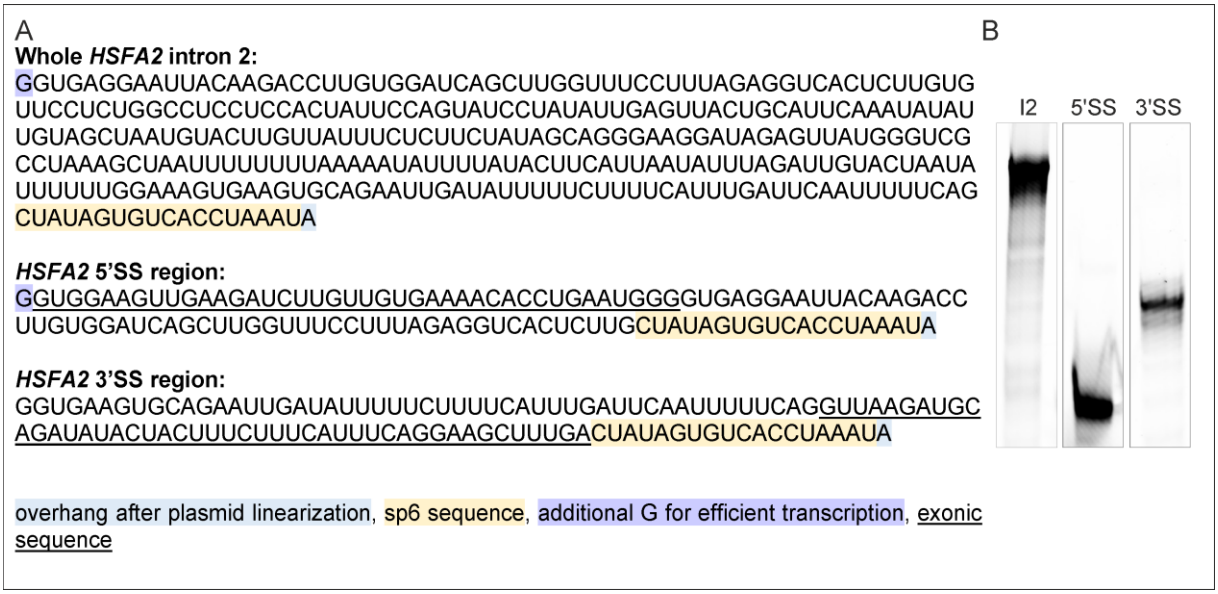

Supplemental Figure 1. *In vitro* transcribed RNAs for RNA EMSA. (A) Nucleotide sequences. **(B)** Confirmation of indirect RNA labeling by labeling 30 pmol of the respective RNA followed by separation in a 5% native polyacrylamide gel.

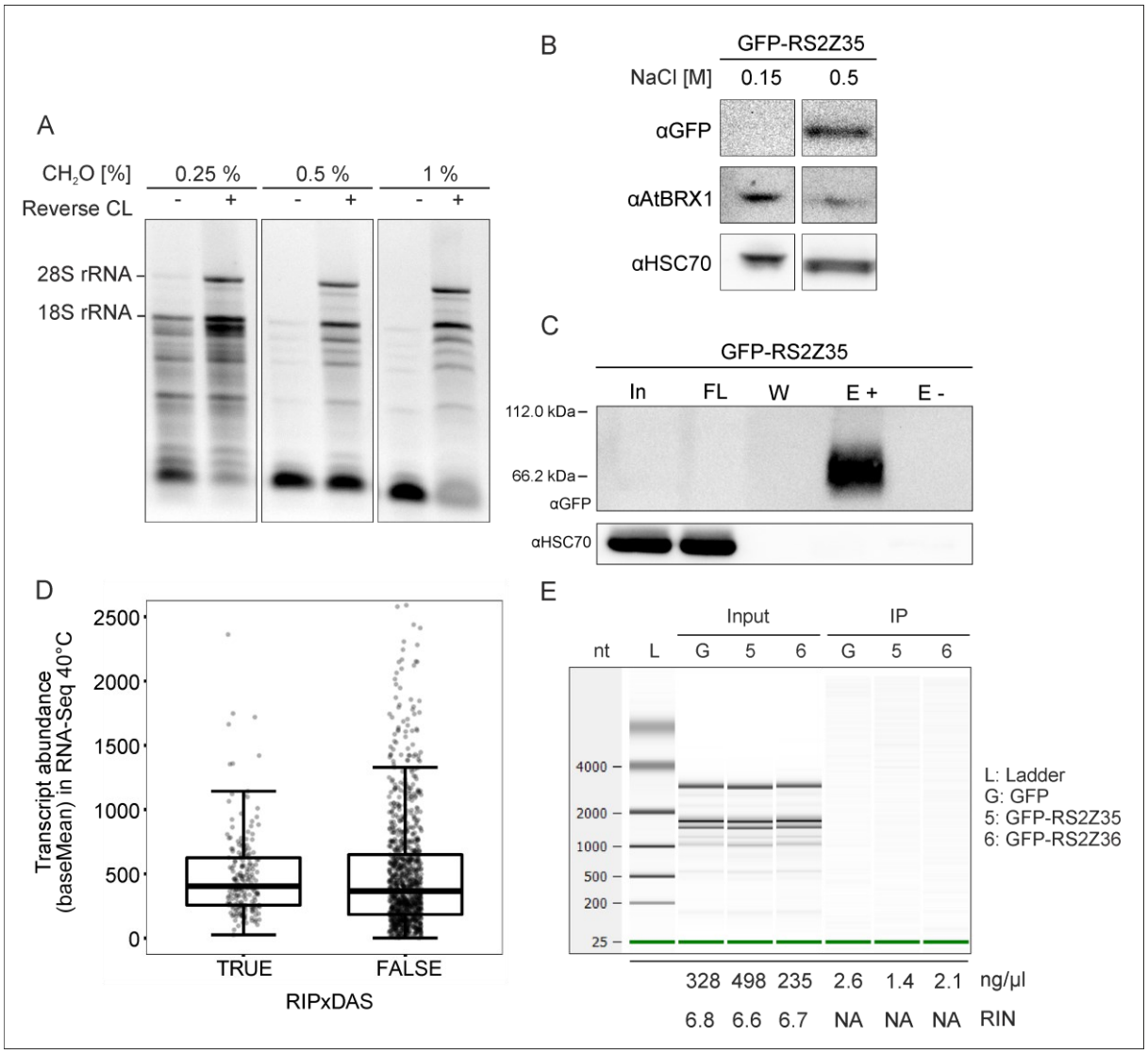

Supplemental Figure 2. Establishing RNA immunoprecipitation (RIP) in tomato. (A) Determination of crosslinking efficiency by crosslinking for 20 min using the indicated formaldehyde concentrations followed by RNA extraction with and without reverse crosslinking (reverse CL). Crosslinking efficiency was evaluated by rRNA. **(B)** Assessment of optimal extraction buffer conditions for nuclear lysis monitored by nuclear protein BRX1 and for RS2Z protein extraction shown by immunoblot after extraction using different salt concentrations. A representative blot with 20 µg total protein extract from *GFP-RS2Z35* plants is depicted. **(C)** Evaluation of unspecific binding to Ni-NTA beads by immunoblot following IP with (+) and without (-) nanobody binding to Ni-NTA agarose coated beads. In: Input (2%), FL: flowthrough (2%), W: last wash (2%), E: elution (40%). **(D)** Transcript abundance as baseMean across all RNA-Seq samples from WT and *rs2z* mutant leaves exposed to 1 h 40°C. Indicated is the transcript abundance of RIP genes identified as DAS in rs2z mutants compared to WT (under HS conditions) (TRUE) and those that were not (FALSE). **(E)** Simulated gel picture after RNA integrity assessment using the bioanalyzer. Depicted are RIP input and IP samples of replicate 1 with indicated concentrations and RNA integrity number (RIN) below. L: Ladder. G: GFP. 5: GFP-RS2Z35. 6: GFP-RS2Z36.

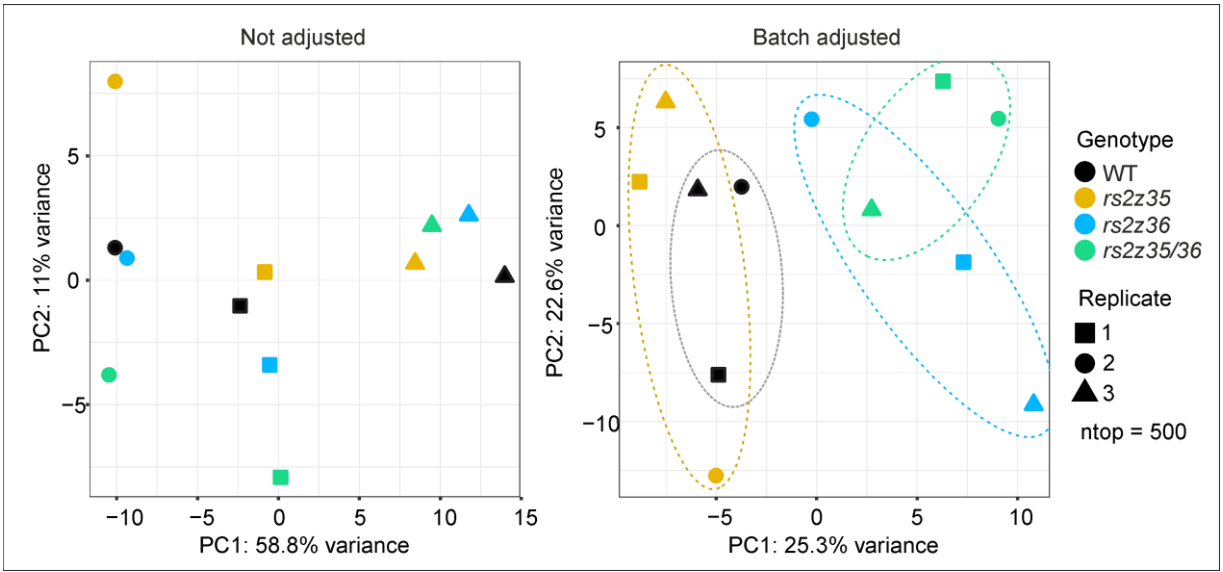

Supplemental Figure 3. Visualisation of sample similarity via principal component analysis (PCA). Before (left) and after (right) batch correction. Ellipses were manually drawn to indicate clustering. The 500 genes with highest row variance were used.

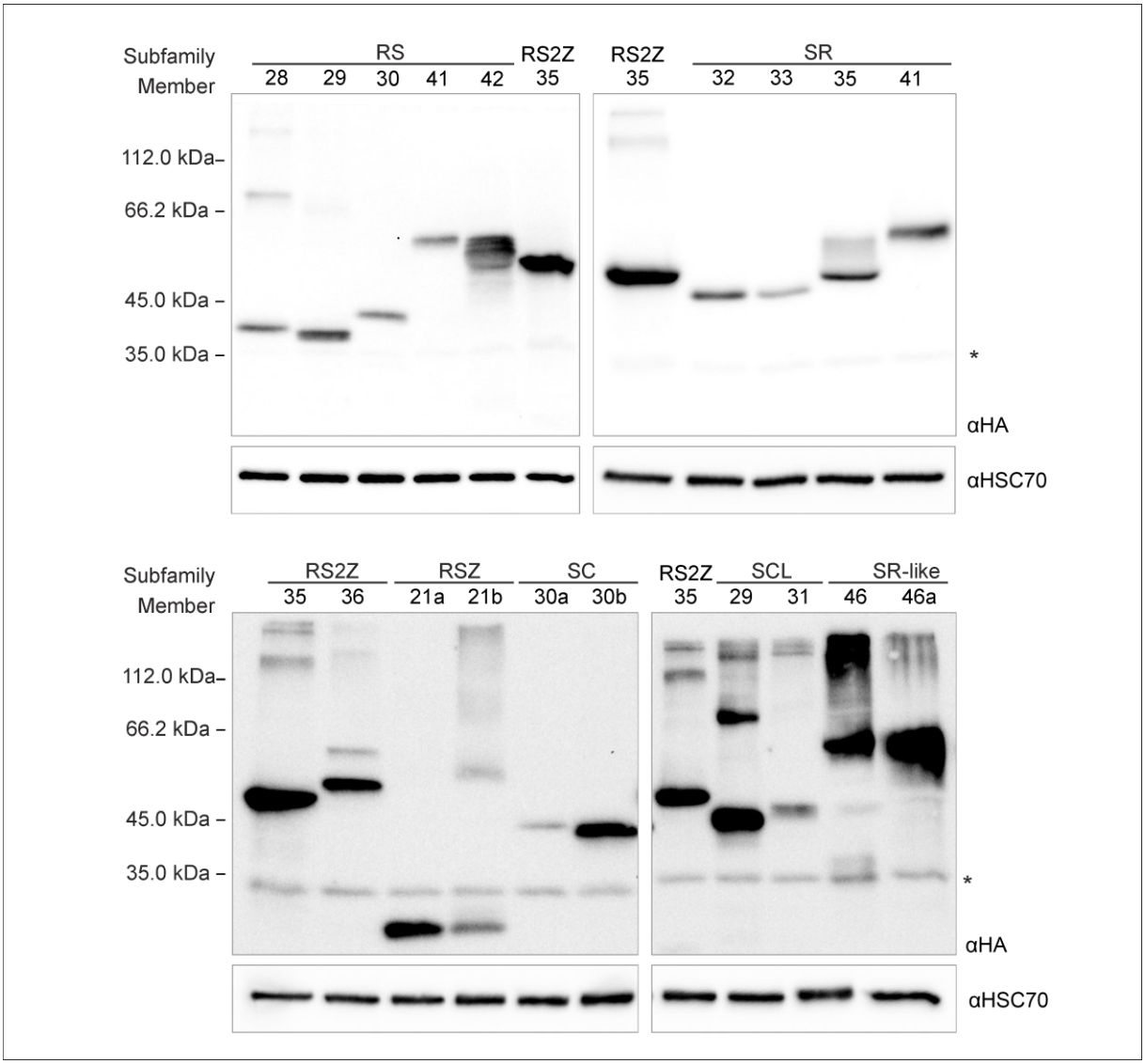

Supplemental Figure 4. **Expression of HA-SR proteins in tomato protoplasts.** Immunoblot analysis depicting HA-SR protein signals in tomato protoplasts transformed with 10 µg HA-SR protein encoding plasmid per $1x10^5$ protoplasts. HA-RS2Z35 serves as reference in each blot and HSC70 serves as loading control. The asterisk indicates unspecific signal.

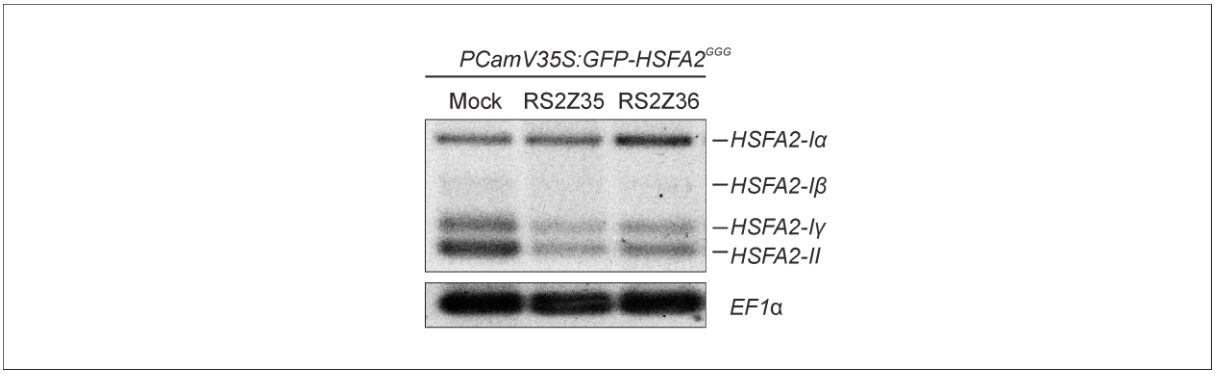

Supplemental Figure 5. RT-PCR using a constitutively expressed *GFP-HSFA2* minigene. Agarose gel after RT-PCR as described in Fig. 9A-B. In contrast to the minigene assay in Fig. 9, the minigene depicted here is driven by the CaMV35S promoter as in Fig. 6.

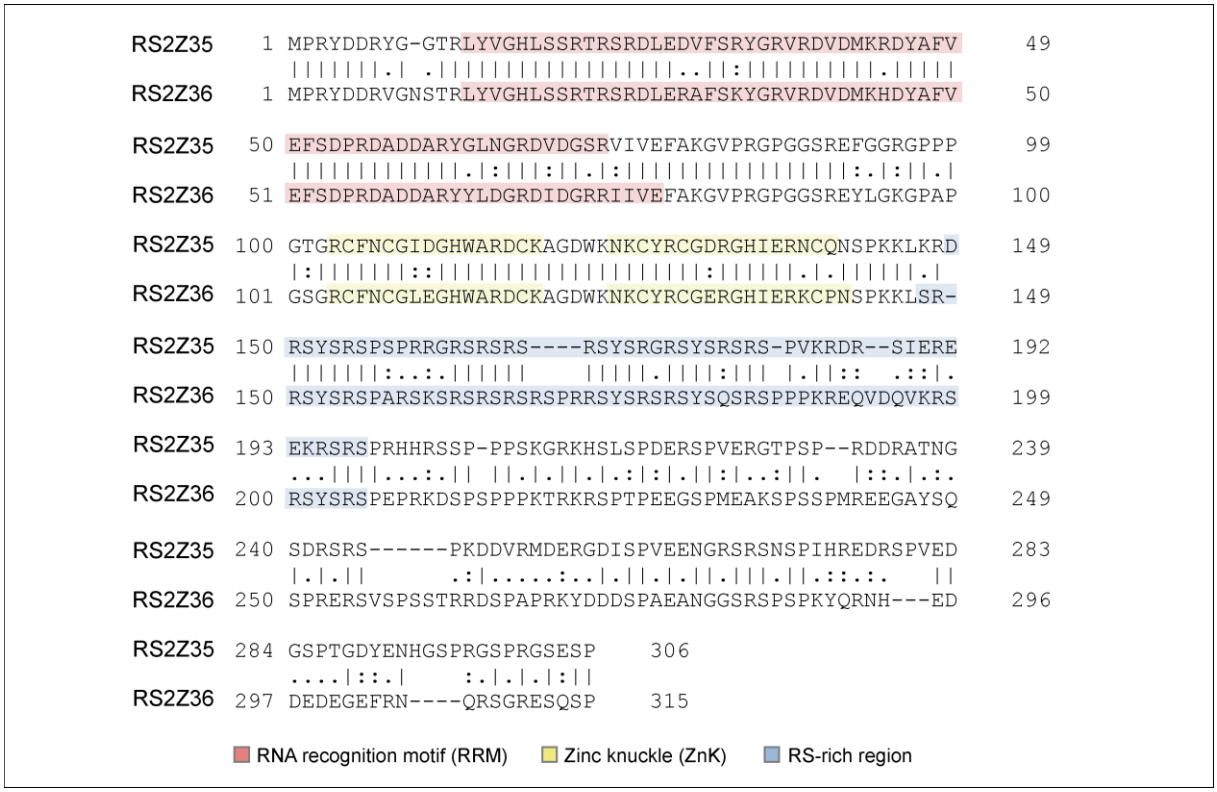

Supplemental Figure 6. Pairwise amino acid sequence alignment of RS2Z35 and RS2Z36. Domains (RRM, ZnK, RS-rich region) are highlighted in red, yellow, and blue colour, respectively. Lines between amino acids represent identical, single dots indicate different aa identity, colons indicate differences in aa identity but general similarity in properties. Hyphens indicate missing aa. The pairwise alignment was performed using EMBOSS Needle (Rice et al, 2000).

RS2Z35

WT:

MVFYPYDVPDYAGYPYDVPDYAGSYPYDVPDYAAQVPPRYDDRYGGTRLYVGHLSSRTRSRDLEDVFSRYGRVRDVD
MKRDYAFVEFSDPRDADDARYGLNGRDVDGSRVIVEFAKGVPRGPGGSREFGGRGPPPGTGRCFNCGIDGHWARDC
KAGDWKNKCYRCGDRGHIERNCQNSPKKLKRDRSYSRSPSPRRGRSRSRSRSYSRGRSYSRSRSPVKRDRSIEREEK
RSRSPRHHRSSPPPSKGRKHSLSPDERSPVERGTPSPRDDRATNGSDRSRSPKDDVRMDERGDISPVEENGRSRSNS
PIHREDRSPVEDGSPTGDYENHGSPRGSPRGSESP

ΔRRM:
MVFYPYDVPDYAGYPYDVPDYAGSYPYDVPDYAAQVPPRYDDRYGGTR~~LYVGHLSSRTRSRDLEDVFSRYGRVRDVD~~
~~MKRDYAFVEFSDPRDADDARYGLNGRDVDGSRVIVE~~FAKGVPRGPGGSREFGGRGPPPGTGRCFNCGIDGHWARDC
KAGDWKNKCYRCGDRGHIERNCQNSPKKLKRDRSYSRSPSPRRGRSRSRSRSYSRGRSYSRSRSPVKRDRSIEREEK
RSRSPRHHRSSPPPSKGRKHSLSPDERSPVERGTPSPRDDRATNGSDRSRSPKDDVRMDERGDISPVEENGRSRSNS
PIHREDRSPVEDGSPTGDYENHGSPRGSPRGSESP

ΔZnk:
MVFYPYDVPDYAGYPYDVPDYAGSYPYDVPDYAAQVPPRYDDRYGGTRLYVGHLSSRTRSRDLEDVFSRYGRVRDVD
MKRDYAFVEFSDPRDADDARYGLNGRDVDGSRVIVEFAKGVPRGPGGSREFGGRGPPPGT~~GRCFNCGIDGHWARDC~~
~~KAGDWKNKCYRCGDRGHIERNCQ~~NSPKKLKRDRSYSRSPSPRRGRSRSRSRSYSRGRSYSRSRSPVKRDRSIEREEK
RSRSPRHHRSSPPPSKGRKHSLSPDERSPVERGTPSPRDDRATNGSDRSRSPKDDVRMDERGDISPVEENGRSRSNS
PIHREDRSPVEDGSPTGDYENHGSPRGSPRGSESP

ΔRS:
MVFYPYDVPDYAGYPYDVPDYAGSYPYDVPDYAAQVPPRYDDRYGGTRLYVGHLSSRTRSRDLEDVFSRYGRVRDVD
MKRDYAFVEFSDPRDADDARYGLNGRDVDGSRVIVEFAKGVPRGPGGSREFGGRGPPPGTGRCFNCGIDGHWARDC
KAGDWKNKCYRCGDRGHIERNCQNSPKKLKRDRSYSRSPSPRRGRSRSRSRSYSRGRSYSRSRS~~PVKRDRSIEREEK~~
RSRSPRHHRSSPPPSKGRKHSLSPDERSPVERGTPSPRDDRATNGSDRSRSPKDDVRMDERGDISPVEENGRSRSNS
PIHREDRSPVEDGSPTGDYENHGSPRGSPRGSESP

RS2Z36

WT:
MVFYPYDVPDYAGYPYDVPDYAGSYPYDVPDYAAQVPPRYDDRVGNSTRLYVGHLSSRTRSRDLERAFSKYGRVRDV
DMKHDYAFVEFSDPRDADDARYYLDGRDIDGRRIIVEFAKGVPRGPGGSREYLGKGPAPGSGRCFNCGLEGHWARDC
KAGDWKNKCYRCGERGHIERKCPNSPKKLSRRSYSRSPARSKSRSRSRSRSPRRSYSRSRSYSQSRSPPPKREQVD
QVKRSRSYSRSPEPRKDSPSPPPKTRKRSPTPEEGSPMEAKSPSSPMREEGAYSQSPRERSVSPSSTRRDSPAPRKY
DDDSPAEANGGSRSPSPKYQRNHEDDEDEGEFRNQRSGRESQSP

ΔRRM:
MVFYPYDVPDYAGYPYDVPDYAGSYPYDVPDYAAQVP~~PRYDDRVGNSTRLYVGHLSSRTRSRDLERAFSKYGRVRDV~~
~~DMKHDYAFVEFSDPRDADDARYYLDGRDIDGRRIIVEFAK~~GVPRGPGGSREYLGKGPAPGSGRCFNCGLEGHWARDC
KAGDWKNKCYRCGERGHIERKCPNSPKKLSRRSYSRSPARSKSRSRSRSRSPRRSYSRSRSYSQSRSPPPKREQVD
QVKRSRSYSRSPEPRKDSPSPPPKTRKRSPTPEEGSPMEAKSPSSPMREEGAYSQSPRERSVSPSSTRRDSPAPRKY
DDDSPAEANGGSRSPSPKYQRNHEDDEDEGEFRNQRSGRESQSP

ΔZnk:
MVFYPYDVPDYAGYPYDVPDYAGSYPYDVPDYAAQVPPRYDDRVGNSTRLYVGHLSSRTRSRDLERAFSKYGRVRDV
DMKHDYAFVEFSDPRDADDARYYLDGRDIDGRRIIVEFAKGVPRGPGGSREYLGKGPAPGSG~~RCFNCGLEGHWARDC~~
~~KAGDWKNKCYRCGERGHIERKCPN~~SPKKLSRRSYSRSPARSKSRSRSRSRSPRRSYSRSRSYSQSRSPPPKREQVD
QVKRSRSYSRSPEPRKDSPSPPPKTRKRSPTPEEGSPMEAKSPSSPMREEGAYSQSPRERSVSPSSTRRDSPAPRKY
DDDSPAEANGGSRSPSPKYQRNHEDDEDEGEFRNQRSGRESQSP

ΔRS:
MVFYPYDVPDYAGYPYDVPDYAGSYPYDVPDYAAQVPPRYDDRVGNSTRLYVGHLSSRTRSRDLERAFSKYGRVRDV
DMKHDYAFVEFSDPRDADDARYYLDGRDIDGRRIIVEFAKGVPRGPGGSREYLGKGPAPGSGRCFNCGLEGHWARDC
KAGDWKNKCYRCGERGHIERKCPNSPKKL~~SRRSYSRSPARSKSRSRSRSRSPRRSYSRSRSYSQSRS~~PPPKREQVD
QVKRSRSYSRSPEPRKDSPSPPPKTRKRSPTPEEGSPMEAKSPSSPMREEGAYSQSPRERSVSPSSTRRDSPAPRKY
DDDSPAEANGGSRSPSPKYQRNHEDDEDEGEFRNQRSGRESQSP

RRM, Znk, RS domain (max length), RS domain (max percentage) 6xHA tag and linker sequence

Supplemental Figure 7. Amino acid sequences of WT and deletion mutant HA-RS2Z constructs. The RRM is highlighted in red, the Znks in yellow. The RS domain is highlighted in blue colour, whereby the region of highest RS/SR dipeptide content was depicted in lighter colour and underlined. HA-tag and linker sequence are underlined. Deleted regions are crossed out.

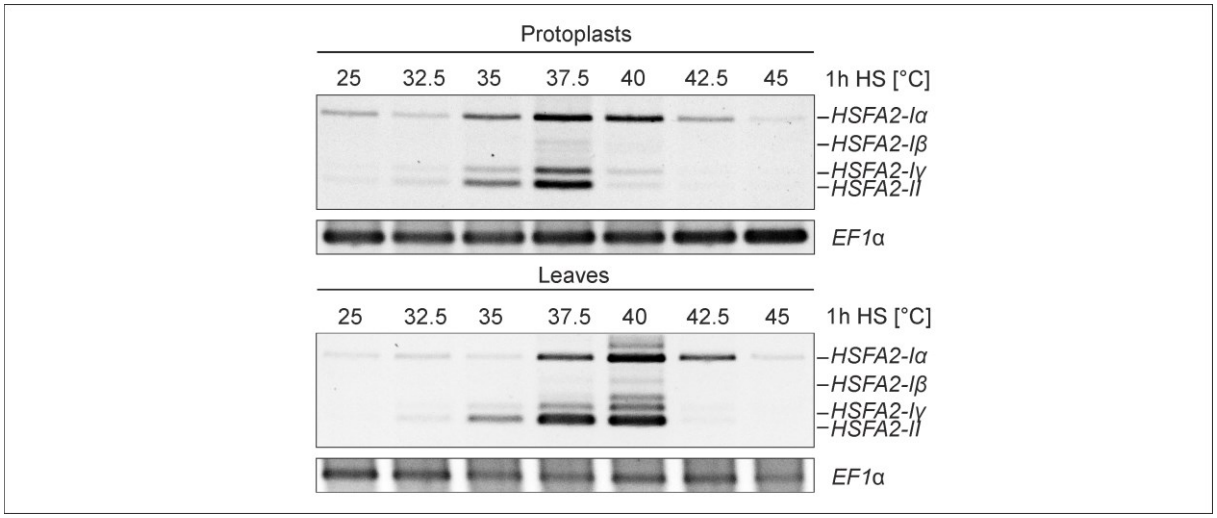

Supplemental Figure 8. Comparison of *HSFA2* splicing profiles in tomato protoplasts and leaves in response to different temperatures. Protoplasts (top) or leaves (bottom) were exppsed tp 1 h HS at the indicated temperature. RT-PCR was performed as in Fig. 6F. *EF1α* serves as control.

RS2Z35

WT:
MPRYDDRYGGTRLYVGHLSSRTRSRDLEDVFSRYGRVRDVDMKRDYAFVEFSDPRDADDARYGLNGRDVDGSRVIVE
FAKGVPRGPGGSREFGGRGPPPGTGRCFNCGIDGHWARDCKAGDWKNKCYRCGDRGHIERNCQNSPKKLKRDRSY
SRSPSPRRGRSRSRSRSYSRGRSYSRSRSPVKRDRSIEREEKRSRSPRHHRSSPPPSKGRKHSLSPDERSPVERGTP
SPRDDRATNGSDRSRSPKDDVRMDERGDISPVEENGRSRSNSPIHREDRSPVEDGSPTGDYENHGSPRGSPRGSESP

rs2z35:
MPRYDDRYGGTRLLLDICLPGRDLETWRTSLADMGEYVMWI

RS2Z36

WT:
MPRYDDRVGNSTRLYVGHLSSRTRSRDLERAFSKYGRVRDVDMKHDYAFVEFSDPRDADDARYYLDGRDIDGRRIIVE
FAKGVPRGPGGSREYLGKGPAPGSGRCFNCGLEGHWARDCKAGDWKNKCYRCGERGHIERKCPNSPKKLSRRSYSR
SPARSKSRSRSRSRSPRRSYSRSRSYSQSRSPPPKREQVDQVKRSRSYSRSPEPRKDSPSPPPKTRKRSPTPEEGSP
MEAKSPSSPMREEGAYSQSPRERSVSPSSTRRDSPAPRKYDDDSPAEANGGSRSPSPKYQRNHEDDEDEGEFRNQR
SGRESQSP

rs2z36:
MPRYDDRVGNSTRLYVGHLSSRTRSR

RRM, Znk, RS domain (max length), RS domain (max percentage), aa sequence different from WT

Supplemental Figure 9. Amino acid sequences of RS2Z35 and RS2Z36 proteins in WT and mutant plants.

RS2Z35:
MPRYDDRYGGTRLYVGHLSSRTRSRDLEDVFSRYGRVRDVDMKRDYAFVEFSDPRDADDARYGLNGRDVDGSRVIVE
FAKGVPRGPGGSREFGGRGPPPGTGRCFNCGIDGHWARDCKAGDWKNKCYRCGDRGHIERNCQNSPKKLKRDRSY
SRSPSPRRGRSRSRSRSYSRGRSYSRSRSPVKRDRSIEREEKRSRSPRHHRSSPPPSKGRKHSLSPDERSPVERGTP
SPRDDRATNGSDRSRSPKDDVRMDERGDISPVEENGRSRSNSPIHREDRSPVEDGSPTGDYENHGSPRGSPRGSESP

GB1-His-RS2Z35 (RBD)
MQYKLILNGKTLKGETTTEAVDAATAEKVFKQYANDNGVDGEWTYDDATKTFTVTEGSHHHHHHGSPRYDDRYGGTRL
YVGHLSSRTRSRDLEDVFSRYGRVRDVDMKRDYAFVEFSDPRDADDARYGLNGRDVDGSRVIVEFAKGVPRGPGGSR
EFGGRGPPPGTGRCFNCGIDGHWARDCKAGDWKNKCYRCGDRGHIERNCQNSP

RS2Z36:
MPRYDDRVGNSTRLYVGHLSSRTRSRDLERAFSKYGRVRDVDMKHDYAFVEFSDPRDADDARYYLDGRDIDGRRIIVE
FAKGVPRGPGGSREYLGKGPAPGSGRCFNCGLEGHWARDCKAGDWKNKCYRCGERGHIERKCPNSPKKLSRRSYSR
SPARSKSRSRSRSRSPRRSYSRSRSYSQSRSPPPKREQVDQVKRSRSYSRSPEPRKDSPSPPPKTRKRSPTPEEGSP
MEAKSPSSPMREEGAYSQSPRERSVSPSSTRRDSPAPRKYDDDSPAEANGGSRSPSPKYQRNHEDDEDEGEFRNQR
SGRESQSP

GB1-His-RS2Z36 (RBD)
MQYKLILNGKTLKGETTTEAVDAATAEKVFKQYANDNGVDGEWTYDDATKTFTVTEGSHHHHHHGSPRYDDRVGNSTR
LYVGHLSSRTRSRDLERAFSKYGRVRDVDMKHDYAFVEFSDPRDADDARYYLDGRDIDGRRIIVEFAKGVPRGPGGSR
EYLGKGPAPGSGRCFNCGLEGHWARDCKAGDWKNKCYRCGERGHIERKCPNSPK

SC30b:
MSHFGRTGPPDIADTYSLLVLNITFRTSADDLFPLFDKYGKVVDIFIPRDRRTGESRGFAFVRYKYAEEAQKAVDRLDGR
VVDGREMAVQFAKYGPNAERIHQGRIIEKVPGFKGSSRSRSPRRRYRDDYHRDREYRRSRSRSVDRYERDRYRQRER
DYRHRSRSRSLSPDYDRDRGRRRDRKHYRRSPSVDSASPSRRSPSPHRKESPPRSLSPTKGSPVRRVRNERSPTPRS
RSPPGRAMDSRSPSPRVDED

GB1-His-SC30b (RRM)
MQYKLILNGKTLKGETTTEAVDAATAEKVFKQYANDNGVDGEWTYDDATKTFTVTEGSHHHHHHGSSHFGRTGPPDIA
DTYSLLVLNITFRTSADDLFPLFDKYGKVVDIFIPRDRRTGESRGFAFVRYKYAEEAQKAVDRLDGRVVDGREMAVQFAK
YGPNAERIHQGRIIEKV

GB1, 6xHis, RRM, Znk, RS domain (max length), RS domain (max percentage)

Supplemental Figure 10. Amino acid sequences of RS2Z35, RS2Z36, SC30b and corresponding recombinant SR proteins (GB1-His-RS2Z35(RBD), GB1-His-RS2Z36(RBD), GB1-His-SC30b(RRM)).

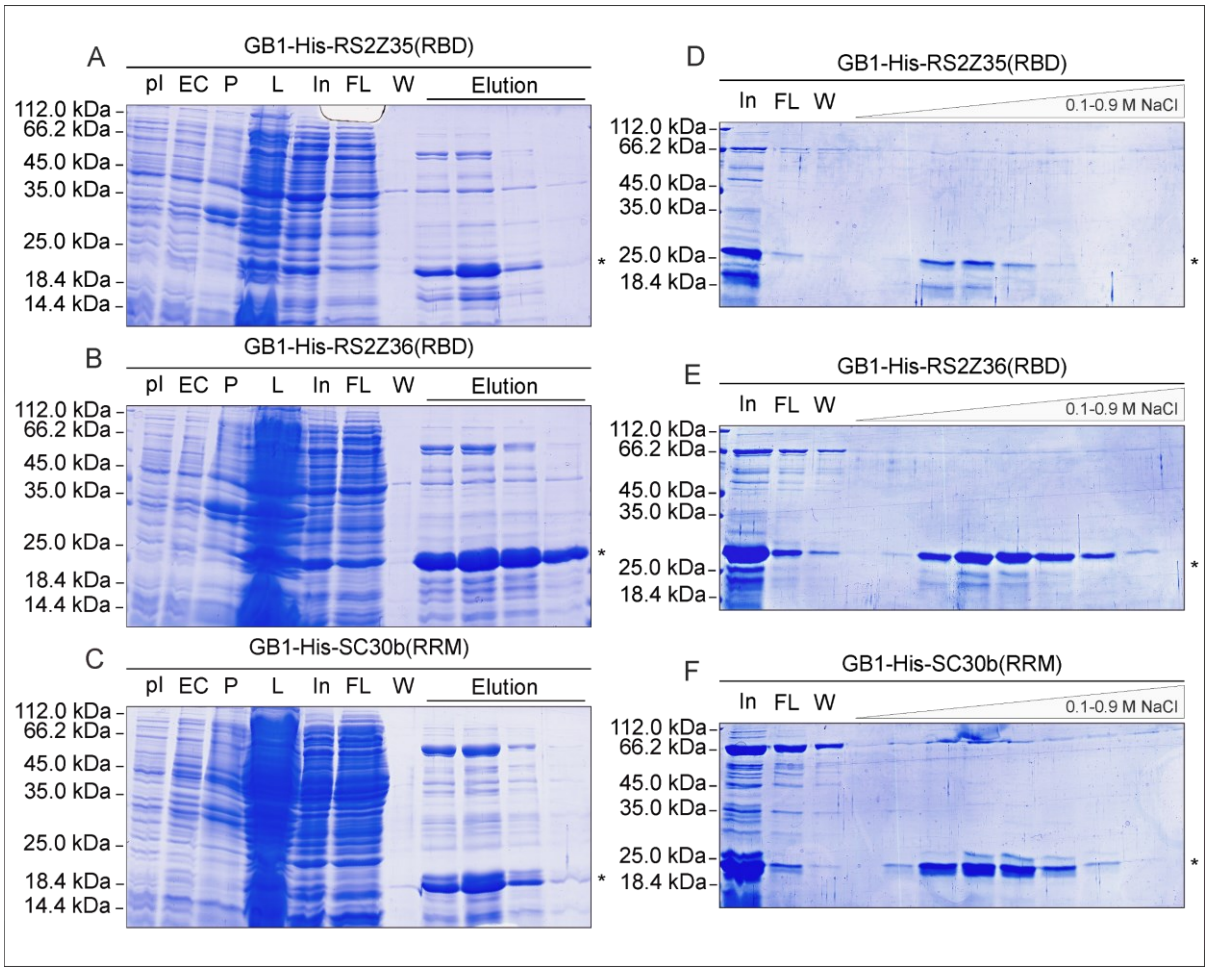

Supplemental Figure 11. Expression and purification of recombinant SR proteins from *E. coli*. SDS-PAGE following large-scale expression of GB1-His-RS2Z35(RBD) **(A)**, GB1-His-RS2Z36(RBD) **(B)** and GB1-His-SC30b(RRM) **(C)** in 2 L E. coli BL21 LEMO (DE3) and subsequent immobilized metal affinity chromatography. pI: pre-induction (0.05%), EC: expression control (0.05%), P: pellet (0.05%), L: lysate (0.05%), In: Input (0.05%), FL: flowthrough (0.05%), W: last wash (0.05%). Elution (1%). Subsequent cation exchange chromatography of GB1-His-RS2Z35(RBD) **(D)**, GB1-His-RS2Z36(RBD) **(E)** and GB1-His-SC30b(RRM) **(F)**. In: Input (0.75%), FL: flowthrough (0.75%). W: first wash (0.75%). Elution (0.75%). Asterisks indicate expected signal for the respective recombinant protein.

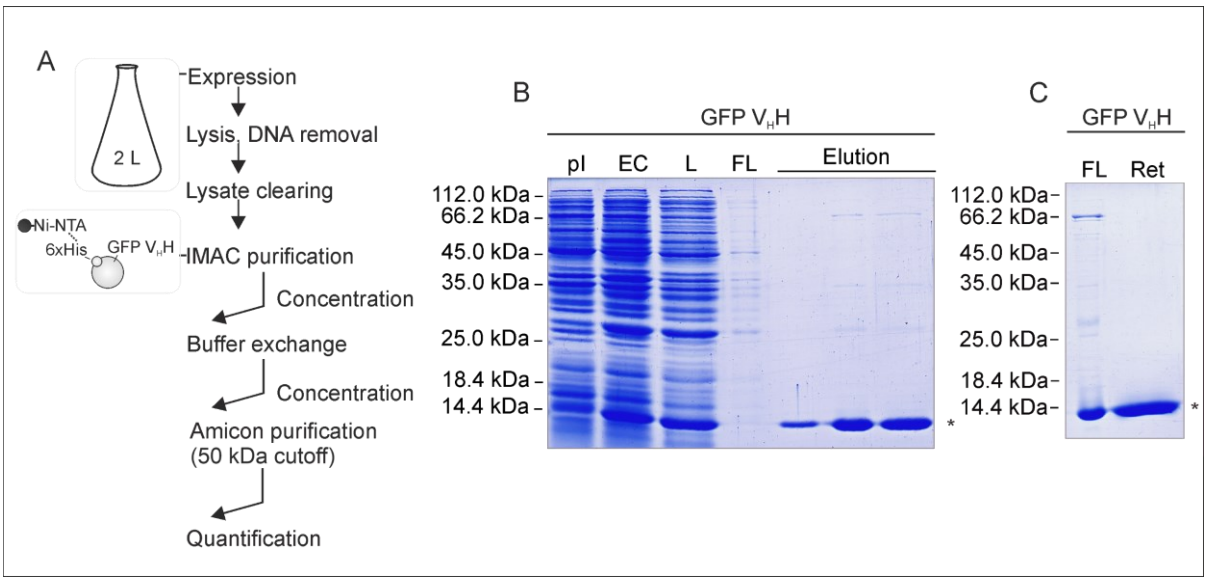

Supplemental Figure 12. Expression and purification of GFP V$_H$H nanobody from *E. coli*. (A) Purification workflow. **(B)** SDS-PAGE following large-scale expression in 2 L E. coli BL21 star (DE3) and subsequent immobilized metal affinity chromatography. pI: pre-induction (0.01%), EC: expression control (0.01%), L: lysate = Input (0.1%), FL: flowthrough (0.01%), Elution (1%). **(C)** SDS-PAGE following separation of nanobodies from higher MW contaminants by Amicon purification. FL: flowthrough (0.1%). Ret = Retention (0.1%). Asterisks indicate signal corresponding to GFP nanobody. Depicted are Coomassie-stained 15% polyacrylamide gels.

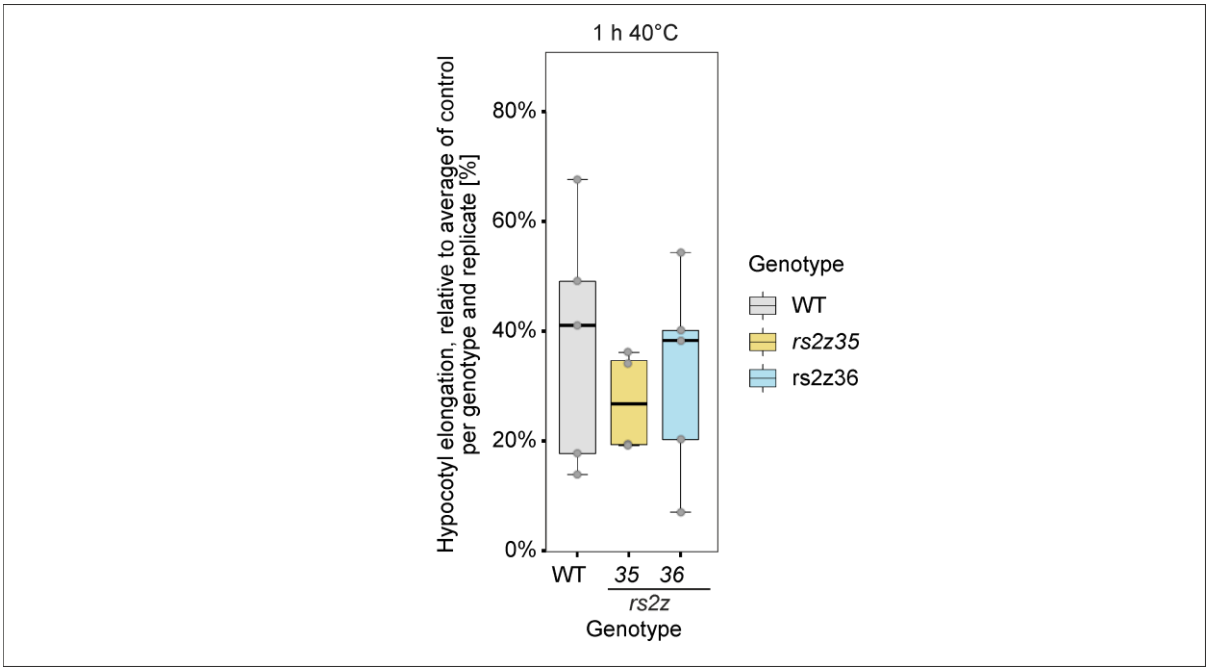

Supplemental Figure 13. Preliminary assessment of basal thermotolerance of *rs2z* single mutant plants. Relative hypocotyl elongation as described for Figure 23 and performed by Samia Bachiri. Statistical analysis showed no significant difference between the genotypes.

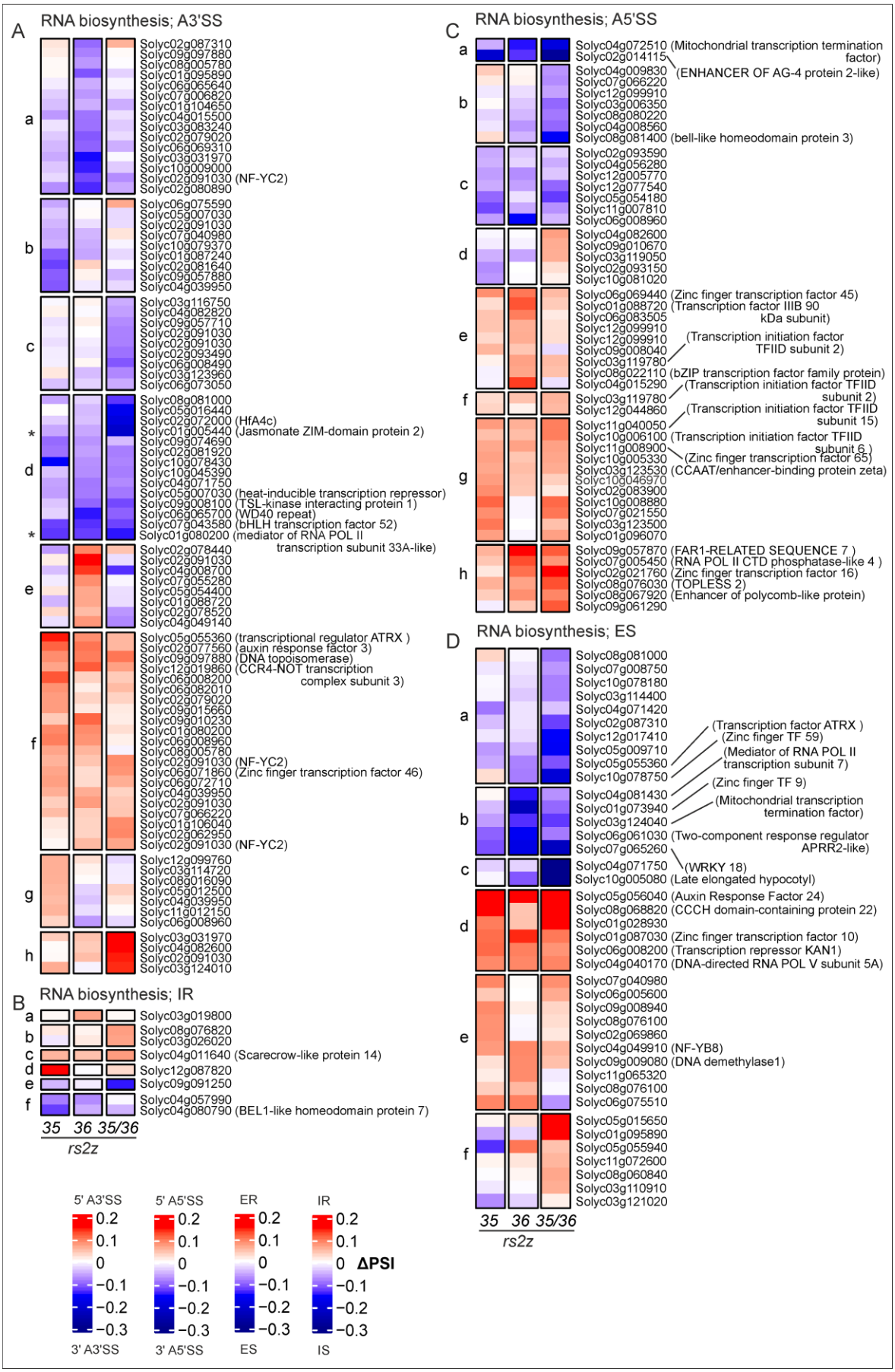

Supplemental Figure 14. Heatmaps depicting alternative splicing changes in genes coding for proteins involved in RNA biosynthesis in *rs2z* mutants relative to WT under HS. Heatmaps were generated as described in Fig. 34.

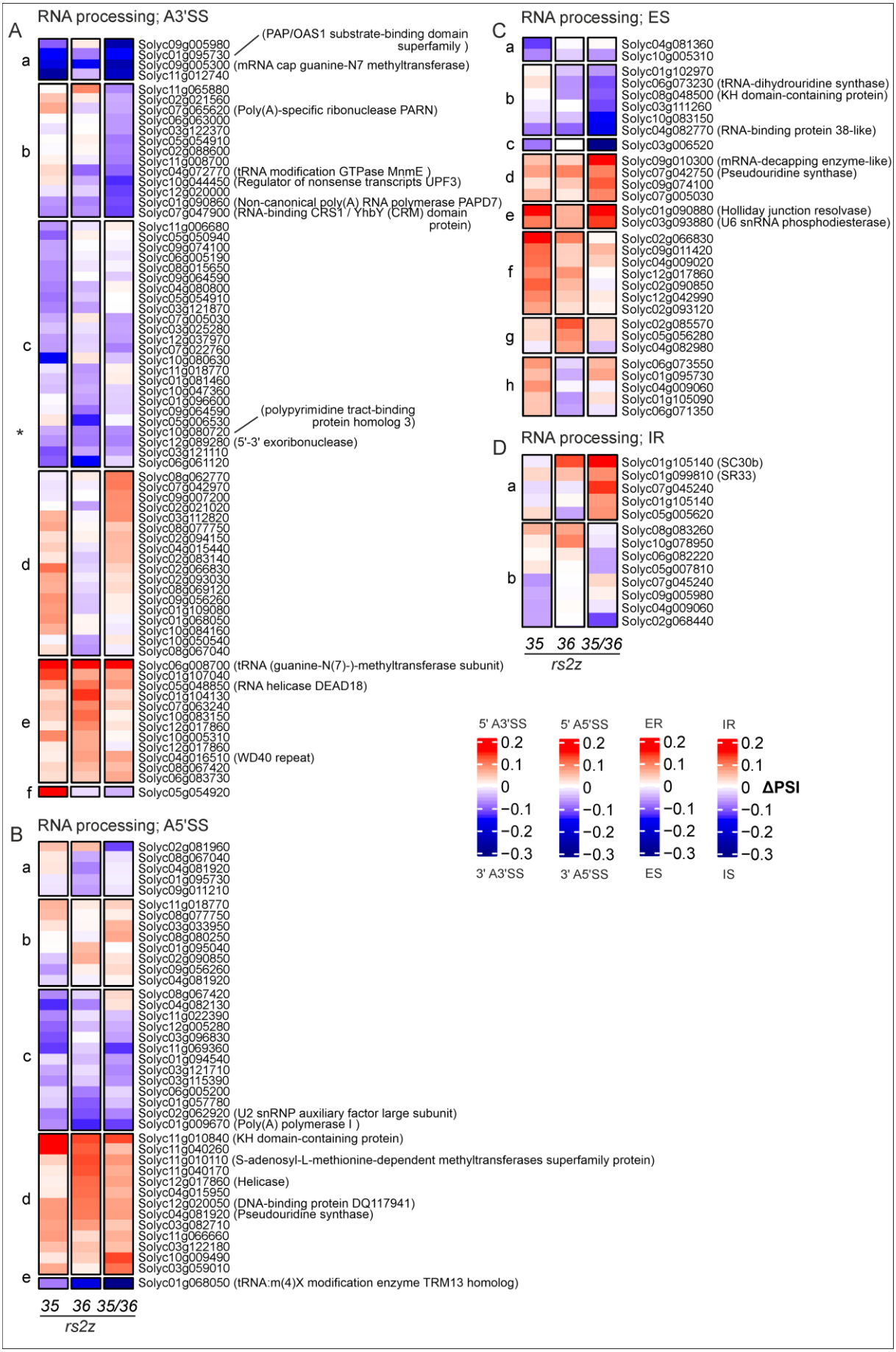

Supplemental Figure 15. Heatmaps depicting alternative splicing changes in genes coding for proteins involved in RNA processing in *rs2z* mutants relative to WT under HS. Heatmaps were generated as described in Fig. 34.

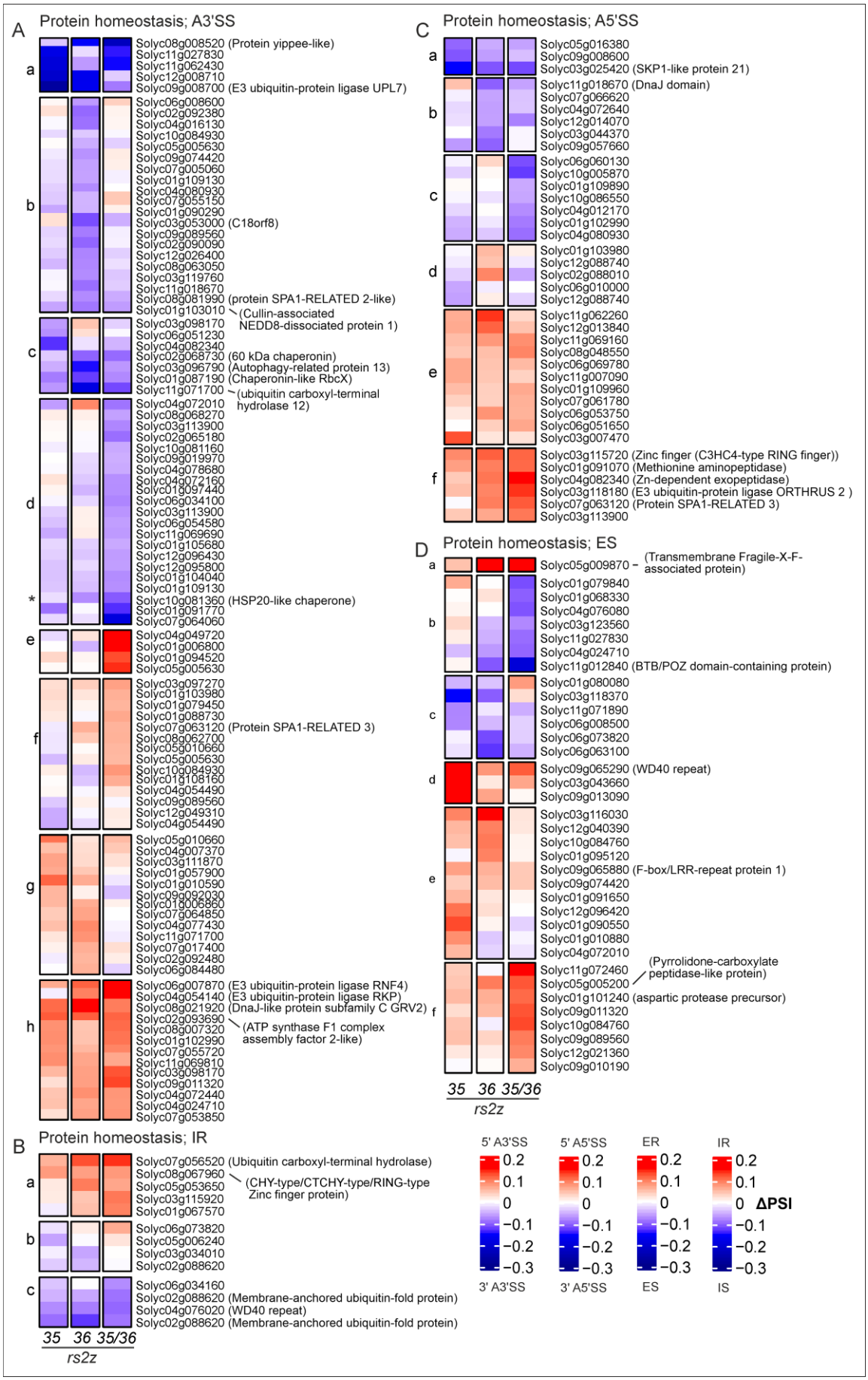

Supplemental Figure 16. Heatmaps depicting alternative splicing changes in genes coding for proteins involved in protein homeostasis in *rs2z* mutants relative to WT under HS. Heatmaps were generated as described in Fig. 34.

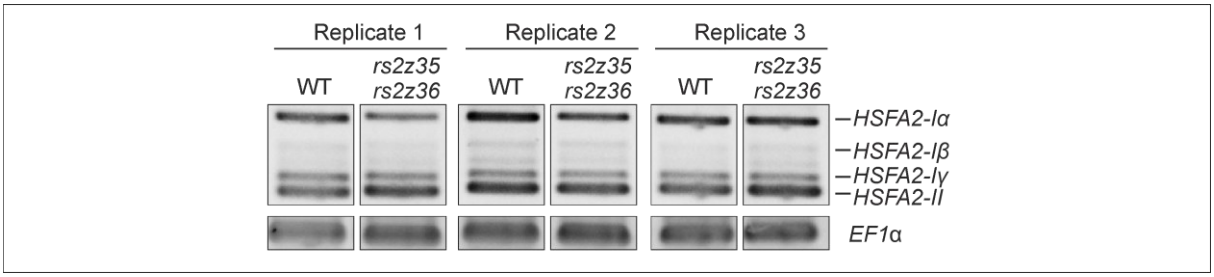

Supplemental Figure 17. Splicing profiles of *HSFA2* in RNA-Seq samples obtained by RT-PCR. RT-PCRs were performed as described Fig. 6F. Splicing profiles of *HSFA2* intron 2 are depicted for the WT and the *rs2z35 rs2z36* mutant amplified from cDNA synthesized from RNA of the three replicates that were sent for sequencing.

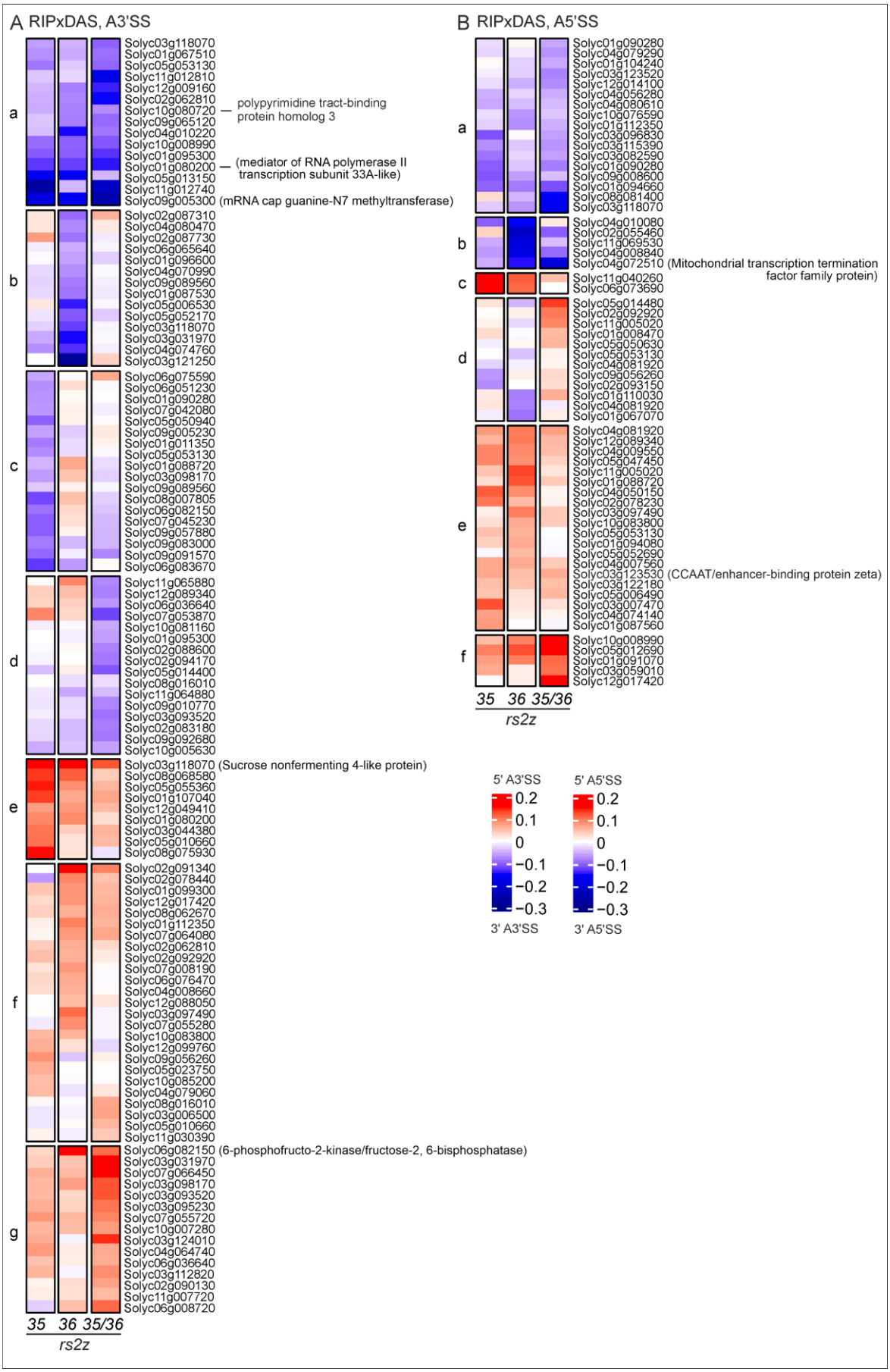

Supplemental Figure 18. Heatmaps depicting alternative splicing changes in genes associated with RS2Z proteins and differentially alternatively spliced by A3'SS or A5'SS in *rs2z* mutants. Heatmaps were generated as described in Fig. 34.

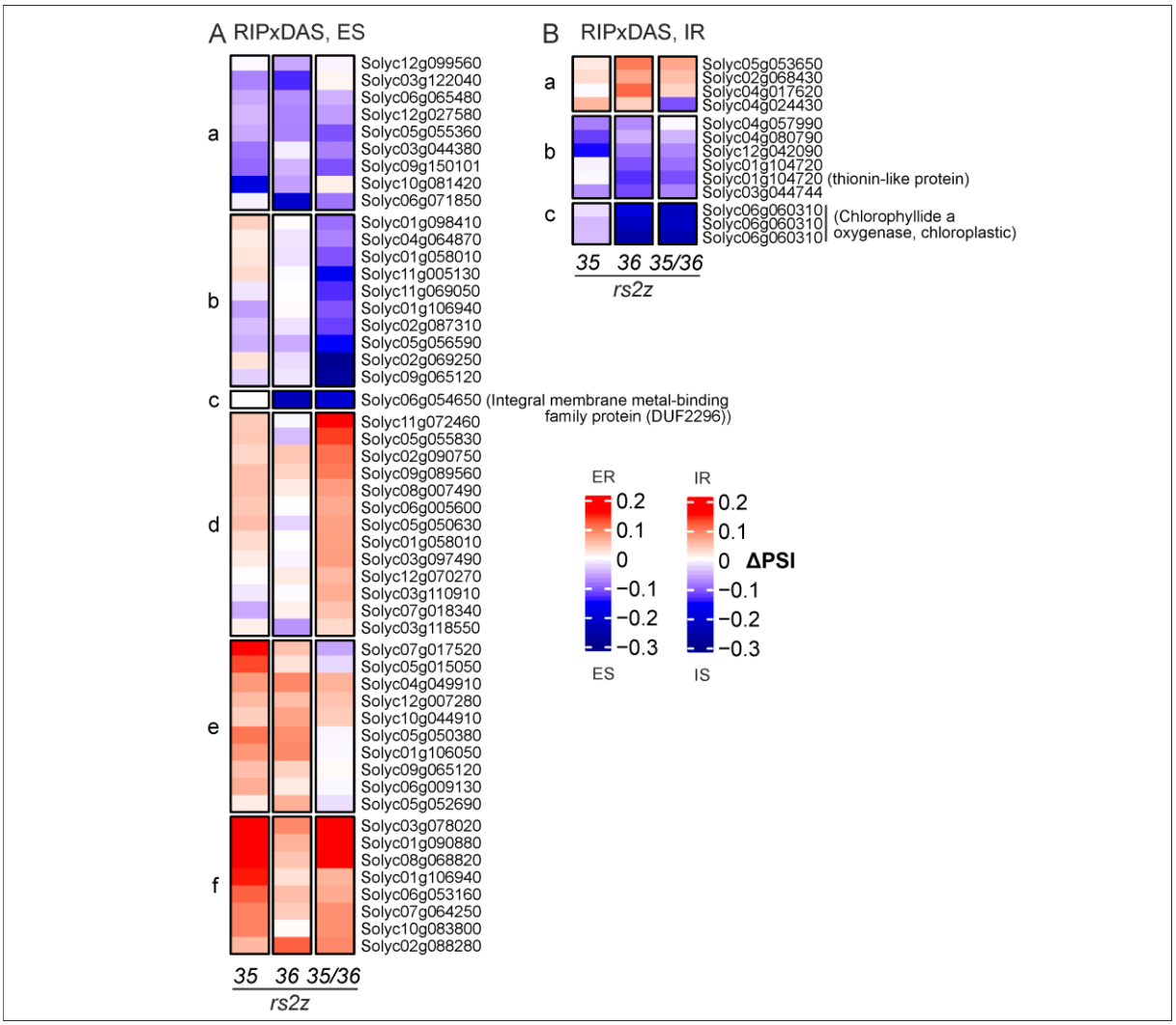

Supplemental Figure 19. Heatmaps depicting alternative splicing changes in genes associated with RS2Z proteins and differentially alternatively spliced by ES or IR in *rs2z* mutants. Heatmaps were generated as described in Fig. 34). **(A)** ES, **(B)** IR.

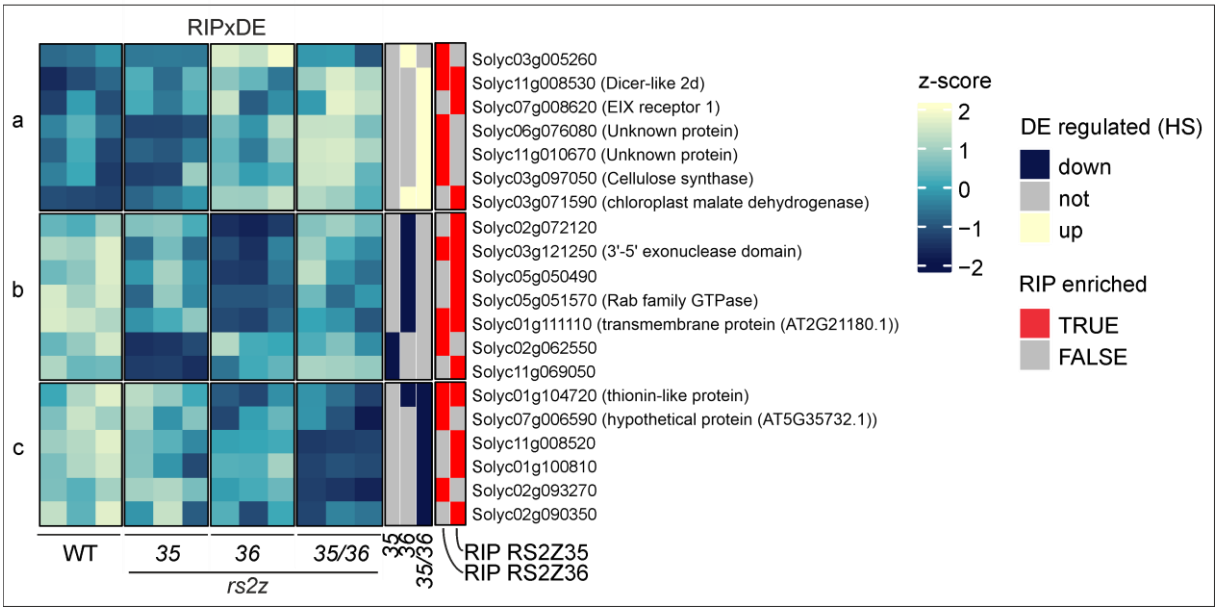

Supplemental Figure 20. Heatmap depicting read counts of genes associated with RS2Z and shown to be differentially expressed in *rs2z* mutants under HS. The heatmap depicts log-transformed z-score normalised read counts as described in Fig. 26. Columns on the right side indicate significant differential expression in *rs2z* mutants relative to WT under HS conditions (I LFC I > 0.5849, padj < 0.05) and RIP-enrichment in *GFP-RS2Z* relative to *GFP*.

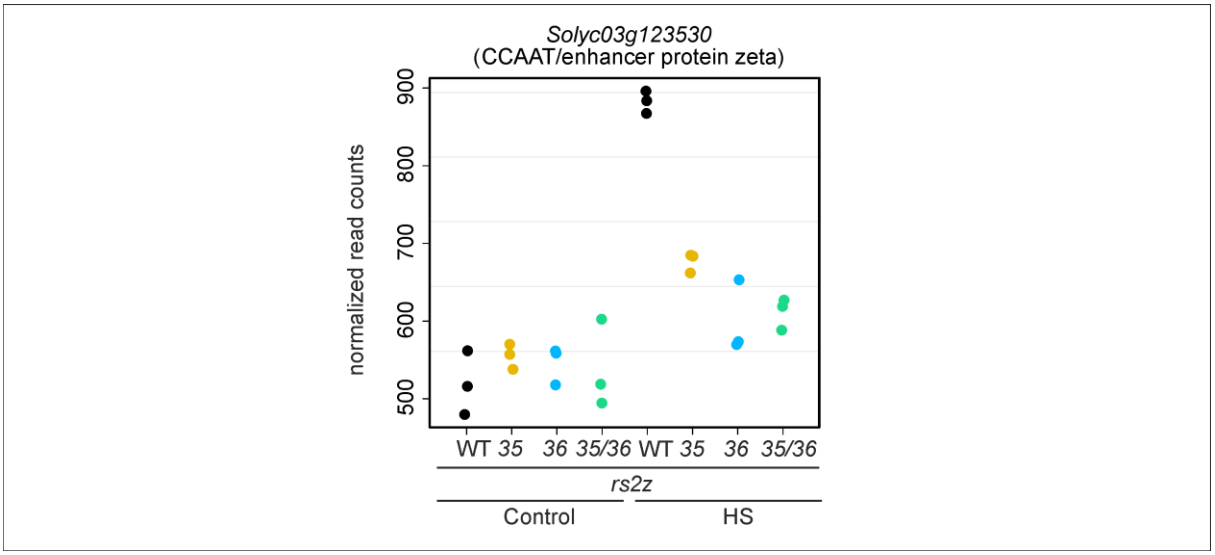

Supplemental Figure 21. Library size normalised read counts for *Solyc03g123530* (CCAAT/enhancer-binding protein zeta) in control and HS (1 h 40°C) samples from WT and *rs2z* mutants.

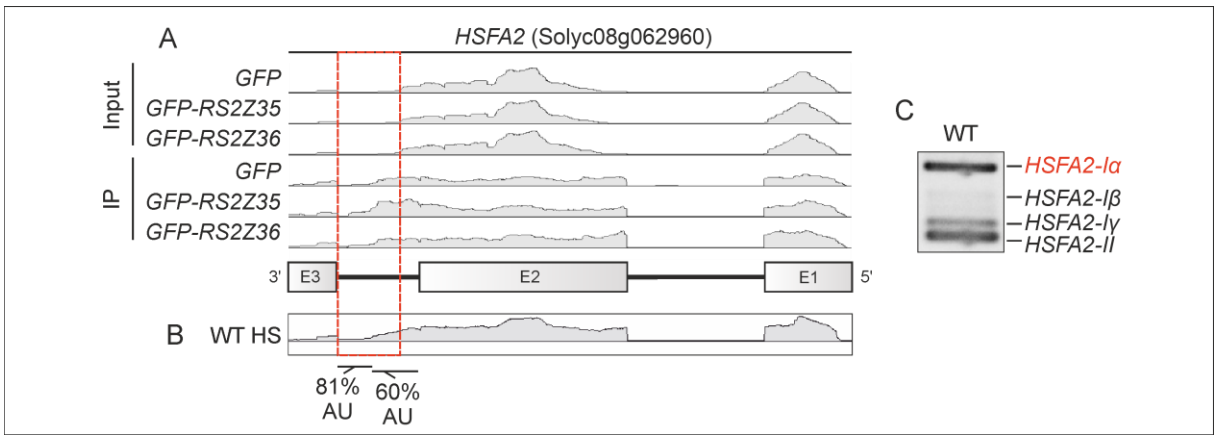

Supplemental Figure 22. *HSFA2* coverage in RIP Input and IP samples. Coverage plot depicting merged read coverage of the *HSFA2* gene in 3 RIP-Seq replicates of *GFP*, *GFP-RS2Z35* and *GFP-RS2Z36* Input and IP samples. **(A)** as well as in one representative replicate from RNA-Seq of the WT under HS **(B)**. The red box highlights the region specific for *HSFA2-Iα*. **(C)** Representative *HSFA2* intron 2 splicing profile obtained from RT-PCR from the same RNA depicted in (B). The AU content is indicated for the 5' and 3'-region of intron 2.

Acknowledgements

First and foremost, I'd like to thank Prof. Dr. Enrico Schleiff for the opportunity to conduct this study in his multi-cultural and multi-national group and thereby providing an inspiring environment not only for tackling many different aspects of plant molecular biology but also for interpersonal growth and connections. Second of all, I'd like to sincerely thank Dr. Sotirios Fragkostefanakis for his supervision and guidance. You are an endless source of ideas and I'm eager to see all the crazy things you will accomplish in the future. Lots of thanks go to Prof. Dr. Michaela Müller-McNicoll for being the second examiner of this study and for introducing me to the world of SR proteins that I fell in love with.

Moreover, I'd like to thank Daniela Bublak, Stavros Vraggalas, Samia Bachiri and Karin Löchli (in no particular order) for their contribution to this study. You were an essential part of its success, and I cannot thank you enough. I wish you all the best in your further academic careers and I'm sure you will thrive greatly! Also, thanks to Uwe Bodenson for providing your never-ending knowledge, your positive attitude, and your willingness to help and tackle all sorts of problems (protein-related and beyond). You are a gem.

Many thanks go to Dr. Kathi Zarnack and Dr. Mario Keller for your supervision and guidance on diving into the territory of bioinformatic analyses.

Furthermore, many thanks to Holger Schranz for taking great care of the tomato plants in the green house. I admire your positive spirit and wish that you will forever keep it.

Of course, many thanks to all current and former members of the Chaperone lab and the whole Schleiff group for creating a pleasant atmosphere to work in, especially the people mentioned above as well as Sarah Ulrich and Nicole Spies. Despite the global pandemic taking place during our PhD which created many obstacles both within our studies and in our private life, we tried to push through and stay focused. While it was not always successful and there were many bad times, I am deeply proud of us all.

Furthermore, I'd like to thank my family and friends for the emotional support and for keeping in touch although I made the lab my second home. Last but not least, I like to address special thanks to my dear grandmother who lost the battle with cancer during this study. You had no doubts that I would make it and I wish you could see that I did. You are missed so much.